

**Development of thermodynamic methods for quantification and
understanding of non-covalent interactions in molecular and ionic systems**

Dissertation

zur Erlangung des Grades

doctor rerum naturalium (Dr. rer. nat)

am Institut für Chemie

der Mathematisch-Naturwissenschaftlichen Fakultät

der Universität Rostock

vorgelegt von

Kondratev Stanislav

aus Samara, Russland

Rostock, 2021



Dieses Werk ist lizenziert unter einer
Creative Commons Namensnennung 4.0 International Lizenz.

Gutachter:

Prof. Dr. habil. Sergey P. Verevkin, Universität Rostock, Institut für Chemie

Prof. Dr. Stefano Vecchio Cipriotti, Sapienza University of Rome, Department of Basic and Applied Science for Engineering

Jahr der Einreichung: 2021

Jahr der Verteidigung: 2021

Acknowledgement

I am grateful to Sergey Vostrikov, Andrey Pimerzin, and Sergey Verevkin for a given opportunity to do this research. Also, I would like to thank Dzmitry Zaitsau for a profound comprehensive scientific and technical support, Peter Kumm and Martin Riedel for helping me to improve my research devices, and Andranik Petrosyan and my parents for a substantial moral support during my stay in Rostock.

Selbstständigkeitserklärung

Ich versichere hiermit an Eides statt, dass diese Arbeit selbstständig und ausschließlich mit Hilfe der von mir angegebenen Quellen und Hilfsmittel angefertigt wurde.

Stanislav Kondratev

08.11.2021

Universität Rostock
Institut für Chemie
Abteilung Physikalische Chemie
Dr. Lorenz Weg 2
D-18051

Summary

The attractive part of the van der Waals potential is commonly referred to as dispersion forces. Dispersion forces are a ubiquitous phenomenon with significant implications for chemistry, biochemistry, and materials science. For example, dispersion helps explain the mutual attraction of σ - π systems, the π - π attractive interactions in graphene, and even why alkanes become liquid with increasing chain length. Dispersion and non-covalent interactions are often responsible for the intramolecular stabilization of flexible or strained molecules, so taking these forces into account is a crucial contribution to rationalizing the unexpected stabilities of such molecules. Qualitatively, non-covalent interactions can often be identified as the driving force behind chemical processes, but quantitatively determining the intensity of interplay is a challenging task. Nevertheless, the extent of stabilization or destabilization could be properly assessed, provided that a reference system of molecules with gradual structural changes is established. To quantify non-covalent interactions in such well-defined molecular and ionic systems, we have developed and validated three thermodynamic methods based on the “experimental” enthalpy of vaporization and enthalpy of formation as well as based on the “theoretical” DFT-calculated energy. The first two methods involve experimental thermochemical data. The required experimental data were collected from the literature and validated with complementary own new measurements. The focus of the experimental studies was on vapor pressure measurements (Knudsen effusion method and transpiration method) and DSC measurements. The available experimental thermochemical data were additionally validated with the help of structure-property correlations and high-level quantum chemical calculations. A straightforward “centerpiece” approach, based on group-additivity was developed for the validation and prediction of thermochemical properties. The non-covalent and dispersion interactions for molecular systems including branched alkanes, alcohols, amines, poly-phenyl aromatics, *etc.* were quantified simultaneously with “experimental” and “theoretical” methods. It has been found that the levels derived with both types are quite different in terms of energy, but correlate linearly within each system of molecules taken into consideration. Hence, the quantitative thermodynamic methods developed in this thesis could significantly contribute to understanding of non-covalent interactions in molecular and ionic systems.

Zusammenfassung

Der anziehende Teil des Van-der-Waals-Potentials wird allgemein als Dispersionskräfte bezeichnet. Dispersionskräfte sind ein allgegenwärtiges Phänomen mit erheblichen Auswirkungen auf Chemie, Biochemie und Materialwissenschaften. Zum Beispiel hilft die Dispersion, die gegenseitige Anziehung von σ - π -Systemen, die anziehenden π - π -Wechselwirkungen in Graphen zu erklären und sogar, warum Alkane mit zunehmender Kettenlänge flüssig werden. Dispersion und nicht-kovalente Wechselwirkungen sind oft für die intramolekulare Stabilisierung flexibler oder gespannter Moleküle verantwortlich, daher ist die Berücksichtigung dieser Kräfte ein wichtiger Beitrag zur Erklärung der unerwarteten Stabilitäten solcher Moleküle. Qualitativ lassen sich oft nicht-kovalente Wechselwirkungen als treibende Kraft chemischer Prozesse identifizieren, aber die Intensität des Zusammenspiels quantitativ zu bestimmen, ist eine anspruchsvolle Aufgabe. Dennoch könnte das Ausmaß der Stabilisierung oder Destabilisierung richtig beurteilt werden, vorausgesetzt, dass ein Referenzsystem von Molekülen mit schrittweisen Strukturänderungen etabliert wird. Um

nicht-kovalente Wechselwirkungen in solchen gut-definierten molekularen und ionischen Systemen zu quantifizieren, haben wir drei thermodynamische Methoden entwickelt und validiert, die auf der „experimentellen“ Verdampfungs- und Bildungsenthalpien sowie auf der „theoretischen“ DFT-berechneten Energie basieren. Die ersten beiden Methoden beinhalten experimentelle thermochemische Daten. Die erforderlichen experimentellen Daten wurden der Literatur entnommen und mit ergänzenden eigenen neuen Messungen validiert. Der Schwerpunkt der experimentellen Untersuchungen lag auf Dampfdruckmessungen (Knudsen-Effusionsverfahren und Transpirationsverfahren) und DSC-Messungen. Die verfügbaren experimentellen thermochemischen Daten wurden zusätzlich mit Hilfe von Struktur-Eigenschafts-Korrelationen und quantenchemischen Berechnungen auf hohem Niveau validiert. Für die Validierung und Vorhersage thermochemischer Eigenschaften wurde ein unkomplizierter „Herzstück“-Ansatz entwickelt, der auf Gruppenadditivität basiert. Die nichtkovalenten und Dispersionswechselwirkungen für molekulare Systeme einschließlich verzweigter Alkane, Alkohole, Amine, Polyphenylaromaten usw. wurden gleichzeitig mit „experimentellen“ und „theoretischen“ Methoden quantifiziert. Es hat sich gezeigt, dass die mit beiden Typen abgeleiteten Niveaus energetisch recht unterschiedlich sind, aber innerhalb jedes betrachteten Molekülsystems linear korrelieren. Daher könnten die in dieser Arbeit entwickelten quantitativen thermodynamischen Methoden wesentlich zum Verständnis nichtkovalenter Wechselwirkungen in molekularen und ionischen Systemen beitragen.

Table of contents

1. Introduction	1
2. Quantification of dispersion forces with the aid of enthalpy of vaporization	6
2.1. Dispersion forces in amines	6
2.1.1. Dispersion forces in symmetric trialkylamines	6
2.1.2. Dispersion forces in phenyl-substituted amines	9
2.2. Quantification of hydrogen bonding and dispersion forces in pharmaceuticals.....	13
2.2.1. Experimental thermochemical studies.....	13
2.2.2. Validation of vaporization enthalpies of drugs with help of “centerpiece” approach.....	15
2.2.3. Quantification of hydrogen bonding and dispersion forces in ibuprofen.....	18
3. Quantification of dispersion forces with the aid of enthalpy of formation	23
3.1. Extremely strained hydrocarbons: strain vs. dispersion forces.....	23
3.2. Sterically congested alcohols: strain vs. dispersion forces	27
3.3. Dispersion interactions in phenyl substituted benzenes, naphthalenes, and anthracenes	28
3.3.1. Compilation of liquid-gas, solid-gas, and solid-liquid phase transition and adjustment to the reference temperature.....	30
3.3.2. Validation of the experimental data on phase transitions.....	35
3.3.3. Nearest-neighbour interactions: agglomeration of substituents in the benzene ring.....	39
3.3.4. Dispersion interactions in para- and meta-terphenyls	41
3.3.5. Dispersion interactions in phenyl substituted naphthalenes and anthracenes	44
3.4. Non-nearest neighbour interactions: well-balanced reactions	48
4. Nearest-neighbour and non-nearest-neighbour non-covalent interactions between substituents in the aromatic systems. Experimental and theoretical study of functionally substituted acetophenones and benzophenones	56
4.1. Introduction.....	56
4.2. Materials and methods	59
4.3. Results and discussion	59
4.3.1. Absolute vapour pressures and thermodynamics of vaporization/sublimation.....	59
4.3.2. Consistency of vaporization/sublimation enthalpies	64

4.3.3. Whether substituted acetophenones and benzophenones follow the Walden's rule?	68
4.3.4. Gas-phase standard molar enthalpies of formation	69
4.3.5. Development of the “centerpiece” group-contribution approach.....	73
4.4. Conclusions.....	83
5. Ionic systems: dispersion forces from the thermodynamic properties	83
5.1. Dispersion forces in aprotic ammonium and phosphonium ionic liquids from the vaporization enthalpy.....	84
5.2. Dispersion forces in aprotic ammonium ionic liquids from DFT	92
5.3. Trend shift in hexafluorophosphate cation based ionic liquids	93
6. Experimental part.	98
6.1. Transpiration or gas saturation method.....	98
6.1.1. Data processing.....	100
6.1.2. Heat capacity differences determination	101
6.2. Mass loss Knudsen effusion method.....	103
6.2.1. Experimental procedure.....	106
6.3. Differential scanning calorimetry	109
6.4. Computational methods	110
7. References	111
APPENDIX.....	136
A. Supporting information for chapter 2.....	136
B. Supporting information for chapter 3.....	139
C. Supporting information for chapter 4.....	143

List of tables

Table 1.1 Contributions of the CH ₂ group to the enthalpy of vaporization at 298 K for the various homologous series of molecular and ionic compounds	3
Table 2.1.1 Compilation of auxiliary data on Kovats's indices, J_x , normal boiling points, T_b , molar heat capacities and heat capacity differences at $T = 298.15$ K	6
Table 2.1.2 Group-additivity values I_i for calculation of vaporization enthalpies, at 298.15 K.....	8
Table 2.1.3 Experimental vaporization enthalpies of tri-alkyl-amines, the sum of constituting increments and their deviations from additivity (E_{disp}), attributed to the dispersion forces	9
Table 2.1.4 Compilation of enthalpies of sublimation/vaporization of phenyl substituted amines...	10
Table 2.1.5 Phase transitions thermodynamics of tri-phenyl-amine.....	11
Table 2.1.6 Correlation of vaporization enthalpies of ortho-substituted benzenes with their Kovats's indices (J_x).....	11
Table 2.1.7 Experimental vaporization enthalpies, of phenyl substituted amines, the sum of constituting increments, and their deviations from additivity (E_{disp}), attributed to the dispersion forces	12
Table 2.2.1 Phase transitions thermodynamics of profens studied in this work.....	14
Table 2.2.2 Phase transitions thermodynamics of auxiliary for the "centerpiece" approach compounds	14
Table 2.2.3 Compilation of data on molar heat capacities and heat capacity differences at $T = 298.15$ K used for temperature adjustments.....	15
Table 2.2.4 Experimental enthalpies of vaporization of the aromatic monocarboxylic acids and their homomorph methyl esters.....	20
Table 3.1.1 Correlation of strain enthalpies H_S of highly branched hydrocarbons with their amount of dispersion contributions ($E_{\text{disp-D3}}$) calculated by the DFT-D3.....	24
Table 3.3.1 Compilation of enthalpies of sublimation/vaporization of aromatic compounds.....	30
Table 3.3.2 Phase transitions thermodynamics of aromatic compounds	32
Table 3.3.3 Compilation of molar heat capacities and heat capacity differences at $T = 298.15$ K ...	34
Table 3.3.4 Compilation of experimental values for di- and tri-phenylbenzenes.....	34
Table 3.3.5 Correlation of vaporization enthalpies, of substituted benzenes, naphthalenes, and anthracenes with their Lee indices (J_{Lee}).....	36
Table 3.3.6 Correlation of Lee indices with number of phenyl rings in the terphenyl series.	36
Table 3.3.7 Correlation of vaporization enthalpies, of substituted benzenes, naphthalenes, and anthracenes with their Kratz indices (J_{Kratz}).....	36
Table 3.3.8 Correlation of Kratz indices with number of phenyl rings in the terphenyl series.	37

Table 3.3.9 Correlation of experimental fusion temperatures (T_{fus}), with number of phenyl rings in the terphenyl series.....	38
Table 3.3.10 Correlation of experimental fusion enthalpies, with number of phenyl rings in the terphenyl series.	38
Table 3.3.11 Compilation of the experimental values for poly-phenyl-benzenes and correlation of reaction enthalpies and strain enthalpies HS with their amount of dispersion contributions ($E_{disp-D3}$) calculated by the DFT-D3.....	39
Table 3.3.12 Compilation of evaluated thermochemical results for para- and meta-terphenyls with their amount of dispersion contributions ($E_{disp-D3}$) calculated by the DFT-D3.....	42
Table 3.3.13 Compilation of evaluated thermochemical results for phenyl substituted naphthalenes and anthracenes with their amount of dispersion contributions ($E_{disp-D3}$) calculated by the DFT-D3.....	45
Table 3.4.1 Compilation of the standard molar enthalpies of vaporization of phenyl substituted ketones	50
Table 3.4.2 Compilation of data on molar heat capacities and heat capacity differences at $T = 298.15$ K.....	51
Table 3.4.3 Phase transitions thermodynamics of substituted acetophenones and benzophenones ..	51
Table 3.4.4 Thermochemical data at $T = 298.15$ K.....	52
Table 3.4.5 Thermochemical data for aromatic and aliphatic amines at $T=298.15$ K.....	54
Table 4.3.1 Compilation of data on molar heat capacities and heat capacity differences at $T = 298.15$ K.....	60
Table 4.3.2 Compilation of enthalpies of vaporization/sublimation for the acetophenone derivatives derived in this work and from the data available in the literature.....	61
Table 4.3.3 Compilation of enthalpies of vaporization/sublimation for the dimethoxyacetophenones derivatives derived in this work and from the data available in the literature.	61
Table 4.3.4 Compilation of enthalpies of vaporization/sublimation for the benzophenone derivatives derived in this work and from the data available in the literature.....	62
Table 4.3.5 Compilation of enthalpies of vaporization/sublimation for the benzophenone derivatives derived in this work and from the data available in the literature.....	62
Table 4.3.6 Correlation of vaporization enthalpies, of substituted acetophenones and benzophenones with their Kovats's indices (J_x)	64
Table 4.3.7 Correlation of vaporization enthalpies, of benzene and benzophenone derivatives with their Kovats's indices (J_x)	65
Table 4.3.8 Correlation of vaporization enthalpies, of benzene and benzophenone derivatives with their Kovats's indices (J_x)	65

Table 4.3.9 Correlation of vaporization enthalpies, of benzene and benzophenone derivatives with their normal boiling temperatures (T_b).....	66
Table 4.3.10 Phase transitions thermodynamics of substituted acetophenones and benzophenones	67
Table 4.3.11 Thermochemical data for substituted acetophenones at $T = 298.15$ K.....	70
Table 4.3.12 Thermochemical data for substituted benzophenones at $T = 298.15$ K.....	70
Table 4.3.13 Thermochemical data at $T = 298.15$ K ($p^\circ = 0.1$ MPa) for auxiliary reference compounds.	73
Table 4.3.14 Parameters and pairwise nearest and non-nearest neighbour interactions of substituents on the “centerpieces” for calculation of thermodynamic properties of substituted benzenes and benzophenones at 298.15 K	74
Table 4.3.15 Analysis of the total amount of pairwise nearest and non-nearest neighbour non-covalent interactions of substituents on the “centerpieces” in terms of enthalpy of formation in gaseous phase for di-methoxy-substituted acetophenones at 298.15 K.....	82
Table 5.1.1 Quantification of dispersion forces for tetra-alkylammonium-based ILs with the [NTf ₂] anion.....	87
Table 5.1.2 Quantification of dispersion forces for tetra-alkylphosphonium-based ILs and alkyl phosphines.....	87
Table 5.2.1 Quantum chemical quantification of dispersion forces for tetra-alkylammonium-based ILs with the [NTf ₂] anion.....	92
Table 5.3.1 The molar enthalpies of vaporization for [C _n mim][PF ₆] family derived from QCM results.	95
Table 5.3.2 Contributions for CH ₂ group into the enthalpy of vaporization , for different classes of molecular and ionic compounds.	97
Table 5.3.3 Chain-length dependence of dispersion forces, $E_{\text{disp-D}}$, in [C _n mim][PF ₆] series at 298.15 K	97
Table 6.2.1 The precise dimensions of the orifices used in this work	106
Table 6.2.2 Results of the test experiments with benzoic acid	107
Table A.1 Results of transpiration method for substituted acetophenones and benzophenones: absolute vapor pressures p , standard molar vaporization enthalpies and standard molar vaporization entropies.....	136
Table A.2 Results of Knudsen effusion method for tri-phenyl-amine: absolute vapor pressures p , standard molar sublimation enthalpies and standard molar sublimation entropies	138
Table A.3 Results from the Knudsen Method: absolute vapour pressures, standard molar sublimation enthalpies and standard molar sublimation entropies measured in this work.....	139

Table B.1 Results of transpiration method for 1-phenyl-naphthalene: absolute vapor pressures p , standard molar vaporization enthalpies and standard molar vaporization/ entropies	139
Table B.2 Results of Knudsen effusion method for aromatic compounds: absolute vapor pressures p , standard molar vaporization/sublimation enthalpies and standard molar vaporization/sublimation entropies.	140
Table B.3 Results of transpiration method: absolute vapour pressures p , standard ($p_0 = 0.1$ MPa) molar vaporization enthalpies and standard ($p_0 = 0.1$ MPa) molar vaporization entropies.	141
Table C.1 Results of transpiration method for substituted acetophenones and benzophenones: absolute vapor pressures p , standard molar vaporization/sublimation enthalpies and standard molar vaporization/sublimation entropies	143
Table C.2 Results of Knudsen effusion method for benzophenone derivatives: absolute vapor pressures p , standard molar sublimation enthalpies and standard molar sublimation entropies.....	147

List of figures

Figure 1.1 Crowding destabilizes experimentally unknown hexaphenylethane, while the more crowded all-meta-tert-butylhexaphenylethane can be crystallized.....	1
Figure 1.2 Calculated Gibbs energy difference at 100 K $\Delta G^{\circ} = G^{\circ}_{\text{hairpin}} - G^{\circ}_{\text{all-trans}}$ versus chain length data from	2
Figure 1.3 Vaporization enthalpies of <i>n</i> -alkanes C_nH_{2n+2} at 298 K from pentane to hexaheptacontane as a function of the number of carbon atoms, N_C , in the alkyl chain.....	3
Figure 2.1.1 Series of symmetrical tri-alkyl-amines with $n = 3-8$ studied in this work.	6
Figure 2.1.2 Correlation of the vaporization enthalpies, of the tri-alkyl-amines with the normal boiling temperatures T_b (left) and with the Kovats' s indices J_x (right).....	7
Figure 2.1.3 One of the possible structures of trioctylamine $(C_8H_{19})_3N$	8
Figure 2.1.4 Series of phenyl substituted amines studied in this work.....	10
Figure 2.1.5 Structures of phenyl-substituted amines optimized by the DFT-D3 method.....	12
Figure 2.2.1 Structures of ibuprofen, flurbiprofen, indoprofen, ketoprofen, and naproxen	13
Figure 2.2.2 Validation of the “centerpiece” approach for vaporization enthalpy of Flurbiprofen...	16
Figure 2.2.3 Evaluation vaporization enthalpy of (S)-naproxen methyl ester with help of the “centerpiece” approach.	16
Figure 2.2.4 Evaluation vaporization enthalpy of ketoprofen with help of the “centerpiece” approach.....	17
Figure 2.2.5 Evaluation vaporization enthalpy of indoprofen with help of the “centerpiece” approach	18
Figure 2.2.6 Structure of the cyclic dimer of ibuprofen with two equivalent O-H...O hydrogen bonds between the functional COOH group of each molecule	18
Figure 2.2.7 Development of the intermolecular hydrogen bonding energy in aliphatic carboxylic acids and ibuprofen according to the homomorph model.....	20
Figure 2.2.8 Experimental vaporization enthalpies of alkyl acetates plotted versus the total number of carbon atoms (N_C) in the side chains.	21
Figure 2.2.9 Correction of the intermolecular hydrogen bonding energy in aliphatic carboxylic acids due to redundant CH_3 contribution.	21
Figure 2.2.10 B3LYP/6-31G* (squares) and B3LYP-D3/6-31G* (circles) calculated binding energies ΔE per molecule of ibuprofen clusters $n = 3-12$	22
Figure 3.1.1 Conventional equations for the evaluation of protobranching (a) and branching (b and c)	24

Figure 3.2.1 Comparison of the strain energies, H_s , and dispersion forces, $E_{\text{disp-D3}}$, in alkyl and phenyl congested carbinols.	27
Figure 3.3.1 Structures of phenyl substituted benzenes, naphthalenes, and anthracenes studied in this work.	29
Figure 3.3.2 The DFT-D3 optimized structures of phenyl substituted benzenes and their dispersion interactions.	41
Figure 3.3.3 Calculation of the dispersion interaction in biphenyl, p-terphenyl, p-quaterphenyl, and m-terphenyl with help of the well-balanced reactions.	42
Figure 3.3.4 Correlation of dispersion interactions $E_{\text{disp-D3}}$ with number of phenyl-rings, N_{ring} , constituting molecules of p-terphenyls (left) and meta-terphenyls (right).	43
Figure 3.3.5 The DFT-D3 optimized structures of para-terphenyls: p-terphenyl, p-quaterphenyl, p-quinquephenyl, p-sexiphenyl, and p-septiphenyl.	44
Figure 3.3.6 The DFT-D3 optimized structures of meta-terphenyls: m-quaterphenyl, m-quinquephenyl, m-sexiphenyl, m-septiphenyl, and m-deciphenyl.	44
Figure 3.3.7 Calculation of the dispersion interaction in phenyl substituted naphthalenes with help of the well-balanced reactions.	45
Figure 3.3.8 The DFT-D3 optimized structures of phenyl-substituted naphthalenes.	46
Figure 3.3.9 Calculation of the dispersion interaction in phenyl substituted anthracenes with help of the well-balanced reactions.	47
Figure 3.3.10 The DFT-D3 optimized structures of phenyl-substituted naphthalenes.	47
Figure 3.4.1 Structures of 1,3-diphenyl-propan, diphenyl carbonate, and 1,3-diphenyl-2-propanone	48
Figure 3.4.2 Calculation of the energetics π - π interaction in 1,2-diphenyl-ethane, 1,3-diphenyl-propane, and diphenyl carbonate with help of the well-balanced reactions.	49
Figure 3.4.3 Phenyl-substituted ketones studied in this work.	50
Figure 3.4.4 Calculation of the dispersion interaction in methyl benzyl ketone, ethyl benzyl ketone, and dibenzyl ketone with help of the well-balanced reactions.	52
Figure 3.4.5 Calculation of the dispersion interaction in 4-phenyl-2-butanone and 1,3-diphenyl-1-propanone with help of the well-balanced reactions.	53
Figure 3.4.6 Calculation of the dispersion interaction in phenyl-substituted amines with help of the well-balanced reactions.	54
Figure 3.4.7 3D-models of structures of 1,3-diphenyl-propan, diphenyl carbonate, and 1,3-diphenyl-2-propanone	56
Figure 4.1.1 Methoxy-acetophenones studied in this work	58
Figure 4.1.2 Mono-substituted benzophenones studied in this work.	58

Figure 4.1.3 Poly-substituted benzophenones studied in this work.....	58
Figure 4.3.1 Stable conformers for 2-hydroxy-benzophenone as calculated with the G4.....	72
Figure 4.3.2 Graphical presentation of the idea of a “centerpiece” group-contribution approach	74
Figure 4.3.3 Quantification of the enthalpic contributions for the hydroxy-, carbonyl-, and methoxy substituents.....	74
Figure 4.3.4 Construction of a strain-free theoretical framework for 3-methoxy-acetophenone and 2,4-dihydroxy-benzophenone	75
Figure 4.3.5 Example for a quantification of the 1,3-non-nearest neighbour interactions of the carbonyl-group with the CH ₃ O substituent in the 3-methoxy-acetophenone.	76
Figure 4.3.6 Example of calculation of the enthalpy of vaporization of the 2-methyl-benzophenone using the “centerpiece” approach with the numerical values from Table 4.3.14.....	77
Figure 4.3.7 Example of calculation of the enthalpy of vaporization of the 2-hydroxy-benzophenone using the “centerpiece” approach with the numerical values from Table 4.3.14.....	78
Figure 4.3.8 Example of calculation of the enthalpy of vaporization of the 2,4-dihydroxy-benzophenone using the “centerpiece” approach with the numerical values from Table 4.3.14.....	79
Figure 4.3.9 Example of calculation of the enthalpy of formation of the 2-hydroxy-benzophenone using the “centerpiece” approach with the numerical values from Table 4.3.14.....	80
Figure 4.3.10 Example of calculation of the enthalpy of formation of the 2-hydroxy-4-methoxy-benzophenone using the “centerpiece” approach with the numerical values from Table 4.3.14.....	81
Figure 4.3.11 Agglomeration of the enthalpic contributions for the nearest and non-nearest neighbour interactions in the three substituted benzene derivatives.	82
Figure 4.3.12 Isomeric 2,4-dimethoxy-acetophenone, 2,5-dimethoxy-acetophenone, 2,6-dimethoxy-acetophenone, and 3,4-dimethoxy-acetophenone: agglomeration of the enthalpic contributions for the nearest and non-nearest neighbour interactions in the three substituted benzene derivatives.	82
Figure 5.1.1 Structures of cations and anions: tetra-alkyl-ammonium cation based ILs and tetra-alkyl-phosphonium cation.	84
Figure 5.1.2 Vaporization enthalpies chain-length dependences of molecular and ionic compounds.	85
Figure 5.1.3 . Differences between vaporization enthalpy values for the <i>ionic</i> and <i>molecular</i> compounds	86
Figure 5.1.4 (a) The chain length dependence of the vaporization enthalpy for n-alkanes	88
Figure 5.1.5 (a) The chain length dependence of the vaporization enthalpy for n-alkanes	90
Figure 5.1.6 The gas phase dispersive interaction between alkyl chains for ammonium-based ILs with [NTf ₂] ⁻ anion, as derived from experimental vaporization enthalpies	91

Figure 5.1.7 Illustration of the long-chained tetra-alkylammonium based IL $[N_{1888}][NTf_2]$ with the structurally predestinated dispersion interactions between the chain segments.	92
Figure 5.2.1 The correlation gas phase dispersive interaction between alkyl chains for ammonium-based ILs with $[NTf_2]^-$ anion calculated at D3(BJ) corrected B3LYP level of theory and results of experimental evaluation with “step by step” method.....	93
Figure 5.3.1 Structures of imidazolium-based ILs 1-alkyl-3-methylimidazolium hexafluorophosphate $[C_nmim][PF_6]$ family with $n = 2, 4, 6, 8, 10, 12, 14, 16,$ and 18	94
Figure 5.3.2 The alkyl chain length dependence of the enthalpy of vaporization for $[C_nmim][PF_6]$ (left) and for $[C_nmim][NTf_2]$ from [4] (right).....	95
Figure 5.3.3 Visualizations of the nano-structuring in $[C_nmim][PF_6]$ series from MD simulations.	96
Figure 5.3.4 Chain-length dependence of dispersion forces, E_{disp-D} , in $[C_nmim][PF_6]$ series at 298.15 K	98
Figure 6.1.1 Transpiration apparatus scheme (left) and a photo of a saturator (right).	99
Figure 6.2.1 Knudsen apparatus scheme.....	104
Figure 6.2.2 Photo of Knudsen apparatus	104
Figure 6.2.3 Scheme of the Knudsen cell with an effusing substance.....	106
Figure 6.2.4 5x scaled microscopic image of the 2 mm membrane.....	106
Figure 6.2.5 Photos of the Knudsen cell.	106
Figure 6.2.6 Results of Knudsen effusion test experiments with benzoic acid	108
Figure 6.2.7 Deviation plot of experimental values from fitting equation	109

1. Introduction

Dispersion is the superordinate concept for attractive forces that act between separate molecules or molecule fragments even without charges or permanent electrical moments. These interactions are generally responsible for the thermodynamic stability and the structuring of the *liquid* and *solid* state. Dispersion forces between molecules are much weaker than the covalent bonds within molecules. For this reason, it is not easy to give a quantitative interpretation of dispersion since the size of the attraction varies considerably with the size of interacting molecules and their shape. Recent advances in quantum chemical methods supported the understanding the phenomenon of "dispersion". With the dispersion-corrected DFT methods, both the short to medium and long-range dispersion components can now be identified for the *gas-phase* species [1]. Most studies on the relevance of dispersion forces were carried out in the *gas phase*. At the same time, most of the practical chemistry takes place in the *liquid phase* or in solution. Following this, a thorough understanding and quantification of the dispersion forces in the *liquid phase* is of practical importance and should also help to elucidate aspects of condensed matter by analysing the additivity vs. cooperativity when going from the separated molecules to the bulk phase.

Numerous remarkable examples of the importance of dispersion forces in the gaseous, liquid, and crystal phase can be found in the recent literature. Admittedly, the hexaphenylethane is unstable, and this phenomenon traditionally attributed to steric repulsion between the six phenyl rings. However, adding 12 bulky tert-butyl groups, one to each of the 12 meta positions, gives a stable ethane derivative (see Figure 1.1).

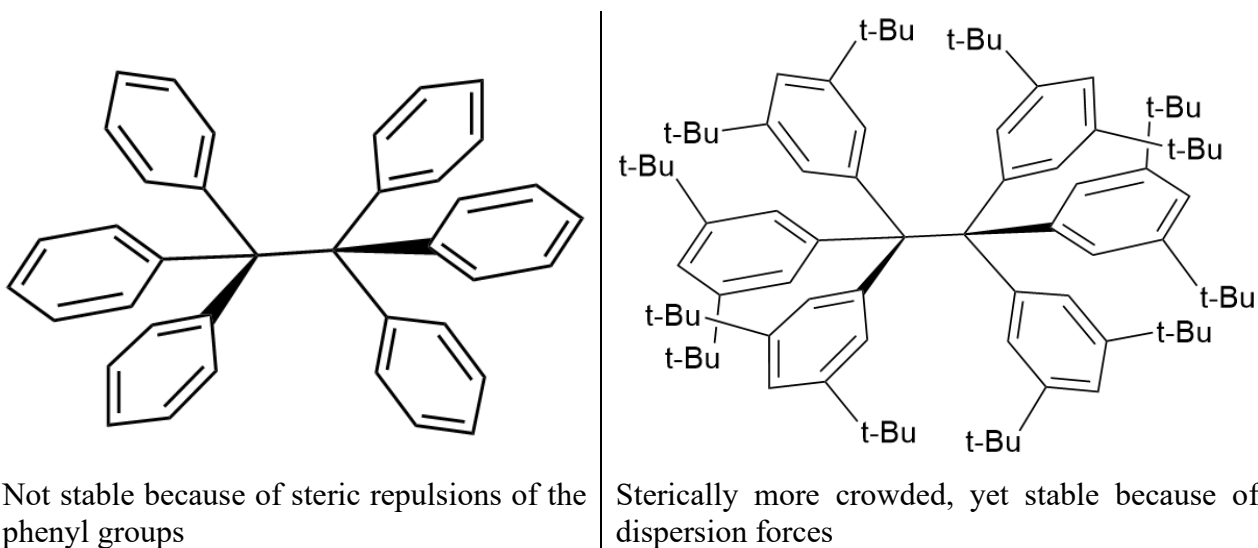


Figure 1.1 Crowding destabilizes experimentally unknown hexaphenylethane, while the more crowded all-meta-tert-butylhexaphenylethane can be crystallized [2]

This unexpected stabilization can be explained in terms of the attractive dispersive forces between the t-butyl groups, which outweigh the otherwise unfavourable interactions of the phenyl units [2]. Lüttschwager *et al.*[3] have shown that at low temperatures, linear alkanes C_nH_{2n+2} of moderate length are known to prefer a fully extended (all-trans) conformation, in analogy to the simplest case of butane. Owing to weak *dispersion interactions* between chain segments, this cannot hold up to $n \rightarrow \infty$. Only quite moderate amount of energy is required to bend an extended chain into a hairpin structure by trans-gauche isomerisation (with reaction enthalpy of about $2 \text{ kJ}\cdot\text{mol}^{-1}$) [3]. The last globally stable extended non-folded alkane was predicted to be with $n=17$ according to spectroscopic study at 100–150 K combined with quantum chemical calculations [3].

Obviously, at temperatures above 100-150 K, the smearing of structural transitions occurs, which leads to an equilibrium mixture of trans-gauche conformations. At the reference temperature $T = 298 \text{ K}$, however, this equilibrium shifts completely to the all-trans conformations and it energetically manifested in the constant contribution of the methylene-group, $\Delta_1^{\text{g}}H_{\text{m}}^{\circ}(\text{CH}_2) = 4.95 \pm 0.12 \text{ kJ}\cdot\text{mol}^{-1}$ [4] to the vaporization enthalpy in the homologous series of *n*-alkanes.

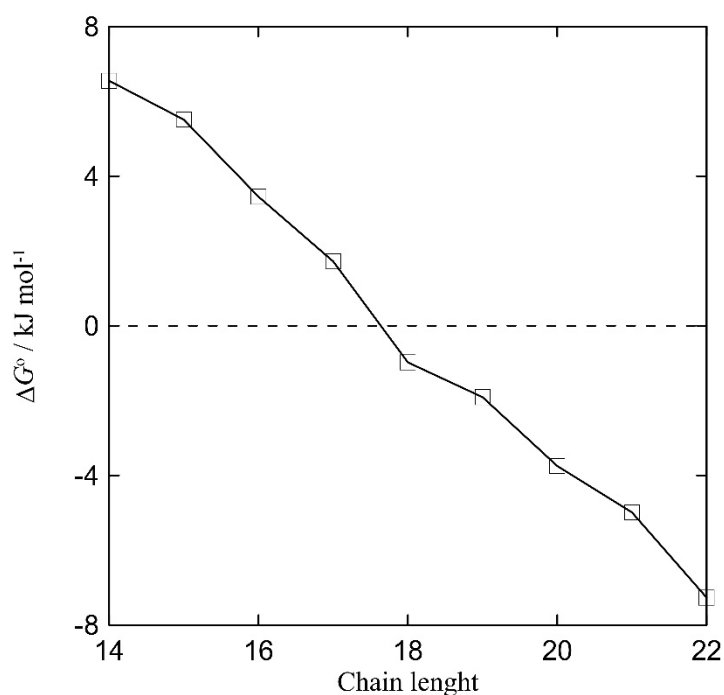


Figure 1.2 Calculated Gibbs energy difference at 100 K $\Delta G^{\circ} = G^{\circ}_{\text{hairpin}} - G^{\circ}_{\text{all-trans}}$ versus chain length data from [3]

A remarkably linear dependence of the chain lengths of the enthalpy of vaporization for *n*-alkanes is given in Table 1.1 and shown in Figure 1.3.

Table 1.1 Contributions of the CH₂ group to the enthalpy of vaporization $\Delta_1^g H_m^o$ at 298 K for the various homologous series of molecular and ionic compounds [4]

Homologous series	$\Delta_1^g H_m^o(\text{CH}_2)$, kJ·mol ⁻¹
C _n H _{2n+2}	4.95±0.12
C _n H _{2n+1} CN	4.44±0.12
C _n H _{2n+1} OH	4.71±0.08
C _n H _{2n+1} C ₆ H ₅	4.48±0.04
CH ₂ =CH-C _n H _{2n+1}	4.97±0.21
HS-C _n H _{2n+1}	4.76±0.18
Cl-C _n H _{2n+1}	4.85±0.10
Br-C _n H _{2n+1}	4.80±0.10
C _n H _{2n+1} CO ₂ -CH ₃	5.03±0.08
[C _n mim][NTf ₂]	3.89±0.20

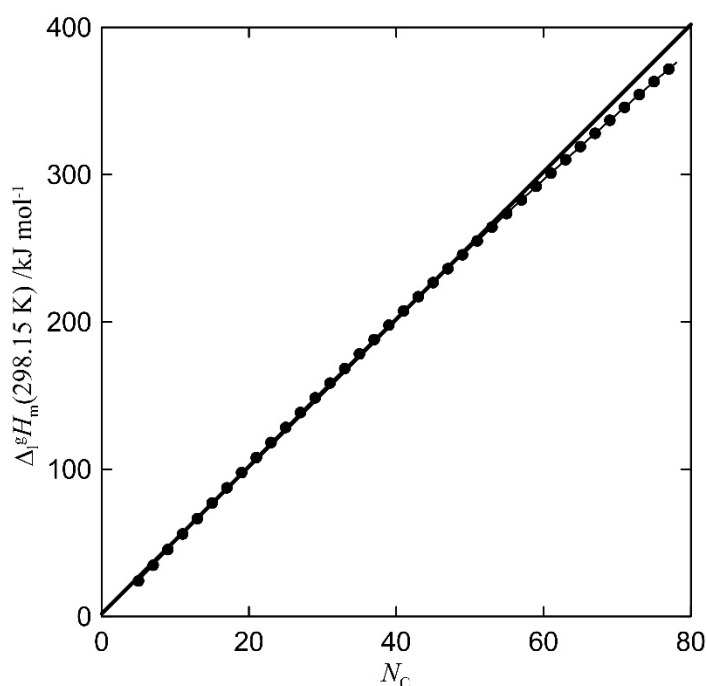


Figure 1.3 Vaporization enthalpies of *n*-alkanes C_nH_{2n+2} at 298 K from pentane to hexaheptacontane as a function of the number of carbon atoms, *N_C*, in the alkyl chain, data from [5].

However, some curvature is observed when the number of carbon atoms exceeds sixty [5]. This observation assumes that the dispersion forces in the long-chain *n*-alkanes are constant and that some additional contributions only occur when the chain is enlarged beyond sixty atoms (see deviation from the linear trend in Figure 1.3). Let us note that thermochemical properties such as enthalpy of vaporization seem to be a good indicator of dispersion forces.

What happens when we introduce a functional group (OH, Cl, Br, *etc.*) into the long alkyl chain? We could hardly expect a change in the $\Delta_1^g H_m^o(\text{CH}_2)$ contribution, since the long alkyl chain must dominate the possible influence of the single functional group. Contrary to this expectation, most of

the homologous series show (CH₂) group contributions to the enthalpy of vaporization that differ those inherent for pure n-alkane (see Table 1.1). Significantly lower (CH₂)-contributions were observed for n-alkylbenzenes and for n-alkyl-nitriles, which are known to have strong dipole-dipole and π - π interactions. The decrease could be a result of dispersion interactions that occur in these *molecular liquids*. What about *ionic liquids*? As it can be seen from Table 1.1, the lowest (CH₂)-contribution of 3.89 kJ·mol⁻¹ [4] was observed for the archetypal series of ionic liquids [C_nmim][NTf₂]. The intensive interplay of dispersion and Coulomb forces specific for ionic liquids probably also have a consequence for the reduction of the $\Delta_1^{\text{g}}H_m^{\text{o}}(\text{CH}_2)$ contribution for the *ionic liquids*.

Dispersion interactions are already successfully derived from quantum chemical and spectroscopic methods [6,7]. Complementary to those well-established procedures we have developed thermodynamic tools based on the standard molar enthalpy of vaporization the $\Delta_1^{\text{g}}H_m^{\text{o}}$ and the standard molar enthalpy of formation $\Delta_f H_m^{\text{o}}$. The gas-phase standard molar enthalpy of formation, $\Delta_f H_m^{\text{o}}(\text{g})$, of interest is the comprehensive experimental thermochemical property that includes all enthalpies of phase transitions (sublimation, vaporization, and fusion) in combination with the condensed phase enthalpy of formation. The enthalpy of vaporization is related to the enthalpy of formation via the following basic thermodynamic equation (conventionally referenced to $T = 298 \text{ K}$):

$$\Delta_f H_m^{\text{o}}(\text{g}, 298 \text{ K}) = \Delta_1^{\text{g}} H_m^{\text{o}}(298 \text{ K}) + \Delta_f H_m^{\text{o}}(\text{liq}, 298 \text{ K}) \quad (1.1)$$

where the liquid-phase standard molar enthalpies, $\Delta_f H_m^{\text{o}}(\text{liq}, 298 \text{ K})$, are usually measured by the high-precision combustion or reaction calorimetry. The enthalpies of vaporisation, $\Delta_1^{\text{g}} H_m^{\text{o}}(298 \text{ K})$, are mainly measured directly by calorimetry or derived from vapor pressure temperature dependences indirectly. The resulting *experimental* values of $\Delta_f H_m^{\text{o}}(\text{g}, 298 \text{ K})$, derived according to Eq. (1.1) can also be calculated using high-level quantum chemical methods (G4, CBS-QB3, *etc.*) to prove the consistency of the *experimental* and *theoretical* results.

Loosely speaking, the gas-phase enthalpy of formation, $\Delta_f H_m^{\text{o}}(\text{g}, 298 \text{ K})$, represents the total amount of energy that is stored in an isolated molecule that hangs in the ideal gas phase. This energy consists of elements and their bonds, as well as intramolecular through space interactions of substituents. The latter interactions could also include the dispersion forces as exemplarily shown for all-meta-tert-butylhexaphenylethane in Figure 1.1. Admittedly, separating the dispersive forces from other available interactions is a challenging but possible task, as discussed in this work.

According to the textbook definition, the vaporization enthalpy, $\Delta_1^{\text{g}} H_m^{\text{o}}(298 \text{ K})$, is an amount of energy required to disrupt “*intermolecular interactions*” in the liquid phase and to transfer 1 mole of molecules into the gas phase. Obviously, the “*intermolecular interactions*” in the liquid phase also

include not only dispersion forces. Therefore, the separation of the dispersion from Van der Waals forces, hydrogen bonding, Coulomb interactions, *etc.* requires well-chosen systems of structurally similar molecules [8] to quantify the amount of dispersion contributions through differences in the properties. As can be seen in Table 1.1, the variation in the contribution for the methylene-group, $\Delta_1^g H_m^o(\text{CH}_2)$, is apparently small (within 1 $\text{kJ}\cdot\text{mol}^{-1}$). However, it is important to note that these contributions were determined very precisely ($\pm 0.1 - 0.2 \text{ kJ}\cdot\text{mol}^{-1}$). The observed differences are therefore meaningful, and experimental studies of the enthalpy of vaporization appear to be a valuable tool for the reliable quantification of the dispersion forces in the *liquid* and *gas* phases.

In the past decade, treating dispersion interactions in the gas phase with the DFT-D3 [10] has received a standard status. A comparison of the energies calculated with the methods B3LYP and B3LYP-D3 (BJ) provides an estimate of the stabilization due to the dispersion $E_{\text{disp-D3}} = \Delta E(\text{B3LYP-D3(BJ)}) - \Delta E(\text{B3LYP})$. The $E_{\text{disp-D3}}$ correction is not exactly equal to the dispersion stabilization, since the correction depends on the functional used, but gives a reasonable level of the magnitude of this interaction. In this work, all calculations were carried out with def2-TZVPP basis set [10]. Further details can be found elsewhere [8,11]

In our laboratory, we systematically used a bunch of experimental thermodynamic methods (combustion calorimetry, solution calorimetry, differential scanning calorimetry, thermogravimetry, vapour pressure determination with combined Quartz Crystal Microbalance, Knudsen method, transpiration technique) to measure and validate the thermodynamic properties required to quantify the dispersion forces in molecular and ionic systems. The aim of the present work is to demonstrate the quantification of the intramolecular dispersion interaction in terms of $\Delta_f H_m^o(\text{g})$ through systematic comprehensive investigations of the thermodynamic (energetic) properties in the gas and the condensed (liquid/crystal) phase. The complementary DFT-D3 calculations should contribute to an understanding of the derived quantities. The enthalpies of vaporization are considered to be an independent method of assessing dispersion forces in terms of enthalpic contributions to $\Delta_1^g H_m^o$. The focus of this work is on demonstrating the application of thermodynamic tools to quantify dispersion forces in both *molecular* and *ionic* systems.

2. Quantification of dispersion forces with the aid of enthalpy of vaporization

2.1. Dispersion forces in amines

2.1.1. Dispersion forces in symmetric trialkylamines

One of the most unexpected opportunities to recognise importance of dispersion forces on the bulk thermodynamic properties came from the studying the homologous series of symmetrical trialkylamines (C_nH_{2n+1})₃N given in Figure 2.1.1

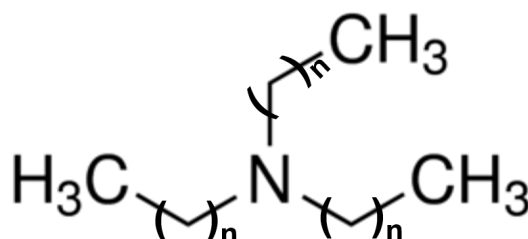


Figure 2.1.1 Series of symmetrical tri-alkyl-amines with $n = 3-8$ studied in this work.

Our results on experimental vaporization enthalpies, $\Delta_1^g H_m^o(298\text{ K})$, of tri-alkyl-amines are given in Table A.1.

The compilation of molar heat capacities $C_{p,m}^o(\text{cr or liq})$ and heat capacity differences $\Delta_{\text{cr,l}}^g C_{p,m}^o$ required for the adjustment of vaporization enthalpies to the reference temperature $T = 298.15\text{ K}$ is given in Table 2.1.1

Table 2.1.1 Compilation of auxiliary data on Kovats's indices, J_x , normal boiling points, T_b , molar heat capacities $C_{p,m}^o(\text{cr or liq})$ and heat capacity differences $\Delta_{\text{cr,l}}^g C_{p,m}^o$ at $T = 298.15\text{ K}$

Compounds	J_x^a	T_b^b K	$C_{p,m}^o(\text{liq})^c$ $\text{J}\cdot\text{K}^{-1}\cdot\text{mol}^{-1}$	$-\Delta_1^g C_{p,m}^o^d$ $\text{J}\cdot\text{K}^{-1}\cdot\text{mol}^{-1}$
tri-ethylamine	680	362	190.8	36±3
tri-n-propyl-amine	937	430	286.5	55±6
tri-n-butyl-amine	1192	485	382.2	78±1
tri-n-pentyl-amine	1420	516	477.9	83±1
tri-n-hexyl-amine	1740	564	573.6	89±1
tri-n-heptyl-amine	2012	603	669.3	99±1
tri-n-octyl-amine	2297	639	750.8 [12]	120±3
tri-phenyl-amine ^e			363.3	105 ^f
benzylamine			207.2 [13]	64.5 ^f
dibenzylamine			351.9	102 ^f

^a Kovats's indices, J_x , on standard non-polar column from [14].

^b Normal boiling temperatures from [15].

^c Calculated by the group-contribution procedure developed by Chickos *et al.* [16].

^d Calculated according to the Clarke and Glew equation [17].

^e The heat capacity $C_{p,m}^o(\text{cr}) = 325.9\text{ J}\cdot\text{K}^{-1}\cdot\text{mol}^{-1}$ and $\Delta_{\text{cr,l}}^g C_{p,m}^o = 49.6\text{ J}\cdot\text{K}^{-1}\cdot\text{mol}^{-1}$ were calculated according to the procedure developed by Acree and Chickos [18].

^f Calculated according to the procedure developed by Acree and Chickos [18].

What is unusual about the series of the symmetrical trialkylamines? It is well established, that the vaporization enthalpy and normal boiling temperature are linearly related within the homologous series [19,20]. To our surprise, the $\Delta_1^g H_m^o(298.15 \text{ K})$ -values for the trialkylamines depend exponentially on the T_b -values (see Figure 2.1.2, left). Also exponentially depend the $\Delta_1^g H_m^o(298.15 \text{ K})$ -values on the Kovats's indices, J_x , as it can be seen in Figure 2.1.2, right.

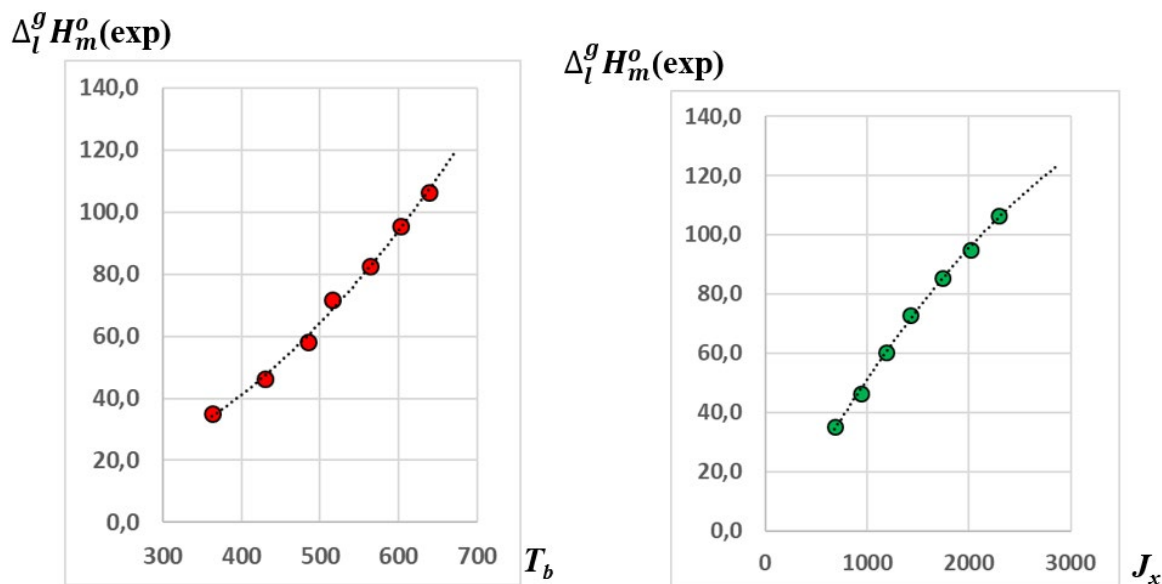


Figure 2.1.2 Correlation of the vaporization enthalpies, $\Delta_1^g H_m^o(298.15 \text{ K})$, of the tri-alkyl-amines with the normal boiling temperatures T_b (left) and with the Kovats's indices J_x (right).

The most plausible explanation for the observed phenomena is to invoke additional dispersion forces in the long-chain molecules. If these attractive forces are specific to the liquid phase, they must be responsible for significant interdigitation and interlocking of alkyl chains. In this case, however, the energy required to extract the interlocking trialkylamine from the well-structured liquid into the gas phase should be higher and the appropriate enthalpy of vaporization should increase. Therefore, the only way to explain the relative decrease in the enthalpy of vaporization is to assume that the dispersion forces are partly entrained to the gas phase. One of the possible structures of trioctylamine that could justify this assumption is shown in Figure 2.1.3, where the significant interlocking of alkyl chains in the gas phase due to dispersion forces is obvious. Our preliminary quantum-chemical calculations supported the existence of such dispersion-stabilized conformers in the gas phase.

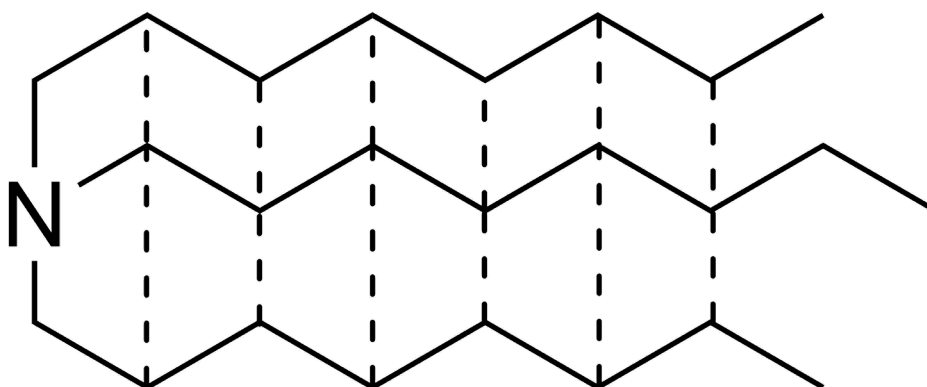


Figure 2.1.3 One of the possible structures of trioctylamine (C_8H_{19})₃N.

How can the amount of dispersion forces in trialkylamines be quantified? One possibility is to compare the experimental enthalpies of vaporization measured in this work (see Table A.1) with the values estimated by the group additivity (GA). Indeed, the GA-estimate of the vaporization enthalpy is collected from reasonably small contributions, with all “non-additive” interactions being deliberately excluded during the parametrization. Such a comparison enables the recognition of special effects that are inherent in the considered thermodynamic function (vaporization enthalpy in this case). The only four increments are generally required to predict the enthalpies of vaporization for this family of trialkylamines. They are $CH_3[C] = CH_3[N] = 5.65 \text{ kJ}\cdot\text{mol}^{-1}$ and $CH_2[2C] = 4.98 \text{ kJ}\cdot\text{mol}^{-1}$ for hydrocarbons and the increments for amines $CH_2[N,C] = 2.45 \text{ kJ}\cdot\text{mol}^{-1}$ and $N[3C] = 5.05 \text{ kJ}\cdot\text{mol}^{-1}$ are given in Table 2.1.2. An example of a typical calculations: the sum of increments for tri-*n*-butylamine, $\Sigma(\text{increments}) = 59.2 \text{ kJ}\cdot\text{mol}^{-1}$, was calculated as the sum of the following increments: $(3\times CH_3[C] + 6\times CH_2[N,C] + N[3C])$. Based on our experiences [21], the vaporization enthalpy is highly additive thermodynamic property. Hence, as usual [22,23], we expected reasonable agreement between the experimental $\Delta_1^g H_m^o(298 \text{ K})$ -values and the sum of appropriate increments, referred to as $\Sigma \Gamma_i(\Delta_1^g H_m^o)$. As it can be seen in Table 2.1.3, the differences E_{disp} between experimental and additive values systematically increase with the growing chains length, so that this discrepancy for trioctylamine is an impressive $-12.6 \text{ kJ}\cdot\text{mol}^{-1}$ reached.

Table 2.1.2 Group-additivity values Γ_i for calculation of vaporization enthalpies, $\Delta_1^g H_m^o$, at 298.15 K in $\text{kJ}\cdot\text{mol}^{-1}$. Numerical values were taken from Ducros *et al.* [20,21].

	$\Gamma_i(\Delta_1^g H_m^o)$		$\Gamma_i(\Delta_1^g H_m^o)$		$\Gamma_i(\Delta_1^g H_m^o)$
Alkanes		Amines		Aromatics^a	
$CH_3[C]$	5.65	$CH_2[N,C]$	2.45	$C_b[H]$	5.65
$CH_2[2C]$	4.98	$CH[N,2C]$	-1.84	$C_b[2C_b,C]$	4.10
$CH[3C]$	3.01	$C[N,3C]$	-5.9	$CH_2[C_b,C]$	4.30
$C[4C]$	0.0	$NH_2[C]$	18.6	$CH[C_b,2C]$	0.96
		$NH[2C]$	14.1	$C[C_b,3C]$	0.0
		$N[3C]$	5.05	$C_b[2C_b,N]$	8.50
				$CH_2[C_b,N]$	5.80

^a Carbone atom in benzene ring is designated as C_b .

^b Derived from vaporization enthalpy of benzylamine $\Delta_1^g H_m^o(298\text{ K}) = 52.3 \pm 0.8\text{ kJ}\cdot\text{mol}^{-1}$ [15].

Table 2.1.3 Experimental vaporization enthalpies, $\Delta_1^g H_m^o(298\text{ K})$, of tri-alkyl-amines (in $\text{kJ}\cdot\text{mol}^{-1}$), the sum of constituting increments ($\Sigma I_i(\Delta_1^g H_m^o)$) and their deviations from additivity (E_{disp}), attributed to the dispersion forces

Trialkyl amine	$\Delta_1^g H_m^o(\text{exp})^a$	$\Sigma I_i(\Delta_1^g H_m^o)^b$	E_{disp}^c
(C ₃ H ₉) ₃ N	46.2±0.2 [16]	44.3	1.9
(C ₄ H ₁₁) ₃ N	58.3±0.6	59.2	-0.9
(C ₅ H ₁₃) ₃ N	71.6±0.5	74.2	-2.6
(C ₆ H ₁₅) ₃ N	82.7±0.8	89.1	-6.4
(C ₇ H ₁₇) ₃ N	95.7±0.8	104.1	-8.4
(C ₈ H ₁₉) ₃ N	106.5±1.0	119.1	-12.6

^a From Table A.1.

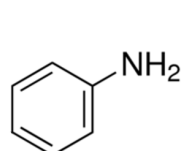
^b Increments are given in Table 2.1.2.

^c Difference between column 2 and 3 in this table.

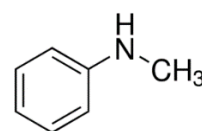
Therefore, the significant decrease in the enthalpies of vaporization of trialkylamines can be attributed to the dispersion interaction between the long chains bound to the nitrogen. This finding is also supported by similar observation for the long-chained alkanes shown in Figure 1.3. Indeed, the decrease of vaporization enthalpies when the number of carbon atoms exceeds sixty also assumes that the straight chain becomes balled due to the dispersion forces between interlocked long-chains in the gas phase. It is quite obvious that the differences, E_{disp} , between the experimental and additive values do not represent the full energy of the dispersive forces between alkyl chains in such a star-like molecules as the trialkylamines. Nevertheless, the E_{disp} values can be considered as a reliable measure of the dispersion forces, at least within this particular homologous series.

2.1.2. Dispersion forces in phenyl-substituted amines

The molecular structures of diphenylamine, triphenylamine, and tribenzylamines are also anticipated to have a significant amount of dispersion interactions among the phenyl-rings around the central N-atom. The series of phenyl-substituted amines selected for the quantification of the dispersion forces is given in Figure 2.1.4



aniline



N-methyl-aniline

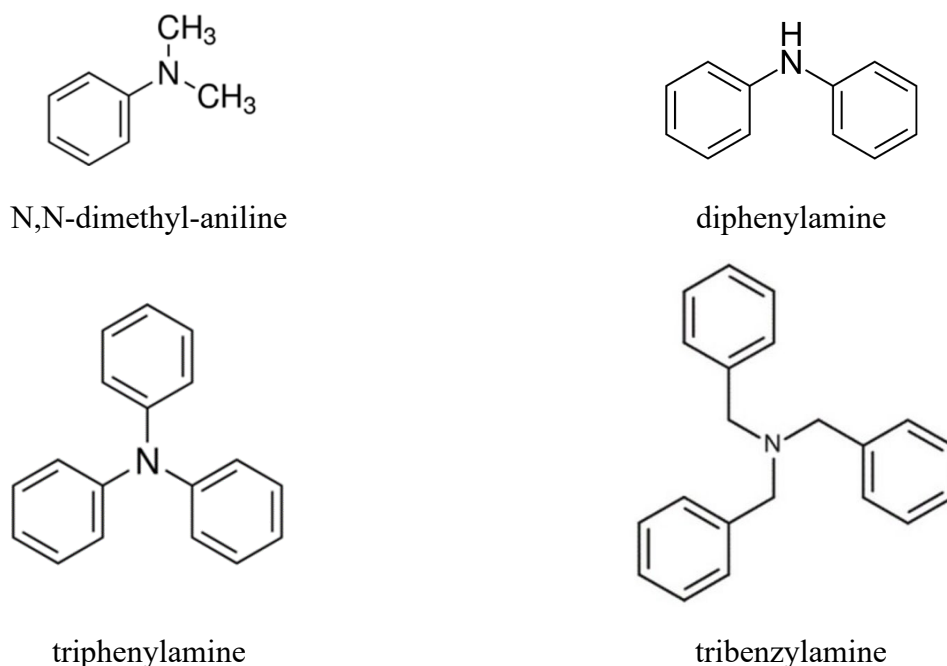


Figure 2.1.4 Series of phenyl substituted amines studied in this work

Results of Knudsen effusion study of triphenylamine are given in Table 2.1.3. It has turned out, that the experimental sublimation and vaporization enthalpies of tri-phenyl-amine reported in the literature are irrationally close to one another (see Table A.2). This observation is very strange, because the triphenylamine is the high-melting compound and the fusion enthalpy $\Delta_{\text{cr}}^{\text{l}}H_{\text{m}}^{\circ}$ cannot be negligible (see Table 2.1.4) if we want to reconcile $\Delta_{\text{cr}}^{\text{g}}H_{\text{m}}^{\circ}$ and $\Delta_{\text{l}}^{\text{g}}H_{\text{m}}^{\circ}$ values for this compound.

Table 2.1.4 Compilation of enthalpies of sublimation/vaporization $\Delta_{\text{cr,l}}^{\text{g}}H_{\text{m}}^{\circ}$ of phenyl substituted amines

Compound	M ^a	<i>T</i> - range K	$\Delta_{\text{cr,l}}^{\text{g}}H_{\text{m}}^{\circ}(T_{\text{av}})$	$\Delta_{\text{cr,l}}^{\text{g}}H_{\text{m}}^{\circ}(298.15 \text{ K})^{\text{b}}$	Ref.
			kJ·mol ⁻¹	kJ·mol ⁻¹	
tri-phenyl-amine (cr)	BG	322-373	87.8±1.3	(91.5±1.4)	[24]
	K	323.3-374.9	118.8±3.2	121.3±3.3	Table A.2
tri-phenyl-amine (liq)	IT	473-573	66.8±1.4	(90.1±2.0)	[25]
	CGC	298		(90.2±1.2)	[26]
	<i>T</i> _{fus}			102.0±3.7	Table 2.1.5
	<i>J</i> _x			102.1±2.0	Table 2.1.6
				102.1±1.8 ^c	average
tri-benzyl-amine (liq)	CGC	298		(92.4±1.4)	[27]
	<i>J</i> _x			112.0±2.0	Table 2.1.6

^a Techniques: BG = Bourdon gauge; K = Knudsen effusion method; IT = isoteniscope; CGC = correlation gas-chromatography; *J*_x – from correlation of experimental vaporization enthalpies with Kovat's indices (see text); *T*_{fus} – derived from experimental data according as the difference $\Delta_{\text{cr}}^{\text{g}}H_{\text{m}}^{\circ} - \Delta_{\text{cr}}^{\text{l}}H_{\text{m}}^{\circ}$ (see Table 2.1.5).

^b Uncertainties of the vaporization and sublimation enthalpies is expressed as is the expanded uncertainty (0.95 level of confidence). They include uncertainties from the experimental conditions and the fitting equation, vapour pressures, and uncertainties from adjustment of sublimation/vaporization enthalpies to the reference temperature *T* = 298.15 K [28,29].

^c Weighted mean value (the uncertainty was taken as the weighing factor). Uncertainty of the sublimation/vaporization enthalpy is expressed as the expanded uncertainty (0.95 level of confidence, *k* = 2). Values in brackets were excluded by the averaging. Value highlighted in bold were recommended for thermochemical calculations.

Table 2.1.5 Phase transitions thermodynamics of tri-phenyl-amine (in kJ·mol⁻¹)^a

Compounds	T_{fus}, K	$\Delta_{\text{cr}}^{\text{l}}H_{\text{m}}^{\text{o}}$	$\Delta_{\text{cr}}^{\text{l}}H_{\text{m}}^{\text{o} \text{ b}}$	$\Delta_{\text{cr}}^{\text{g}}H_{\text{m}}^{\text{o} \text{ c}}$	$\Delta_{\text{l}}^{\text{g}}H_{\text{m}}^{\text{o} \text{ d}}$
		at T_{fus}		298.15 K	
tri-phenylamine [30]	400.2±0.5	24.9±0.4	19.3±1.7	121.3±3.3	102.0±3.7

^a Uncertainties are presented as expanded uncertainties (0.95 level of confidence with k=2).

^b The experimental enthalpies of fusion $\Delta_{\text{cr}}^{\text{l}}H_{\text{m}}^{\text{o}}$ measured at T_{fus} were adjusted to 298.15 K with help of the equation [18]:
 $\Delta_{\text{cr}}^{\text{l}}H_{\text{m}}^{\text{o}}(298.15 \text{ K})/(\text{J}\cdot\text{mol}^{-1}) = \Delta_{\text{cr}}^{\text{l}}H_{\text{m}}^{\text{o}}(T_{\text{fus}}/\text{K}) - (\Delta_{\text{cr}}^{\text{g}}C_{p,m}^{\text{o}} - \Delta_{\text{l}}^{\text{g}}C_{p,m}^{\text{o}}) \times [(T_{\text{fus}}/\text{K}) - 298.15 \text{ K}]$

where $\Delta_{\text{cr}}^{\text{g}}C_{p,m}^{\text{o}}$ and $\Delta_{\text{l}}^{\text{g}}C_{p,m}^{\text{o}}$ were taken from Table 2.1.1. Uncertainties in the temperature adjustment of fusion enthalpies from T_{fus} to the reference temperature are estimated to account with 30 % to the total adjustment [18].

^c Experimental values measured by the Knudsen method (see Table A.3).

^d Calculated as the difference between column 5 and 4 in this table.

The significant disarray of phase transition thermodynamics of triphenylamines has prompted an additional validation of our new results. A Correlation Gas-Chromatographic (CGC) method is conventionally used for validation of the experimental vaporization enthalpies [31,32]. This method is based on correlating the experimental $\Delta_{\text{l}}^{\text{g}}H_{\text{m}}^{\text{o}}(298.15 \text{ K})$ -values with their Kovats's indices [33]. The literature data available on the Kovats's retention indices, J_x , for aromatic amines and amino-substituted benzenes [34] were taken for correlation with the $\Delta_{\text{l}}^{\text{g}}H_{\text{m}}^{\text{o}}(298.15 \text{ K})$ -values collected in Table 2.1.6.

Table 2.1.6 Correlation of vaporization enthalpies, $\Delta_{\text{l}}^{\text{g}}H_{\text{m}}^{\text{o}}(298.15 \text{ K})$, of ortho-substituted benzenes with their Kovats's indices (J_x)^a

Compound	J_x ^b	$\Delta_{\text{l}}^{\text{g}}H_{\text{m}}^{\text{o}}(298.15 \text{ K})_{\text{exp}}$ kJ·mol ⁻¹	$\Delta_{\text{l}}^{\text{g}}H_{\text{m}}^{\text{o}}(298.15 \text{ K})_{\text{calc}^{\text{c}}}$ kJ·mol ⁻¹	Δ^{d} kJ·mol ⁻¹
N-Me-aniline	1035	55.0±0.2 [35]	55.5	-0.5
2-Me-aniline	1068	57.3±0.2 [36]	57.0	0.3
3-Me-aniline	1082	58.3±0.4 [36]	57.6	0.7
4-Me-aniline	1068	57.8±0.3 [36]	57.0	0.8
N-butylaniline	1300	65.5±0.5 [37]	67.6	-2.1
diphenylamine	1537	79.5±0.4 [38]	78.4	1.1
dibenzylamine	1698	85.8±1.0 [39]	85.8	0.0
tri-phenylamine	2055		102.1±2.0	
tribenzylamine	2271		112.0±2.0	

^a Uncertainty is given as expanded uncertainties (0.95 level of confidence with k=2).

^b Kovats's indices, J_x , on standard non-polar columns from [34].

^c Calculated using Eq. (6.3.1).

^d Difference between experimental and calculated by Eq.(6.3.1) values.

As it was anticipated, the selected $\Delta_{\text{l}}^{\text{g}}H_{\text{m}}^{\text{o}}(298.15 \text{ K})$ -values correlated linearly with J_x values for the structurally parent sets of substituted benzenes. Indeed, the following high quality linear correlation was obtained:

$$\Delta_{\text{l}}^{\text{g}}H_{\text{m}}^{\text{o}}(298.15 \text{ K}) / (\text{kJ}\cdot\text{mol}^{-1}) = 8.2 + 0.0457 \times J_x \quad \text{with } (R^2 = 0.9992) \quad (2.1.1)$$

The result for triphenylamine the $\Delta_1^g H_m^o(298.15 \text{ K}) = 102.1 \text{ kJ}\cdot\text{mol}^{-1}$ obtained from this correlation is in excellent agreement with those the $\Delta_1^g H_m^o(298.15 \text{ K}) = 102.0 \pm 3.7 \text{ kJ}\cdot\text{mol}^{-1}$ derived in Table 2.1.5. Such good agreement can be seen as additional validation of the experimental data measured in this work by using the Knudsen method (see Table A.2 and Table 2.1.5). Moreover, the vaporization enthalpy of the tribenzylamine $\Delta_1^g H_m^o(298.15 \text{ K}) = 112.0 \text{ kJ}\cdot\text{mol}^{-1}$ was calculated according to Eq. (6.3.1). Since the structure of tribenzylamine is parent to the triphenylamine, this value should be considered reliable. It can be seen from Table 2.1.6, that differences between experimental and calculated according to Eq. (6.3.1) values are mostly below $1 \text{ kJ}\cdot\text{mol}^{-1}$. Hence, the uncertainties of enthalpies of vaporization which are estimated from the correlation the $\Delta_1^g H_m^o(298.15 \text{ K}) - J_x$ are evaluated with $\pm 2.0 \text{ kJ}\cdot\text{mol}^{-1}$. The $\Delta_1^g H_m^o(298.15 \text{ K})$ -values for phenyl-substituted amines evaluated in Table 2.1.4 and Table 2.1.6 can be now used for discussion of the dispersion forces in these molecules.

Qualitatively, the constellation of phenyl rings in diphenylamine, triphenylamine and tribenzylamine enables the existence of the attractive interactions between the substituents (see Figure 2.1.5)

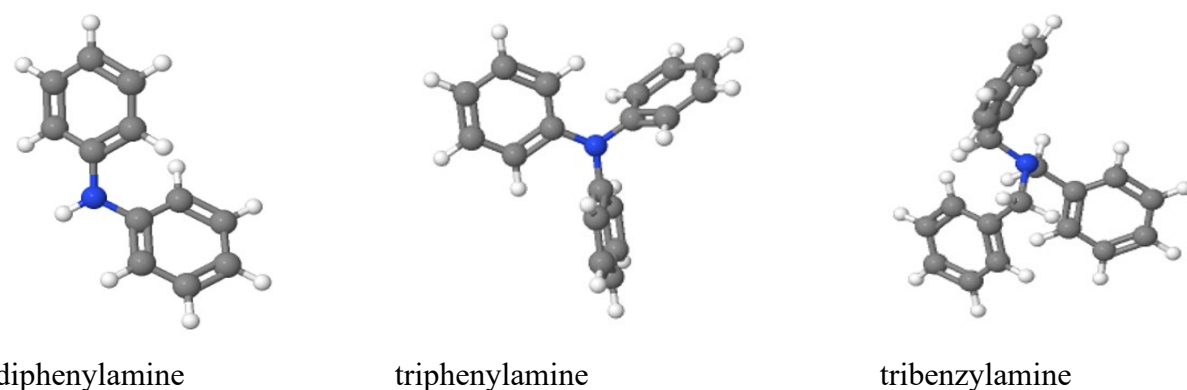


Figure 2.1.5 Structures of phenyl-substituted amines optimized by the DFT-D3 method

Quantitatively, the amount of dispersion interactions stored in the phenyl substituted amines was calculated using the group contributions shown in Table 2.1.2. The calculations were carried out in the same way as shown for trialkylamines (see 2.1.1). Results are given in Table 2.1.7.

Table 2.1.7 Experimental vaporization enthalpies, $\Delta_1^g H_m^o(298 \text{ K})$, of phenyl substituted amines, the sum of constituting increments ($\Sigma \Gamma_i(\Delta_1^g H_m^o)$), and their deviations from additivity (E_{disp}), attributed to the dispersion forces ((in $\text{kJ}\cdot\text{mol}^{-1}$)).

Phenyl amines	$\Delta_1^g H_m^o(\text{exp})^a$	$\Sigma \Gamma_i(\Delta_1^g H_m^o)^a$	E_{disp}^b
$(\text{C}_6\text{H}_5)\text{NH}_2$	55.8 ± 0.2 [40]	55.4	0.4
$(\text{C}_6\text{H}_5)\text{NH}(\text{CH}_3)$	55.0 ± 0.2 [35]	56.5	-1.5
$(\text{C}_6\text{H}_5)\text{N}(\text{CH}_3)_2$	54.0 ± 0.5 [37]	53.1	0.9
$(\text{C}_6\text{H}_5)_2\text{NH}$	79.5 ± 0.4 [39]	87.6	-8.1

$(\text{C}_6\text{H}_5)_3\text{N}$	102.1 ± 1.8^c	110.3	-8.2
$(\text{C}_6\text{H}_5\text{-CH}_2\text{-})_3\text{N}$	112.0 ± 2.0^c	119.5	-7.5

^a The increments are given in Table 2.1.2.

^b Difference between column 2 and 3 in this table.

^c From Table 2.1.4.

As it follows from this table, the dispersion interactions are not important for the methyl-substituted anilines, however in diphenyl- and triphenylamines the significant amount of the attractive forces between phenyl rings (at the level of $-8 \text{ kJ}\cdot\text{mol}^{-1}$) was calculated. The attractive interactions in tribenzylamine are slightly lower (at the level of $-7 \text{ kJ}\cdot\text{mol}^{-1}$) most probably due to the increased size and flexibility of this molecule.

To draw the final conclusion, the significant decrease in enthalpies of vaporization of trialkylamines and phenyl-substituted amines in general can be attributed to the dispersion interaction between the long chains attached to the nitrogen or to attractive interactions between the phenyl rings around the central nitrogen atom. The experimental enthalpies of vaporization in combination with the group additivity method serve as a suitable tool for quantifying such interactions.

2.2. Quantification of hydrogen bonding and dispersion forces in pharmaceuticals

2.2.1. Experimental thermochemical studies

Ibuprofen, flurbiprofen, indoprofen, ketoprofen, and naproxen (see Figure 2.2.1) are an interesting example of the subtle balance between different types of intermolecular interactions that occur in these pharmaceuticals.

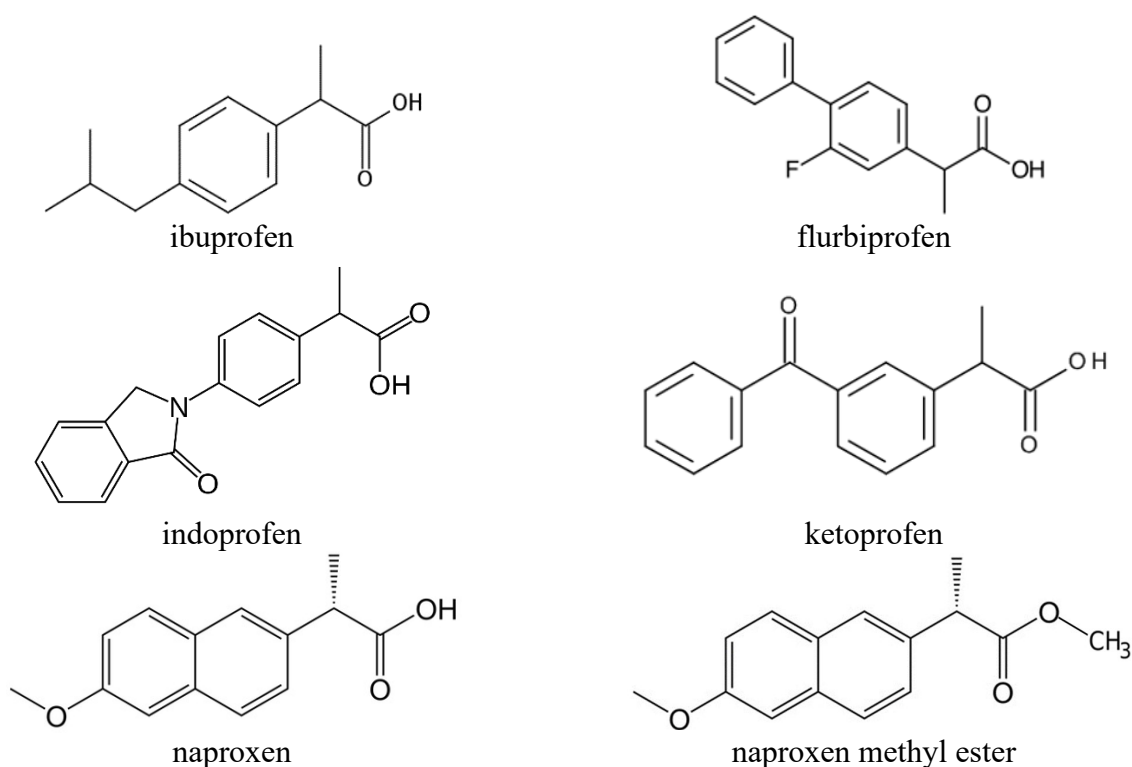


Figure 2.2.1 Structures of ibuprofen, flurbiprofen, indoprofen, ketoprofen, and naproxen

Unfortunately, the thermodynamic data on these compounds are very limited and contradicting [11]. New experimental results compiled in Table A.3 and Table 2.2.1 have significantly contributed to the current state knowledge.

Table 2.2.1 Phase transitions thermodynamics of profens studied in this work (in $\text{kJ}\cdot\text{mol}^{-1}$)^a

Compounds	T_{fus} , K	$\Delta_{\text{cr}}^1 H_m^{\circ}$ at T_{fus}	298.15 K		
			$\Delta_{\text{cr}}^1 H_m^{\circ}$ ^b	$\Delta_{\text{cr}}^g H_m^{\circ}$	$\Delta_1^g H_m^{\circ}$
1	2	3	5	6	7
(±)-ibuprofen	348.4±0.1	25.0±0.1 [41]	21.6±1.1	111.0±1.1 [11]	89.4±0.8[11]
flurbiprofen	387.1 ^c	28.6±0.1 ^c	22.6±1.3	136.1±0.9 ^c	113.5±1.6 ^d
(S)-naproxen methyl ester	365.3	29.3 ± 0.1 ^c	24.7±1.4	120.9±0.8	96.2±1.6
indoprofen	483.0 ^c	37.5±1.0 ^c	22.5±4.6	177.1±4.7 ^c	154.6±1.3 ^f
ketoprofen	367.2	28.3±0.3 [42,43]	23.0±1.6	149.6±1.9 ^c	126.6±1.0 ^f
(S)-naproxen [44]	429.2	31.6±0.1	24.1±2.3	129.1±0.9	105.0±2.5

^a Uncertainty is expressed as the standard uncertainty (0.683 level of confidence, $k = 1$)

^b The experimental enthalpies of fusion $\Delta_{\text{cr}}^1 H_m^{\circ}$ measured at T_{fus} were adjusted to 298.15 K with help of the equation [18]:
 $\Delta_{\text{cr}}^1 H_m^{\circ}(298.15 \text{ K})/(\text{J}\cdot\text{mol}^{-1}) = \Delta_{\text{cr}}^1 H_m^{\circ}(T_{\text{fus}}/\text{K}) - (\Delta_{\text{cr}}^g C_{p,m}^{\circ} - \Delta_1^g C_{p,m}^{\circ}) \times [(T_{\text{fus}}/\text{K}) - 298.15 \text{ K}]$

where $\Delta_{\text{cr}}^g C_{p,m}^{\circ}$ and $\Delta_1^g C_{p,m}^{\circ}$ were taken from Table 2.2.3. Uncertainties in the temperature adjustment of fusion enthalpies from T_{fus} to the reference temperature are estimated to account with 30 % to the total adjustment [18].

^c Measured in this work

^d Calculated as the difference between column 6 and 5 in this table.

^e Calculated as the sum of column 5 and 6 in this table.

^f Calculated according to the “centerpiece” approach [45,46].

Table 2.2.2 Phase transitions thermodynamics of auxiliary for the “centerpiece” approach compounds (in $\text{kJ}\cdot\text{mol}^{-1}$)^a

Compounds	T_{fus} , K	$\Delta_{\text{cr}}^1 H_m^{\circ}$ at T_{fus}	298.15 K		
			$\Delta_{\text{cr}}^1 H_m^{\circ}$ ^b	$\Delta_{\text{cr}}^g H_m^{\circ}$	$\Delta_1^g H_m^{\circ}$
1	2	3	4	5	6
benzene [71-43-2]					33.9±0.1[40]
biphenyl [92-52-4]					66.7±0.1[47]
fluorobenzene [462-06-6]					31.2±0.1[40]
2-fluorobiphenyl [321-60-8]					64.0±0.5 ^c
benzophenone [191-16-9]	321.0	18.2±0.1[48]	17.0±0.3	95.0±0.4[49]	78.0±0.2 ^d
N-methyl-pyrrolidone [872-50-4]					54.9±0.1[40]
1-indanone [83-33-0]	312.9	17.8±0.2	17.2±0.3	83.5±0.7[51]	66.3±0.8 ^d
cyclopentanone [120-92-3]					42.8±0.1[40]
2-methyl-iso-indoline-1-one [5342-91-6]					72.1±0.8 ^c
methyl 2-phenylpropanoate [31508-44-8]					62.0±0.7[52]
2-methoxy-naphthalene [93-04-9]					69.3±0.9[53]

^a Uncertainty is expressed as the standard uncertainty (0.683 level of confidence, $k = 1$)

^b The experimental enthalpies of fusion $\Delta_{\text{cr}}^1 H_m^{\circ}$ measured at T_{fus} were adjusted to 298.15 K with help of the equation [18]:
 $\Delta_{\text{cr}}^1 H_m^{\circ}(298.15 \text{ K})/(\text{J}\cdot\text{mol}^{-1}) = \Delta_{\text{cr}}^1 H_m^{\circ}(T_{\text{fus}}/\text{K}) - (\Delta_{\text{cr}}^g C_{p,m}^{\circ} - \Delta_1^g C_{p,m}^{\circ}) \times [(T_{\text{fus}}/\text{K}) - 298.15 \text{ K}]$

where $\Delta_{\text{cr}}^g C_{p,m}^{\circ}$ and $\Delta_1^g C_{p,m}^{\circ}$ were taken from Table 2.2.3. Uncertainties in the temperature adjustment of fusion enthalpies from T_{fus} to the reference temperature are estimated to account with 30 % to the total adjustment [18].

^c Calculated according to the “centerpiece” approach [45,46] (see Figure 2.2.5)

^d Calculated as the difference between column 4 and 5 in this table.

Table 2.2.3 Compilation of data on molar heat capacities $C_{p,m}^{\circ}(\text{cr or liq})$ and heat capacity differences $\Delta_{\text{cr,l}}^{\text{g}}C_{p,m}^{\circ}$ (in $\text{J}\cdot\text{K}^{-1}\cdot\text{mol}^{-1}$) at $T = 298.15\text{ K}$ used for temperature adjustments.

Compounds	$C_{p,m}^{\circ}(\text{cr})^{\text{a}}$	$-\Delta_{\text{cr,l}}^{\text{g}}C_{p,m}^{\circ}^{\text{b}}$	$C_{p,m}^{\circ}(\text{liq})^{\text{a}}$	$-\Delta_{\text{l}}^{\text{g}}C_{p,m}^{\circ}^{\text{b}}$
flurbiprofen	297.5	45.4	396.5	113.7
indoprofen	370.2	56.3	487.3	137.3
ketoprofen	314.4	47.9	438.2	124.5
(S)-naproxen	294.4	44.9	351.8	102.0
(S)-naproxen methyl ester	318.5	48.5	411.0	117.4
benzophenone	224.8 [48]	34.5	298.0	88.1
1-indanone	175.3	27.0	219.0	67.5

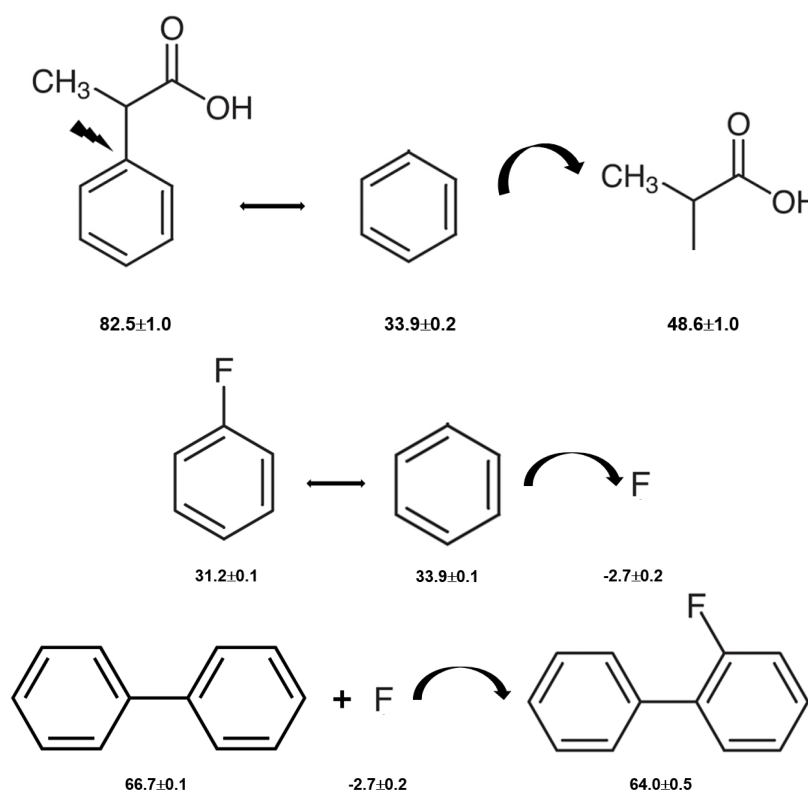
^a Calculated by the group-contribution procedure developed by Chickos *et al.*[16].

^b Calculated according to the procedure developed by Chickos and Acree [18].

These new thermochemical data have been used for the development the “centerpiece” approach for validation of the experimental data and for prediction vaporization enthalpies of drugs.

2.2.2. Validation of vaporization enthalpies of drugs with help of “centerpiece” approach

The main idea of the “centerpiece” approach was shown in previous chapter. In order to demonstrate the principle of the applicability of the “centerpiece” approach for the case of flurbiprofen it is reasonable to select biphenyl as the “centerpiece” and attach all required substituents to this molecule. The algorithm of calculation the vaporization enthalpy of the flurbiprofen using the “centerpiece” is shown in Figure 2.2.2. The auxiliary data for development of numerical values of substituents are taken from Table 2.2.2.



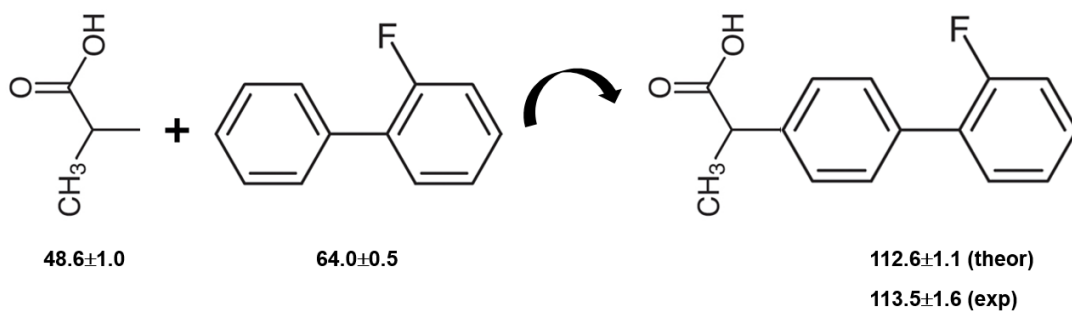


Figure 2.2.2 Validation of the “centerpiece” approach for vaporization enthalpy of flurbiprofen. All numerical values of vaporization enthalpies of auxiliary molecules are given in Table 2.2.2 (in $\text{kJ}\cdot\text{mol}^{-1}$). Experimental result was derived using results from Knudsen effusion method and enthalpy of fusion (see Table 2.2.1).

It has turned out that the *theoretical* enthalpy of vaporization of flurbiprofen, $\Delta_1^{\text{g}}H_m^{\text{o}}(298.15\text{ K}) = 112.6 \pm 1.1\text{ kJ}\cdot\text{mol}^{-1}$, is in very good agreement with the experimental value, $\Delta_1^{\text{g}}H_m^{\text{o}}(298.15\text{ K}) = 113.5 \pm 1.6\text{ kJ}\cdot\text{mol}^{-1}$, evaluated in Table 2.2.1 from the new experimental data.

The next example is calculation of vaporization enthalpy of the (S)-naproxen methyl ester, starting from the 2-methoxy-naphthalene as the “centerpiece”. The algorithm of the calculations is shown in Figure 2.2.3.

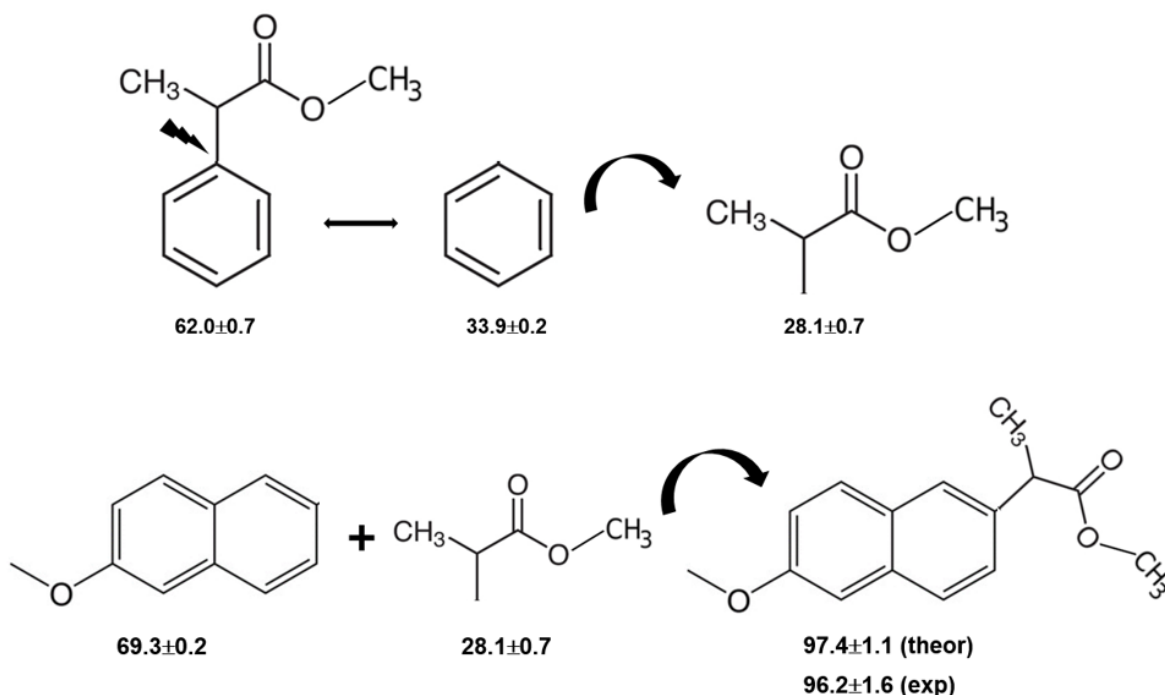


Figure 2.2.3 Evaluation vaporization enthalpy of (S)-naproxen methyl ester with help of the “centerpiece” approach. All numerical values of vaporization enthalpies of auxiliary molecules are given in Table 2.2.2 (in $\text{kJ}\cdot\text{mol}^{-1}$). Experimental result was derived using results from Knudsen effusion method and enthalpy of fusion (see Table 2.2.1).

Also in this case, the *theoretical* enthalpy of vaporization of (S)-naproxen methyl ester, $\Delta_1^{\text{g}}H_{\text{m}}^{\circ}(298.15 \text{ K}) = 97.4 \pm 1.1 \text{ kJ}\cdot\text{mol}^{-1}$, is in very good agreement with the experimental value, $\Delta_1^{\text{g}}H_{\text{m}}^{\circ}(298.15 \text{ K}) = 96.2 \pm 1.6 \text{ kJ}\cdot\text{mol}^{-1}$, evaluated in Table 2.2.1 from the new experimental data.

The last example is calculation of vaporization enthalpy of the ketoprofen, starting from the benzophenone as the “centerpiece”. The algorithm of the calculations is shown in Figure 2.2.4.

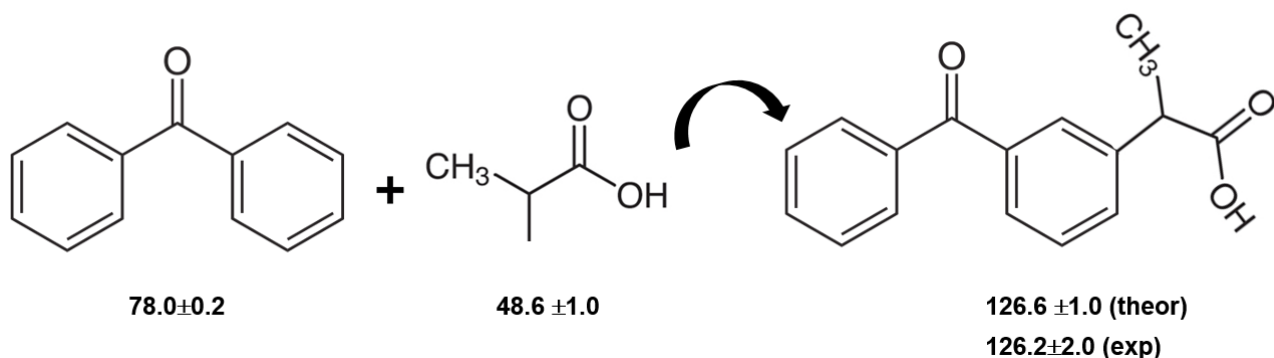
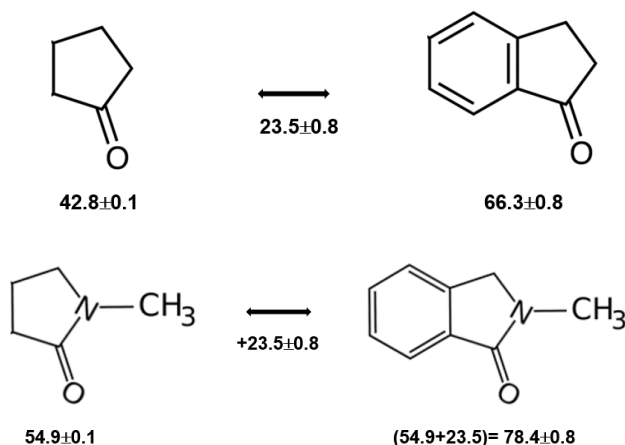


Figure 2.2.4 Evaluation vaporization enthalpy of Ketoprofen with help of the “centerpiece” approach. All numerical values of vaporization enthalpies of auxiliary molecules are given in Table 2.2.2 (in $\text{kJ}\cdot\text{mol}^{-1}$). Experimental result was derived using correlation-gas-chromatography [54].

Also in this case, the *theoretical* enthalpy of vaporization of ketoprofen, $\Delta_1^{\text{g}}H_{\text{m}}^{\circ}(298.15 \text{ K}) = 126.6 \pm 1.0 \text{ kJ}\cdot\text{mol}^{-1}$, is in very good agreement with the experimental value, $\Delta_1^{\text{g}}H_{\text{m}}^{\circ}(298.15 \text{ K}) = 126.2 \pm 2.0 \text{ kJ}\cdot\text{mol}^{-1}$ [54] evaluated in Table 2.2.1 from the new experimental data.



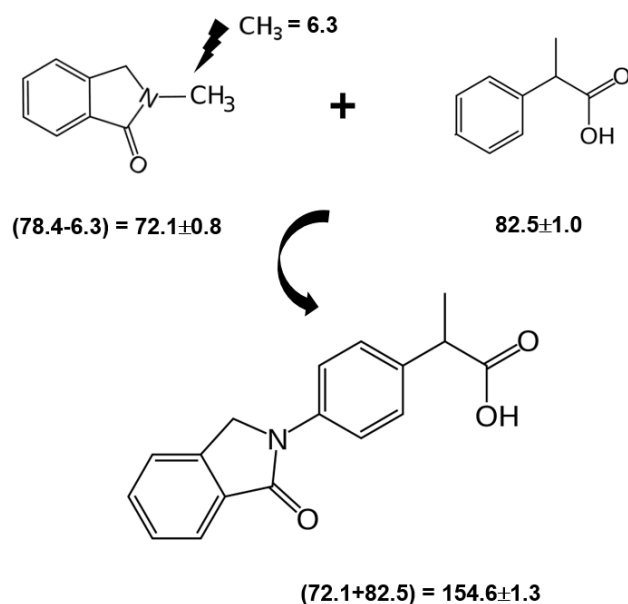


Figure 2.2.5 Evaluation vaporization enthalpy of Indoprofen with help of the “centerpiece” approach. All numerical values of vaporization enthalpies of auxiliary molecules are given in Table 2.2.1 (in $\text{kJ}\cdot\text{mol}^{-1}$).

The results discussed in Figure 2.2.2, Figure 2.2.3, and Figure 2.2.4, show that the “centerpiece” approach can be successfully applied for prediction of vaporization enthalpies of aromatic systems related to pharmaceuticals. For this reason, the vaporization enthalpy of indoprofen, $\Delta_1^{\text{g}}H_{\text{m}}^{\circ}(298.15\text{ K}) = 154.6 \pm 1.3\text{ kJ}\cdot\text{mol}^{-1}$, calculated using “centerpiece” approach using the 2-methyl-iso-indoline-1-one as the “centerpiece” (see Figure 2.2.5), should be considered as reliable.

2.2.3. Quantification of hydrogen bonding and dispersion forces in ibuprofen

One of the key features defining the ibuprofen structure is the doubly intermolecular $\text{O}\cdots\text{O}=\text{C}$ hydrogen bond in cyclic dimers (see Figure 2.2.6).

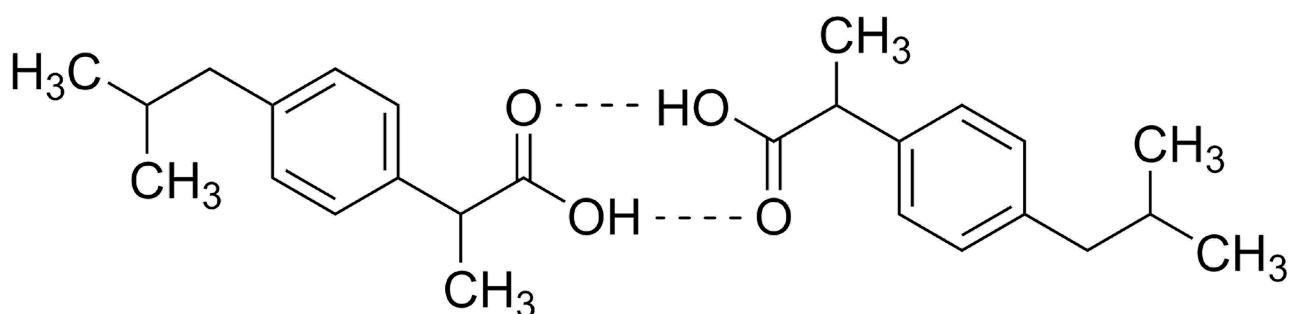


Figure 2.2.6 Structure of the cyclic dimer of ibuprofen with two equivalent $\text{O}\cdots\text{O}$ hydrogen bonds between the functional COOH group of each molecule

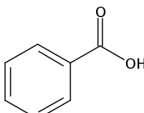
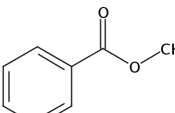
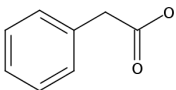
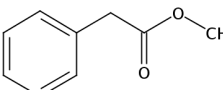
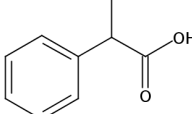
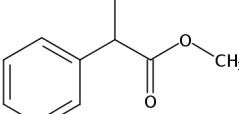
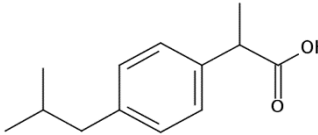
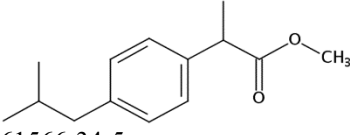
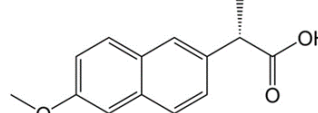
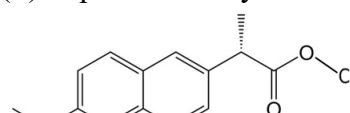
The reliable value of the vaporization enthalpy of ibuprofen, $\Delta_1^{\text{g}}H_{\text{m}}^{\circ}(298\text{ K}) = 89.4 \pm 0.8\text{ kJ}\cdot\text{mol}^{-1}$, was derived from thermochemical experiments [11]. Is it possible to dissect the experimental vaporization enthalpy, which represents the overall interaction energies in contributions for hydrogen

bonding and dispersion forces as both present in ibuprofen? A combined approach of thermodynamic measurements and quantum chemical calculations was applied to obtain detailed information about the structure and interactions in ibuprofen.

One way to quantify the strength of the intermolecular hydrogen bonding in the liquid phase is the concept of homomorphs [55]. Molecules with the same or very similar molecular dimensions are called "homomorphs". The concept of homomorphs permits a useful correlation between the chemical properties of molecules of widely different functions, but of similar sizes and shapes [56]. For ibuprofen its homomorph is α -methyl-4-(2-methylpropyl)-benzeneacetic acid methyl ester (see Table 2.2.4). The exchange of the OH group in ibuprofen with the similarly dimensioned methyl group enables the correlation of their thermodynamic properties. For example, the experimental vaporization enthalpy is $\Delta_1^g H_m^o(298\text{ K}) = 89.4 \pm 0.8\text{ kJ}\cdot\text{mol}^{-1}$ for ibuprofen and $\Delta_1^g H_m^o(298\text{ K}) = 69.4 \pm 0.3\text{ kJ}\cdot\text{mol}^{-1}$ for its homomorph (see Table 2.2.4), hence the difference $\Delta(\Delta_1^g H_m^o) = -19.4 \pm 0.9\text{ kJ}\cdot\text{mol}^{-1}$ between ibuprofen and homomorph is obviously related to the formation of hydrogen bonding in ibuprofen, which is prevented in the ester by substituting the hydroxy group by the methyl group. This $\Delta(\Delta_1^g H_m^o)$ -value is similar to those for the three other pairs of acids and esters as given in Table 2.2.4, column 3. These differences in enthalpies of vaporization for the aromatic species are also at the same level as for a large set of aliphatic monocarboxylic acids and their homomorph methyl alkanoates with $\Delta(\Delta_1^g H_m^o)$ -values in the range of 18 to 23 $\text{kJ}\cdot\text{mol}^{-1}$ [11]. The differences of enthalpies of vaporization for the acetic acid ($-18.0 \pm 0.5\text{ kJ}\cdot\text{mol}^{-1}$) and ibuprofene ($-20.3 \pm 1.5\text{ kJ}\cdot\text{mol}^{-1}$) relative to their esters are illustrated in Figure 2.2.7. They will be used for developing the intermolecular HB-strength in aliphatic acids and ibuprofen in terms of the $\Delta(\Delta_1^g H_m^o)$. Before doing this, however, we need to correct the HB strength for the presence of the methyl group in the esters used for comparison. Indeed, the CH_3 -group is contributing to the vaporization enthalpy of esters and this contribution should be evaluated and excluded by assessment of the HB-strength. For evaluation of the CH_3 -group contribution, we plotted experimental enthalpies of vaporization $\Delta_1^g H_m^o(298\text{ K})$ of alkyl acetates versus the number of carbon atoms, N_C , present in these compounds. In Figure 2.2.8 we observe a clear slope decreasing about $4.3\text{ kJ}\cdot\text{mol}^{-1}$ with each removed methylene group. This behavior is well-known for *n*-alkanes, *n*-alcohols or even for ionic liquids with cations bearing alkyl chain groups [4]. However, the desired value here is given by the intercept. At $N_C = 0$ only the contribution for the CH_3 group present in the alkyl acetates remains. This value of about $27\text{ kJ}\cdot\text{mol}^{-1}$ can be now used for correcting the intermolecular HB-strength in aliphatic acids due to the redundant methyl contribution. This procedure finally allows us to determine the HB energies present in the aliphatic carboxylic acids and ibuprofen, respectively. The approach to evaluate the CH_3 -group correction is illustrated in Figure 2.2.9. The total HB energy results from the difference of the enthalpies of vaporization of aliphatic

carboxylic acids and their esters ($-18 \text{ kJ}\cdot\text{mol}^{-1}$) corrected for the redundant CH_3 contribution ($-27 \text{ kJ}\cdot\text{mol}^{-1}$). The HB energy in the doubly hydrogen bonded aliphatic carboxylic acids sums up to a total of $45 \text{ kJ}\cdot\text{mol}^{-1}$, which is twice as high as the HB energies in water and alcohols [55,57].

Table 2.2.4 Experimental enthalpies of vaporization $\Delta_1^{\text{g}}H_{\text{m}}^{\circ}$ (298 K) of the aromatic monocarboxylic acids and their homomorph methyl esters (in $\text{kJ}\cdot\text{mol}^{-1}$) [11].

Acid	$\Delta_1^{\text{g}}H_{\text{m}}^{\circ}$	Ester	$\Delta_1^{\text{g}}H_{\text{m}}^{\circ}$	$\Delta(\Delta_1^{\text{g}}H_{\text{m}}^{\circ})$
benzoic acid  65-85-0	75.9 ± 1.6	methyl benzoate  93-58-3	55.6 ± 0.1	-20.3 ± 1.6
phenyl-ethanoic acid  103-82-2	79.1 ± 0.3	methyl phenylethanoate  101-41-7	57.4 ± 1.0	-21.7 ± 1.1
2-phenylpropanoic acid  492-37-5	82.5 ± 1.0	methyl 2-phenylpropanoate  31508-44-8	62.0 ± 0.7	-20.5 ± 1.2
ibuprofen  15687-27-1	89.4 ± 0.8	α -methyl-4-(2-methylpropyl)-benzeneacetic acid methyl ester  61566-34-5	69.5 ± 0.3	-19.9 ± 0.9
(S)-naproxen 	105.0 ± 2.5	(S)-naproxen methyl ester 	96.2 ± 1.6	8.8 ± 3.0

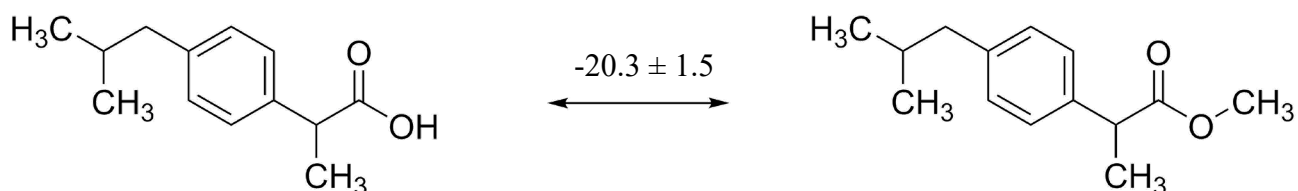
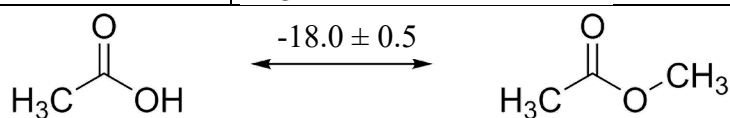


Figure 2.2.7 Development of the intermolecular hydrogen bonding energy in aliphatic carboxylic acids and ibuprofen according to the homomorph model. The differences $\Delta(\Delta_1^{\text{g}}H_{\text{m}}^{\circ})$ are given in $\text{kJ}\cdot\text{mol}^{-1}$.

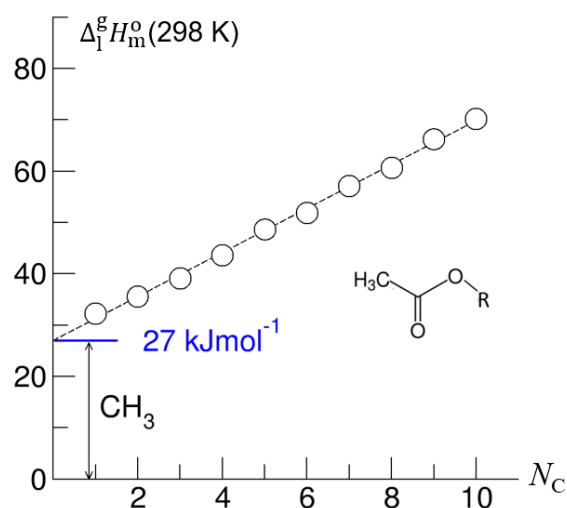


Figure 2.2.8 Experimental vaporization enthalpies, $\Delta_1^g H_m^o(298 \text{ K}, \text{kJ}\cdot\text{mol}^{-1})$, of alkyl acetates plotted versus the total number of carbon atoms (N_C) in the side chains. The intercept of about $27 \text{ kJ}\cdot\text{mol}^{-1}$ at $N_C=0$ gives the contribution of the CH_3 group and allows the correction of the intermolecular HB energy in aliphatic carboxylic acids.

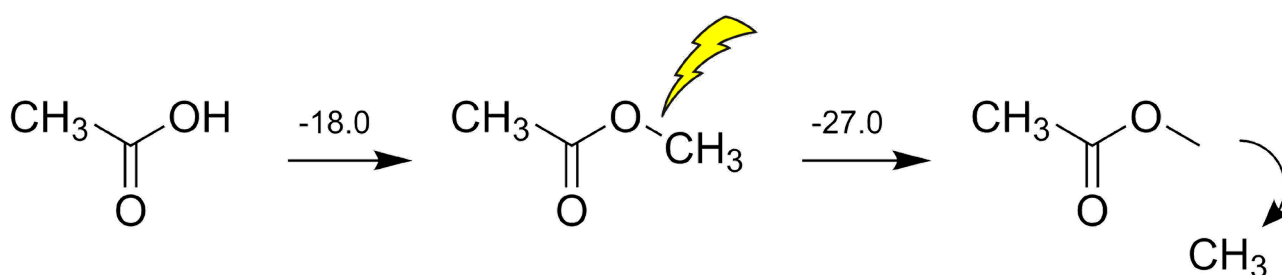


Figure 2.2.9 Correction of the intermolecular hydrogen bonding energy in aliphatic carboxylic acids due to redundant CH_3 contribution. The corrected HB energy was calculated as the sum $[(-18.0) + (-27.0)] = -45.0 \text{ kJ}\cdot\text{mol}^{-1}$.

For dissecting the vaporization enthalpy of ibuprofen into contributions from hydrogen bonding and dispersion interaction, we calculated clusters n including up to twelve molecules ($n = 12$) at the B3LYP/6-31G* level of theory. The clusters with even numbers of molecules consist exclusively of cyclic dimers showing the typical double hydrogen bonds in carboxylic acids. The clusters with odd numbers of molecules include one molecule which is not involved in stable cyclic dimers. Thus, the binding energies for $n = 3, 5, 7, 9, 11$ are slightly lower compared to those for the other clusters comprised of cyclic dimers only. In Figure 2.2.10 we show that with increasing cluster size the binding energies ΔE converge to $45 \text{ kJ}\cdot\text{mol}^{-1}$. Both values are only half of the experimental vaporization enthalpies of ibuprofen of about $89.4 \pm 0.8 \text{ kJ}\cdot\text{mol}^{-1}$, but almost perfectly agree with the dissected HB energy at the level of $45 \text{ kJ}\cdot\text{mol}^{-1}$. It seems that the larger clusters describe the amount of hydrogen bonding present in liquid ibuprofen. We could show earlier that such a cluster size is sufficient to mimic liquid phase properties [58–64]. The agreement between experimental and

calculated HB energies also suggests that liquid ibuprofen mainly consists of cyclic dimers as observed solely in the solid material. It is well-known, that DFT methods fail to describe dispersion interaction properly. Thus, we re-optimized the ibuprofen clusters by using Grimme's D3 dispersion correction [9,10]. A comparison of the DFT and DFT-D3 energies provides a lower bound estimate of the stabilization due to dispersion $E_{\text{disp-D3}} = \Delta E(\text{B3LYP-D3}) - \Delta E(\text{B3LYP})$. The $\Delta\Delta E_{\text{disp}}$ correction is not exactly equal to the dispersion stabilization as the correction depends on the repulsiveness of the functional employed, but it provides an excellent estimate of the magnitude of this interaction.

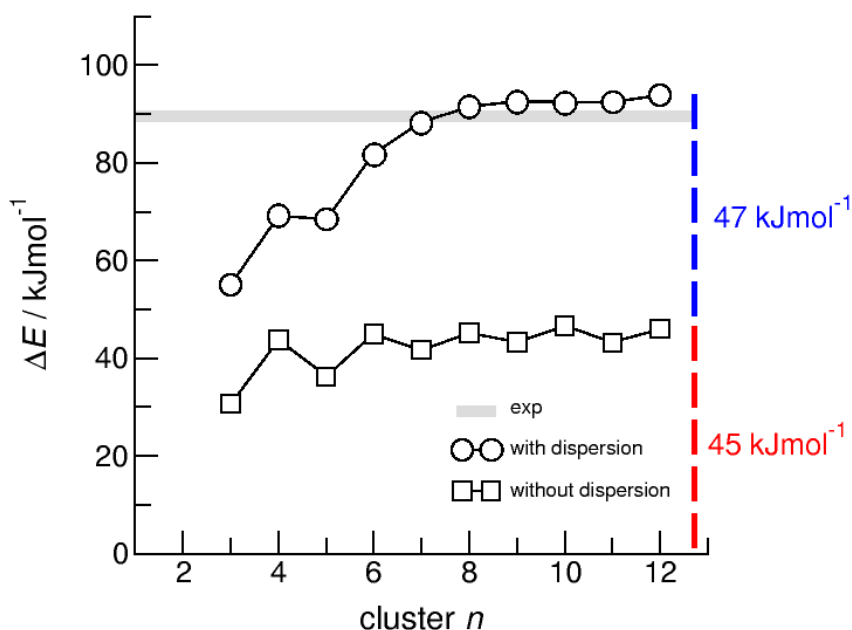


Figure 2.2.10 B3LYP/6-31G* (squares) and B3LYP-D3/6-31G* (circles) calculated binding energies ΔE per molecule of ibuprofen clusters $n = 3-12$.

In Figure 2.2.10 we show that the “odd/even effect” disappears for larger clusters, suggesting that the differences in hydrogen bonding are compensated by taking dispersion interaction into account. However, the main result is that the binding energies for the larger clusters ($n > 8$) now perfectly describe the experimental enthalpy of vaporization. The calculated ΔE values of about 92 $\text{kJ}\cdot\text{mol}^{-1}$ lie only slightly above the experimental values of $89.4 \pm 0.8 \text{ kJ}\cdot\text{mol}^{-1}$. Obviously, the experimental enthalpy of vaporization is reasonably described by the calculated interaction energies present in larger clusters. Moreover, we can dissect the binding energies into hydrogen bonding and dispersion interaction, both being of equal magnitude with 45 $\text{kJ}\cdot\text{mol}^{-1}$ and 47 $\text{kJ}\cdot\text{mol}^{-1}$, respectively. In particular, the HB energies are in almost perfect agreement with the experimentally derived value of about 45 $\text{kJ}\cdot\text{mol}^{-1}$. This suggests that the experimental approach to dissecting HB energy also seems appropriate. The HB contribution in the order of 50% of the overall interaction energy as calculated here, is substantially higher than the HB contribution calculated for the crystal lattice from force fields estimated to be about 30% [65]. It seems to be surprising that for the strongly hydrogen

bonded carboxylic acids (more than twice strong as the HB bonds in water or alcohols due to the cyclic dimers), dispersion interaction plays such an important role and definitely has to be considered for describing thermodynamic properties. At this point we understand the liquid/gas phase transition for ibuprofen on the basis of hydrogen bonding and dispersion forces.

To conclude, the hydrogen bond energy within the cyclic dimers of about $45 \text{ kJ}\cdot\text{mol}^{-1}$ could be derived exclusively from the experimental vaporization enthalpy of ibuprofen and related aromatic carboxylic acids, homomorph methyl esters and alkyl acetates. It could be confirmed by DFT calculations on clusters including up to twelve molecules that the enthalpies of vaporization of ibuprofen consists of almost equal contributions from hydrogen bonding and dispersion interaction. Our combined approach including thermodynamic methods and DFT calculations allowed comprehensive understanding of structure and molecular interaction in ibuprofen and related compounds.

3. Quantification of dispersion forces with the aid of enthalpy of formation

3.1. Extremely strained hydrocarbons: strain vs. dispersion forces

Qualitatively, organic chemists usually recognize a strained molecule when they see its structural formula. Quantitative knowledge of the strain offers the possibility of predicting the stability or reactivity of a molecule. Advances in computational chemistry and molecular modelling methods have increasingly been used by organic chemists to gain quantitative insights into molecular energetics and to better predict feasibility of organic and biochemical reactions. An accurate and reliable experimental $\Delta_f H_m^0(\text{g})$ -values are required to develop and test theoretical methods. The strained hydrocarbons and in particular highly branched and extremely strained hydrocarbons like tri-tert-butylmethane, octamethylhexane and hexaethylethane collected in Table 1.1 are considered to be a very tough test for any methodology, but they can be considered as optimal test systems for determining dispersion effects.

As early as 1956, Pitzer and Catalano [66] pointed out that the relative stabilities of branched versus linear alkanes are due to intramolecular dispersion forces. The general lack of intrinsic polarization in alkanes enables their energies to be easily separated into dispersion and covalent contributions. Several approaches are suitable for such a separation. Schleyer *et al.* [67] suggested the concept of “protobranching” in order to rationalize the importance of electron correlation for attractive interactions of 1,3-alkyl groups in alkanes. They used the bond separation or isodesmic reactions to quantify the stabilizing effects in branched alkanes compared to the linear species. For example, (see Figure 3.1.1), propane has one protobranch (or 1,3-alkyl contacts) and is stabilized appreciably, by $-11.5 \text{ kJ}\cdot\text{mol}^{-1}$, relative to methane and ethane. Neopentane has six protobranches but n-pentane only three.

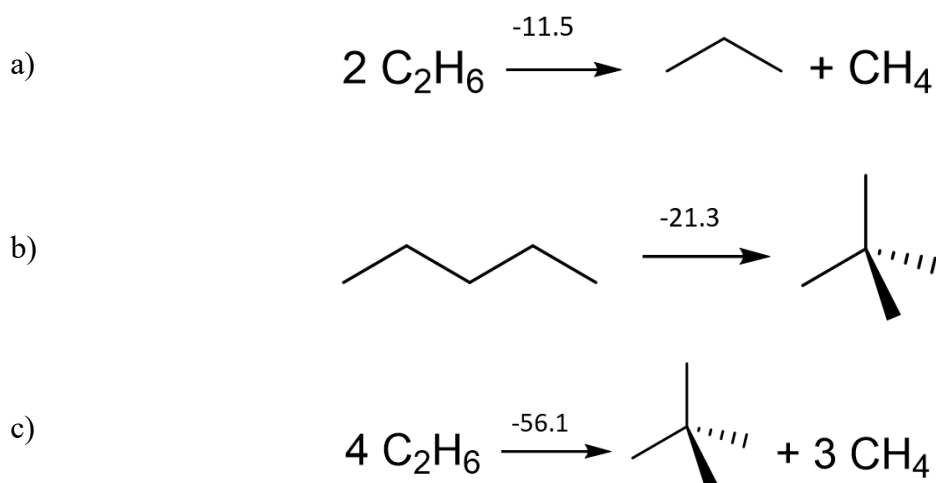
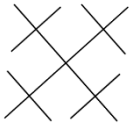
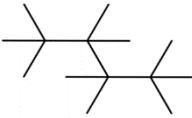
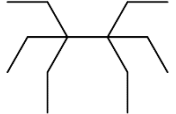
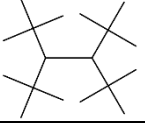


Figure 3.1.1 Conventional equations for the evaluation of protobranching (a) and branching (b and c). Values in $\text{kJ}\cdot\text{mol}^{-1}$ are based on experimental standard molar enthalpies of formation at 298 K [68]

Although the concept of protobranching has been criticized [69], it clearly shows that the attractive interactions of 1,3-alkyl groups are responsible for the general stabilization of branched alkanes. However, the application of this approach to quantifying the dispersion forces is difficult in practice, since the selection of suitable modelling reactions does not become trivial as the molecule size increases (*e.g.*, for the list of alkanes given in Table 3.1.1). Indeed, as can be seen from Figure 3.1.1, even the enthalpies of two modelling reactions for neopentane differ considerably and could provide an ambiguous interpretation of the amount of dispersion forces in the branched alkane.

Table 3.1.1 Correlation of strain enthalpies H_s of highly branched hydrocarbons with their amount of dispersion contributions ($E_{\text{disp-D3}}$) calculated by the DFT-D3.

Formula	Structure	$\Delta_f H_m^0(\text{g})^a$	H_s^b	$E_{\text{disp-D3}}^c$
C_5H_{12}		-168.1 ± 0.8	1.4	-32.4
C_9H_{20}		-241.6 ± 1.4	34.7	-77.8
$\text{C}_{10}\text{H}_{22}$		(-241.0 ± 4.1)	64.9	-93.9
$\text{C}_{12}\text{H}_{26}$		(-251.1 ± 4.1)	106.1	-121.0
$\text{C}_{13}\text{H}_{28}$		-235.2 ± 4.3 [70]	156.1	-136.2

C ₁₇ H ₃₆		(-147.6±4.1)	362.0	-211.8
C ₁₄ H ₃₀		-248.3±2.4 [70]	172.2	-155.7
C ₁₄ H ₃₀		-265.5±2.6 [70]	118.1	-146.5
C ₁₈ H ₃₈		-250.6±3.8 [71]	277.0	-186.0

^a Experimental values taken from Pedley *et al.* [68] or from the references specified for each structure. Uncertainties are expressed as the twice standard deviations. Values in parentheses were calculated in this work by using G3MP2 method and the atomisation procedure. The atomisation enthalpies were corrected according to equation: $\Delta_f H_m^0(g)_{G3MP2} = 0.8376 \times \Delta_f H_m^0(g)_{AT} - 31.3$ ($R^2 = 0.9673$). The latter was derived with help of experimental enthalpies of formation of the branched alkanes collected in this table.

^b Calculated according to Eq. (3.1.1)

^c Calculated with the DFT-3D in this work.

To avoid ambiguity, we tried to invoke an idea of “Spannungsenergie” or “strain energy” introduced by A. von Baeyer [72] (and further developed by Schleyer *et al.* [73]) to correlate the strain energies with the amount of dispersion forces available in the branched alkane according to the DFT-D3 calculations (see Table 3.1.1).

The concept of “strain”, H_S , in organic molecules, although not unambiguously defined, is conceptually useful, because in the value of H_S the sum of overall interactions in a molecule is collected [74]. The strain, H_S , of a molecule is conventionally defined as the difference between its experimental $\Delta_f H_m^0(g)$ and that for its corresponding hypothetically strain-free model, calculated from “strain-free” group contributions (increments) [73]:

$$H_S = (\Delta_f H_m^0(g) - \Sigma \text{ increments}) \quad (3.1.1)$$

A group is defined by Benson [75] as a polyvalent atom in a molecule together with all of its ligands. The system of strain-free increments is based on the standard enthalpies of formation $\Delta_f H_m^0(g)$ of simple homologous (“strain-less”) molecules [73]. Their advantage with respect to the classic Benson increments [75] is the possibility of the determining of strain enthalpies. Schleyer *et al.* [73] established the values of “strain-free” increments for hydrocarbons: $\text{CH}_3[\text{C}] = -42.05 \text{ kJ}\cdot\text{mol}^{-1}$; $\text{CH}_2[2\text{C}] = -21.46 \text{ kJ}\cdot\text{mol}^{-1}$; $\text{CH}[3\text{C}] = -9.04 \text{ kJ}\cdot\text{mol}^{-1}$; $\text{C}[4\text{C}] = -1.26 \text{ kJ}\cdot\text{mol}^{-1}$, Beckhaus [76] extended this methodology to arenes: $\text{C}_B\text{H}[2\text{C}_B] = 13.72 \text{ kJ}\cdot\text{mol}^{-1}$ (C_B represents the aromatic C atoms); $\text{C}_B[\text{C}, 2\text{C}_B] = 23.51 \text{ kJ}\cdot\text{mol}^{-1}$. As an example, strain of neopentane, $H_S = 1.4 \text{ kJ}\cdot\text{mol}^{-1}$, can be calculated using its enthalpy of formation $\Delta_f H_m^0(g) = -168.1 \pm 0.8 \text{ kJ}\cdot\text{mol}^{-1}$ [68] and the sum of the strain-free increments: $(4 \times \text{CH}_3[\text{C}] + \text{C}[4\text{C}])$.

Total amount of a molecule strain reflects the quantitative structure – energy relationships. The strain in organic molecules can generally be explained in terms of the angular strain, non-bonded atoms repulsions, or stereoelectronic effects. It is not easy, but it is always of interest to extract contributions to the strain enthalpy in order to understand their regularities.

In the case of the series of extremely branched hydrocarbons collected in Table 3.1.1, the following procedure has been applied. We derived their strain enthalpies H_s , according to Eq. (3.1.1), and for each molecule, the contribution $E_{\text{disp-D3}}$ due to the dispersion forces was calculated using the DFT-D3 method. It should be noted that the contribution $E_{\text{disp-D3}} = -32.4 \text{ kJ}\cdot\text{mol}^{-1}$, calculated according to the DFT-D3 method for the neopentane is more or less the average value between $-21.3 \text{ kJ}\cdot\text{mol}^{-1}$ and $-56.1 \text{ kJ}\cdot\text{mol}^{-1}$ suggested by Wodrich *et al.* [67] as a measure of the stabilization through dispersion forces (see Figure 3.1.1). Anyway, the strong stabilization of neopentane quantified via $E_{\text{disp-D3}}$ completely overwhelmed the faint value of the strain $H_s = 1.4 \text{ kJ}\cdot\text{mol}^{-1}$. Table 3.1.1 shows that the degree of crowding of the alkane increases starting from neopentane. The 2,2,4,4-tetra-methyl-pentane is already strained by $H_s = 34.7 \text{ kJ}\cdot\text{mol}^{-1}$, nevertheless this strain is effectively compensated by the increased dispersion forces with $E_{\text{disp-D3}} = -77.8 \text{ kJ}\cdot\text{mol}^{-1}$. Similarly, in 2,2,3,4,4-penta-methyl-pentane and in 2,2-(3-isopropyl)-4,4-pentamethyl-pentane, the rising strain due to the sterical crowding is still compensated by the increasing amount of stabilizing dispersion interactions (see Table 3.1.1). In contrast, in tri-tert-butyl-methane, which is obviously sterically more encumbered, compared to the previous entries in Table 3.1.1, the enormous strain of $H_s = 156.1 \text{ kJ}\cdot\text{mol}^{-1}$ already somewhat overwhelms the attractive forces of $E_{\text{disp-D3}} = -136.2 \text{ kJ}\cdot\text{mol}^{-1}$. Similarly, in 2,2,3,3,4,4,5,5-octamethylhexane, the even greater strain of $H_s = 177.2 \text{ kJ}\cdot\text{mol}^{-1}$ is no longer counteracted with the attractive forces of $E_{\text{disp-D3}} = -155.7 \text{ kJ}\cdot\text{mol}^{-1}$.

The evaluation of the $H_s - E_{\text{disp-D3}}$ relationships with increasing overcrowding of the alkane shows the clear concerting trend between the two values. A remarkably linear correlation:

$$E_{\text{disp-D3}} / \text{kJ}\cdot\text{mol}^{-1} = -0.393 \times H_s - 77.4 \quad \text{with } R^2 = 0.921 \quad (3.1.2)$$

was derived from H_s and $E_{\text{disp-D3}}$ collected in Table 3.1.1. This trend can be helpful in rationalizing the potential success or failure of synthetic efforts to prepare sterically hindered molecules.

For example, for tri-tert-butyl-methane and 2,2,3,3,4,4,5,5-octamethylhexane, the balance of repulsive and attractive forces evaluated in Table 3.1.1 is only slightly shifted to the steric repulsions. Admittedly, adding a dispersion correction to the DFT levels does not fully correct the energy difference. With the most modern DFT-D3 approaches, an error up to 30% remains, possible [77], therefore the counter play of strain and dispersion in tri-tert-butyl-methane and 2,2,3,3,4,4,5,5-octamethylhexane can be considered as the game ended in a draw. This conclusion is fully supported with the successful synthesis of these extremely strained alkanes reported in our previous work [70]. More striking example of counter play of strain and intramolecular attraction come from tetra-tert-

butyl-methane. The highest strain of $H_s = 362.0 \text{ kJ}\cdot\text{mol}^{-1}$ has no chance of being covered by the attractive forces of $E_{\text{disp-D3}} = -211.8 \text{ kJ}\cdot\text{mol}^{-1}$. Consequently, the experimental efforts to synthesize this molecule are in vain.

The example of extremely strained alkanes has shown, that despite our conceptually incomplete understanding of “steric demand” (as a balance of repulsive and attractive forces), the steric crowding cannot be made solely responsible for the thermodynamic feasibility of strained molecules, since the intramolecular dispersion interactions can decisively stabilize molecules that otherwise have labile bonds. Such a “dispersion glue” around reactive molecules (not just bonds) is able to stabilize them to the degree that they can be isolated and characterized [6].

3.2. Sterically congested alcohols: strain vs. dispersion forces

The sterically congested carbinols (see Figure 3.2.1) are also a remarkable pattern for studying the individual types of strains in these molecules and provide a valuable test case for semi-empirical, empirical, and quantum-chemical calculations. This set of compounds is interesting because it allows one to observe the gradual changes in the interplay of the strain and intramolecular dispersive forces that result from the arrangement of various bulky alkyl or phenyl groups around the C-OH moiety.

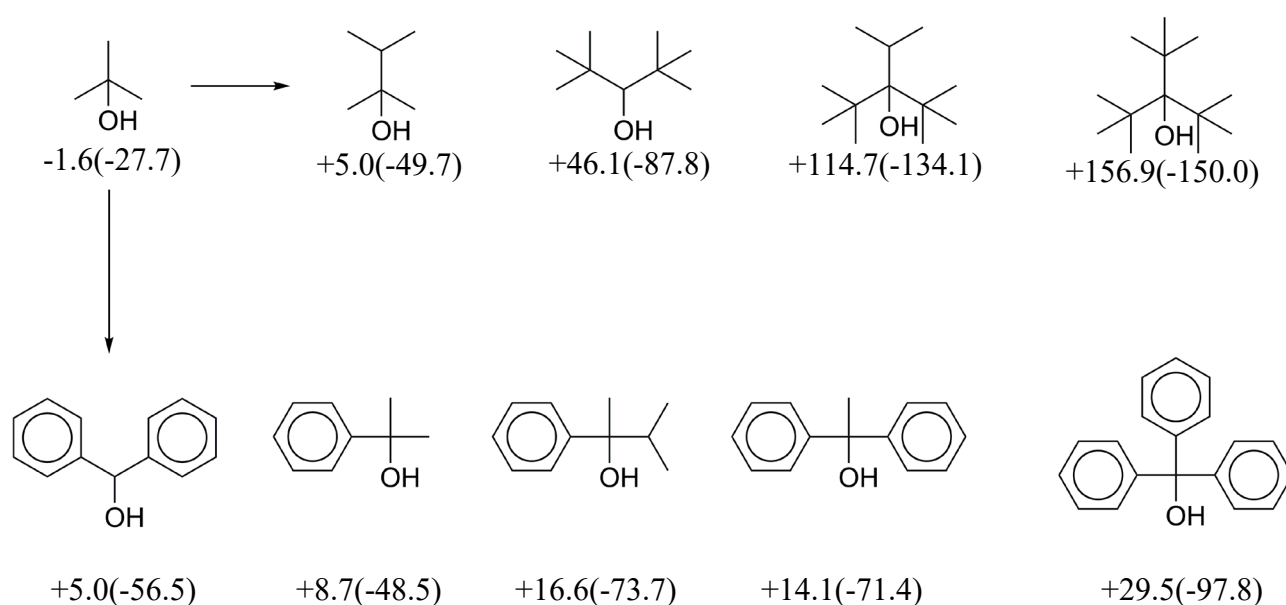


Figure 3.2.1 Comparison of the strain energies, H_s , and dispersion forces, $E_{\text{disp-D3}}$, in alkyl and phenyl congested carbinols. The experimental data (in $\text{kJ}\cdot\text{mol}^{-1}$) were taken from our previous work [78]. The $E_{\text{disp-D3}}$ -contributions (given in parentheses, in $\text{kJ}\cdot\text{mol}^{-1}$) were calculated in this work by DFT-D3.

The gradual evolution of the strain enthalpies (calculated according to Eq. (3.1.1)) of alkyl and phenyl congested carbinols is shown in Figure 3.2.1. If the trimethyl-methanol (tert-butanol) claimed to be strain-free ($H_s = -1.6 \text{ kJ}\cdot\text{mol}^{-1}$), the interaction of two methyls with the iso-propyl group in 2,3-dimethyl-2-butanol already led to a weak destabilization of $5.0 \text{ kJ}\cdot\text{mol}^{-1}$. The strain increases rapidly

by the further congestion of the C-OH moiety with the bulky tert-butyl groups. The most strained compound in this set is tri-tert-butyl-methanol with the strain $H_s = 156.9 \text{ kJ}\cdot\text{mol}^{-1}$ due to steric repulsions among the bulky tert-butyl groups. The dispersion forces contributions, $E_{\text{disp-D3}}$, calculated for this set increase simultaneously with increasing degree of strain (see Figure 3.2.1). In tri-tert-butylmethanol, the destabilization due to the sterical repulsions of the bulky substituents is completely compensated with the equal amount of attractive dispersion forces.

Development of the strain-dispersion competition is shown in Figure 3.2.1 (right). The phenyl substituent is less spacious compared to the tert-butyl group. In addition, the phenyl substituent can exert the attractive π - π interactions with the neighbouring phenyl group. Consequently, the strain effects in phenyl-congested carbinols are less profound with the common level of strain of around $10 \text{ kJ}\cdot\text{mol}^{-1}$. Only in tri-phenyl-methanol did steric repulsions of phenyl rings lead to stronger destabilization of $29.5 \text{ kJ}\cdot\text{mol}^{-1}$. The ability of the phenyl substituents to exert mutual attractive p-p interactions is clearly manifested in diphenyl-carbinol ($E_{\text{disp-D3}} = -56.5 \text{ kJ}\cdot\text{mol}^{-1}$) and 1,1-diphenyl-ethanol ($E_{\text{disp-D3}} = -71.4 \text{ kJ}\cdot\text{mol}^{-1}$), when their dispersion contributions are compared with those of the least stabilised 1-phenyl-1-methyl-ethanol ($E_{\text{disp-D3}} = -48.5 \text{ kJ}\cdot\text{mol}^{-1}$). It is also evident that the large dispersion contribution in tri-phenyl-methanol ($E_{\text{disp-D3}} = -97.8 \text{ kJ}\cdot\text{mol}^{-1}$) results from the triple mutual attractive p-p interactions of the phenyls and completely eliminates the steric repulsions of phenyl rings around the C-OH unit.

Similar to the trend observed for the strained alkanes, the evaluation of the $H_s - E_{\text{disp-D3}}$ relationships with the increasing crowding of the C-OH unit shows the clear concerting trend between the two values. For the alkyl-congested carbinols we observed the following linear correlation:

$$E_{\text{disp-D3}} / \text{kJ}\cdot\text{mol}^{-1} = -0.740 \times H_s - 42.5 \quad \text{with } R^2 = 0.958 \quad (3.2.1)$$

For the phenyl-congested carbinols the following linear correlation was observed:

$$E_{\text{disp-D3}} / \text{kJ}\cdot\text{mol}^{-1} = -2.167 \times H_s - 36.5 \quad \text{with } R^2 = 0.936 \quad (3.2.2)$$

It makes oneself conspicuous, that the greater slope in the case of phenyl-substitution can be considered as evidence of the less profound stabilization due to the attractive π - π interactions, in comparison to the strong dispersion contributions of the tert-butyl groups. Moreover, if this conclusion is correct, the even smaller slope of Eq. (3.1.1) can be seen as a manifestation of paramount importance of dispersion forces for the stabilization of extremely strained hydrocarbons.

3.3. Dispersion interactions in phenyl substituted benzenes, naphthalenes, and anthracenes

If one looks at the structures of phenyl-substituted benzenes, naphthalenes, and anthracenes, it becomes clear (see Figure 3.1.1) that these are predestined for dispersion interactions between phenyl rings.

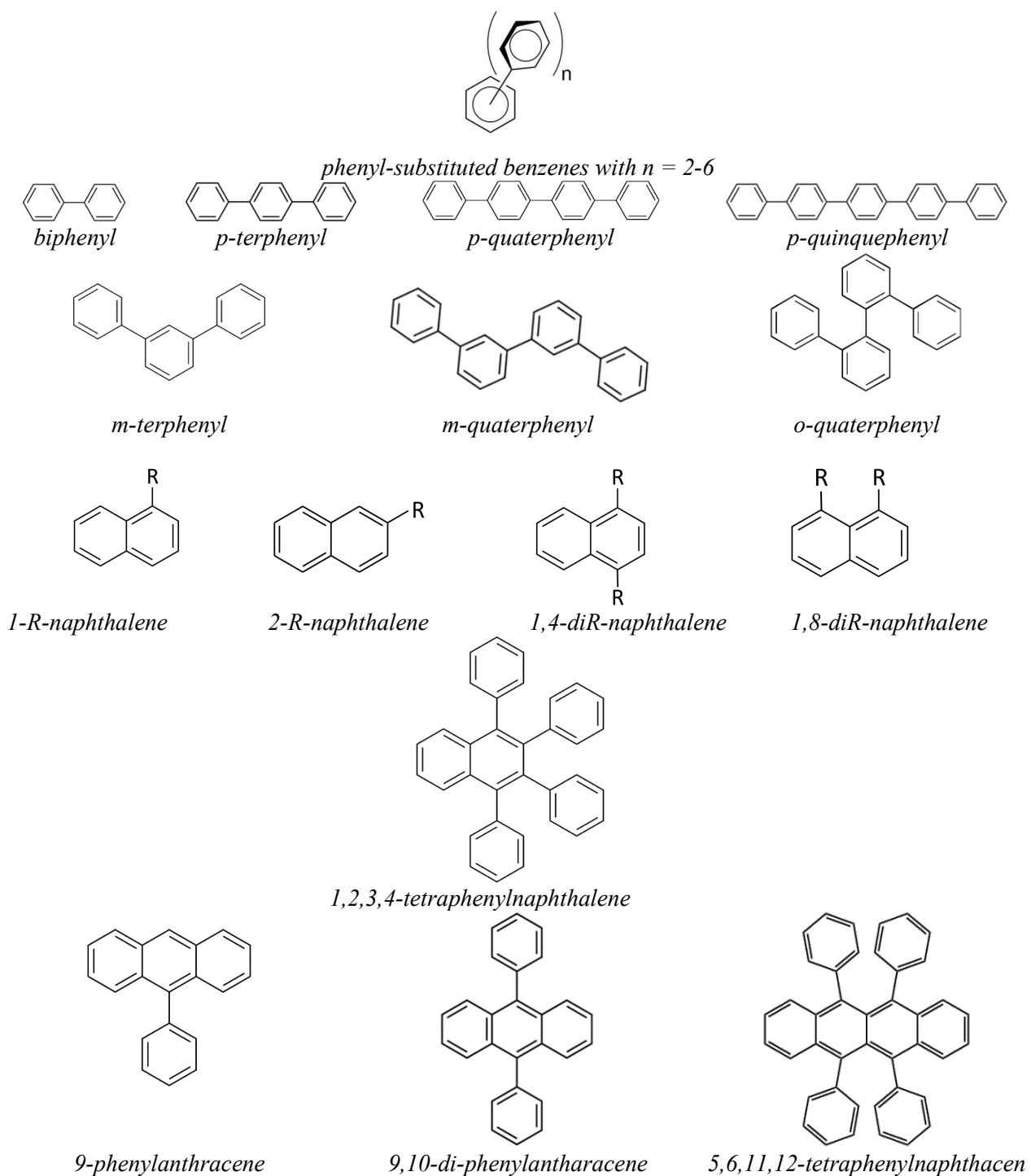


Figure 3.3.1 Structures of phenyl substituted benzenes, naphthalenes, and anthracenes studied in this work.

It was shown in the previous sections 3.1 and 3.2 that the gas phase standard molar enthalpies of formation could be successfully used to derive the dispersion interactions. Admittedly, the network of equations (3.3.1), (3.3.2), and (3.3.3) relates the thermochemical quantities that lead to the target $\Delta_f H_m^\circ(\text{g})$ - value:

$$\Delta_f H_m^\circ(\text{g}) = \Delta_f H_m^\circ(\text{cr/liq}) + \Delta_{\text{cr,l}}^{\text{g}} H_m^\circ \quad (3.3.1)$$

$$\Delta_{\text{cr}}^{\text{g}} H_m^\circ = \Delta_{\text{l}}^{\text{g}} H_m^\circ + \Delta_{\text{l}}^{\text{cr}} H_m^\circ \quad (3.3.2)$$

$$\Delta_{\text{cr}}^{\text{l}}H_{\text{m}}^{\text{o}} = \Delta_{\text{cr}}^{\text{g}}H_{\text{m}}^{\text{o}} - \Delta_{\text{l}}^{\text{g}}H_{\text{m}}^{\text{o}} \quad (3.3.3)$$

According to the common rule, all these values must refer to the same temperature (T = 298.15 K in this work). We collected available literature data on thermochemical quantities involved in the above equations and adjusted them to the reference temperature T = 298.15 K.

3.3.1. Compilation of liquid-gas, solid-gas, and solid-liquid phase transition and adjustment to the reference temperature

The compilation of enthalpies of sublimation/vaporization enthalpies $\Delta_{\text{cr,l}}^{\text{g}}H_{\text{m}}^{\text{o}}$ is given in Table 3.3.1. The compilation of enthalpies of fusion $\Delta_{\text{cr}}^{\text{l}}H_{\text{m}}^{\text{o}}$ is given in Table 3.3.2. The compilation of the molar heat capacities $C_{\text{p,m}}^{\text{o}}$ (cr or liq) and heat capacity differences $\Delta_{\text{cr,l}}^{\text{g}}C_{\text{p,m}}^{\text{o}}$ required for the temperature adjustment according to the Kirchhoff's Law is given in Table 3.3.3. The quality of the experimental data taken from the literature should be validated and checked for internal consistency. The best way to validate is to use your own complementary measurements and structure-property correlations. The sublimation/vaporization enthalpies $\Delta_{\text{cr,l}}^{\text{g}}H_{\text{m}}^{\text{o}}$ measured in this work using the transpiration method and the Knudsen-effusion method are given in Table B.1 and Table B.2. The enthalpies of fusion $\Delta_{\text{cr}}^{\text{l}}H_{\text{m}}^{\text{o}}$ measured in this work by using DSC are given in Table 3.3.2.

Table 3.3.1 Compilation of enthalpies of sublimation/vaporization $\Delta_{\text{cr,l}}^{\text{g}}H_{\text{m}}^{\text{o}}$ of aromatic compounds

Compound	M ^a	T- range	$\Delta_{\text{cr,l}}^{\text{g}}H_{\text{m}}^{\text{o}}(T_{\text{av}})$	$\Delta_{\text{cr,l}}^{\text{g}}H_{\text{m}}^{\text{o}}(298.15 \text{ K})^{\text{b}}$	Ref.
CAS		K	kJ·mol ⁻¹	kJ·mol ⁻¹	
1,2-diphenylbenzene (liq) 84-15-1	S	343.5-462.4	77.5±0.2	88.2±0.5	[79]
	T	335.5-368.4	81.1±0.6	86.7±0.7	[80]
	T	343.5-377.4	79.5±0.4	86.1±0.6	[81]
	S	450.7-650.1	64.0±0.9	90.5±1.5	[82]
	J_x			86.3±2.0	Table 3.3.5
	J_x			87.2±2.0	Table 3.3.7
				87.3±0.3 ^c	average
1,2-diphenylbenzene (cr)	K	312.3-328.6	103.4±2.4	104.4±2.4	[83]
	SC			105.7±2.0	[81]
	T_{fus}			102.4±0.7	Table 3.3.2
					102.8±0.6 ^c
1,3-diphenylbenzene (liq) 92-06-8	T_{fus}			97.9±3.0	Table 3.3.2
	J_x			98.2±2.0	Table 3.3.5
	J_x			98.7±2.0	Table 3.3.7
					98.4±1.3 ^c
1,3-diphenylbenzene (cr)				118.2±2.8	[81]
1,4-diphenylbenzene (liq) 92-94-4	T_{fus}			100.6±4.3	Table 3.3.2
	J_x			99.7±2.0	Table 3.3.5
	J_x			100.7±2.0	Table 3.3.7
					100.2±1.3 ^c
1,4-diphenylbenzene (cr)				123.8±2.4	[81]
1,3,5-triphenylbenzene (liq) 612-71-5	T_{fus}			129.4±3.8	Table 3.3.2
	J_x			131.4±2.0	Table 3.3.5
	J_x			130.8±2.0	Table 3.3.7
					130.9±1.3 ^c
1,2,3-triphenylbenzene (cr) [1165-14-6]	K	373.2-395.0	131.7±1.3	136.4±1.8	[84]
	SC	298.15		138.6±1.4	[81]
					137.8±1.1 ^c
1,2,4-triphenylbenzene (cr) [1165-53-3]	K-QCM	359.2-370.2	130.9±0.5	134.5±2.1	[85]
1,2,3,4-tetraphenylbenzene (cr) [1487-12-3]	K-QCM	411.2-433.1	149.8±3.3	158.3±3.6	[86]
1,2,4,5,-tetraphenylbenzene (cr) [3383-32-2]	K-QCM	439.3-456.3	155.3±2.1	165.6±3.0	[85]
pentaphenylbenzene (cr) [18631-82-8]	K-QCM	447.7-467.5	164.9±2.4	177.9±3.1	[86]

hexaphenylbenzene (cr) 992-04-1	mIs	625-678	163.6±5.0	197.1±5.4	[87]
	TGA	573-606	167.9±6.0	195.4±6.7	[88]
	K-QCM	491.4-510.5	166.9±6.5	186.1±6.6	[89]
	QCM	445.6-493.6	180.4±2.0	196.6±2.3	[81]
	SC	298.15		197.1±5.4	[81]
				195.8±1.8	average
hexaphenylbenzene (liq)	mIs	730-830	84.1±5.0	194.1±5.5	[87]
	T_{fus}			195.0±17.2	Table 3.3.2
				194.2±5.2 ^c	average
p-quaterphenyl (cr) 135-70-6	K	440-470	156.0±5.0	164.7±5.2	[90]
	n/a			168.4±1.6	[83]
	QCM	390-430	153.0±2.0	159.2±2.2	[91]
	K	438.7-472.5	159.9±3.2	168.6±3.4	this work
				165.6±1.2 ^c	average
p-quaterphenyl (liq)	T_{fus}			137.4±7.3	Table 3.3.2
	CGC	298.15		136.1±3.2	[92]
	J_x			137.0±2.0	Table 3.3.5
	J_x			136.7±2.0	Table 3.3.7
				136.7±1.3 ^c	average
p-quinquephenyl (cr)	QCM	470-510	196.9±2.4	210.1±2.8	[91]
p-quinquephenyl (liq) 3073-05-0	T_{fus}			182.5±12.9	Table 3.3.2
	J_x			176.5±4.0	Table 3.3.5
	J_x			172.6±4.0	Table 3.3.7
				174.9±2.8 ^c	average
m-quaterphenyl (liq) 1166-18-3	K	388.7-409.2	116.7±0.8	130.5±1.1	this work
	J_x			132.2±2.0	Table 3.3.5
	J_x			131.8±2.0	Table 3.3.7
				131.1±0.6 ^c	average
m-quaterphenyl (cr)	T_{fus}			153.0±1.9	Table 3.3.2
o-quaterphenyl (liq) 641-96-3	J_x			108.3±2.0	Table 3.3.5
	J_x			107.6±2.0	Table 3.3.7
				108.0±1.4 ^c	average
o-quaterphenyl (cr)	T_{fus}			127.6±2.8	Table 3.3.2
1-phenyl-naphthalene (liq) 605-02-7	T	313-373	88.6±2.0	(92.7±2.1)	[93]
	DC	386	103.3±0.5	81.1±1.8	[94]
	IP+E	375.0-630.2	67.3±0.3	84.3±1.0	[95]
	T	318.5-371.0	78.4±1.0	82.5±1.1	[81]
	SC	298.15		82.7±1.6	[81]
	T	313.1-369.8	79.2±0.5	83.2±0.5	Table B.1
	J_x			83.2±2.0	Table 3.3.5
	J_x			83.7±2.0	Table 3.3.7
					83.2±0.4 ^c
2-phenyl-naphthalene (liq) 612-94-2	S	373.2-462.9	75.9±0.3	86.8±0.7	[96]
	E	482.9-604.1	67.2±0.4	89.4±1.2	[95]
	T_{fus}			87.6±1.8	Table 3.3.2
	J_x			89.0±2.0	Table 3.3.5
	J_x			88.4±2.0	Table 3.3.7
				87.6±0.5 ^c	average
2-phenyl-naphthalene (cr)	K	331.1-353.2	106.6±0.8	108.9±1.2	[94]
2-(biphenyl-4-yl)naphthalene (cr) [68862-02-2]	K	405.2-437.2	137.0±0.9	143.2±1.4	[94]
2-(biphenyl-4-yl)naphthalene (liq)	T_{fus}			132.4±4.5	Table 3.3.2
2-(biphenyl-3-yl)naphthalene (liq)	K	381.1-413.2	104.4±2.5	116.7±2.6	[94]
2-(biphenyl-3-yl)naphthalene (cr) [87294-80-2]	T_{fus}			131.6±2.8	Table 3.3.2
1,2,3,4-teraphenyl-naphthalene (cr) 751-38-2	K-QCM	430.3-448.3	150.9±2.8	161.4±3.4	[89]
	QCM	338.1-370.6	156.2±0.8	160.4±1.1	[81]
	SC	298.15		164.8±3.4	[81]
	K	405.7-455.8	146.8±1.2	156.7±1.5	this work
				159.5±0.8 ^c	average
1,2,3,4-teraphenyl-naphthalene (liq)	T_{fus}			153.4±6.1	Table 3.3.2
1,4-diphenyl-naphthalene (cr) [796-30-5]	K-QCM	372.3-399.5	125.2±2.6	129.5±2.8	[89]
1,8-diphenyl-naphthalene (cr) [1038-67-1]	K-QCM	361.4-389.2	124.8±0.8	128.7±1.2	[89]
1-([1,1'-biphenyl]-4-yl)-naphthalene (cr) 82777-03-5	K-QCM	390.2-414.3	136.1±0.9	141.2±1.5	[89]
1,8-di([1,1'-biphenyl]-4-yl)naphthalene (cr) 82777-02-4	K-QCM	454.3-473.4	174.0±3.0	186.3±3.6	[89]
9-phenyl-anthracene (cr) 602-55-1	K	353-426	115.3±3.0	119.3±3.1	[97]
	TE	353-428	115.6±2.5	119.6±2.6	[98]
	T	373-453	118.7±2.0	123.9±2.1	[93]
	SC	298.15		125.5±0.8	[81]

9-phenyl-anthracene (liq)	TE	435-507	84.5±2.5	103.9±2.6	124.6±0.7 ^c	average
	T_{fus}			108.0±2.8		[98]
	J_x			108.3±2.0		Table 3.3.2
	J_x			108.0±2.0		Table 3.3.5
						107.3±1.2 ^c
9,10-diphenyl-anthracene (cr) 1499-10-1	HSA	481-502	156.9±5.0	168.1±5.4		[99]
	K	393-433	143.6±5.0	150.3±5.1		[100]
	T	423-453	137.5±5.0	145.6±5.2		[93]
	QCM	341-373	149.3±0.8	153.6±1.1		[81]
	SC	298.15		152.9±2.0		[81]
	K	404.0-454.0	148.2±3.9	155.7±4.0		this work
					153.6±0.9 ^c	average
9,10-diphenyl-anthracene (liq)	T_{fus}			138.3±5.9		Table 3.3.2
	J_x			135.9±3.0		Table 3.3.5
	J_x			135.6±3.0		Table 3.3.7
					136.0±2.0 ^c	average
5,6,11,12-tetraphenyltetracene (cr) 517-51-1	K	453-523	162.8±4.2	(180.2±5.0)		[100]
	K-QCM	503.5-522.6	177.7±2.2	197.4±3.3		[101]
	QCM	450.5-490.7	198.0±1.3	213.8±1.8		[81]
	SC	298.15		213.2±4.0		[81]
					210.5±1.5 ^c	average

^a Techniques: T = transpiration method; J_x – from correlation of experimental vaporization enthalpies with retention indices (see text); T_{fus} = derived from experimental data according to Eq. (3.3.2) or (3.3.3)(see text); CGC = correlation gas-chromatography; DC = drop microcalorimetry; S = static method; n/a = method is not available; QCM = quartz-crystal-microbalance; K = Knudsen effusion method; K-QCM = Knudsen effusion method combined with quartz-crystal-microbalance for mass-loss measurements; mIs = micro-isoteniscope; TE = torsion-effusion method; SC = indirect method based on the data from high-precision solution calorimetry; HAS = head-space-analysis; E = ebulliometry; IP = inclined-piston method; TGA = thermogravimetry.

^b Experimental values the vaporization and sublimation enthalpies measured at T_{av} were adjusted to the reference temperature using the heat capacity differences given in Table B.1. Uncertainties is expressed as expanded uncertainties (0.95 level of confidence with $k=2$). They include uncertainties from the experimental conditions and the fitting equation, vapour pressures, and uncertainties from adjustment of sublimation/vaporization enthalpies to the reference temperature $T = 298.15$ K [28,29].

^c Weighted mean value (the uncertainty was taken as the weighing factor). Uncertainty of the sublimation/vaporization enthalpy is expressed as the expanded uncertainty (0.95 level of confidence, $k = 2$). Values in brackets were excluded by the averaging. Values highlighted in bold were recommended for thermochemical calculations.

Table 3.3.2 Phase transitions thermodynamics of aromatic compounds (in $\text{kJ}\cdot\text{mol}^{-1}$)^a

Compounds	T_{fus} , K	$\Delta_{cr}^1 H_m^o$ at T_{fus}	$\Delta_{cr}^1 H_m^o$ ^b	$\Delta_{cr}^g H_m^o$ ^c	$\Delta_1^g H_m^o$ ^d
			298.15 K		
1	2	3	4	5	6
1,4-diphenylbenzene	486.3±0.5	35.5±1.3 [102]			
	493.1±1.0	(41.6±0.8)[103]			
	487.0±0.5	35.3±1.0 [104]			
	486.3±0.5	35.5±0.5 [105]			
	482.4±1.0	35.3±0.2 [80]			
	490.9±0.5	32.9±0.6 [106]			
	487.0±0.5	35.4±0.5 [107]			
	487.2±0.2^c	35.2±0.2^c	23.2±3.6	123.8±2.4 [81]	100.6±4.3
1,3-diphenylbenzene	360.0±1.0	22.6±1.0 [108]			
	361.0±1.0	25.3±0.5 [109]			
	361.2±0.5	(31.0±0.2) [80]			
	361.8±0.6	25.5±0.4 [106]			
	361.0±0.5	23.8±0.2 [110]			
	361.0±0.5	24.7±0.5 [110]			
	361.1±0.3^c	24.3±0.2^c	20.3±1.2	118.2±2.8 [81]	97.9±3.0
1,2-diphenylbenzene	329.4±0.5	17.2±0.1 [111]			
	328.4±0.5	17.2±1.0 [112]			
	327.8±0.5	16.8±0.2 [80]			
	329.4±0.2	17.0±0.4 [106]			
	329.4±0.5	17.2±0.5 [111]			
	329.1±0.2^c	17.1±0.1^c	15.1±0.6	102.4±0.7^f	87.3±0.3
1,3,5-triphenylbenzene	448.5±0.5	22.9±0.6 [109]			

	446.0±1.0	33.4±0.5 [113]			
	445.2±0.2	32.6±0.5 [80]			
	448.0±0.5	31.1±1.0 [114]			
	447.3±0.1	31.1±0.8 [115]			
	446.9±0.1^c	32.5±0.3^c	20.4±3.6	149.8±1.6 [116]	129.4±3.9
1,2,3-triphenylbenzene	431.0±2.0 [117]	31.0±1.0 (WC=72) ^j	20.0±3.3	138.6±0.8 [81]	118.6±3.4
1,2,4-triphenylbenzene	393.6±2.0 [117]	28.3±1.0 (WC=72)	20.4±2.4	134.5±2.1 [85]	114.1±3.2
1,2,3,4-tetraphenylbenzene	467.0±3.0 [118]	35.5±1.0 (WC=76)	18.9±5.0	158.3±3.6 [86]	139.4±6.2
1,2,4,5-tetraphenylbenzene	547.5±2.0 [117]	41.6±1.0 (WC=76)	17.1±7.5	165.6±3.0 [85]	148.5±8.1
pentaphenylbenzene	700.0±3.0 [118]	53.9±1.0 (WC=77)	7.3±14.0	177.9±3.1 [86]	170.6±14.3
hexaphenylbenzene	723.8±0.8	57.6±0.9 [this work]	0.8±17.1	195.8±1.8	195.0±17.2
p-quaterphenyl	587.2±0.3	(37.8±1.1) [102]			
	586.7±0.3	(57.6±0.9) [103]			
	587.2±0.8	(37.8±1.0) [119]			
	594.4±0.5	(53.4±1.1) [106]			
	587.2±0.9	(60.8±3.0) [120]			
	593.0±0.4	50.9±1.1 [this work]			
	593.5±0.5^c	52.2±0.8^c	28.2±7.2	165.6±1.2	137.4±7.3
o-quaterphenyl	390.6±0.4	27.2±0.5 [106]	19.6±2.4	127.6±2.8 ^f	108.0±1.4
m-quaterphenyl	360.0±0.1	27.7±0.5 [106]			
	359.2±0.5	27.1±1.5 [this work]			
	360.0±0.2^c	27.6±0.5^c	22.5±1.6	153.0±1.9^f	130.5±1.1
p-quinquephenyl	(659.6±0.6)	(42.3±2.7) [102]			
	(661.0±2.0)	(44.0±2.0) [121]			
	(663.4±3.9)	(48.8±3.9) [106]			
	718±3 [122]	68.9±2.0^g	27.6±12.6	210.1±2.8	182.5±12.9
2-phenyl-naphthalene	373.5±0.2	(17.9±0.2) [94]			
	374.8±0.1	22.6±0.1 [95]			
		25.7±0.5^h	21.4±1.4	108.9±1.2	87.5±1.8
1,4-diphenyl-naphthalene	409.0±3.0 [118]	25.8±1.0 (WC=63) ^j	17.4±2.7	129.5±2.8	112.1±3.9
1,8-diphenyl-naphthalene	418.0±2.0 [117]	26.3±1.0 (WC=63)	17.3±2.9	128.7±1.2	111.4±3.1
1-([1,1'-biphenyl]-4-yl)-naphthalene	424.0±3.0 [118]	26.7±1.0 (WC=63)	17.3±3.0	141.2±1.5	123.9±3.4
1,8-di([1,1'-biphenyl]-4-yl)naphthalene	477±3 [118]	34.3±1.0 (WC=72)	14.4±6.1	186.3±3.6	171.9±7.1
1,2,3,4-tetra-phenylnaphthalene	479.0±0.1	24.8±0.6 [115]			
	477.1±0.2	26.4±0.1 [this work]			
	478.6±0.1^c	26.3±0.2^c	6.1±6.0	159.5±0.8	153.4±6.1
2-(biphenyl-4-yl)naphthalene	489.5±0.5	25.10±0.1 [94]	10.8±4.3	143.2±1.4	132.4±4.5
2-(biphenyl-3-yl)naphthalene	346.3±0.1	18.5±0.2 [94]	14.9±1.1	131.6±2.8 ^f	116.7±2.6
9-phenyl-anthracene	427.6±0.8	25.5±0.4 [123]	16.6±2.7	124.6±0.7	108.0±2.8
9,10-diphenyl-anthracene	523.2±0.2	30.6±0.7 [124]			
	521.3±1.1	30.1±1.0 [124]			
	524.0±0.2	31.4±0.5 [this work]			
	523.6±0.2^c	31.0±0.4^e (34.7±0.4)ⁱ	15.3±5.8	153.6±0.9	138.3±5.9
5,6,11,12-tetraphenyltetracene	603.1±1.0	46.6±2.3 [124]			
	603.1±1.1	46.6±2.5 [124]			
	603.1±0.7^c	46.6±1.7^c	6.1±12.2	210.5±1.5	204.4±12.3

^a Uncertainties are presented as expanded uncertainties (0.95 level of confidence with k=2).

^b The experimental enthalpies of fusion $\Delta_{cr}^l H_m^o$ measured at T_{fus} were adjusted to 298.15 K with help of the equation [18]: $\Delta_{cr}^l H_m^o(298.15\text{ K})/(\text{J}\cdot\text{mol}^{-1}) = \Delta_{cr}^l H_m^o(T_{fus}/\text{K}) - (\Delta_{cr}^g C_{p,m}^o - \Delta_{cr}^g C_{p,m}^o) \times [(T_{fus}/\text{K}) - 298.15\text{ K}]$ where $\Delta_{cr}^g C_{p,m}^o$ and $\Delta_{cr}^g C_{p,m}^o$ were taken from Table 3.3.3. Uncertainties in the temperature adjustment of fusion enthalpies from T_{fus} to the reference temperature are estimated to account with 30 % to the total adjustment [18].

^c Experimental values from Table 3.3.1

^d Calculated as the difference between column 5 and 4 in this table.

^e Weighted average value (with the experimental uncertainty used as the weighing factor). Values highlighted in bold were used for thermochemical calculations.

^f Calculated according to Eq. (3.3.2) with experimental vaporization enthalpies from Table 3.3.1 and fusion enthalpy from this table.

^g Calculated according to structure property relationships shown in Table 3.3.9.

^h The solid-solid phase transition enthalpy 3.1±0.5 at 331.4±0.5 K [95] was added to the fusion enthalpy.

ⁱ The solid-solid phase transition enthalpy 3.7±0.1 at 459.4±0.2 K measured by DSC [124] was added to the fusion enthalpy.

^j The *Walden's Constant* (WC) calculated according to Eq. (4.3.8)

Table 3.3.3 Compilation of molar heat capacities $C_{p,m}^{\circ}(\text{cr or liq})$ and heat capacity differences $\Delta_{\text{cr,l}}^{\text{g}}C_{p,m}^{\circ}$ at $T = 298.15 \text{ K}$ (in $\text{J}\cdot\text{K}^{-1}\cdot\text{mol}^{-1}$)

Compounds	$C_{p,m}^{\circ}(\text{cr})^{\text{a}}$	$-\Delta_{\text{cr}}^{\text{g}}C_{p,m}^{\circ}{}^{\text{b}}$	$C_{p,m}^{\circ}(\text{liq})^{\text{a}}$	$-\Delta_{\text{l}}^{\text{g}}C_{p,m}^{\circ}{}^{\text{b}}$
1,2-diphenylbenzene	274.7 [111]	42.0	369.1 [111]	106.5
1,3-diphenylbenzene	277.4 [125]	42.4	366.4	105.8
1,4-diphenylbenzene	278.1 [105]	42.5	366.4	105.8
1,3,5-triphenylbenzene	361.0 [113]	54.9	484.2	136.5
1,2,3-triphenylbenzene	356.2 [125]	54.2	484.2	136.5
1,2,4-triphenylbenzene	356.2 ^c	54.2	484.2	136.5
1,2,3,4-tetraphenylbenzene	453.0	68.7	602.0	167.1
1,2,4,5-tetraphenylbenzene	453.0	68.7	602.0	167.1
penta-phenylbenzene	540.0	81.8	719.8	197.7
hexa-phenylbenzene	627.0	94.8	837.6	228.4
p-quaterphenyl	363.5 [125]	55.3	484.2	136.5
p-quinquephenyl	455.5 [106]	69.0	602.0	167.1
m-quaterphenyl	359.5 [106]	54.7	484.2	136.5
o-quaterphenyl	359.1 [106]	54.7	484.2	136.5
1-phenyl-naphthalene	-	-	310.7 [95]	91.4
2-phenyl-naphthalene	274.8 [95]	37.9	310.7 ^c	91.4
1,4-diphenyl-naphthalene	324.0 [89]	49.4	440.0	125.0
1,8-diphenyl-naphthalene	328.3 [89]	50.0	440.0	125.0
1-([1,1'-biphenyl]-4-yl)-naphthalene	328.3 [89]	50.0	440.0	125.0
1,8-di([1,1'-biphenyl]-4-yl)naphthalene	490.9 [89]	74.4	675.6	186.2
1,2,3,4-tetra-phenyl-naphthalene	491.6 [89]	74.5	675.6	186.2
2-(biphenyl-4-yl)naphthalene	330.4 [94]	50.3	440.0	125.0
2-(biphenyl-3-yl)naphthalene	330.4 ^c	50.3	440.0	125.0
9-phenyl-anthracene	294.8	45.0	395.8	113.5
9,10-diphenyl-anthracene	381.8	58.0	513.6	144.1
5,6,11,12-tetraphenyltetracene	607.2	91.8	822.8	224.5

^a Calculated by the group-contribution procedure developed by Chickos *et al.* [16].

^b Calculated according to the procedure developed by Acree and Chickos [18].

^c Supposed to be the same as for the appropriate isomer with the known experimental heat capacity.

It has been found, that experimental $\Delta_{\text{f}}H_{\text{m}}^{\circ}(\text{cr})$ -values for di- and tri-phenylbenzenes have been reported several times (see Table 3.3.4). The available results are consistent within their experimental uncertainties. Therefore, the weighted mean values were calculated for 1,2-, 1,3-, 1,4-diphenylbenzene and 1,3,5-triphenylbenzene (the uncertainty was used as a weighing factor). These values were used to derive experimental $\Delta_{\text{f}}H_{\text{m}}^{\circ}(\text{g})$ -values and to further develop the dispersion interactions.

Table 3.3.4 Compilation of experimental $\Delta_{\text{f}}H_{\text{m}}^{\circ}(\text{cr})$ -values for di- and tri-phenylbenzenes (in $\text{kJ}\cdot\text{mol}^{-1}$, at $T = 298.15 \text{ K}$ and $p^{\circ} = 0.1 \text{ MPa}$)^a

Compound	$\Delta_{\text{f}}H_{\text{m}}^{\circ}(\text{cr})$
1,2-diphenylbenzene	178.3±1.2 [80]
	182.5±3.6 [83]

	178.7±1.1^b
1,3-diphenylbenzene	161.8±1.2 [80] 161.3±3.8 [83] 161.7±1.2^b
1,4-diphenylbenzene	162.6±5.2 [90] 152.5±0.9 [80] 158.8±3.4 [83] 153.2±0.9^b
1,3,5-triphenylbenzene	224.6±5.4 [126] 218.8±5.7 [127] 220.0±1.2 [80] 219.0±4.8 [84] 220.1±1.1^b

^a Uncertainties are expressed as the twice standard deviations.

^b Weighted mean value (the uncertainty was taken as the weighing factor). Values highlighted in bold were recommended for thermochemical calculations.

3.3.2. Validation of the experimental data on phase transitions

A valuable option for establishing the consistency of experimental data on phase transitions (liquid-gas, solid-gas, and solid-liquid) for the compound examined is the common thermochemical equation Eqs. (3.3.2) and (3.3.3). As an example, let us consider the collection of phase transition for 1,2-diphenylbenzene (ortho-terphenyl). Indeed, for this compound, the averaged vaporization enthalpy $\Delta_1^g H_m^o(298.15 \text{ K}) = 87.3 \pm 0.3 \text{ kJ}\cdot\text{mol}^{-1}$ was derived from six entries included in Table 3.3.1. In contrast, the sublimation enthalpy $\Delta_{cr}^g H_m^o(298.15 \text{ K}) = 102.8 \pm 0.6 \text{ kJ}\cdot\text{mol}^{-1}$ is less reliable, because it was derived only from three entries (see Table 3.3.1). The consistency of phase transitions available for 1,2-diphenylbenzene can be easily established with help of Eq. (3.3.3) and the averaged experimental enthalpy of fusion for this compound $\Delta_{cr}^l H_m^o(298.15 \text{ K}) = 15.1 \pm 0.6 \text{ kJ}\cdot\text{mol}^{-1}$ (see Table 3.3.2) as follows:

$$\Delta_{cr}^l H_m^o(298.15 \text{ K}, 1,2\text{-diphenylbenzene}) = 102.8 - 87.3 = 15.5 \pm 0.7 \text{ kJ}\cdot\text{mol}^{-1} \quad (3.3.4)$$

This estimate is in an excellent agreement with the experiment $\Delta_{cr}^l H_m^o(298.15 \text{ K}) = 15.1 \pm 0.6 \text{ kJ}\cdot\text{mol}^{-1}$ (see Table 3.3.2). In the same way we checked the consistency of phase transitions for other compounds compiled in Table 3.3.1 and Table 3.3.2. The consistency of the $\Delta_{cr}^g H_m^o(298.15 \text{ K})$, $\Delta_1^g H_m^o(298.15 \text{ K})$, and $\Delta_{cr}^l H_m^o(298.15 \text{ K})$ phase transitions for benzene, naphthalene, and anthracene derivatives proved in this work could be regarded as an indirect support of the reliability of these thermochemical results.

Another valuable option for establishing the consistency of experimental data on liquid-gas phase transitions is correlation of vaporization enthalpies with retention indices. The literature data available on the Lee retention indices, [128–130] and Kratz retention indices, [131] for substituted benzenes, naphthalenes, and anthracenes were taken for correlation with the $\Delta_1^g H_m^o(298.15 \text{ K})$ -values

evaluated in Table 3.3.2). Results from these correlations are given in Tables 3.3.7 and 3.3.9. It has turned out, that the required indices for p-quaterphenyl and p-quinquephenyl are absent in the literature, however they were derived from linear correlations developed for Lee retention indices (see Table 3.3.6) and Kratz retention indices (see Table 3.3.8)

Table 3.3.5 Correlation of vaporization enthalpies, $\Delta_1^g H_m^o(298.15 \text{ K})$, of substituted benzenes, naphthalenes, and anthracenes with their Lee indices (J_{Lee})^a

Compound	J_{Lee} ^b	$\Delta_1^g H_m^o(298.15 \text{ K})_{\text{exp}}$ ^c kJ·mol ⁻¹	$\Delta_1^g H_m^o(298.15 \text{ K})_{\text{calc}}$ ^d kJ·mol ⁻¹	Δ^e kJ·mol ⁻¹
1-phenyl-naphthalene	312.7	83.2	83.5±2.0	-0.3
2-phenyl-naphthalene	330.7	87.8	89.0±2.0	-1.2
o-terphenyl	322	87.9	86.3±2.0	1.6
m-terphenyl	361	97.9	98.2±2.0	-0.3
p-terphenyl	366	100.6	99.7±2.0	0.9
1,3,5-triphenyl-benzene	469.5	129.4	131.4±2.0	-2.0
o-quaterphenyl	394		108.3±2.0	
m-quaterphenyl	471	130.5	131.8±2.0	-1.3
p-quaterphenyl	488	137.4	137.0±2.0	0.4
p-quinquephenyl	617		176.5±2.0	
9-phenylanthracene	394	108	108.3±2.0	-0.3
9,10-diphenylanthracene	484.3	138.7	135.9±3.0	2.8

^a Uncertainties are presented as expanded uncertainties (0.95 level of confidence with k=2).

^b Lee indices, J_{Lee} , on standard non-polar columns from [128–130]

^c From Table 3.3.1.

^d Calculated using equation: $\Delta_1^g H_m^o(298.15 \text{ K}) / (\text{kJ} \cdot \text{mol}^{-1}) = -12.1 + 0.3056 \times J_{Lee}$ with ($R^2 = 0.9957$)

^e Difference between experimental and calculated values.

Table 3.3.6 Correlation of Lee indices with number of phenyl rings in the terphenyl series.

Compound	N_{rings} ^a	$J_{Lee}(\text{exp})$ ^b	$J_{Lee}(\text{calc})$ ^c	Δ^d
biphenyl	2	234	236	-2
p-terphenyl	3	366	363	3
p-quaterphenyl	4	488	490	-2
p-quinquephenyl	5		617	

^a Number of phenyl rings in the compound.

^b From Table 3.3.5

^c Calculated using equation: $J_{Lee} = -18.3 + 127 \times N_{rings}$ with ($R^2 = 0.9957$)

^d Difference between experimental and calculated values.

Table 3.3.7 Correlation of vaporization enthalpies, $\Delta_1^g H_m^o(298.15 \text{ K})$, of substituted benzenes, naphthalenes, and anthracenes with their Kratz indices (J_{Kratz})^a

Compound	J_{Kratz} ^b	$\Delta_1^g H_m^o(298.15 \text{ K})_{\text{exp}}$ ^c kJ·mol ⁻¹	$\Delta_1^g H_m^o(298.15 \text{ K})_{\text{calc}}$ ^d kJ·mol ⁻¹	Δ^e kJ·mol ⁻¹
biphenyl	1392	65.8 [47]	64.7±2.0	1.1
1-phenyl-naphthalene	1822	83.2	83.7±2.0	-0.5
2-phenyl-naphthalene	1930	87.8	88.4±2.0	-0.6
o-terphenyl	1903	87.9	87.2±2.0	0.7
m-terphenyl	2164	97.9	98.7±2.0	-0.8
p-terphenyl	2208	100.6	100.7±2.0	-0.1

1,3,5-triphenylbenzene	2891	129.4	130.8±2.0	-1.4
o-quaterphenyl	2365		107.6±2.0	
m-quaterphenyl	2923	130.5	132.2±2.0	-1.7
p-quatrephenyl	3024	137.4	136.7±2.0	0.7
p-quinquephenyl	3840		172.6±2.0	
9-phenylanthracene	2374	108.0	108.0±2.0	0.0
9,10-diphenylanthracene	3000	138.7	135.6±3.0	3.1

^a Uncertainties are presented as expanded uncertainties (0.95 level of confidence with k=2).

^b Kratz indices, J_x , on standard non-polar columns from [131].

^c From Table 3.3.1.

^d Calculated using equation: $\Delta_1^{\text{g}}H_m^{\text{o}}(298.15 \text{ K}) / (\text{kJ}\cdot\text{mol}^{-1}) = 3.3 + 0.0441 \times J_{\text{Kratz}}$ with ($R^2 = 0.9971$).

^d Difference between experimental and calculated values.

Table 3.3.8 Correlation of Kratz indices with number of phenyl rings in the terphenyl series.

Compound	$N_{\text{rings}}^{\text{a}}$	$J_{\text{Kratz}}(\text{exp})^{\text{b}}$	$J_{\text{Kratz}}(\text{calc})^{\text{c}}$
biphenyl	2	1392	1392
p-terphenyl	3	2208	2208
p-quaterphenyl	4		3024
p-quinquephenyl	5		3840

^a Number of phenyl rings in the compound.

^b From Table 3.3.7

^c Calculated using equation: $J_{\text{Kratz}} = -240 + 816 \times N_{\text{rings}}$ with ($R^2 = 0.9999$)

It is known, that the $\Delta_1^{\text{g}}H_m^{\text{o}}(298.15 \text{ K})$ -values correlate linearly with retention indices in various homologous series of alkylbenzenes, alkanes, aliphatic ethers, alcohols, or in a series of structurally similar compounds [132]. As expected, the $\Delta_1^{\text{g}}H_m^{\text{o}}(298.15 \text{ K})$ -values of substituted benzenes, naphthalenes, and anthracenes correlated linearly with J_{Lee} values (see correlation as a footnote to Table 3.3.5) as well as with J_{Kratz} (see correlation as a footnote to Table 3.3.8). The results of the correlations with retention indices are in a good agreement with those experimental results evaluated in Table 3.3.2. Such good agreement can be seen as additional validation of the experimental data validated and evaluated in this work (see Table 3.3.1 and Table 3.3.2). It can be seen from Table 3.3.5 and Table 3.3.7, that differences between experimental and calculated according to values are mostly below $1.0 \text{ kJ}\cdot\text{mol}^{-1}$. Hence, the uncertainties of enthalpies of vaporization which were estimated from the correlation the $\Delta_1^{\text{g}}H_m^{\text{o}}(298.15 \text{ K}) - J_x$ are evaluated with these uncertainties of $\pm 2.0 \text{ kJ}\cdot\text{mol}^{-1}$. The agreement for the anthracene derivatives is somewhat lower, and the uncertainties of $\pm 3.0 \text{ kJ}\cdot\text{mol}^{-1}$ were ascribed for this series.

An additional structure-property correlations have been performed in order to establish reliable enthalpy of fusion of p-quinquephenyl as follows. A thermal analysis data available for the p-quinquephenyl reveal at least three solid–solid transitions below the melting point: I (ring flips), II (crystal-nematic), and III (nematic-isotropic) [106]. The enthalpy of sublimation for this compound was measured between 470 and 510 K (see Table 3.3.1). In order to derive the enthalpy of fusion for

this compound we decided to correlate the fusion properties within the series of p-terphenyls as follows. The possibility of a robust linear correlation between the melting temperature and the number of rings in the p-terphenyl series was already shown by Rodrigues *et al.* [106]. In Table 3.3.9 we collected T_{fus} of biphenyl, p-terphenyl, p-quaterphenyl, p-quinquephenyl, and p-sexiphenyl and correlated these values with the number of phenyl rings, N_{rings} , in each compound.

Table 3.3.9 Correlation of experimental fusion temperatures (T_{fus}), with number of phenyl rings in the terphenyl series.

Compound	N_{rings} ^a	$T_{fus}(\text{exp})$ ^b	$T_{fus}(\text{calc})$ ^c	Δ^d
		K	K	K
biphenyl	2	342 [47]	351	-9
p-terphenyl	3	487	474	14
p-quaterphenyl	4	594	596	-2
p-quinquephenyl	5	718 [122]	718	0
p-sexiphenyl	6	838 [133]	841	-3

^a Number of phenyl rings in the compound.

^b From Table 3.3.2

^c Calculated using equation: $\Delta_{cr}^1 H_m^o(T_{fus}) = 106.7 + 122.3 \times N_{rings}$ with ($R^2 = 0.9981$).

^d Difference between experimental and calculated values.

A remarkable linear $T_{fus} - N_{rings}$ correlation (see footnote in Table 3.3.9) has inspired to correlate the fusion enthalpies in this series with the N_{rings} . Data required for this correlation are collected in Table 3.3.10.

Table 3.3.10 Correlation of experimental fusion enthalpies, $\Delta_{cr}^1 H_m^o(T_{fus})$, with number of phenyl rings in the terphenyl series.

Compound	N_{rings} ^a	$\Delta_{cr}^1 H_m^o(T_{fus})(\text{exp})$ ^b	$\Delta_{cr}^1 H_m^o(T_{fus})(\text{calc})$ ^c	Δ^d
		$\text{kJ} \cdot \text{mol}^{-1}$	$\text{kJ} \cdot \text{mol}^{-1}$	$\text{kJ} \cdot \text{mol}^{-1}$
biphenyl	2	18.6	18.5	0.1
p-terphenyl	3	35.2	35.3	-0.1
p-quaterphenyl	4	52.2	52.1	0.1
p-quinquephenyl	5		68.9	

^a Number of phenyl rings in the compound.

^b From Table 3.3.2

^c Calculated using equation: $\Delta_{cr}^1 H_m^o(T_{fus}) = -15.1 + 16.8 \times N_{rings}$ with ($R^2 = 0.9999$)

^d Difference between experimental and calculated values.

It has turned out that also a perfect ($R^2 = 0.9999$) linear correlation is established between $\Delta_{cr}^1 H_m^o(T_{fus})$ and N_{rings} (see footnote in Table 3.3.10). Using this correlation, a theoretical $\Delta_{cr}^1 H_m^o(T_{fus}) = 68.9 \pm 2.0 \text{ kJ} \cdot \text{mol}^{-1}$ was estimated and used to reconcile phase transitions of p-quinquephenyl in Table 3.3.1 and Table 3.3.2. The thermochemical quantities evaluated in Table 3.3.1 and Table 3.3.2 have been used to derive the gas-phase enthalpy of formation of phenyl substituted benzenes,

naphthalenes, and anthracenes according to Eq. (3.3.1). The resulting $\Delta_f H_m^0(g)$ -values have been used to discuss nearest-neighbour interactions on the aromatic rings as manifestation of the dispersion forces in these molecules.

3.3.3. Nearest-neighbour interactions: agglomeration of substituents in the benzene ring

Mono-, di-, tri-, tetra-, penta-, and hexa-phenylbenzenes are interesting but still simple poly-aromatic compounds. In these poly-phenylbenzenes, the attractive part of the van der Waals dispersion forces is the main component of the intramolecular interactions. The gradual agglomeration of phenyl substituents distributed around the central benzene ring makes poly-phenylbenzenes an interesting example for tracking the energetics of nearest-neighbour interactions and structural changes at the molecular level. The experimental $\Delta_f H_m^0(g, 298\text{ K})$ -values required for the thermodynamic analysis are collected in Table 3.3.11.

Table 3.3.11 Compilation of the experimental $\Delta_f H_m^0(g)$ -values for poly-phenyl-benzenes and correlation of reaction enthalpies $\Delta_r H_m^0(g)R$ and strain enthalpies H_S with their amount of dispersion contributions ($E_{\text{disp-D3}}$) calculated by the DFT-D3 (in $\text{kJ}\cdot\text{mol}^{-1}$, at $T = 298.15\text{ K}$ and $p^\circ = 0.1\text{ MPa}$)^a

Compound	$\Delta_f H_m^0(\text{cr})_{\text{exp}}$	$\Delta_{\text{cr}}^g H_m^0$	$\Delta_f H_m^0(g)_{\text{exp}}$ ^b	$\Delta_r H_m^0(g)R$ ^c	H_S ^d	$E_{\text{disp-D3}}$ ^e
1	2	3	4	5	6	7
benzene			82.9±0.9 [116]	-	-	-13.4
biphenyl	97.9±1.1 [134]	81.8±0.2 [134]	179.7±1.1	-	-4.5	-40.2
1,2-diphenylbenzene	178.7±1.1 ^f	102.4±0.7 ^g	281.1±1.3	4.6	-5.0	-76.7
1,3-diphenylbenzene	161.7±1.2 ^f	118.2±2.8 [81]	279.9±3.0	3.4	-6.2	-67.9
1,4-diphenylbenzene	153.2±0.9 ^f	123.8±2.8 [81]	277.0±2.9	0.5	-9.1	-67.2
1,2,3-triphenylbenzene	242.6±5.3 [84]	137.8±1.1 ^g	380.4±5.4	7.1	-7.6	-115.1
1,2,4-triphenylbenzene	243.6±4.4 [85]	134.5±2.1 ^g	378.1±4.9	4.8	-9.9	-104.6
1,3,5-triphenylbenzene	220.1±1.1 ^f	149.8±1.6 [116]	369.9±1.9	-3.4	-18.1	-96.5
1,2,3,4-tetraphenylbenzene	330.5±7.3 [86]	158.3±3.6 ^g	488.8±8.1	18.7	-1.1	-153.7
1,2,4,5-tetraphenylbenzene	311.8±5.9 [85]	165.6±3.0 ^g	477.4±6.6	7.3	-12.5	-142.2
pentaphenylbenzene	426.3±9.0 [86]	177.9±3.1 ^g	604.2±9.5	37.3	12.4	-193.1
hexaphenylbenzene	520.1±8.0 [85]	195.8±1.8 ^g	715.9±8.2	52.2	22.2	-244.3

^a Uncertainties are expressed as the twice standard deviations.

^b Calculated as sum of column 2 and 3 from this table.

^c Calculated according to Eq. (3.3.5) using the Hess's Law and $\Delta_f H_m^0(g)_{\text{exp}}$ given in this table.

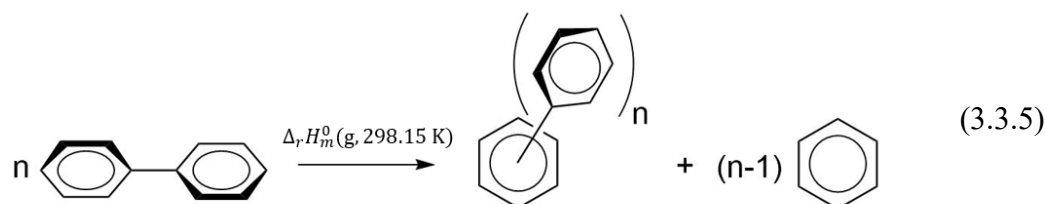
^d Calculated according to Eq. (3.1.1) with the strain-free increments $C_B H[2C_B] = 13.72\text{ kJ}\cdot\text{mol}^{-1}$ and $C_B[C, 2C_B] = 23.51\text{ kJ}\cdot\text{mol}^{-1}$ from Beckhaus [76].

^e Calculated with the DFT-D3 in this work.

^f Averaged values from Table 3.3.4.

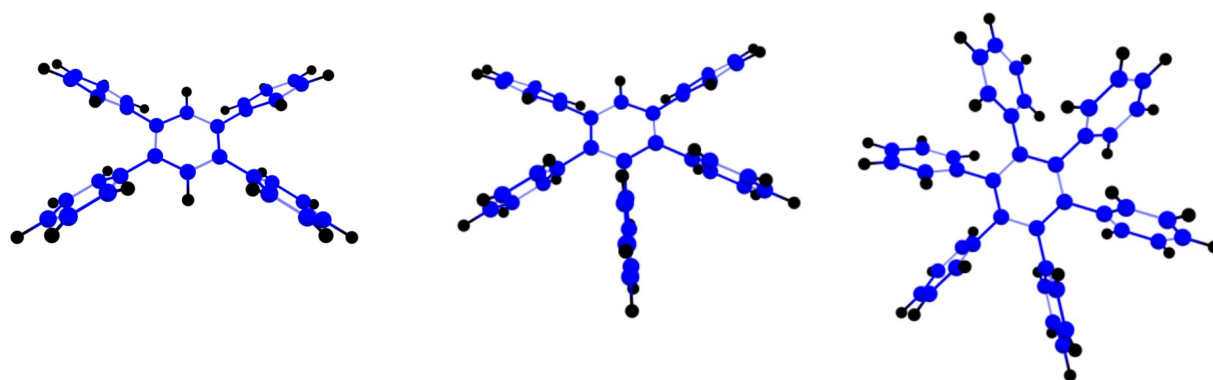
^g Recommended values from Table 3.3.1.

There are few possibilities (or scales) to discuss substituents interactions between phenyl rings. The first scale is to use a homodesmotic reaction [135] according to Eq. (3.3.6) to assess the overall number of substituent interactions in poly-phenylbenzenes.



The results are given in Table 3.3.11, column 5. The repulsions of two phenyl rings in ortho-position on the benzene ring leads to a weak destabilization $\Delta_r H_m^{\circ}(\text{g})_{\text{R}} = 4.6 \text{ kJ}\cdot\text{mol}^{-1}$ for 1,2-diphenylbenzene and 1,2,4-triphenylbenzene ($\Delta_r H_m^{\circ}(\text{g})_{\text{R}} = 4.8 \text{ kJ}\cdot\text{mol}^{-1}$). This destabilization increased only slightly in 1,2,3-triphenylbenzene ($\Delta_r H_m^{\circ}(\text{g})_{\text{R}} = 7.1 \text{ kJ}\cdot\text{mol}^{-1}$) and 1,2,4,5-tetraphenylbenzene ($\Delta_r H_m^{\circ}(\text{g})_{\text{R}} = 7.3 \text{ kJ}\cdot\text{mol}^{-1}$). The destabilization increased gradually with the agglomeration of phenyl rings in 1,2,3,4-tetraphenylbenzene ($\Delta_r H_m^{\circ}(\text{g})_{\text{R}} = 18.7 \text{ kJ}\cdot\text{mol}^{-1}$), pentaphenylbenzene ($\Delta_r H_m^{\circ}(\text{g})_{\text{R}} = 37.3 \text{ kJ}\cdot\text{mol}^{-1}$) and hexaphenylbenzene ($\Delta_r H_m^{\circ}(\text{g})_{\text{R}} = 52.2 \text{ kJ}\cdot\text{mol}^{-1}$). Where is the preferred conjugation of the phenyl rings and the expected stabilization of the π system? Perhaps the homodesmotic reaction (Eq. (3.3.5)) is not suitable for revealing the intramolecular aromatic stacking interactions? Another alternative option, discussed in Section 2.1 is to derive the strain enthalpies, H_s , of poly-phenylbenzenes (see Table 3.3.11, column 6) according to Eq. (3.1.1). It has turned out, that in terms of H_s , the all di-, tri-, and tetra-phenyl-substituted benzenes are moderately stabilized at the level of -5 to -12.5 $\text{kJ}\cdot\text{mol}^{-1}$. However, in penta- and hexa-phenylbenzene the significant destabilization up to 22 $\text{kJ}\cdot\text{mol}^{-1}$ was observed due to steric repulsions of crowding phenyl substituents. Obviously, the two scales $\Delta_r H_m^{\circ}(\text{g})_{\text{R}}$ and H_s , fail to reflect properly the increasing stabilization of molecules through agglomeration of substituents on the benzene ring.

The only way to understand the total amount of interactions expressed as $\Delta_r H_m^{\circ}(\text{g})_{\text{R}}$ or H_s -values, is to use the DFT-D3 calculation in order estimate the contributions due to the dispersion forces (see Table 3.3.11, column 7). Indeed, in terms of dispersion forces, $E_{\text{disp-D3}}$, already benzene is stabilized by $E_{\text{disp-D3}} = -13.4 \text{ kJ}\cdot\text{mol}^{-1}$, followed by stabilization by $E_{\text{disp}} = -40.2 \text{ kJ}\cdot\text{mol}^{-1}$ for diphenyl. The further accumulation of phenyl substituents around the benzene ring shows a gradual increase in stabilization with each unit introduced. It is not a surprize, that the most stabilized in this series are penta- ($E_{\text{disp-D3}} = -193.1 \text{ kJ}\cdot\text{mol}^{-1}$) and hexa-phenylbenzene ($E_{\text{disp-D3}} = -244.3 -40.2 \text{ kJ}\cdot\text{mol}^{-1}$).



1,2,4,5-tetraphenylbenzene

$$E_{\text{disp-D3}} = -142.2 \text{ kJ}\cdot\text{mol}^{-1}$$

1,2,3,4,5-pentaphenylbenzene

$$E_{\text{disp-D3}} = -193.1 \text{ kJ}\cdot\text{mol}^{-1}$$

hexaphenylbenzene

$$E_{\text{disp-D3}} = -244.3 \text{ kJ}\cdot\text{mol}^{-1}$$

Figure 3.3.2 The DFT-D3 optimized structures of phenyl substituted benzenes and their dispersion interactions.

Such a tremendous amount of stabilizing dispersion interactions plays in contrast to the strong next-neighbouring steric repulsions of crowding phenyl substituents. The result of this counterplay is the very moderate destabilization (in terms of $\Delta_r H_m^0(\text{g})_R$) in most poly-substituted benzenes except for penta- and hexa-phenyl-benzene. Also, in terms of strain H_S -values, the counterplay of the attractive forces between the π systems and steric repulsions is not properly reflected in the weak stabilisation observed in the poly-phenyl-substituted benzenes (see Table 3.3.11, column 6). Nevertheless, it has turned out that similar to the strained alkanes and carbinols, the DFT-D3 calculated dispersion contributions (see Table 3.3.11, column 6) are linearly correlate, *e.g.*, with the $\Delta_r H_m^0(\text{g})_R$ -values (see Table 3.3.11, column 5) as follows:

$$E_{\text{disp-D3}} / \text{kJ}\cdot\text{mol}^{-1} = -3.0 \times \Delta_r H_m^0(\text{g})_R - 85.8 \quad \text{with } R^2 = 0.882 \quad (3.3.6)$$

The somewhat lower quality of the correlation ($R^2 = 0.882$) compared to those developed in Sections 3.1 and 3.2 is more likely to be attributed to a very individual counterplay of strain and stabilization in tri- and tetra-substituted poly-phenyl-benzenes. Even if we could not quantify the dispersion interactions in poly-phenyl-benzenes only with the help of the thermodynamic properties, the enthalpic contributions evaluated in Table 3.3.11 allow a better understanding of the energetics in this series of molecules.

3.3.4. Dispersion interactions in *para*- and *meta*-terphenyls

The available thermochemical data for *para*- and *meta*-terphenyls are compiled in Table 3.3.11. Unfortunately, the amount and purity of the commercially available samples from both series were not sufficient for thermochemical experiments. For this reason, the only enthalpies of formation of biphenyl, *p*-terphenyl, *p*-quaterphenyl, and *m*-terphenyl were disposable for calculation of interactions (see Figure 3.3.3). Nevertheless, we used the DFT-D3 calculations to further evaluate the total amount of dispersion interactions (see Table 3.3.12, column 5).

Table 3.3.12 Compilation of evaluated thermochemical results for para- and meta-terphenyls with their amount of dispersion contributions ($E_{\text{disp-D3}}$) calculated by the DFT-D3 (in $\text{kJ}\cdot\text{mol}^{-1}$, at $T = 298.15\text{ K}$ and $p^\circ = 0.1\text{ MPa}$)^a

Compound	$\Delta_f H_m^\circ(\text{cr})^b$	$\Delta_{\text{cr}}^g H_m^\circ^c$	$\Delta_f H_m^\circ(\text{g})_{\text{exp}}^d$	$E_{\text{disp-D3}}^e$
1	2	3	4	5
benzene			82.9±0.9 [116]	-13.4
biphenyl			179.7±1.1	-40.2
p-terphenyl	153.2±0.9	123.8±2.8	277.0±2.9	-67.2
p-quaterphenyl	227.0±7.0 [116]	165.6±1.2	392.6±7.1	-94.2
p-quinquephenyl	-	210.1±2.8	-	-121.2
p-sexiphenyl	-	-	-	-148.3
p-septiphenyl	-	-	-	-175.3
m-terphenyl	161.7±1.2	118.2±2.8	279.9±3.0	-67.9
m-quaterphenyl	-	153.0±1.9	-	-95.9
m-quinquephenyl	-	-	-	-121.2
m-sexiphenyl	-	-	-	-160.3
m-septiphenyl	-	-	-	-202.3
m-deciphphenyl	-	-	-	-357.8

^a Uncertainties are expressed as the twice standard deviations.

^b Recommended values from Table 3.3.4.

^c Recommended values from Table 3.3.1.

^d Calculated as sum of column 2 and 3 from this table.

^e Calculated with the DFT-D3 in this work.

In section 3.3.2 we have already shown, that the homodesmotic reaction according to Eq. (3.3.5) can be used to assess the overall number of substituent interactions in poly-phenylbenzenes. It is interesting to explore ability of such type of well-balanced reactions (WBR) to obtain a suitable scale for evaluating the dispersive forces in similarly shaped compounds like those collected in Table 3.3.12 and Table 3.3.13.

For biphenyl, p-terphenyl, p-quaterphenyl, and m-terphenyl we constructed the following WBR given in Figure 3.3.3. The dispersion forces, E_{disp} , in these compounds were calculated according to the Hess's Law by using experimental enthalpies of formation, $\Delta_f H_m^\circ(\text{g})_{\text{exp}}$, of the reaction participants given in Table 3.3.12, column 4. The dispersion forces calculated with the DFT-D3, $E_{\text{disp-D3}}$, are also given in this figure for comparison.

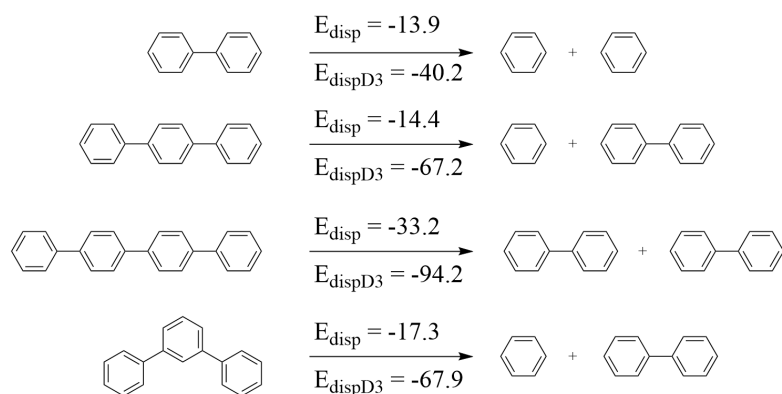


Figure 3.3.3 Calculation of the dispersion interaction in biphenyl, p-terphenyl, p-quaterphenyl, and m-terphenyl with help of the well-balanced reactions. The standard molar enthalpies of formation

of reaction participants are given (in $\text{kJ}\cdot\text{mol}^{-1}$) below the formulas. E_{disp} = dispersion forces calculated (in $\text{kJ}\cdot\text{mol}^{-1}$) according to Hess's Law. $E_{\text{disp-D3}}$ = dispersion forces calculated (in $\text{kJ}\cdot\text{mol}^{-1}$) with the DFT-D3.

The E_{disp} and $E_{\text{disp-D3}}$ values belong to different scales that measure the amount of dispersion forces in molecules. Nevertheless, it is apparent, that these values reproduce the similar trend in biphenyl, p-terphenyl, p-quaterphenyl, and m-terphenyl. The DFT-D3 calculations provide more broad insight in development of amount of dispersion interactions in para- and meta-terphenyls (see Table 3.3.12, column 5). As can be seen from this table, in both series, the amount of dispersion forces gradually increases as the sequence of phenyl rings increases. To our surprise, the correlation of the dispersion interactions $E_{\text{disp-D3}}$ with number of phenyl-rings that form para-terphenyls and meta-terphenyls series has shown different trends (see Figure 3.3.4).

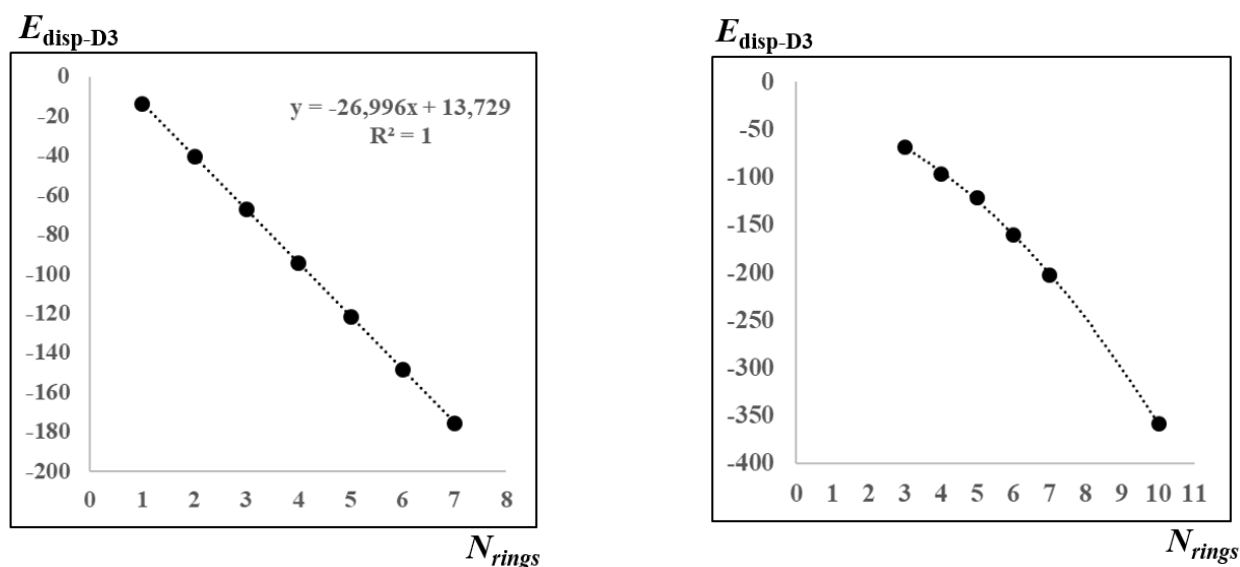


Figure 3.3.4 Correlation of dispersion interactions $E_{\text{disp-D3}}$ with number of phenyl-rings, N_{ring} , constituting molecules of p-terphenyls (left) and meta-terphenyls (right).

The para-terphenyl series shows a perfect linear dependence on the N_{ring} , while the dispersion forces in the meta series increase exponentially. The reason for these different trends can be revealed from the structures optimized using DFT-D3 given in Figure 3.3.5 and Figure 3.3.6.

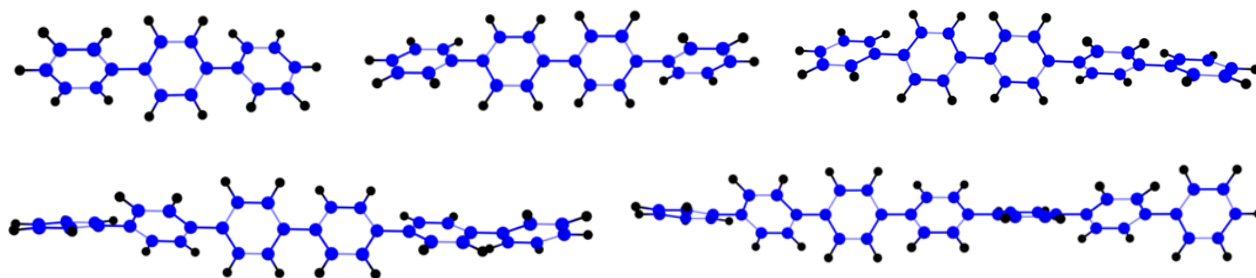


Figure 3.3.5 The DFT-D3 optimized structures of para-terphenyls: p-terphenyl, p-quaterphenyl, p-quinquephenyl, p-sexiphenyl, and p-septiphenyl. The numerical values of $E_{\text{disp-D3}}$ are given in Table 3.3.12, column 5.

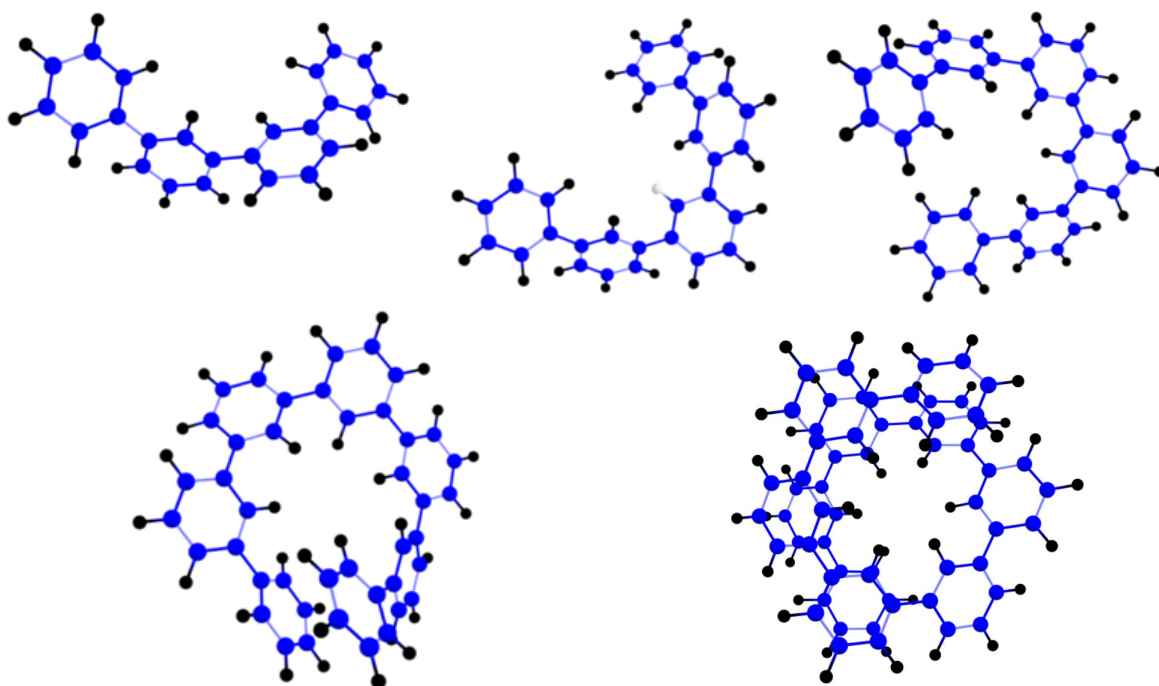


Figure 3.3.6 The DFT-D3 optimized structures of meta-terphenyls: m-quaterphenyl, m-quinquephenyl, m-sexiphenyl, m-septiphenyl, and m-deciphphenyl. The numerical values of $E_{\text{disp-D3}}$ are given in Table 3.3.12, column 5.

It makes oneself conspicuous, that in the para-terphenyls series, the chain formed from phenyl rings remains straight and the dispersion interactions in this series accumulate due to the π interactions of the flat rings that are not significantly screwed along the chain (see Figure 3.3.5). In contrast, the chain formed from phenyl rings in the meta-terphenyl series shows the crooked trend. This trend is twisted more and more with each phenyl ring added. As can be seen in Figure 3.3.6, the chain of m-septiphenyl becomes round. In m-deciphphenyl, the edge rings are already overlapped and exert the direct π - π dispersion interactions. It is interesting that the amount of dispersion interactions in p-quaterphenyl and m-quaterphenyl is quantitatively practically equal. The same applies to p-quinquephenyl and m-quinquephenyl. However, already with m-sexiphenyl and m-septiphenyl, the amount of dispersion forces is significantly greater than that of their para-isomers.

3.3.5. Dispersion interactions in phenyl substituted naphthalenes and anthracenes

The available thermochemical data for phenyl substituted naphthalenes and anthracenes are compiled in Table 3.3.13. There were enough experimental data on this type of compounds, and we derived the dispersion interactions from both experimental enthalpies of formation (see Figure 3.3.7 and Figure 3.3.9) and from the DFT-D3 calculations (see Table 3.3.13, column 5).

Table 3.3.13 Compilation of evaluated thermochemical results for phenyl substituted naphthalenes and anthracenes with their amount of dispersion contributions ($E_{\text{disp-D3}}$) calculated by the DFT-D3 (in $\text{kJ}\cdot\text{mol}^{-1}$, at $T = 298.15 \text{ K}$ and $p^\circ = 0.1 \text{ MPa}$)^a

Compound	$\Delta_f H_m^\circ(\text{cr,l})$	$\Delta_{\text{cr,l}}^g H_m^\circ$ ^b	$\Delta_f H_m^\circ(\text{g})_{\text{exp}}$ ^c	$E_{\text{disp-D3}}$ ^d
	1	2	3	4
1-phenyl-naphthalene (liq)	166.1±1.5 [95]	83.2±0.4	249.3±1.6	-60.5
2-phenyl-naphthalene (cr)	140.2±3.0 [89]	108.9±1.2	249.1±3.2	-56.9
1,4-diphenyl-naphthalene (cr)	222.7±4.3 [89]	129.5±2.8	352.2±5.1	-91.7
1,8-diphenyl-naphthalene (cr)	243.5±4.3 [89]	128.7±1.2	372.2±4.5	-106.1
1-([1,1'-biphenyl]-4-yl)-naphthalene (cr)	212.0±4.2 [89]	141.2±1.5	353.2±4.5	-87.7
1,8-di([1,1'-biphenyl]-4-yl)naphthalene (cr)	376.7±6.5 [89]	186.3±3.6	563.0±7.4	-174.8
2-(biphenyl-3-yl)naphthalene (cr)	-	131.6±2.8	-	-84.7
2-(biphenyl-4-yl)naphthalene (cr)	198.3±4.1 [89]	143.2±1.4	341.5±4.3	-83.9
1,2,3,4-tetra-phenylnaphthalene	409.7±6.4 [89]	159.5±0.8	569.2±6.4	-179.7
9-phenylanthracene (cr)	-	124.6±0.7	-	-81.3
9,10-diphenylanthracene (cr)	308.7±3.0 [116]	153.6±0.9	462.3±3.1	-117.0
5,6,11,12-tetraphenyltetracene (cr)	581.4±8.2 [101]	210.5±1.5	791.9±8.3	-244.6

^a Uncertainties are expressed as the twice standard deviations.

^b Recommended values from Table 3.3.1.

^c Calculated as sum of column 2 and 3 from this table.

^d Calculated with the DFT-D3 in this work.

For phenyl substituted naphthalenes we constructed the following WBR given in Figure 3.3.7.

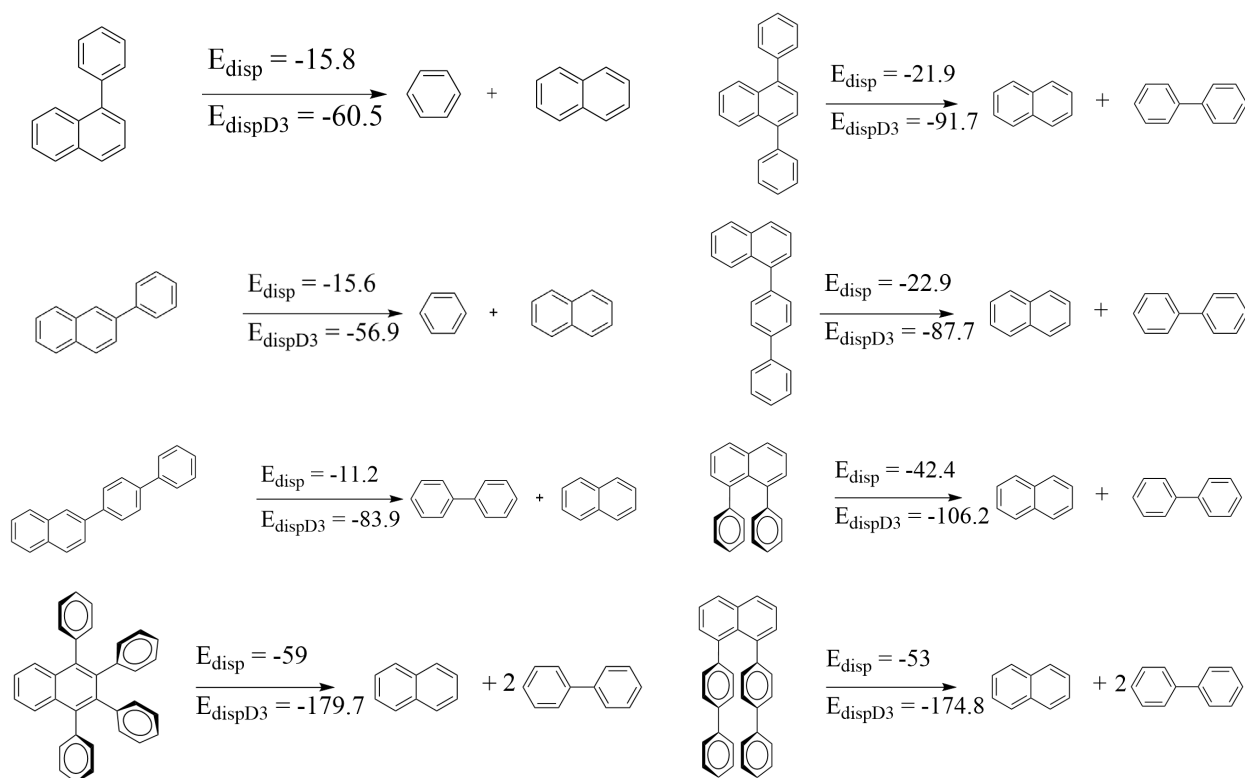


Figure 3.3.7 Calculation of the dispersion interaction in phenyl substituted naphthalenes with help of the well-balanced reactions. The standard molar enthalpies of formation of reaction participants are given (in $\text{kJ}\cdot\text{mol}^{-1}$) below the formulas. E_{disp} = dispersion forces calculated (in $\text{kJ}\cdot\text{mol}^{-1}$) according to Hess's Law. $E_{\text{disp-D3}}$ = dispersion forces calculated (in $\text{kJ}\cdot\text{mol}^{-1}$) with the DFT-D3

According to these reactions, the dispersion interactions in 1-phenyl-naphthalene and 2-phenyl-naphthalene are the lowest in this series, followed by 2-(biphenyl-4-yl)naphthalene and 1-([1,1'-biphenyl]-4-yl)-naphthalene, and 1,4-diphenyl-naphthalene. The most impressive π -interactions are observed with 1,8-diphenyl-naphthalene and 1,8-di ([1,1'-biphenyl]-4-yl)naphthalene, where the phenyl rings are closest together and exert the force of attraction like a pair of tweezers. Also the large amount of dispersion forces was observed in 1,2,3,4-tetra-phenylnaphthalene. It is interesting that according to the DFT-D3 calculations, the $E_{\text{disp-D3}} = -179.7 \text{ kJ}\cdot\text{mol}^{-1}$ in 1,2,3,4-tetra-phenylnaphthalene is significantly larger than $E_{\text{disp-D3}} = -153.7 \text{ kJ}\cdot\text{mol}^{-1}$ in similarly shaped 1,2,3,4-tetraphenylbenzene. Obviously, the naphthalene ring provides the additional stabilization of the π system. The DFT-D3 optimized structures of phenyl-substituted naphthalenes are given in Figure 3.3.8.

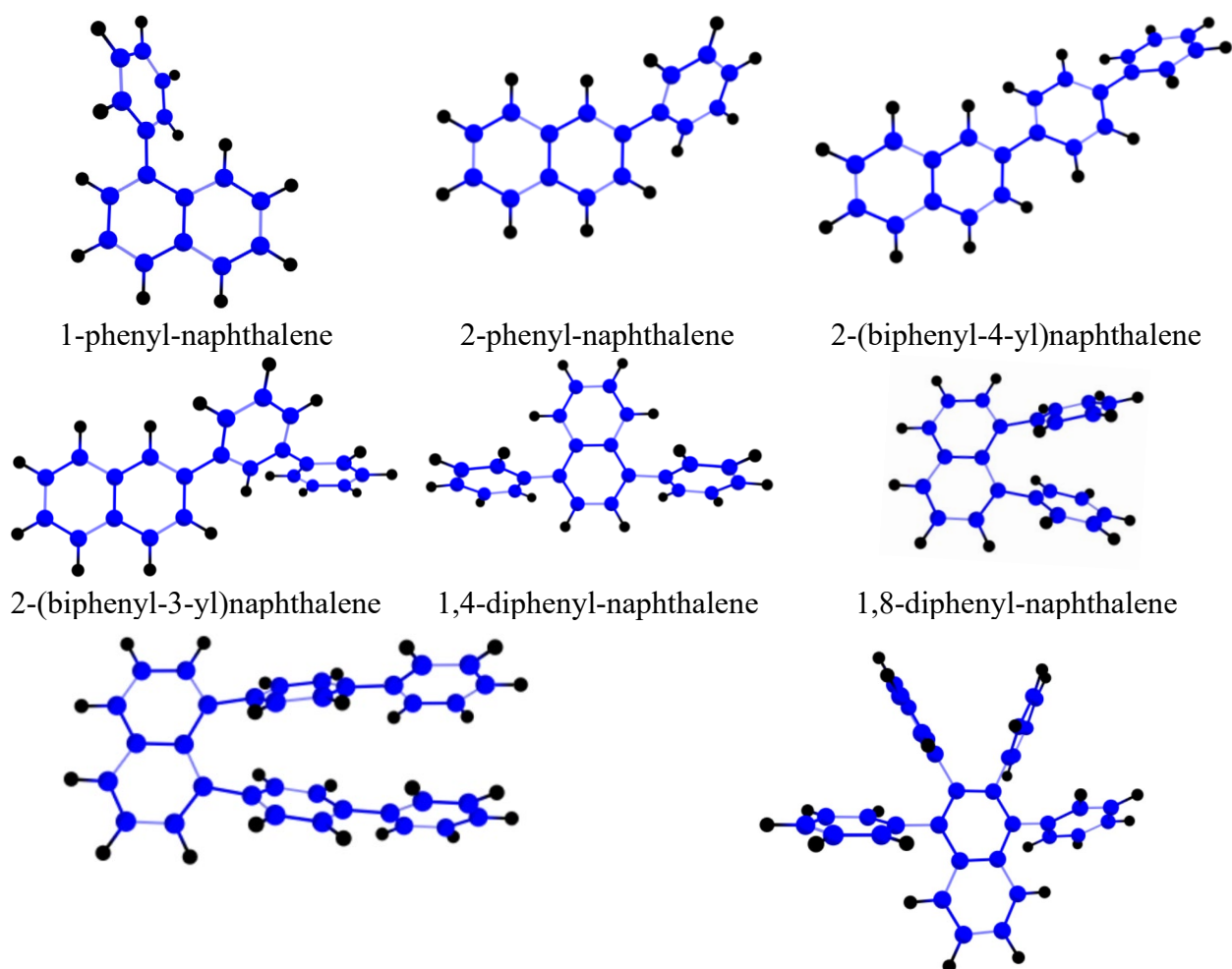


Figure 3.3.8 The DFT-D3 optimized structures of phenyl-substituted naphthalenes. The numerical values of $E_{\text{disp-D3}}$ are given in Table 3.3.15, column 5.

For phenyl substituted anthracenes we constructed the following WBR given in Figure 3.3.9.

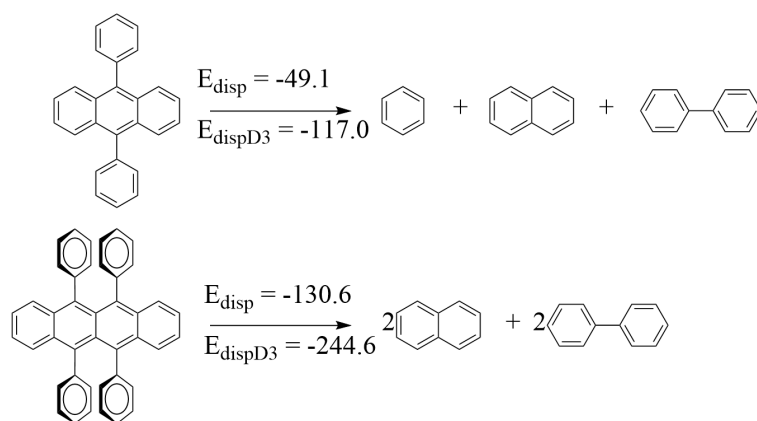


Figure 3.3.9 Calculation of the dispersion interaction in phenyl substituted anthracenes with help of the well-balanced reactions. The standard molar enthalpies of formation of reaction participants are given (in $\text{kJ}\cdot\text{mol}^{-1}$) below the formulas. E_{disp} = dispersion forces calculated (in $\text{kJ}\cdot\text{mol}^{-1}$) according to Hess's Law. $E_{\text{disp-D3}}$ = dispersion forces calculated (in $\text{kJ}\cdot\text{mol}^{-1}$) with the DFT-D3.

It has turned out that the dispersion interactions in phenyl substituted anthracene and tetracene are significantly more profound than in phenyl-substituted naphthalenes. According to the DFT-D3 calculations, the $E_{\text{disp-D3}} = -117.0 \text{ kJ}\cdot\text{mol}^{-1}$ in 9,10-diphenylanthracene is larger than $E_{\text{disp-D3}} = -91.7 \text{ kJ}\cdot\text{mol}^{-1}$ in similarly shaped 1,4-di-phenylnaphthalene. Also, in the case of anthracenes, the detached ring provides the additional stabilization of the π system compared to naphthalene derivatives. The $E_{\text{disp-D3}} = -244.6 \text{ kJ}\cdot\text{mol}^{-1}$ in 5,6,11,12-tetraphenyltetracene is identical to the stabilization observed for hexaphenylbenzene ($E_{\text{disp-D3}} = -244.3 \text{ kJ}\cdot\text{mol}^{-1}$). The DFT-D3 optimized structures of phenyl-substituted naphthalenes are given in Figure 3.3.10.

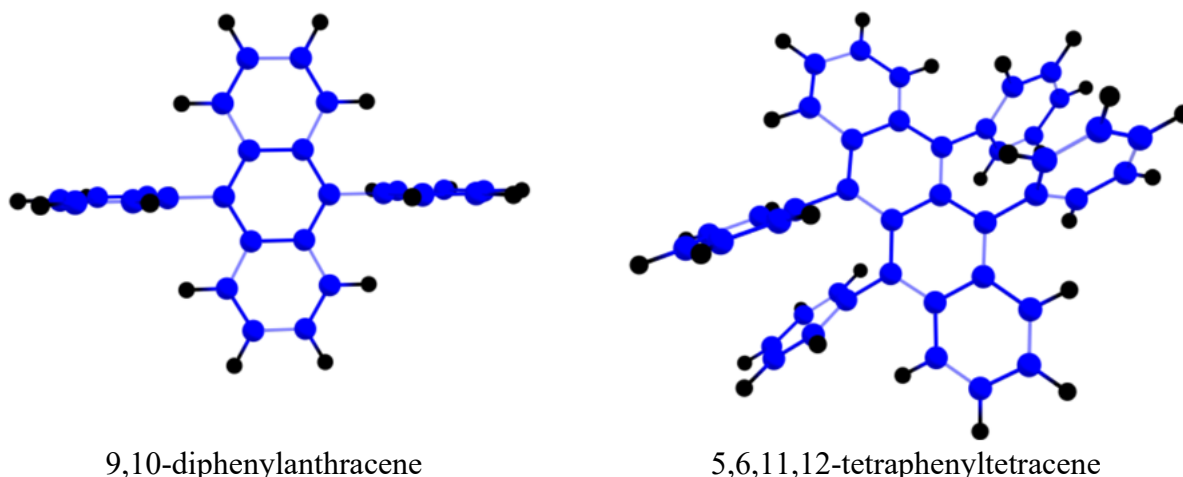


Figure 3.3.10 The DFT-D3 optimized structures of phenyl-substituted naphthalenes. The numerical values of $E_{\text{disp-D3}}$ are given in Table 3.3.13, column 5.

Results shown in Figure 3.3.7 and Figure 3.3.9 make it obvious, that for both series the DFT-D3 calculated dispersion contributions are systematically overestimated, but they linearly correlate

with the E_{disp} values, *e.g.*, for the data compiled in Table 3.3.12 and Table 3.3.13 the following linear correlation was observed:

$$E_{\text{disp-D3}} / \text{kJ}\cdot\text{mol}^{-1} = 1.68 \times E_{\text{disp-D3}} - 45.0 \quad \text{with } R^2 = 0.876 \quad (3.3.7)$$

The moderate quality of this correlation ($R^2 = 0.876$) is understandable due to the relatively large experimental uncertainties (up to $8 \text{ kJ}\cdot\text{mol}^{-1}$) of the gas-phase enthalpies of formation. From our experience, however, such large uncertainties are typical of such large and heavy volatile molecules.

3.4. Non-nearest neighbour interactions: well-balanced reactions

The intramolecular long-range substituents interactions with non-nearest neighbours is an important example of dispersion manifestation. They become increasingly important with growing molecule size. A simple example of the interactions of non-nearest neighbours in the molecular system is shown in Figure 3.4.1. The flexible structures of 1,3-diphenyl-propan, diphenyl carbonate, and 1,3-diphenyl-2-propanone, expect free rotation of phenyl rings. However, the ability of the phenyl rings to interact with one another through π - π interactions can produce the conformation with the aromatic rings in a stacked arrangement (see Figure 3.4.1) stabilized by these attractive interactions.

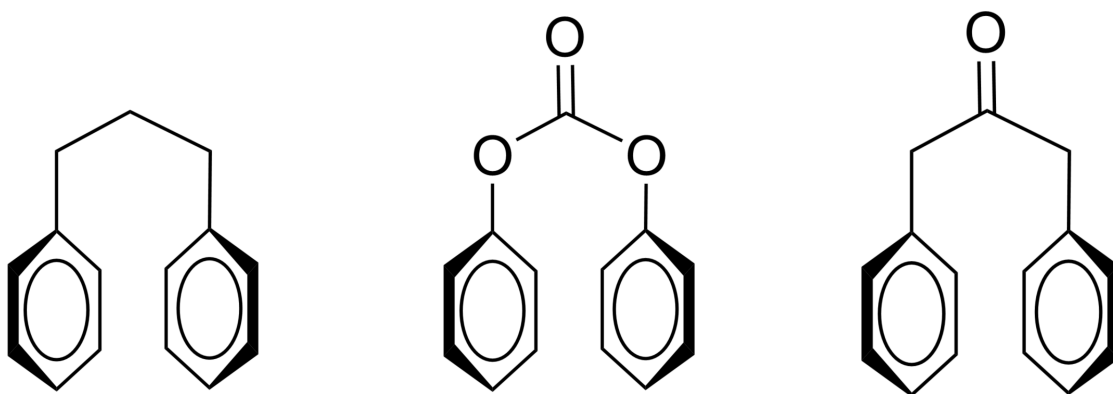


Figure 3.4.1 Structures of 1,3-diphenyl-propan, diphenyl carbonate, and 1,3-diphenyl-2-propanone

How can these interactions be quantified? The strength of this π - π interaction can be derived using the Hess's Law applied to the well-balanced reaction (WBR) designed *e.g.*, for 1,2-diphenyl-ethane in Figure 3.4.2. Indeed, on the one hand, the reaction is deliberately constructed in such a way that all atomic contributions on the left and right are compensated. On the other hand, the "pure" π - π interaction of the phenyl rings on the right side of the reaction should be released. The contribution of dispersion forces effective 1,2-diphenyl-ethane ($E_{\text{disp-D3}} = -46.1 \text{ kJ}\cdot\text{mol}^{-1}$) derived by the Hess's Law is significantly lower compared to those derived from the DFT-D3 calculations ($E_{\text{disp-D3}} = -59.6 \text{ kJ}\cdot\text{mol}^{-1}$).

Similarly, the WBR for 1,3-diphenyl-propan and diphenyl carbonate were constructed, and the contribution of the dispersion forces derived (see Figure 3.4.2). It has turned out, that the π - π interactions in all three molecular systems are very close in size at the general level of $E_{\text{disp-D3}} \approx -60.1 \text{ kJ}\cdot\text{mol}^{-1}$. However, the results of DFT-D3 for all three species are systematically overestimated (see Figure 3.4.2).

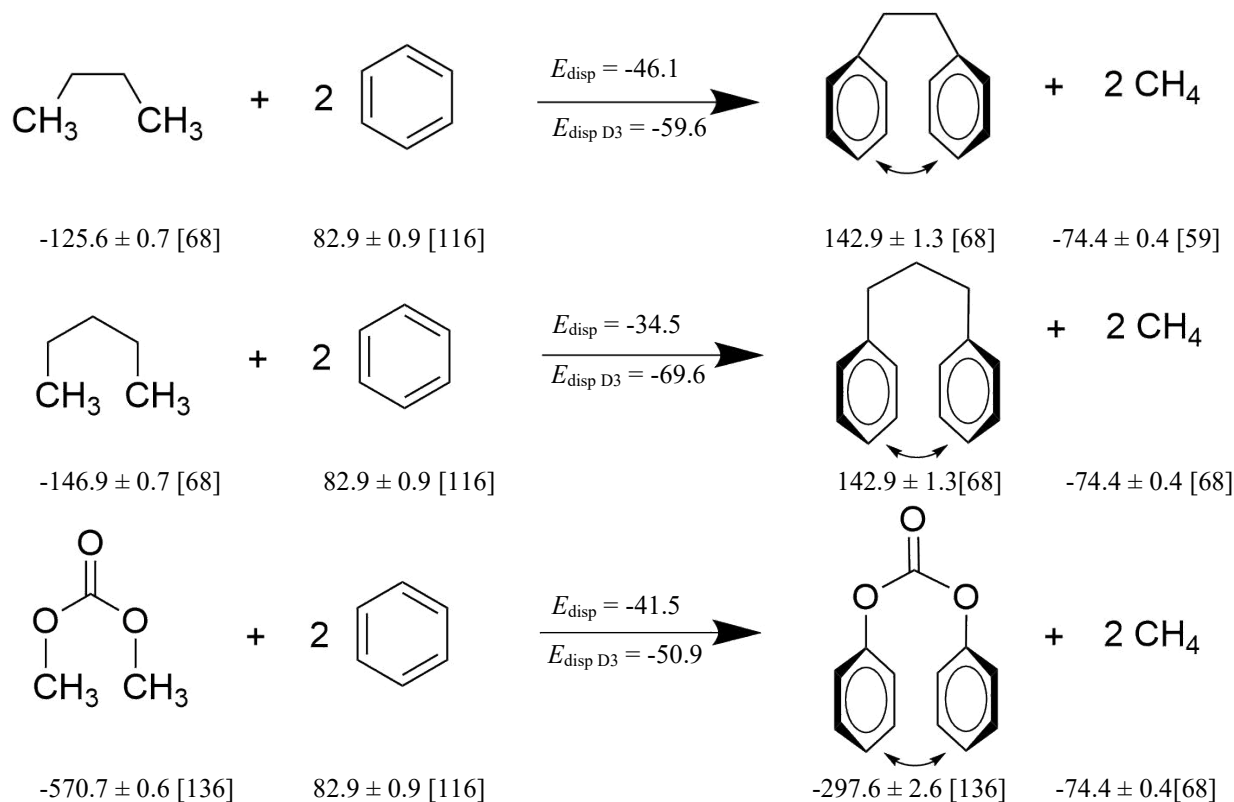
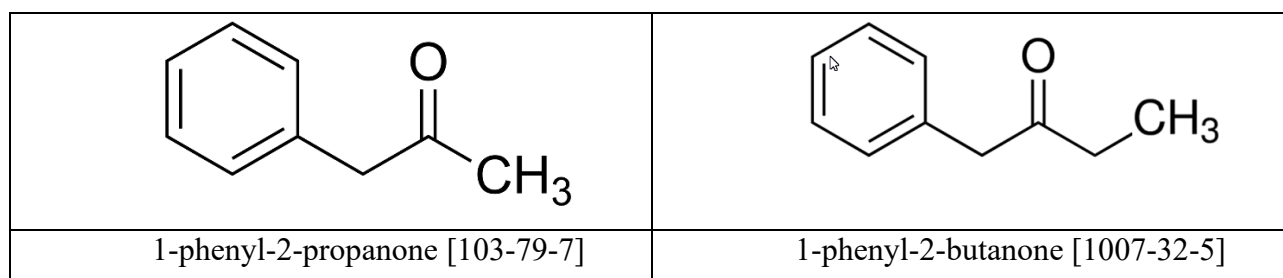


Figure 3.4.2 Calculation of the energetics π - π interaction in 1,2-diphenyl-ethane, 1,3-diphenyl-propane, and diphenyl carbonate with help of the well-balanced reactions. The standard molar enthalpies of formation of reaction participants are given (in $\text{kJ}\cdot\text{mol}^{-1}$) below the formulas. E_{disp} = dispersion forces calculated (in $\text{kJ}\cdot\text{mol}^{-1}$) according to Hess's Law. $E_{\text{disp-D3}}$ = dispersion forces calculated (in $\text{kJ}\cdot\text{mol}^{-1}$) with the DFT-D3.

In order to identify the reason for such systematic deviations, the experimental thermochemical studies and the DFT-D3 calculations were carried out in the series of phenyl-substituted ketones: methyl benzyl ketone, ethyl benzyl ketone and dibenzyl ketone (see Figure 3.4.3)



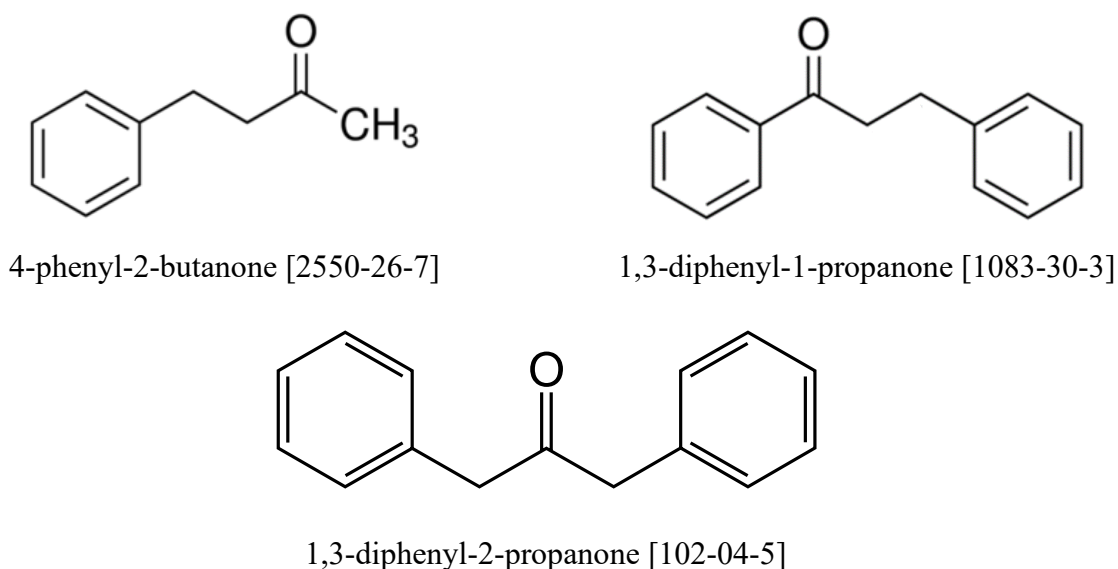


Figure 3.4.3 Phenyl-substituted ketones studied in this work.

Results of vapor pressure measurements are collected in Table B.3.

The compilation of the standard molar enthalpies of vaporization $\Delta_1^g H_m^o$ of phenyl substituted ketones available in the literature and comparison of these values with our results is given in Table 3.4.1.

Table 3.4.1 Compilation of the standard molar enthalpies of vaporization $\Delta_1^g H_m^o$ of phenyl substituted ketones

Compound	M ^a	<i>T</i> - range K	$\Delta_1^g H_m^o(T_{av})$	$\Delta_1^g H_m^o(298.15 \text{ K})^b$	Ref.
			kJ·mol ⁻¹	kJ·mol ⁻¹	
1-phenyl-2-propanone	EM	275-3320	55.2±3.0	55.2±3.0	[137]
	S	273-328		57.7±2.0	[138]
	CGC	298.15		56.1±2.0	[139]
	SF	323.2-489.7	53.3±1.2	60.8±1.3	Table B.3
				58.7±0.9^c	average
1-phenyl-2-butanone	T	295.3-345.2	62.2±0.6	63.7±0.7	Table B.3
4-phenyl-2-butanone	T	293.2-333.5	62.0±0.7	63.2±0.8	Table B.3
1,3-diphenyl-1-propanone (liq)	T	368.8-403.4	76.1±0.9	85.2±1.0	Table B.3
1,3-diphenyl-2-propanone (cr)	EM	283-308	89.1±3.0	89.5±3.0	[137]
	C	365.6	129.8±2.0	111.6±2.3	[77]
	<i>T_{fus}</i>			108.6±0.8	Table 3.4.3
				108.9±0.9^c	average
1,3-diphenyl-2-propanone (liq)	n/a	398.7-603.7	64.6±2.8	84.4±3.0	[140]
	C	365.6	103.0±2.3	84.6±2.5	[77]
	T	315.7-363.9	85.1±0.7	89.4±0.8	Table B.3
				88.7±0.7^c	average

^a Techniques: T = transpiration method; n/a = method is not available; EM = Balson effusion manometer; C = calorimetry; *T_{fus}* = calculated as the sum $\Delta_1^g H_m^o$ and $\Delta_{cr}^l H_m^o$; SF - from experimental boiling temperatures reported at different pressures compiled by SciFinder [118] (see text).

^b Uncertainties of the vaporization enthalpies is expressed as expanded uncertainty (0.95 level of confidence, *k* = 2). They include uncertainties from the experimental conditions and the fitting equation, vapour pressures, and uncertainties from adjustment of vaporization enthalpies to the reference temperature *T* = 298.15 K [28,29].

^c Weighted mean value (the uncertainty was taken as the weighing factor). Uncertainty of the vaporization enthalpy is expressed as the expanded uncertainty (0.95 level of confidence, $k = 2$). Values highlighted in bold were recommended for thermochemical calculations.

The available in the literature vapor pressures were treated in the same way as our own results in Table B.3 with help of heat capacity differences $\Delta_{\text{cr,l}}^{\text{g}}C_{\text{p,m}}^{\text{o}}$ collected in Table 3.4.2.

Table 3.4.2 Compilation of data on molar heat capacities $C_{\text{p,m}}^{\text{o}}$ (cr or liq) and heat capacity differences $\Delta_{\text{cr,l}}^{\text{g}}C_{\text{p,m}}^{\text{o}}$ at $T = 298.15$ K (in $\text{J}\cdot\text{K}^{-1}\cdot\text{mol}^{-1}$)

Compounds	$C_{\text{p,m}}^{\text{o}}$ (cr) ^a	$-\Delta_{\text{cr}}^{\text{g}}C_{\text{p,m}}^{\text{o}}$ ^b	$C_{\text{p,m}}^{\text{o}}$ (liq) ^a	$-\Delta_{\text{l}}^{\text{g}}C_{\text{p,m}}^{\text{o}}$ ^b
1-phenyl-2-propanone			240.5	73.1
1-phenyl-2-butanone			272.4	81.4
4-phenyl-2-butanone			272.4	81.4
1,3-diphenyl-1-propanone	280.3	42.8	361.8	104.6
1,3-diphenyl-2-propanone	280.3	42.8	361.8	104.6

^a Calculated by the group-contribution procedure developed by Chickos *et al.* [16].

^b Calculated according to the procedure developed by Acree and Chickos [18].

The significant disagreement of vaporization enthalpies for 1-phenyl-2-propanone prompted us to use experimental boiling temperatures at different pressures compiled by SciFinder [118]. The accuracy of this data is questionable as it comes from the distillation of a compound after its synthesis and not from special physico-chemical studies. However, numerous data on boiling temperatures at standard pressure, as well as at reduced pressures provide a reliable level of experimental vapour pressures and trend of the dependence of vapour pressure with temperature. In our recent work on amino-alcohols we have demonstrated that SF-data can be considered sufficient to obtain the reliable trend of the temperature dependencies of the vapour pressures. The vaporization enthalpy for 1-phenyl-2-propanone calculated from SciFinder data is given in Table 3.4.1 and it is in fair agreement with other available results.

The 1,3-diphenyl-2-propanone is solid at the room temperature. The enthalpy of fusion for this compound was measured using DSC (see Table 3.4.3) and it was used to derive the sublimation enthalpy in the independent way (see Table 3.4.1 and Table 3.4.3) in order to ascertain the latter value.

Table 3.4.3 Phase transitions thermodynamics of substituted acetophenones and benzophenones (in $\text{kJ}\cdot\text{mol}^{-1}$)^a

Compounds	T_{fus} , K	$\Delta_{\text{cr}}^{\text{l}}H_{\text{m}}^{\text{o}}$ at T_{fus}	$\Delta_{\text{cr}}^{\text{l}}H_{\text{m}}^{\text{o}}$ ^b	$\Delta_{\text{l}}^{\text{g}}H_{\text{m}}^{\text{o}}$ ^c	$\Delta_{\text{cr}}^{\text{g}}H_{\text{m}}^{\text{o}}$ ^d
			298.15 K		
1	2	3	4	5	6
1-phenyl-2-butanone	222.5	14.8±0.4			
1,3-diphenyl-2-propanone	307.2	20.2±0.5 [30]			
	307.1	19.6±0.2			
		19.7±0.2	19.2±0.2	89.4±0.8	108.6±0.8

^a Uncertainties are presented as expanded uncertainties (0.95 level of confidence with $k=2$).

^b The experimental enthalpies of fusion $\Delta_{\text{cr}}^{\text{l}}H_{\text{m}}^{\text{o}}$ measured at T_{fus} were adjusted to $T = 298.15$ K with help of the following equation [18]:

$$\Delta_{\text{cr}}^{\text{l}}H_{\text{m}}^{\text{o}}(298.15 \text{ K})/(\text{J}\cdot\text{mol}^{-1}) = \Delta_{\text{cr}}^{\text{l}}H_{\text{m}}^{\text{o}}(T_{\text{fus}}/\text{K}) - (\Delta_{\text{cr}}^{\text{g}}C_{\text{p,m}}^{\text{o}} - \Delta_{\text{l}}^{\text{g}}C_{\text{p,m}}^{\text{o}}) \times [(T_{\text{fus}}/\text{K}) - 298.15 \text{ K}],$$

where $\Delta_{\text{cr}}^{\text{g}}C_{\text{p,m}}^{\circ}$ and $\Delta_{\text{l}}^{\text{g}}C_{\text{p,m}}^{\circ}$ were taken from Table 3.4.2. Uncertainties in the temperature adjustment of fusion enthalpies from T_{fus} to the reference temperature are estimated to account with 30 % to the total adjustment [18].

^c Experimental values of vaporization enthalpies (see Table B.3).

^d Calculated as the sum column 4 and 5 in this table.

The experimental thermochemical studies reported in Table B.3, Table 3.4.1, Table 3.4.2, and Table 3.4.3 lead to the gas-phase standard molar enthalpy of formation, $\Delta_{\text{f}}H_{\text{m}}^{\circ}(\text{g})$, of phenyl substituted ketones as the sum of vaporization/sublimation enthalpies and condensed phase standard molar enthalpy of formation, $\Delta_{\text{f}}H_{\text{m}}^{\circ}(\text{liq/cr})$ (see Table 3.4.4).

Table 3.4.4 Thermochemical data at $T = 298.15 \text{ K}$ ($p^{\circ} = 0.1 \text{ MPa}$, in $\text{kJ} \cdot \text{mol}^{-1}$)^a

Compound	$\Delta_{\text{f}}H_{\text{m}}^{\circ}(\text{liq/cr})$	$\Delta_{\text{l,cr}}^{\text{g}}H_{\text{m}}^{\circ \text{b}}$	$\Delta_{\text{f}}H_{\text{m}}^{\circ}(\text{g})$
1-phenyl-2-propanone (liq)	-151.9 ± 2.0 [68]	58.7 ± 0.9	-93.2 ± 2.2
1-phenyl-2-butanone (liq)		63.7 ± 0.7	-118.6 ± 3.5 ^c
4-phenyl-2-butanone (liq)		63.2 ± 0.8	-124.4 ± 3.5 ^c
1,3-diphenyl-1-propanone (liq)		85.2 ± 1.0	5.6 ± 3.5 ^c
1,3-diphenyl-2-propanone (cr)	-95.2 ± 3.0 [77]	108.9 ± 0.9	13.7 ± 3.1

^a The uncertainties are given as the twice standard deviation.

^b Evaluated experimental values from Table 3.4.1.

^c Calculated using the G4 method

The $\Delta_{\text{f}}H_{\text{m}}^{\circ}(\text{g})$ -values for 1-phenyl-2-butanone, 4-phenyl-2-butanone, and 1,3-diphenyl-1-propanone were calculated using the high-level G4 method. These values can be now use for interpretation of dispersion interactions in these compounds, as it shown in Figure 3.4.4.

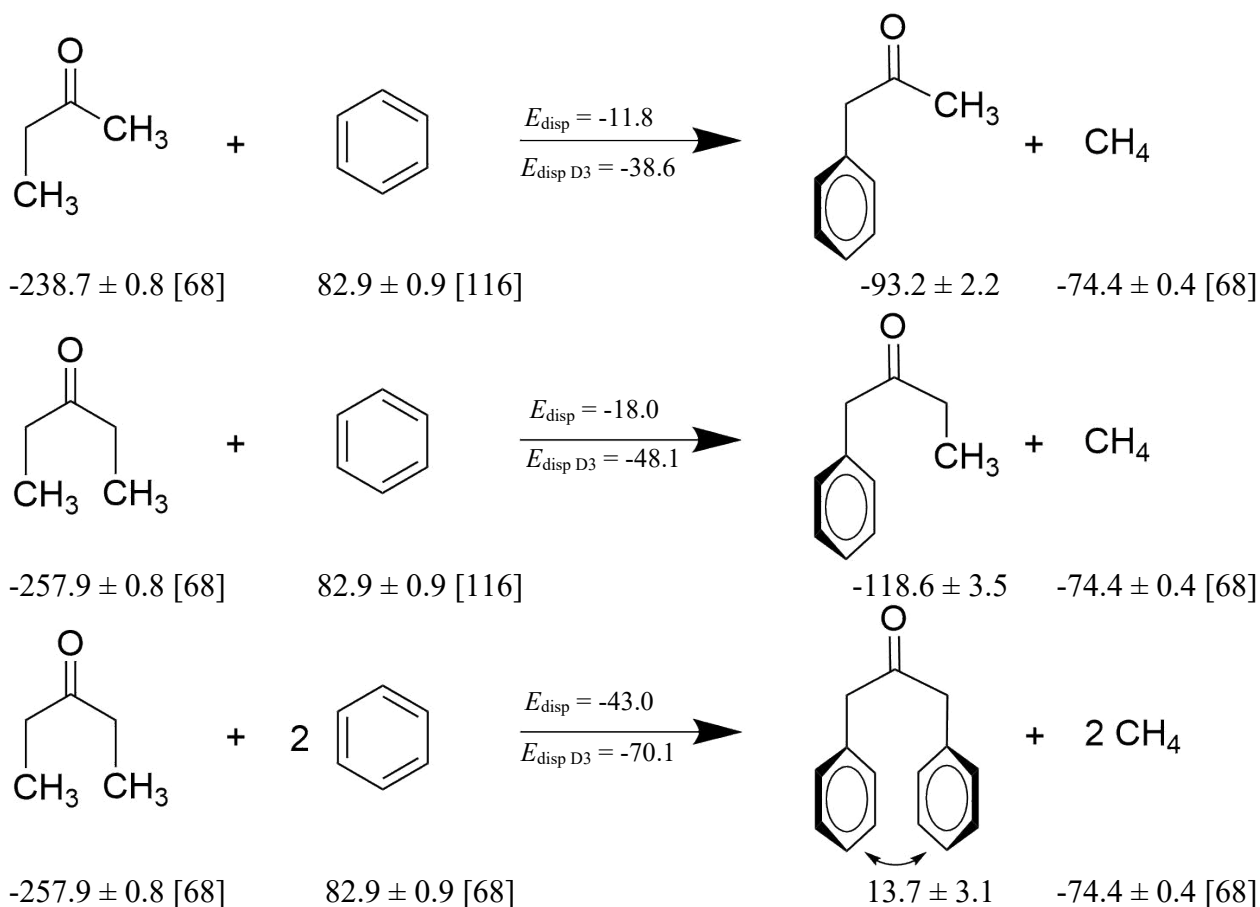


Figure 3.4.4 Calculation of the dispersion interaction in methyl benzyl ketone, ethyl benzyl ketone,

and dibenzyl ketone with help of the well-balanced reactions. The standard molar enthalpies of formation of reaction participants are given (in $\text{kJ}\cdot\text{mol}^{-1}$) below the formulas. E_{disp} = dispersion forces calculated (in $\text{kJ}\cdot\text{mol}^{-1}$) according to Hess's Law. $E_{\text{disp-D3}}$ = dispersion forces calculated (in $\text{kJ}\cdot\text{mol}^{-1}$) with the DFT-D3.

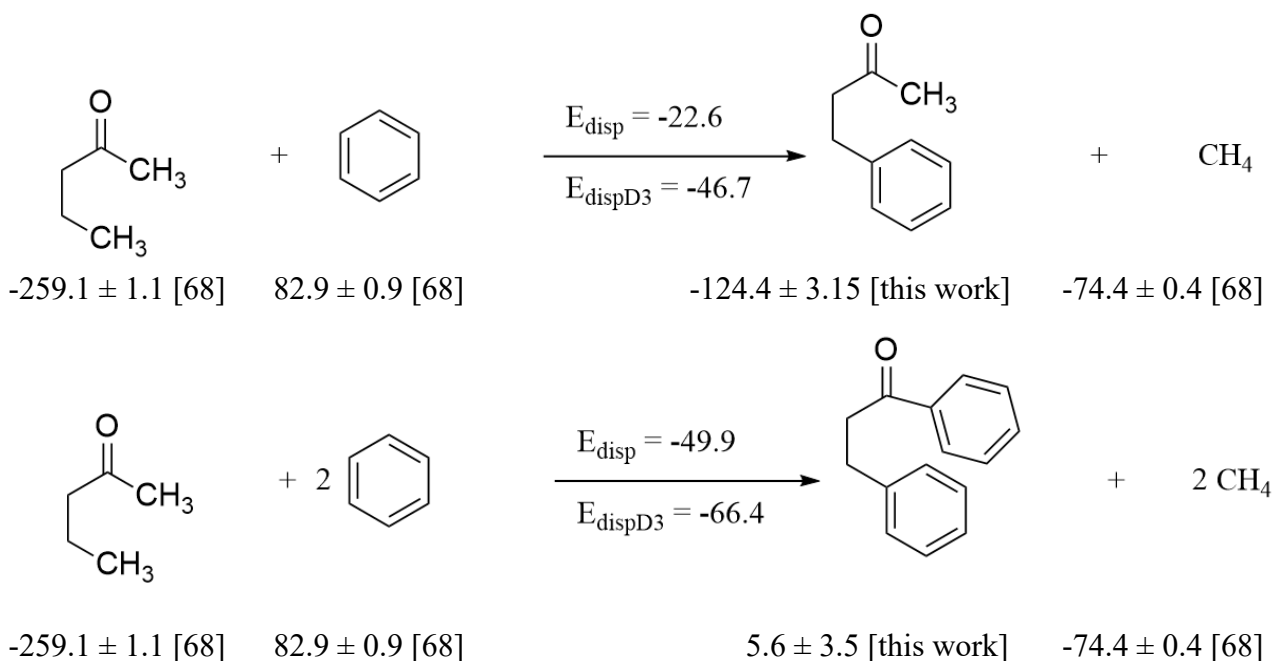


Figure 3.4.5 Calculation of the dispersion interaction in 4-phenyl-2-butanone and 1,3-diphenyl-1-propanone with help of the well-balanced reactions. The standard molar enthalpies of formation of reaction participants are given (in $\text{kJ}\cdot\text{mol}^{-1}$) below the formulas. E_{disp} = dispersion forces calculated (in $\text{kJ}\cdot\text{mol}^{-1}$) according to Hess's Law. $E_{\text{disp-D3}}$ = dispersion forces calculated (in $\text{kJ}\cdot\text{mol}^{-1}$) with the DFT-D3.

In the methyl benzyl ketone and ethyl benzyl ketone the π - π interactions are absent. In the dibenzyl ketone, the π - π interactions are expected to be similar to those in 1,2-diphenyl-ethane, 1,3-diphenyl-propane, and diphenyl carbonate. The results of the DFT-D3 calculations are given in Figs. Figure 3.4.4 and Figure 3.4.5 and are compared to those that derived from the experimental enthalpies of formation according to WBR shown in Figure 3.4.4 and Figure 3.4.5. It has turned out that also for this system the DFT-D3 calculated dispersion contributions are systematically overestimated, but they linearly correlate with the E_{disp} values, *e.g.*, for the data on Figure 3.4.4 as follows:

$$E_{\text{disp}} / \text{kJ}\cdot\text{mol}^{-1} = 0.972 \times E_{\text{disp-D3}} - 28.7 \quad \text{with } R^2 = 0.988 \quad (3.4.1)$$

The reason of this scaling is not yet quite apparent, but the good quality correlation between two independent procedures encourages the use of the thermodynamic values and WBR to quantify the dispersion forces.

Also, for the phenyl-substituted amines studied in chapter 2.1.2 the strength of the π - π interaction among the phenyl rings can be derived using the Hess's Law applied to the well-balanced reaction constructed for these molecules in Figure 3.4.6.

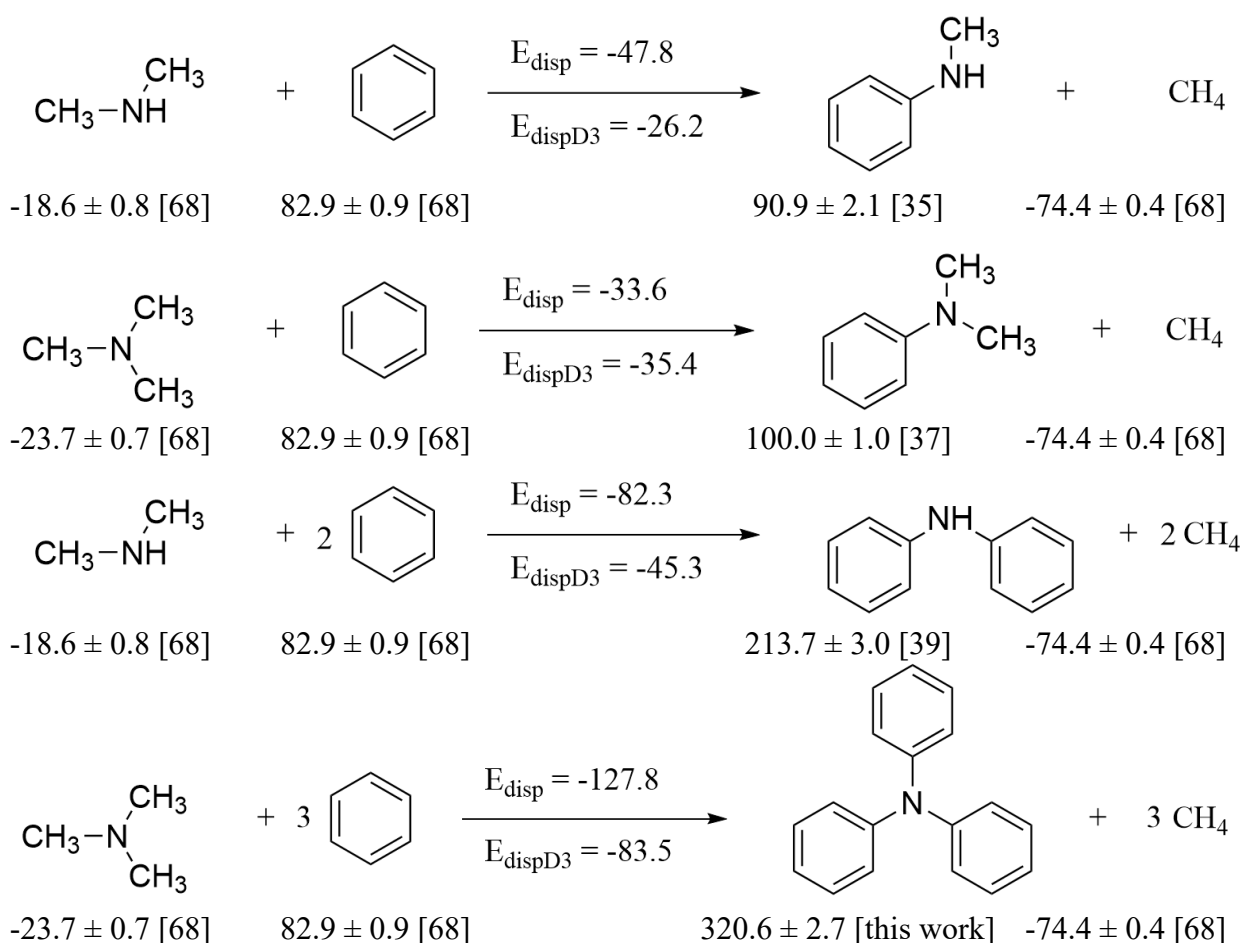


Figure 3.4.6 Calculation of the dispersion interaction in phenyl-substituted amines with help of the well-balanced reactions. The standard molar enthalpies of formation of reaction participants are given (in $\text{kJ}\cdot\text{mol}^{-1}$) below the formulas. E_{disp} = dispersion forces calculated (in $\text{kJ}\cdot\text{mol}^{-1}$) according to Hess's Law. $E_{\text{disp-D3}}$ = dispersion forces calculated (in $\text{kJ}\cdot\text{mol}^{-1}$) with the DFT-D3.

The *experimental* gas-phase standard molar enthalpies of formation $\Delta_f H_m^0(\text{g}, 298.15 \text{ K})$ of phenyl substituted amines used for the interpretation of dispersion forces are given in Table 3.4.5 (column 3). Last decade, the composite high-level quantum-chemical methods from the G*-family become a valuable tool to obtain *theoretical* $\Delta_f H_m^0(\text{g}, 298.15)$ -values with so-called “chemical accuracy” of 4-5 $\text{kJ}\cdot\text{mol}^{-1}$ [141,142]. The *theoretical* $\Delta_f H_m^0(\text{g}, 298.15)$ -values of aromatic and aliphatic amines were calculated by the G4 method were used in this work for validation of *experimental* results collected in Table 3.4.5. An agreement or disagreement between the *theoretical* and *experimental* $\Delta_f H_m^0(\text{g}, 298.15 \text{ K})$ -values could be used as an indicator for the mutual consistency.

Table 3.4.5 Thermochemical data for aromatic and aliphatic amines at $T=298.15 \text{ K}$ ($p^0=0.1 \text{ MPa}$, in $\text{kJ}\cdot\text{mol}^{-1}$)^a

	$\Delta_f H_m^0(\text{g})_{\text{G4-AT}}^b$	$\Delta_f H_m^0(\text{g})_{\text{exp}}$	$\Delta_f H_m^0(\text{g})_{\text{theor}}^c$	Δ^d
<i>aromatic amines</i>				
aniline	87.6	87.1±0.8 [68]	87.4	-0.3

N-methyl-aniline	93.1	90.9±2.1 [35]	92.8	-1.9
N,N-dimethyl-aniline	100.8	100.0±1.0 [37]	100.4	-0.4
diphenyl-amine	214.1	213.7±3.0 [39]	211.5	2.2
tri-phenylamine	325.3		320.6 ^e	
<i>aliphatic amines</i>				
tri-methyl-amine	-25.5	-23.7±0.7 [68]	-23.5	-0.2
tri-ethyl-amine	-96.7	-92.8±0.6 [68]	-93.4	0.6
tri-n-propyl-amine	-164.0	-161.0±0.9 [68]	-159.4	-1.6
tri-butyl-amine	-231.0	-223.2±1.3 ^f	-225.1	1.9

^a The uncertainties in this table are expressed as the twice standard deviation.

^b Calculated by the G4 method by using of the atomization reaction (see text). The expanded uncertainty assessed to be of ±3.5 kJ·mol⁻¹ [143].

^c Calculated according to Eq. (3.4.3).

^d Difference between columns 3 and 4.

^e The value $\Delta_f H_m^0(\text{g})_{\text{theor}} = 320.0 \pm 4.1$ kJ·mol⁻¹ was recently calculated by the G3MP2 method by using of the corrected atomization reaction [144].

^f Calculated from $\Delta_f H_m^0(\text{liq})_{\text{exp}} = -281.6 \pm 1.2$ kJ·mol⁻¹ [145] and $\Delta_f^{\text{g}} H_m^0(\text{exp}) = 58.3 \pm 0.6$ kJ·mol⁻¹ measured in this work (see Section 2.1)

The H_{298} -values from the G4 output have been converted to the standard molar enthalpies of formation $\Delta_f H_m^0(\text{g}, 298.15 \text{ K})_{\text{theor}}$ using the atomization (AT) reaction. The atomization reaction is given by the following equation:



Based on our experience with the quantum chemical calculations, the enthalpies of formation from the atomization reaction sometimes systematically deviate from the experimental values [146]. However, a simple linear correlation could be found between calculated by the atomisation reaction and experimental enthalpies of formation of aliphatic and aromatic amines collected in Table 3.4.5:

$$\Delta_f H_m^0(\text{g})_{\text{theor}} / \text{kJ} \cdot \text{mol}^{-1} = 0.9809 \times \Delta_f H_m^0(\text{g}, \text{AT}) + 1.5 \text{ with } R^2 = 0.9999 \quad (3.4.3)$$

Using these correlations, the “corrected” theoretical enthalpies of formation of aliphatic and aromatic amines have been calculated (see Table 3.4.5, column 4). As it apparent from Table 3.4.5, the G4 *theoretical* values $\Delta_f H_m^0(\text{g}, 298.15 \text{ K})_{\text{theor}}$ are practically indistinguishable from the *experimental* results. The good agreement observed among the *theoretical* and *experimental* $\Delta_f H_m^0(\text{g}, 298.15 \text{ K})$ -values for aliphatic and aromatic amines can be considered as an evidence of the internal consistency of thermochemical results evaluated in Table 3.4.5, which can be recommended now as reliable benchmark properties for further thermochemical calculations, *e.g.*, for calculations of dispersion interactions in aromatic amines as it shown in Figure 3.4.6.

As it can be seen in Figure 3.4.6, a surprisingly significant amount of dispersion interactions in all aromatic amines was derived according to the WBR. As expected, the values $E_{\text{disp}} = -82.3$ kJ·mol⁻¹ for diphenylamine and $E_{\text{disp}} = -127.8$ kJ·mol⁻¹ are more profound compared to the aniline derivatives. The results of the DFT-D3 calculations are also given in Figure 3.4.6 for comparison to those that derived from the experimental enthalpies of formation according to WBR. Unexpected the

DFT-D3 calculated dispersion contributions are systematically underestimated, but they linearly correlate with the E_{disp} values, as follows:

$$E_{\text{disp}} / \text{kJ}\cdot\text{mol}^{-1} = 1.31 \times E_{\text{disp-D3}} - 19.4 \quad \text{with } R^2 = 0.9867 \quad (3.4.4)$$

The reason of this scaling requires further investigations, however, the good correlation between two independent methods promotes the use of the thermodynamic values and the WBR to quantify the dispersion forces.

The visualization on Figure 3.4.7 of the diphenyl structures the conformations of which were obtained with the D3-method can provide a clear understanding of how the dispersion forces orient the phenyl rings towards each other.

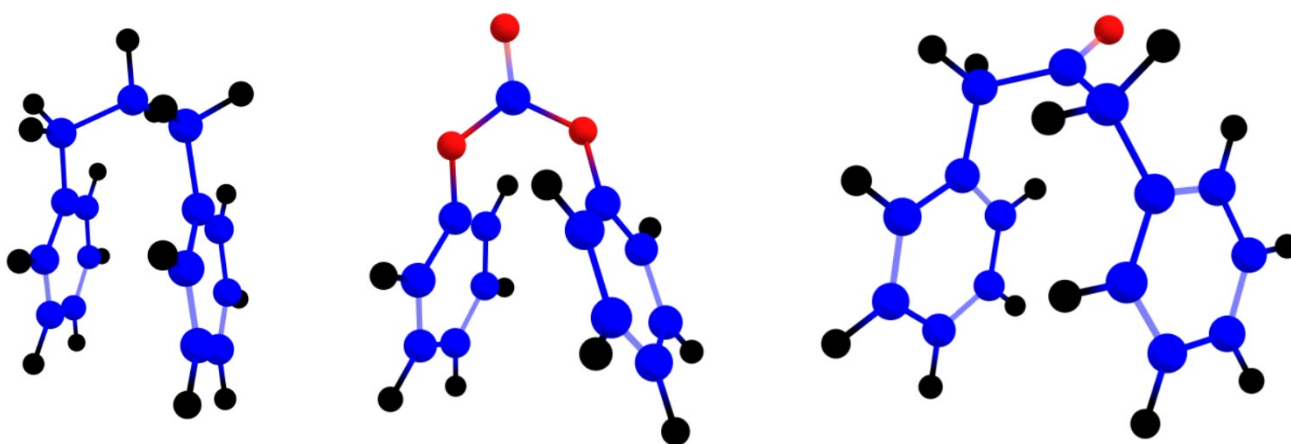


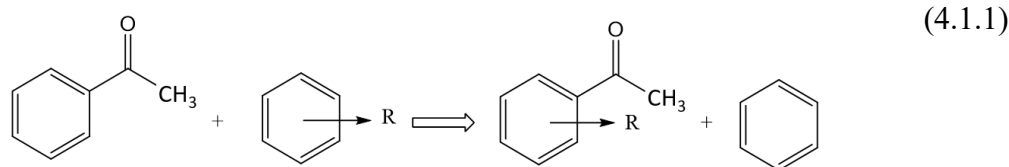
Figure 3.4.7 3D-models of structures of 1,3-diphenyl-propan, diphenyl carbonate, and 1,3-diphenyl-2-propanone

4. Nearest-neighbour and non-nearest-neighbour non-covalent interactions between substituents in the aromatic systems. Experimental and theoretical study of functionally substituted acetophenones and benzophenones

4.1. Introduction

The study of non-bonded interactions between various functional groups in the benzene ring is a very popular topic in physical chemistry [147]. The perturbation of electronic density on the benzene ring due to interactions of the substituents is usually responsible for the distribution of the *ortho*-, *meta*-, and *para*-isomers by synthesis. Numerically the substituent effects are often described by various substituent constants of the substituents X and Y, which are generally divided into the electron-withdrawing group and the electron-donating group. The concept of substituent effects in the benzene ring is not straightforward, but it is successfully realized in organic and inorganic chemistry [148]. Also, in *thermochemistry* the pairwise nearest and non-nearest neighbor interactions between substituents in the benzene ring are also responsible for the distribution of the *ortho*-, *meta*-, and *para*-isomers, *e.g.*, in the case of production of an industrially important antioxidant *para*-tert-

butylphenol via alkylation of phenol with isobutene [149]. Moreover, the knowledge of the pairwise interactions in the benzene ring is essential for prediction of thermochemical properties of the benzene derivatives based on the group-additivity procedure [21,149–152]. Admittedly, a reaction enthalpy, $\Delta_r H_m^0$, of a general distribution reaction (4.1.1) with participation of e.g., acetophenone:



as calculated according to the Hess's Law can be considered as an evidence of the pairwise interaction of substituents R and carbonyl-group in their 2-, 3-, and 4-position on the benzene ring. In comparison to classical values of enthalpies of formation, $\Delta_f H_m^0(\text{g})$, which are mostly responsible for the overall energetics of a molecule, the energetics of the *ortho*-, *meta*-, and *para*- pairwise interactions is more demonstrative for interpretation by using $\Delta_r H_m^0$ -values derived for the disproportionation reaction (4.1.1). From our experiences [21,149–152], the pairwise *meta*-, and *para*-interactions of different substituents R are usually weak, and they hardly exceed a few $\text{kJ}\cdot\text{mol}^{-1}$. On the contrary, the *ortho*-interactions can be strongly destabilizing due to steric interactions or stabilizing due to the *intra*-molecular hydrogen bonding. The *ortho*-repulsions are unique and they are usually dependent on the nature and the size of substituents. However, a general quantification of *ortho*-, *meta*-, and *para*-pairwise interactions is required for the optimization of synthesis and for a quick appraisal of positional isomers distribution in the reaction mixtures. Moreover, the quantitative knowledge of intensity of pairwise nearest-neighbour and non-nearest-neighbour non-covalent interactions is crucially important for validation and evaluation of experimental or theoretical data. Especially for thermochemical data of benzene derivatives, where a dramatic disagreement of available experimental data is often discussed [152–154], the determination and discussion of *ortho*-, *meta*-, and *para*- pairwise interactions is one of the possible ways to establish the reliability and consistency of the available experimental data. Substituted acetophenones and benzophenones have received much attention in the recent thermochemical literature [51,155–168] mainly due to biological, antibacterial activity and application in polymer industry (as UV stabilizers). Thermochemical data for this chemical family like standard molar enthalpies of formation, $\Delta_f H_m^0$, standard molar enthalpies of sublimation, $\Delta_{\text{cr}}^{\text{g}} H_m^0$, standard molar enthalpies of vaporization, $\Delta_{\text{f}}^{\text{g}} H_m^0$, and standard molar enthalpies of fusion, $\Delta_{\text{cr}}^{\text{l}} H_m^0$, are of practical importance for optimization of synthetic procedures.

The aim of this work is to use experimental and computational methods to obtain reliable thermodynamic information for the development of quantitative structure-property relationships in molecules that are relevant for the chemical engineering.

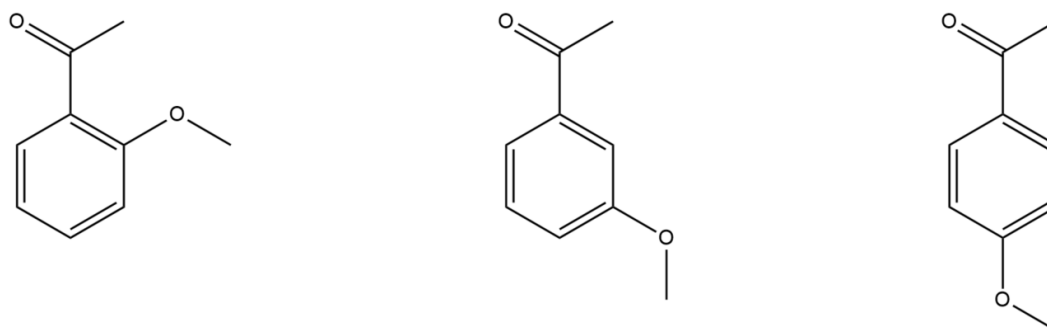


Figure 4.1.1 Methoxy-acetophenones studied in this work

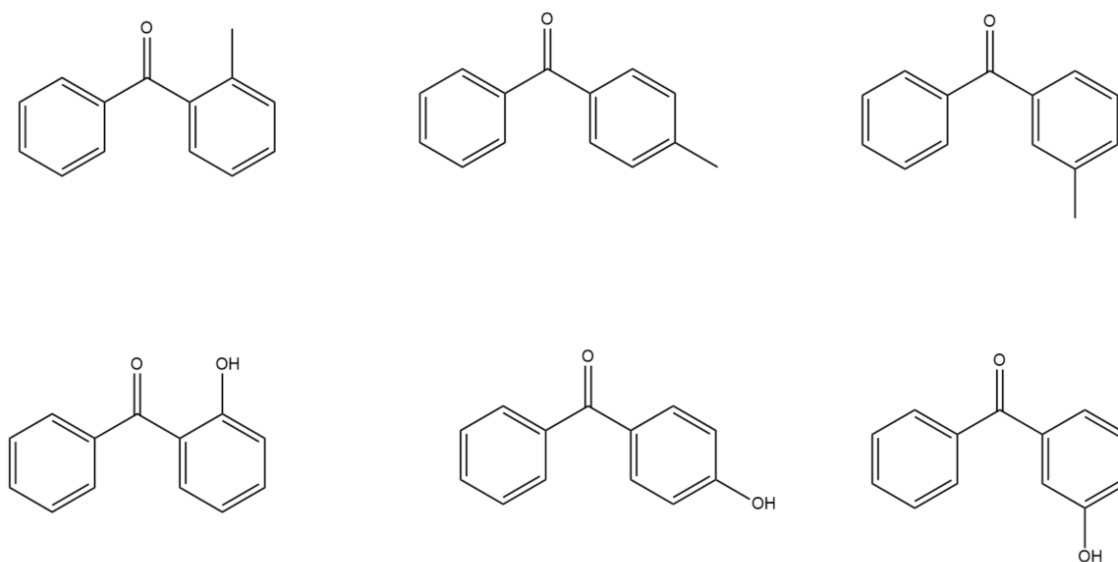


Figure 4.1.2 Mono-substituted benzophenones studied in this work

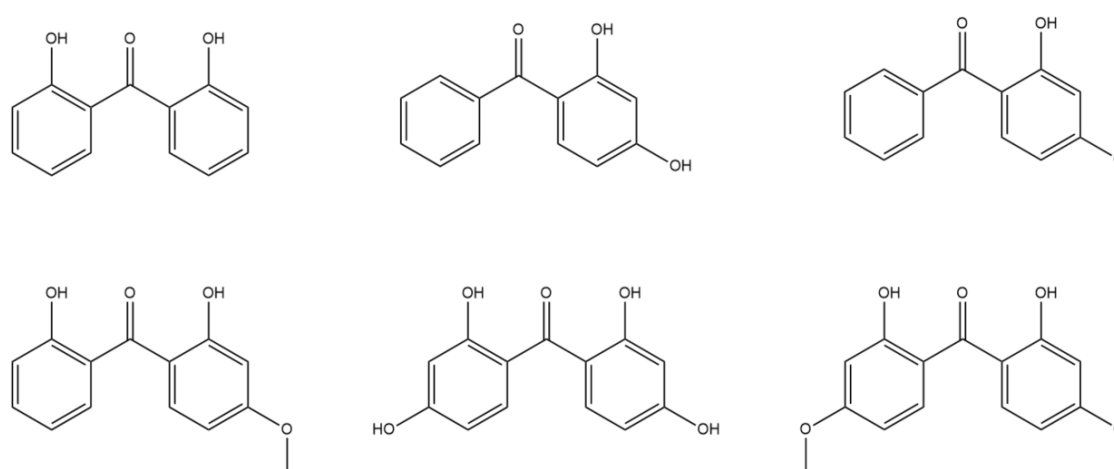


Figure 4.1.3 Poly-substituted benzophenones studied in this work

Here we present results on vapor pressures, enthalpies of phase transitions, and enthalpies of formation, of a series of substituted acetophenones and benzophenones of general formulas given in Figure 4.1.1, Figure 4.1.2, and Figure 4.1.3 . The data available in the literature and new experimental results were evaluated and checked for internal consistency. The consistent thermochemical data sets for substituted acetophenones and benzophenones have been used for the design and the development of a “centerpiece” group-contribution approach being necessary for appraisal of enthalpies of formation and enthalpies of vaporisation of compounds important for the utilisation of renewable feedstock for the platform chemicals.

4.2. Materials and methods

Commercially available samples of substituted acetophenones and benzophenones have been used in this work. Liquid samples were purified by the fractional distillation. Solid samples were purified by the fractional sublimation in a vacuum. Purities were determined using a gas chromatograph equipped with a capillary column HP-5 and a flame ionization detector. No impurities (greater than 0.003 mass fraction) were detected in samples used for vapor pressure measurements. Vapour pressures of substituted acetophenones and benzophenones at different temperatures were measured by using the transpiration method [169,170] and Knudsen effusion method [171]. The standard molar enthalpies of vaporization/sublimation, $\Delta_{l,cr}^g H_m^o$, were derived from the temperature dependences of vapour pressures. Melting temperatures and enthalpies of fusion were measured by DSC [172]. The quantum-chemical composite G4 method from Gaussian 09 software [143] was used for calculations of enthalpies H_{298} -values, which were finally converted to the $\Delta_f H_m^o(g)$ and discussed.

4.3. Results and discussion

4.3.1. Absolute vapour pressures and thermodynamics of vaporization/sublimation

Experimental vapour pressures, p_i , for the substituted acetophenones and benzophenones and their temperature dependence were measured by the transpiration method. Results of transpiration method are given in Table C.1.

Experimental vapour pressures, p_i , for 2,4-di-hydroxy-benzophenone and 2,2'4,4'-di-hydroxy-benzophenone were too low to be measured by the transpiration method within a reasonable time. Their temperature dependences were measured by the Knudsen effusion method. Results of Knudsen method are given in Table C.2.

Vapor pressure results for the substituted acetophenones and benzophenones were fit to the following equation[169,170]:

$$R \times \ln(p_i / p_{ref}) = a + \frac{b}{T} + \Delta_{l,cr}^g C_{p,m}^o \times \ln\left(\frac{T}{T_0}\right) \quad (4.3.1)$$

where $R = 8.31446 \text{ J}\cdot\text{K}^{-1}\cdot\text{mol}^{-1}$ is the molar gas constant, the reference pressure, $p_{ref} = 1 \text{ Pa}$, and a and b are adjustable parameters; the arbitrary temperature T_0 applied in Eq.(4.3.1) was chosen to be $T_0 = 298.15 \text{ K}$ and $\Delta_{l,cr}^g C_{p,m}^o$ is the difference of the molar heat capacities of the gas and the liquid/crystal phases respectively. The isobaric heat capacity differences $\Delta_{l,cr}^g C_{p,m}^o$ are required for temperature adjustments of vaporization/sublimation enthalpies are given in Table 4.3.1.

Table 4.3.1 Compilation of data on molar heat capacities $C_{p,m}^o$ (cr or liq) and heat capacity differences $\Delta_{cr,l}^g C_{p,m}^o$ at $T = 298.15 \text{ K}$ (in $\text{J}\cdot\text{K}^{-1}\cdot\text{mol}^{-1}$)

Compounds	$C_{p,m}^o$ (cr) ^a	$-\Delta_{cr}^g C_{p,m}^o$ ^b	$C_{p,m}^o$ (liq) ^a	$-\Delta_l^g C_{p,m}^o$ ^b
<i>x</i> -methoxy-acetophenone	213.2	32.7	265.0	79.5
<i>x,x</i> -dimethoxy-acetophenone	222.7	34.2	286.5	85.1
<i>x</i> -methyl-benzophenone	254.1	38.9	326.4	95.4
2-hydroxy-benzophenone	225.4 [164]	34.6	366.4	105.8
3-hydroxy-benzophenone	233.7 [164]	35.8	366.4	105.8
4-hydroxy-benzophenone	226.0 [164]	34.7	366.4	105.8
2,4-dihydroxy-benzophenone	254.9	39.0	434.8	123.6
2,2'-dihydroxy-benzophenone	253.0 [162]	38.7	434.8	123.6
2-hydroxy-4-methoxy-benzophenone	286.6	43.8	422.8	120.5
2,2'-hydroxy-4-methoxy-benzophenone	301.0	45.9	491.2	138.3
2,2',4,4'-tetrahydroxy-benzophenone	283.2	43.2	571.6	159.2
2,2'-dihydroxy-4,4'- dimethoxybenzophenone	347.0	52.8	547.6	153.0

^a Calculated by the group-contribution procedure developed by Chickos *et al.*[16].

^b Calculated according to the procedure developed by Acree and Chickos [18].

Vapor pressure measured at different temperatures, T , measured in this work, as well as those available from the literature, have been used to derive the enthalpies of sublimation/vaporization using the following equation:

$$\Delta_{cr,l}^g H_m^o(T) = -b + \Delta_{cr,l}^g C_{p,m}^o \times T \quad (4.3.2)$$

Sublimation entropies at temperatures T were also derived from the vapor pressures temperature dependences using Eq. (4.3.3):

$$\Delta_{cr,l}^g S_m^o(T) = \Delta_{cr,l}^g H_m^o/T + R \ln(p_i/p^o) \quad (4.3.3)$$

with $p^o = 0.1 \text{ MPa}$. Experimental vapor pressures measured at different temperatures, coefficients a and b of Eq. (4.3.1), as well as values of $\Delta_{cr,l}^g H_m^o(T)$ and $\Delta_{cr,l}^g S_m^o(T)$ are given in Table C.1 and Table C.2. The method for calculating the combined uncertainties of the vaporization/sublimation enthalpies includes uncertainties from the experimental conditions of transpiration, uncertainties in vapor pressure and uncertainties due to the temperature adjustment to $T = 298.15 \text{ K}$ as described elsewhere [28,29]. The compilation of available standard molar vaporization/sublimation enthalpies for the compounds shown in Figure 4.1.1 is given in Table 4.3.2. The original absolute vapor

pressures available in the literature have been also treated by using Eqs. (4.3.2) and (4.3.3) to evaluate enthalpies of vaporization/sublimation at 298.15 K (see Table 4.3.2) in the same way as our own results. Uncertainties of the literature results have been also re-assessed in the same way [28,29] as for our own experimental results.

Table 4.3.2 Compilation of enthalpies of vaporization/sublimation $\Delta_{l,cr}^g H_m^o$ for the acetophenone derivatives derived in this work and from the data available in the literature.

Compound	M ^a	T- range	$\Delta_{l,cr}^g H_m^o(T_{av})$	$\Delta_{l,cr}^g H_m^o(298.15 \text{ K})^b$	Ref.
CAS		K	kJ·mol ⁻¹	kJ·mol ⁻¹	
acetophenone [98-86-2]				55.4±0.3	[159]
2'-methoxy-acetophenone (liq)	C	365.4	78.3±0.6	66.7±1.2	[173]
579-74-8	T	293.1-348.1	62.9±0.3	64.6±0.4	Table C.1
	J_x			64.8±0.5	Table 4.3.6
				64.6±0.4^c	average
3'-methoxy-acetophenone (liq)	C	365.3	80.1±0.6	67.8±1.2	[173]
586-37-8	T	293.1-363.2	63.7±0.3	65.8±0.4	Table C.1
	J_x			65.7±0.5	Table 4.3.6
				65.9±0.3^c	average
4'-methoxy-acetophenone (cr)	K	286.8-311.4	93.9±4.0	93.9±4.1	[174]
100-06-1	VG	275.8-300.4	77.7±0.5	(77.4±0.8)	[175]
	C	334.4	94.2±0.6	87.8±1.4	[176]
	S	296.2-308.1	89.6±0.5	89.7±1.4	[176]
	T_{fus}			86.6±0.8	Table 4.3.10
				87.6±0.6^c	average
4'-methoxy-acetophenone (liq)	K	312.8-333.5	66.8±4.4	68.7±4.5	[174]
	S	302.1-355.7	71.4±1.4	73.8±1.5	[176]
	T	317.2-354.1	67.3±0.5	70.1±0.6	Table C.1
	J_x			70.2±0.5	Table 4.3.6
				70.4±0.4^c	average

^a Techniques: T = transpiration method; C = Calvet microcalorimetry; VG = viscosity gauge; K = Knudsen effusion method; S = static method; J_x – from correlation of experimental vaporization enthalpies with Kovats's indices (see text); S = static method; S = static method; T_{fus} = calculated according to Eq. (4.3.7). (see text)

^b Vapor pressures available in the literature were treated using Eqs. (4.3.2) and (4.3.7) with help of heat capacity differences from Table 4.3.1 to evaluate the enthalpy of vaporization at 298.15 K in the same way as our own results in Table C.1 and Table C.2. Uncertainty of the vaporization enthalpy $U(\Delta_l^g H_m^o)$ is the expanded uncertainty (0.95 level of confidence) calculated according to procedure described elsewhere [28,29].

^c Weighted mean value. Values in parenthesis were excluded from the calculation of the mean. Values in bold are recommended for further thermochemical calculations.

Table 4.3.3 Compilation of enthalpies of vaporization/sublimation $\Delta_{l,cr}^g H_m^o$ for the dimethoxy-acetophenones derivatives derived in this work and from the data available in the literature.

Compound	M ^a	T- range	$\Delta_{l,cr}^g H_m^o(T_{av})$	$\Delta_{l,cr}^g H_m^o(298.15 \text{ K})^b$	Ref.
CAS		K	kJ·mol ⁻¹	kJ·mol ⁻¹	
2,4-dimethoxy-acetophenone (cr)	C	355.0	115.0±0.6	102.0±1.5	[177]
2,4-dimethoxy-acetophenone (liq)	T_f			85.9±1.5	Table 4.3.10
	J_x			83.8±2.0	Table 4.3.6
				85.1±1.2^c	average
2,5-dimethoxy-acetophenone (liq)	C	353.0	89.8±0.4	77.3±2.2	[177]
	J_x			79.8±2.0	Table 4.3.6
				78.7±1.5^c	average

2,6-dimethoxy-acetophenone (cr)	C	355.3	110.6±0.4	97.4±1.1	[177]
2,6-dimethoxy-acetophenone (liq)	T_f			78.9±1.3	Table 4.3.10
	J_x			77.3±2.0	Table 4.3.6
				78.4±1.1^c	average
3,4-dimethoxy-acetophenone (cr)	C	355.0	121.0±0.6	108.0±1.5	[177]
3,4-dimethoxy-acetophenone (liq)	T_f			91.8±1.6	Table 4.3.10

^a Techniques: C = Calvet microcalorimetry; J_x – from correlation of experimental vaporization enthalpies with Kovats' indices (see text); T_{fus} = calculated according to Eq. (4.3.7). (see text)

^b Vapor pressures available in the literature were treated using Eqs. (4.3.2) and (4.3.7) with help of heat capacity differences from Table 4.3.1 to evaluate the enthalpy of vaporization at 298.15 K in the same way as our own results in Table C.1 and Table C.2. Uncertainty of the vaporization enthalpy $U(\Delta_{l,cr}^g H_m^o)$ is the expanded uncertainty (0.95 level of confidence) calculated according to procedure described elsewhere [28,29].

^c Weighted mean value. Values in bold are recommended for further thermochemical calculations.

Table 4.3.4 Compilation of enthalpies of vaporization/sublimation $\Delta_{l,cr}^g H_m^o$ for the benzophenone derivatives derived in this work and from the data available in the literature.

Compound	M ^a	T- range	$\Delta_{l,cr}^g H_m^o(T_{av})$	$\Delta_{l,cr}^g H_m^o(298.15\text{ K})^b$	Ref.
CAS		K	$\text{kJ}\cdot\text{mol}^{-1}$	$\text{kJ}\cdot\text{mol}^{-1}$	
benzophenone	IP/E	355-579	64.8±0.3	78.4±0.9	[158]
	S	308.2-384.8	73.7±0.1	77.9±0.3	[163]
	T_f			78.0±0.4	Table 4.3.10
				78.0±0.2^c	average
2-methyl-benzophenone (liq) 131-58-8	n/a	435-580	64.4±2.0	84.4±2.3	[38]
	C	523	141.8±1.7	81.2±1.7	[163]
	J_x	298 K		81.1±0.5	Table 4.3.8
				81.2±0.5^c	average
3-methyl-benzophenone (liq) 643-65-2	n/a	445-585	67.8±2.0	(88.5±2.3)	[38]
	C	523	146.2±1.2	85.6±1.7	[163]
	T	303.2-362.2	77.2±0.5	80.4±0.6	Table C.1
	J_x	298 K		80.8±0.5	Table 4.3.8
				80.9±0.4^c	average
4-methyl-benzophenone (cr)	C	401	120.8±1.0	97.3±1.0	[163]
	SC	298		98.5±1.0	[166]
				97.9±0.7^c	average
4-methyl-benzophenone (liq)	n/a	450-492	71.9±2.0	(88.4±2.3)	[38]
	T_f			81.0±0.9	Table 4.3.10
	J_x	298 K		80.8±0.5	Table 4.3.8
				80.8±0.4^c	average

^a Techniques: T = transpiration method; C = Calvet microcalorimetry; SC = method based on solution calorimetry; IP = inclined-piston gauge manometry; E = ebulliometry; n/a = not available; J_x – from correlation of experimental vaporization enthalpies with Kovats' indices (see text); S = static method; T_{fus} = calculated according to Eq. (4.3.7) (see text)

^b Vapor pressures available in the literature were treated using Eqs. (4.3.2) and (4.3.7) with help of heat capacity differences from Table 4.3.1 to evaluate the enthalpy of vaporization at 298.15 K in the same way as our own results in Table C.1 and Table C.2. Uncertainty of the vaporization enthalpy $U(\Delta_{l,cr}^g H_m^o)$ is the expanded uncertainty (0.95 level of confidence) calculated according to procedure described elsewhere [28,29].

^c Weighted mean value. Values in parenthesis were excluded from the calculation of the mean. Values in bold are recommended for further thermochemical calculations.

Table 4.3.5 Compilation of enthalpies of vaporization/sublimation $\Delta_{l,cr}^g H_m^o$ for the benzophenone derivatives derived in this work and from the data available in the literature.

Compound	M ^a	T- range	$\Delta_{cr}^g H_m^o(T_{av})$	$\Delta_{cr}^g H_m^o(298.15\text{ K})^b$	Ref.
CAS		K	$\text{kJ}\cdot\text{mol}^{-1}$	$\text{kJ}\cdot\text{mol}^{-1}$	
2-hydroxy-benzophenone (cr) [117-99-7]	C	401.6	123.1±1.7	97.9±1.9	[164]

2-hydroxy-benzophenone (liq)	T_f			80.2±2.0	Table 4.3.10
3-hydroxy-benzophenone (cr) [13020-57-0]	K-QCM	361.2-378.2	129.9±0.7	131.7±0.9	[164]
3-hydroxy-benzophenone (liq)	T_f			110.8±2.2	Table 4.3.10
4-hydroxy-benzophenone(cr) [1137-42-4]	K-QCM	377.2-394.2	128.6±0.7	130.3±1.0	[164]
4-hydroxy-benzophenone (liq)	T_f			113.7±2.5	Table 4.3.10
2-methoxy-benzophenone (liq) [2553-04-0]				86.5±3.0 ^c	this work
3-methoxy-benzophenone (liq) [6136-67-0]	T_b	621.4 [178]		87.8±2.0	Table 4.3.9
4-methoxy-benzophenone (liq) [611-94-9]	T_b	628.2 [178]		89.2±2.0	Table 4.3.9
	J_x			93.5±2.0	Table 4.3.8
				91.3±1.4^d	average
2,4-di-hydroxy-benzophenone (cr)	IG	323-363	93±16	(95±16)	[157]
131-56-6	n/a	312-353	134.0±2.0	135.3±2.1	[179]
	K	366.6-406.8	129.5±2.8	133.0±2.9	Table C.2
				134.5±1.7^d	average
2,4-di-hydroxy-benzophenone (liq)	UVS	418-485	86.8±5.0	(105.8±5.0)	[155]
	T_f			112.3±4.2	Table 4.3.10
2-hydroxy-4-methoxy-benzophenone (cr)	n/a	281-337	118.8±5.0	119.3±5.0	[38]
131-57-7	K	306.5-320.5	109.0±5.0	109.6±5.1	[179]
	T_f			117.1±1.3	Table 4.3.10
				116.8±1.2^d	average
2-hydroxy-4-methoxy-benzophenone (liq)	UVS	337-413	74.2±5.0	(83.5±5.0)	[155]
	T	341.2-368.2	91.6±0.9	98.4±1.0	Table C.1
2,2'-dihydroxy-benzophenone (cr) [835-11-0]	T_f			101.9±1.3	Table 4.3.10
2,2'-dihydroxy-benzophenone (liq)	T	363.1-408.4	74.7±0.8	84.9±0.9	Table C.1
2-hydroxy-4-methoxy-benzophenone (liq)	UVS	337-413	74.2±2.0	(83.5±5.0)	[155]
	T	341.2-368.2	91.6±0.9	98.4±1.0	Table C.1
2,2'-dihydroxy-4-methoxy-benzophenone (cr)	n/a	303-342	228±5	(229±5.0)	[38]
131-53-3	T_f			118.6±1.6	Table 4.3.10
2,2'-dihydroxy-4-methoxy-benzophenone (cr)	TGA	343-573	81.8	-	[160]
131-53-3	UVS	342-481	74.1±5.0	(89.7±5.0)	[155]
	T	365.1-430.9	87.1±0.7	100.7±0.9	Table C.1
2,2',4,4'-tetrahydroxy-benzophenone (cr)	n/a	363-471	143.2±5.0	(148.7±5.0)	[38]
131-55-5	K	431.8-453.8	153.6±2.6	159.8±3.1	Table 4.3.10
2,2',4,4'-tetrahydroxy-benzophenone (liq)	TGA	472-573	150.5	-	[160]
	T_f			152.0±6.8	Table 4.3.10
2,2'-dihydroxy-4,4'-dimethoxybenzophenone (cr)	n/a	325-408	146.8±5.0	(150.4±5.0)	[38]
131-54-4	T	368.5-399.3	134.8±2.2	139.4±2.4	Table C.1
2,2'-dihydroxy-4,4'-dimethoxybenzophenone (liq)	TGA	412-573	96.9	-	[160]
	K	412.6-435.1	98.0±2.8	117.2±2.9	Table C.2
	T_f			117.6±4.2	Table 4.3.10
				117.3±2.4^d	average

^a Techniques: T = transpiration method; C = Calvet microcalorimetry; K = Knudsen effusion method; K-QCM = Knudsen effusion method combined with the quartz-crystal microbalance for the mass loss measurements; IP = inclined-piston gauge manometry; E = ebulliometry; UVS = ultraviolet spectrophotometry; IG = ionisation gauge; n/a = not available; J_x – from correlation of experimental vaporization enthalpies with Kovats's indices (see text); S = static method; T_{fus} = calculated according Eq. (4.3.7) (see text); T_b – from correlation of experimental vaporization enthalpies with the normal boiling temperatures(see text); TGA = thermogravimetry.

^b Vapor pressures available in the literature were treated using Eqs. (4.3.2) and (4.3.7) with help of heat capacity differences from Table 4.3.1 to evaluate the enthalpy of vaporization at 298.15 K in the same way as our own results in Table C.1 and Table C.2. Uncertainty of the vaporization enthalpy $U(\Delta_1^g H_m^0)$ is the expanded uncertainty (0.95 level of confidence) calculated according to procedure described elsewhere [28,29].

^c Assessed based on vaporization enthalpy of 3-methoxy-benzopenone (this table) and the difference between vaporization enthalpy of 2-methoxy- and 3-methoxy-acetophenone (Table 4.3.2).

^d Weighted mean value. Values in parenthesis were excluded from the calculation of the mean. Values in bold are recommended for further thermochemical calculations.

4.3.2. Consistency of vaporization/sublimation enthalpies

4.3.2.1. Kovats's retention indices for validation of experimental vaporization enthalpies

A valuable method for validation of the $\Delta_1^{\text{g}}H_{\text{m}}^{\circ}(298.15 \text{ K})$ -values collected in Table 4.3.2, Table 4.3.3, Table 4.3.4, and Table 4.3.5 is a method based on chromatographic retention indices [33,132] available for substituted acetophenones and benzophenones [180,181]. It is known, that the $\Delta_1^{\text{g}}H_{\text{m}}^{\circ}(298.15 \text{ K})$ -values correlate linearly with Kovats's indices in various homologous series of alkanes, alkylbenzenes, aliphatic ethers, alcohols, or in a series of structurally similar compounds [141]. The following linear correlation was obtained when the $\Delta_1^{\text{g}}H_{\text{m}}^{\circ}(298.15 \text{ K})$ -values are correlated with J_x -values for the structurally parent set of methoxy-acetophenones collected in Table 4.3.6:

$$\Delta_1^{\text{g}}H_{\text{m}}^{\circ}(298.15 \text{ K}) / (\text{kJ}\cdot\text{mol}^{-1}) = -53.5 + 0.0932 \times J_x \quad \text{with } (R^2 = 0.9978) \quad (4.3.4)$$

Also, linear correlation was obtained when the $\Delta_1^{\text{g}}H_{\text{m}}^{\circ}(298.15 \text{ K})$ -values are correlated with J_x -values for the structurally parent set of benzophenones collected in Table 4.3.6:

$$\Delta_1^{\text{g}}H_{\text{m}}^{\circ}(298.15 \text{ K}) / (\text{kJ}\cdot\text{mol}^{-1}) = 29.0 + 0.0306 \times J_x \quad \text{with } (R^2 = 0.9685) \quad (4.3.5)$$

Table 4.3.6 Correlation of vaporization enthalpies, $\Delta_1^{\text{g}}H_{\text{m}}^{\circ}(298.15 \text{ K})$, of substituted acetophenones and benzophenones with their Kovats's indices (J_x)

Compound	J_x ^a	$\Delta_1^{\text{g}}H_{\text{m}}^{\circ}(298 \text{ K})_{\text{exp}}$	$\Delta_1^{\text{g}}H_{\text{m}}^{\circ}(298 \text{ K})_{\text{calc}}$	Δ^{b}
		$\text{kJ}\cdot\text{mol}^{-1}$	$\text{kJ}\cdot\text{mol}^{-1}$	$\text{kJ}\cdot\text{mol}^{-1}$
2'-methoxy-acetophenone	1269	64.6±0.4 ^c	64.8 ^d	-0.2
3'-methoxy-acetophenone	1279	65.8±0.4 ^c	65.7 ^d	0.1
4'-methoxy-acetophenone	1327	70.1±0.6 ^c	70.2 ^d	-0.1
benzophenone	1603	78.0±0.2 ^e	78.1 ^f	-0.1
2-methyl-benzophenone	1704	81.2±1.7 ^e	81.1 ^f	0.1
3-methyl-benzophenone	1694	80.4±0.6 ^e	80.8 ^f	-0.4
4-methyl-benzophenone	1694	81.0±0.9 ^e	80.8 ^f	0.2

^a Kovats's indices, J_x , on the standard non-polar column SE-30 [180].

^b Difference between column 4 and 5 in this table.

^c Experimental data measured by using the transpiration method (see Table C.1).

^d Calculated using Eq. (4.3.4): $\Delta_1^{\text{g}}H_{\text{m}}^{\circ}(298.15 \text{ K}) / (\text{kJ}\cdot\text{mol}^{-1}) = -53.5 + 0.0932 \times J_x$ with $(R^2 = 0.9978)$ with the assessed uncertainty of $\pm 0.5 \text{ kJ}\cdot\text{mol}^{-1}$ (expanded uncertainty 0.95 level of confidence).

^e Selected experimental data (given in italic in Table 4.3.4).

^f Calculated using Eq. (4.3.5): $\Delta_1^{\text{g}}H_{\text{m}}^{\circ}(298.15 \text{ K}) / (\text{kJ}\cdot\text{mol}^{-1}) = 29.0 + 0.0306 \times J_x$ with $(R^2 = 0.9685)$ with the assessed uncertainty of $\pm 0.5 \text{ kJ}\cdot\text{mol}^{-1}$ (expanded uncertainty 0.95 level of confidence).

The vaporization enthalpies for methoxy-acetophenones derived from the correlations with Kovats's indices (see Table 4.3.6) are in a good agreement with those obtained by the transpiration method (see Table C.1). Also the vaporization enthalpies for the set of the methyl-substituted benzophenones derived from the J_x -correlation (see Table 4.3.6) are in agreement with those from conventional methods (see Table 4.3.4). Such good agreement can be seen as additional validation of

the experimental data measured and evaluated in this work. It can be seen from Table 4.3.6, that differences between experimental vaporization enthalpies and values calculated according to Eqs. (4.3.4) and (4.3.5) are mostly below 1 kJ·mol⁻¹. Hence, the uncertainties of the “theoretical” enthalpies of vaporization which are estimated from the correlation of $\Delta_1^g H_m^o(298.15 \text{ K})$ with Kovats’s indices are evaluated with an uncertainty of $\pm 0.5 \text{ kJ}\cdot\text{mol}^{-1}$.

With this success of the of the $\Delta_1^g H_m^o - J_x$ -correlations it is reasonable to apply this method to derive vaporization enthalpies of substituted acetophenones (see Table 4.3.7) and substituted benzophenones (see Table 4.3.8), where J_x -values were available from the literature.

Table 4.3.7 Correlation of vaporization enthalpies, $\Delta_1^g H_m^o(298.15 \text{ K})$, of benzene and benzophenone derivatives with their Kovats’s indices (J_x)

Compound	J_x^a	$\Delta_1^g H_m^o(298 \text{ K})_{\text{exp}}$	$\Delta_1^g H_m^o(298 \text{ K})_{\text{calc}}^b$	Δ^c
		kJ·mol ⁻¹	kJ·mol ⁻¹	kJ·mol ⁻¹
methoxybenzene	900 [180]	46.6±0.2 [182]	46.2	0.4
acetophenone	1048 [180]	55.4±0.3 [159]	54.3	1.1
2'-methoxy-acetophenone	1269 [180]	64.6±0.4 ^d	66.4	-1.8
3'-methoxy-acetophenone	1279 [180]	65.8±0.4 ^d	67.0	-1.2
4'-methoxy-acetophenone	1327 [180]	70.4±0.6 ^d	69.6	0.8
2,4-dimethoxy-acetophenone	1586 [181]	85.9±1.5 ^e	83.8±2.0^f	2.1
2,5-dimethoxy-acetophenone	1515 [181]	77.3±2.2 ^e	79.8±2.0^f	-2.5
2,6-dimethoxy-acetophenone	1469 [181]	78.9±1.3 ^e	77.3±2.0^f	1.6

^a Kovats’s indices, J_x , on the standard non-polar columns [180,181]

^b Calculated using equation: $\Delta_1^g H_m^o(298.15 \text{ K}) / (\text{kJ}\cdot\text{mol}^{-1}) = 0.0547 \times J_x - 3.0$ with ($R^2 = 0.9828$)

^c Difference between column 4 and 5 in this table.

^d Experimental data measured by using the transpiration method (see Table C.1).

^e Experimental data measured by using the Calvet calorimetry (see Table 4.3.3).

^f Expanded uncertainty with 0.95 level of confidence.

Table 4.3.8 Correlation of vaporization enthalpies, $\Delta_1^g H_m^o(298.15 \text{ K})$, of benzene and benzophenone derivatives with their Kovats’s indices (J_x)

Compound	J_x^a	$\Delta_1^g H_m^o(298 \text{ K})_{\text{exp}}$	$\Delta_1^g H_m^o(298 \text{ K})_{\text{calc}}^b$	Δ^c
		kJ·mol ⁻¹	kJ·mol ⁻¹	kJ·mol ⁻¹
methoxybenzene	900	46.6±0.2 [182]	46.8	-0.2
acetophenone	1048	55.4±0.3 [159]	54.5	0.9
2'-methoxy-acetophenone	1269	64.6±0.4 ^d	65.9	-1.3
3'-methoxy-acetophenone	1279	65.8±0.4 ^d	66.4	-0.6
4'-methoxy-acetophenone	1327	70.4±0.6 ^d	68.9	1.5
4'-methoxy-benzophenone	1804 [183]	-	93.5±2.0^e	

^a Kovats’s indices, J_x , on the standard non-polar column SE-30 [180].

^b Calculated using equation: $\Delta_1^g H_m^o(298.15 \text{ K}) / (\text{kJ}\cdot\text{mol}^{-1}) = 0.0516 \times J_x + 0.4$ with ($R^2 = 0.9942$)

^c Difference between column 4 and 5 in this table.

^d Experimental data measured by using the transpiration method (see Table C.1).

^e Expanded uncertainty with 0.95 level of confidence.

The “theoretical” results derived from the correlation with the Kovats’s indices are designated as J_x . These results are valuable to support the level of enthalpy of vaporization derived from other methods, especially in cases where data are scarce (*e.g.*, for the dimethoxy-substituted acetophenones

in Table 4.3.3). The experimental and “theoretical” vaporization enthalpies derived for each compound are given in Table 4.3.2, Table 4.3.3, and Table 4.3.4.

4.3.2.2. Normal boiling temperatures for validation of experimental vaporization enthalpies

Another possible option for determining the consistency of the experimental results on vaporization enthalpies for substituted acetophenones and benzophenones is also the correlation of enthalpies of vaporization with normal boiling temperatures [184]. The literature data available on the normal boiling temperatures, T_b , for substituted acetophenones and benzophenones were taken for correlation with the $\Delta_1^g H_m^o(298.15 \text{ K})$ -values measured in this work by the transpiration (see Table C.1), as well as a selected data set for methyl-benzophenones (see Table 4.3.4). Indeed, the $\Delta_1^g H_m^o(298.15 \text{ K})$ -values correlated linearly with T_b values for both selected sets and we derived the following linear correlation:

$$\Delta_1^g H_m^o(298.15 \text{ K}) / (\text{kJ}\cdot\text{mol}^{-1}) = 0.2109 \times T_b - 43.3 \quad \text{with } (R^2 = 0.9887) \quad (4.3.6)$$

Table 4.3.9 Correlation of vaporization enthalpies, $\Delta_1^g H_m^o(298.15 \text{ K})$, of benzene and benzophenone derivatives with their normal boiling temperatures (T_b)

Compound	T_b ^a	$\Delta_1^g H_m^o(298 \text{ K})_{\text{exp}}$	$\Delta_1^g H_m^o(298 \text{ K})_{\text{calc}}$ ^b	Δ ^c
		$\text{kJ}\cdot\text{mol}^{-1}$	$\text{kJ}\cdot\text{mol}^{-1}$	$\text{kJ}\cdot\text{mol}^{-1}$
methoxybenzene	426.8	46.6±0.2 [182]	46.7	-0.1
acetophenone	475.8	55.4±0.3 [159]	57.0	-1.6
2'-methoxy-acetophenone	(511.5) ^d	64.6±0.4 ^e	64.6	0.0
3'-methoxy-acetophenone	513.2	65.8±0.4 ^e	64.9	1.0
4'-methoxy-acetophenone	531.2	70.4±0.6 ^e	68.7	1.7
benzophenone	578.6	78.0±0.2 ^f	78.7	-0.7
2'-methyl-benzophenone	582.7	81.2±1.7 ^f	79.6	1.6
3'-methyl-benzophenone	586.2	80.4±0.6 ^f	80.3	0.1
4'-methyl-benzophenone	599.2	81.0±0.9 ^f	83.1	-2.1
3'-methoxy-benzophenone	621.5 [178]		87.8±2.0	
4'-methoxy-benzophenone	628.2 [178]		89.2±2.0	

^a Normal boiling temperatures, T_b , [38].

^b Calculated using Eq. (4.3.6): $\Delta_1^g H_m^o(298.15 \text{ K}) / (\text{kJ}\cdot\text{mol}^{-1}) = 0.2109 \times T_b - 43.3$ with ($R^2 = 0.9887$).

^c Difference between column 4 and 5 in this table.

^d Assessed by Eq. (4.3.6).

^e Experimental data measured by using the transpiration method (see Table C.1).

^f Selected experimental data (given in italic in Table 4.3.4).

From in Table 4.3.2, Table 4.3.3, Table 4.3.4, and Table 4.3.5 can be seen, that for many compounds agreement among $\Delta_1^g H_m^o(298.15 \text{ K})$ -values, which were derived in different ways, all lie within the assigned error bars. To get more confidence and reliability, we calculated the weighted average (the uncertainty was used as a weighing factor) for the substituted acetophenones and

benzophenones given in Table 4.3.2, Table 4.3.3, Table 4.3.4, and Table 4.3.5. These values are highlighted in bold and are recommended for thermochemical calculations.

4.3.2.3. Phase transitions for validation of experimental vaporization enthalpies

The common thermochemical equation:

$$\Delta_{\text{l}}^{\text{g}}H_{\text{m}}^{\circ}(298.15 \text{ K}) = \Delta_{\text{cr}}^{\text{g}}H_{\text{m}}^{\circ}(298.15 \text{ K}) - \Delta_{\text{cr}}^{\text{l}}H_{\text{m}}^{\circ}(298.15 \text{ K}) \quad (4.3.7)$$

can be also used for establishing the consistency of experimental data on phase transitions (liquid-gas, solid-gas, and solid-liquid) measured or evaluated in this work. Indeed, for 2,2'-dihydroxy-4,4'-dimethoxybenzophenone, the sublimation enthalpy $\Delta_{\text{cr}}^{\text{g}}H_{\text{m}}^{\circ}(298.15 \text{ K}) = 139.4 \pm 2.4 \text{ kJ}\cdot\text{mol}^{-1}$ was measured using the transpiration method below the melting point (see Table C.1) and the vaporization enthalpy $\Delta_{\text{l}}^{\text{g}}H_{\text{m}}^{\circ}(298.15 \text{ K}) = 117.2 \pm 2.9 \text{ kJ}\cdot\text{mol}^{-1}$ was derived from vapour pressures measured above the melting point (see Table C.1). The consistency of phase transitions available for 2,2'-dihydroxy-4,4'-dimethoxybenzophenone can be easily established with help of Eq. (4.3.7) and the experimental enthalpy of fusion for this compound $\Delta_{\text{cr}}^{\text{l}}H_{\text{m}}^{\circ}(298.15 \text{ K}) = 21.8 \pm 3.4 \text{ kJ}\cdot\text{mol}^{-1}$ (see Table 4.3.9) as follows:

$\Delta_{\text{l}}^{\text{g}}H_{\text{m}}^{\circ}(298.15 \text{ K}, 2,2'\text{-dihydroxy-4,4'-dimethoxybenzophenone}) = 139.4 - 21.8 = 117.6 \pm 4.2 \text{ kJ}\cdot\text{mol}^{-1}$. This estimate is in an excellent agreement with the transpiration experiment $\Delta_{\text{l}}^{\text{g}}H_{\text{m}}^{\circ}(298.15 \text{ K}) = 117.2 \pm 2.9 \text{ kJ}\cdot\text{mol}^{-1}$, proving consistency of the energetics of all three phase transitions.

Table 4.3.10 Phase transitions thermodynamics of substituted acetophenones and benzophenones (in $\text{kJ}\cdot\text{mol}^{-1}$)^a

Compounds	T_{fus}, K	$\Delta_{\text{cr}}^{\text{l}}H_{\text{m}}^{\circ}$ at T_{fus}	WC^{b}	298.15 K		
				$\Delta_{\text{cr}}^{\text{l}}H_{\text{m}}^{\circ \text{c}}$	$\Delta_{\text{cr}}^{\text{g}}H_{\text{m}}^{\circ \text{d}}$	$\Delta_{\text{l}}^{\text{g}}H_{\text{m}}^{\circ \text{e}}$
1	2	3	4	5	6	7
acetophenones						
4-methoxy-acetophenone [176]	310.3±0.2	16.8±0.6	54.0	16.2±0.2	86.6±0.8 ^f	70.4±0.4 ^g
2,4-dimethoxy-acetophenone	315±1	17.0±0.5 ^h		16.1±0.5	102.0±1.5	85.9±1.5
2,6-dimethoxy-acetophenone	343±1	18.5±0.5 ^h		16.2±0.5	97.4±1.1	78.9±1.3
3,4-dimethoxy-acetophenone	325±1	17.6±0.5 ^h		16.2±0.5	108.0±1.5	91.8±1.6
benzophenones						
benzophenone [48]	321.0±0.1	18.2±0.1	56.7	17.0±0.3	95.0±0.4 ^f	78.0±0.2 ^g
4-methyl-benzophenone	327±1	18.5±0.5 ⁱ		16.9±0.7	97.7±0.8	80.8±0.4 ^g
2-hydroxy-benzophenone [164]	312.3±0.1	18.7±0.1	59.9	17.7±0.3	97.9±1.9	80.2±2.0
3-hydroxy-benzophenone [164]	390.5±0.3	27.4±0.2	70.2	20.9±2.0	131.7±0.9	110.8±2.2
4-hydroxy-benzophenone [164]	407.7±0.5	24.4±0.1	59.8	16.6±2.3	130.3±1.0	113.7±2.5
2,4-dihydroxy-benzophenone [this work]	417.7±0.2	30.8±0.7	73.7	20.7±3.1	133.0±2.9	112.3±4.2
2,2'-dihydroxy-benzophenone [162]	334.5±0.1	20.1±0.1	60.0	17.0±1.0	101.9±1.3 ^f	84.9±0.9 ^g
2-hydroxy-4-methoxy-benzophenone [179]	336.7±0.5	21.8±0.1	64.7	18.7±0.9	117.1±1.3 ^f	98.4±1.0 ^g
2,2'-hydroxy-4-methoxy-benzophenone [160]	343.0±0.5	22.0±0.5	64.1	17.9±1.3	118.6±1.6 ^f	100.7±0.9 ^g
2,2',4,4'-tetrahydroxy-benzophenone [160]	472.0±0.5	28.0±0.5	59.3	7.8±6.1	159.8±3.1	152.0±6.8
2,2'-dihydroxy-4,4'-dimethoxybenzophenone [160]	412.3±0.5	33.2±0.5	80.5	21.8±3.4	139.4±2.4	117.6±4.2
				64±5^j		

^a Uncertainties are presented as expanded uncertainties (0.95 level of confidence with $k=2$).

^b The *Walden's Constant* (WC) calculated according to Eq. (4.3.8).

^c The experimental enthalpies of fusion $\Delta_{\text{cr}}^{\text{l}}H_{\text{m}}^{\text{o}}$ measured at T_{fus} were adjusted to $T = 298.15$ K with help of the following equation [18]:

$$\Delta_{\text{cr}}^{\text{l}}H_{\text{m}}^{\text{o}}(298.15 \text{ K})/(\text{J}\cdot\text{mol}^{-1}) = \Delta_{\text{cr}}^{\text{l}}H_{\text{m}}^{\text{o}}(T_{\text{fus}}/\text{K}) - (\Delta_{\text{cr}}^{\text{g}}C_{\text{p,m}}^{\text{o}} - \Delta_{\text{l}}^{\text{g}}C_{\text{p,m}}^{\text{o}}) \times [(T_{\text{fus}}/\text{K}) - 298.15 \text{ K}],$$

where $\Delta_{\text{cr}}^{\text{g}}C_{\text{p,m}}^{\text{o}}$ and $\Delta_{\text{l}}^{\text{g}}C_{\text{p,m}}^{\text{o}}$ were taken from Table 4.3.1. Uncertainties in the temperature adjustment of fusion enthalpies from T_{fus} to the reference temperature are estimated to account with 30 % to the total adjustment [9].

^d Experimental values of sublimation enthalpies (see Table 4.3.2, Table 4.3.3, Table 4.3.4, and Table 4.3.5).

^e Calculated as the difference between column 6 and 5 in this table.

^f Calculated as the sum column 7 and 5 in this table.

^g Experimental values of vaporization enthalpies (see Table 4.3.2, Table 4.3.3, Table 4.3.4, and Table 4.3.5)

^h Calculated according to the *Walden's rule* with the *WC* from 4-methoxyacetophenone

ⁱ Calculated according to the *Walden's rule* with the *WC* from benzophenone

^j *Walden's constant WC* calculated as the average value from all data for acetophenones and benzophenones

We calculated vaporization enthalpies for substituted acetophenones and benzophenones according to Eq. (4.3.7) and used these values for comparison with results derived by other techniques (see Table 4.3.2, Table 4.3.3, Table 4.3.4, and Table 4.3.5)

4.3.3. Whether substituted acetophenones and benzophenones follow the *Walden's rule*?

In 1908 Paul Walden found that the ratio according to Eq. (4.3.8) can be considered as a constant (*Walden's Constant*) [185]:

$$WC = \frac{\Delta_{\text{cr}}^{\text{l}}H_{\text{m}}^{\text{o}}}{T_{\text{fus}}} = \Delta_{\text{cr}}^{\text{l}}S_{\text{m}}^{\text{o}} = 56.5 \text{ J}\cdot\text{K}^{-1}\cdot\text{mol}^{-1} \quad (4.3.8)$$

This observation was supported by experimental results from 35 compounds (mostly substituted benzenes like nitrobenzene, aniline, dimethylaniline, diphenylmethane, diphenylamine, acetophenone, *para*-propenylanisole, but also aliphatic esters, anhydrides, *etc.*). The prerequisite for this constancy is that the compounds did not associate in the liquid state. Eq. (4.3.9) is known as *Walden's rule* for thermochemistry [186]. The *Walden's rule* is derived from the general Gibbs–Helmholtz thermodynamic equation:

$$\Delta_{\text{cr}}^{\text{l}}G_{\text{m}}^{\text{o}} = \Delta_{\text{cr}}^{\text{l}}H_{\text{m}}^{\text{o}} - T_{\text{fus}} \times \Delta_{\text{cr}}^{\text{l}}S_{\text{m}}^{\text{o}} \quad (4.3.9)$$

where $\Delta_{\text{cr}}^{\text{l}}G_{\text{m}}^{\text{o}}$ is the standard molar Gibbs energy of the solid-liquid phase transition and $\Delta_{\text{cr}}^{\text{l}}S_{\text{m}}^{\text{o}}$ is the standard molar fusion entropy. At equilibrium $\Delta_{\text{cr}}^{\text{l}}G_{\text{m}}^{\text{o}} = 0$ and the *Walden's Constant* is equal to $\Delta_{\text{cr}}^{\text{l}}S_{\text{m}}^{\text{o}}$. The fundamental meaning of the latter equality is that the structure of the solid and liquid phase is in principle very close and determined (*e.g.*, by “non-associated” compounds) mainly by the weak van-der-Waals forces. The contribution of $56.5 \text{ J}\cdot\text{K}^{-1}\cdot\text{mol}^{-1}$ suggested by Walden may be considered as a constant entropic “penalty” for the re-organization of both “non-associated” phases during fusion [186]. It is obvious that most of substituted acetophenones and benzophenones cannot be considered as the “non-associated” molecules. How different from $56.5 \text{ J}\cdot\text{K}^{-1}\cdot\text{mol}^{-1}$ could the *WC* be for this set of relatively strongly associated molecules? We calculated the *Walden's Constants* according to Eq. (4.3.8) with help of fusion properties collected in Table 4.3.10. Results from *WC* calculations are given in Table 4.3.10, column 4.

It has turned out, that for the set of substituted acetophenones and benzophenones collected in Table 4.3.10 the value of $WC = 64 \pm 5 \text{ J} \cdot \text{K}^{-1} \cdot \text{mol}^{-1}$ is not significantly different from $56.5 \text{ J} \cdot \text{K}^{-1} \cdot \text{mol}^{-1}$. Moreover this value is equal to $WC = 64 \pm 3 \text{ J} \cdot \text{K}^{-1} \cdot \text{mol}^{-1}$ derived for the methoxy-substituted benzaldehydes and vanillins just recently [45], [187]. Why do the acetophenones, benzophenones, and vanillins as the strongly associated compounds follow Walden's rule, which was initially developed for “non-associated” systems? An explanation could be found with help of the concept “ideal associated solution” suggested by Prigogine [188]. Applying this concept of the “ideal associated solution” to the process of fusion of associated compounds considered in current study, we could see that we have strong associated network in the crystal state, but the same strong associated network remains in the liquid after melting. For this reason, Prigogine's "ideally associated" concept is an explanation for the equality of WC observed for differently structured hydroxy-substituted benzaldehydes. Conversely, if the hydrogen bonding network in the liquid phase must be changed, the Walden constants for all examined vanillins must be different since they have significantly different types of hydrogen bonding. The equivalence of the WC values shown in Table 4.3.10 has important consequences. From a practical point of view and based on our experience, Eq. (4.3.8) can be easily adapted for calculations within a range of similarly shaped molecules. We have already observed similarity of *Walden's Constants* for R-acetanilides with R = alkyl, F, Cl, Br, NO₂, NH₂, OH, OCH₃ [151] and for the for R-substituted benzamides [190]. We have found that for these series the WC for each series deviates from the “classic” value $56.5 \text{ J} \cdot \text{K}^{-1} \cdot \text{mol}^{-1}$ by about $\pm 10 \text{ J} \cdot \text{K}^{-1} \cdot \text{mol}^{-1}$. Such a “modified” *Walden's Constant* helps not only in evaluating the consistency of the experimental fusion data within a set of similarly structured compounds (see Table 4.3.10), but also the *Walden's rule* serves as a valuable tool for estimating missing fusion enthalpies of interesting organic compounds, provided that their fusion temperatures are available (e.g., dimethoxy-acetophenones in Table 4.3.10). Moreover, the “modified” *Walden's Rule* often helps to evaluate available phase transition data according to the general equation Eq. (4.3.7), as it was shown in previous section.

4.3.4. Gas-phase standard molar enthalpies of formation

Very limited enthalpies of formation of substituted acetophenones and benzophenones are available in the literature. The numerical data available in the literature are summarized in Table 4.3.11 for substituted acetophenones and in Table 4.3.12 for substituted benzophenones. Since the significant discrepancies among some available data for $\Delta_{\text{l,cr}}^{\text{g}} H_{\text{m}}^{\circ}$ or $\Delta_{\text{f}} H_{\text{m}}^{\circ}(\text{liq})$ have been noticed in Table 4.3.2, Table 4.3.3, Table 4.3.4, Table 4.3.5, Table 4.3.11, and Table 4.3.12, any additional arguments to support the reliability of the evaluated in Table 4.3.11, and Table 4.3.12 $\Delta_{\text{f}} H_{\text{m}}^{\circ}(\text{g}, 298.15 \text{ K})$ -values are required. Recent development of the high-level quantum chemistry methods has led to predicting enthalpies of formation $\Delta_{\text{f}} H_{\text{m}}^{\circ}(\text{g})$ with “chemical accuracy” which is usually defined as

within $\pm 4\text{-}5 \text{ kJ}\cdot\text{mol}^{-1}$ [141,142]. This trend has made the composite methods of the G-family a valuable tool to for the mutual validation of the experimental and computational thermochemistry. A disagreement or agreement between the *experimental* and *theoretical* $\Delta_f H_m^0(\text{g}, 298.15 \text{ K})$ -values could provide a criterion for the mutual validation for both results. Moreover, this valuable information helps in evaluation of the quality of the thermochemical data for compounds under study.

Table 4.3.11 Thermochemical data for substituted acetophenones at $T = 298.15 \text{ K}$ ($p^\circ = 0.1 \text{ MPa}$) (in $\text{kJ}\cdot\text{mol}^{-1}$)^a

Compound	$\Delta_f H_m^0(\text{cr/liq})^a$	$\Delta_{\text{l,cr}}^g H_m^0(298.15 \text{ K})^b$	$\Delta_f H_m^0(\text{g})_{\text{exp}}$	$\Delta_f H_m^0(\text{g})_{\text{G4}}^c$
acetophenone (liq)	-142.5 \pm 1.0 [156]	55.4 \pm 0.3[159]	-87.1 \pm 1.0	
2-methyl-acetophenone (liq) [167]		59.2 \pm 0.3	-110.7 \pm 2.6	-111.6
3-methyl-acetophenone (liq) [167]		59.9 \pm 0.3	-120.1 \pm 2.6	-120.9
4-methyl-acetophenone (liq) [167]		61.5 \pm 0.3	-120.8 \pm 2.6	-121.6
2-hydroxy-acetophenone (liq) [167]	-352.5 \pm 1.8	58.5 \pm 0.4	-294.0 \pm 1.8	-294.2
3-hydroxy-acetophenone (cr) [167]	-370.6 \pm 4.2	106.1 \pm 2.0 (84.7 \pm 2.2)	-264.5 \pm 4.6	-264.8
4-hydroxy-acetophenone (cr) [167]	-368.5 \pm 1.7	103.9 \pm 0.7 (88.8 \pm 1.1)	-264.6 \pm 1.8	-270.0
2'-methoxy-acetophenone (liq)	-298.7 \pm 2.2[173]	64.8 \pm 0.4	-233.9 \pm 2.2	-229.4
3'-methoxy-acetophenone (liq)	-305.5 \pm 2.4 [173]	65.9 \pm 0.3	-239.6 \pm 2.3	-237.4
4'-methoxy-acetophenone (cr)	-328.9 \pm 1.6 [173]	87.6 \pm 0.6 (70.4 \pm 0.4)	-241.3 \pm 1.7	-241.7
2,4-dimethoxy-acetophenone (cr) [177]	-486.6 \pm 1.9	102.0 \pm 1.5 (85.9 \pm 1.5)	-384.6 \pm 2.4	-384.6
2,5-dimethoxy-acetophenone (liq) [177]	-455.6 \pm 2.2	77.3 \pm 2.2	-378.3 \pm 3.1	-377.2
2,6-dimethoxy-acetophenone (cr) [177]	-464.6 \pm 1.8	97.4 \pm 1.1 (78.9 \pm 1.3)	-367.2 \pm 2.1	-369.6
3,4-dimethoxy-acetophenone (cr) [177]	-484.6 \pm 1.9	108.0 \pm 1.5 (91.8 \pm 1.6)	-376.6 \pm 2.4	-377.5

^a Uncertainties in this table are twice standard deviations.

^b Taken from Table 4.3.2 and Table 4.3.3. For the crystalline samples is given $\Delta_{\text{cr}}^g H_m^0$

^c Calculated by the G4 method with help of reactions 4.3.12-15 using experimental $\Delta_f H_m^0(\text{g})$ -values for the reaction participants. The expanded uncertainty assessed to be $\pm 3.5 \text{ kJ}\cdot\text{mol}^{-1}$ [143].

Table 4.3.12 Thermochemical data for substituted benzophenones at $T = 298.15 \text{ K}$ ($p^\circ = 0.1 \text{ MPa}$) (in $\text{kJ}\cdot\text{mol}^{-1}$)^a

Compound	$\Delta_f H_m^0(\text{cr/liq})^a$	$\Delta_{\text{l,cr}}^g H_m^0(298.15 \text{ K})^b$	$\Delta_f H_m^0(\text{g})_{\text{exp}}$
benzophenone	-37.3 \pm 1.4 [158]	95.0 \pm 0.4	57.7 \pm 1.5
2-methyl-benzophenone (liq)	-54.0 \pm 3.3 [163]	81.2 \pm 0.5	27.2 \pm 3.3
3-methyl-benzophenone (liq)	-62.9 \pm 3.8 [163]	80.9 \pm 0.4	18.0 \pm 3.8
4-methyl-benzophenone (cr)	-76.9 \pm 2.8 [163]	97.7 \pm 0.8	20.8 \pm 2.9
2-hydroxy-benzophenone (cr) [164]	-245.7 \pm 3.8	97.9 \pm 1.9	-147.8 \pm 4.3
3-hydroxy-benzophenone (cr) [164]	-247.3 \pm 4.0	131.7 \pm 0.9	-115.6 \pm 3.9
4-hydroxy-benzophenone(cr) [164]	-252.4 \pm 3.3	130.3 \pm 1.0	-122.1 \pm 3.8
2,4-di-hydroxy-benzophenone (cr)		134.5 \pm 1.7	
2-hydroxy-4-methoxy-benzophenone(cr) [179]	-414.2 \pm 4.5	116.8 \pm 1.2	-297.4 \pm 4.7
2,2'-dihydroxy-benzophenone (cr)		101.9 \pm 1.3	
2,2'-dihydroxy-4-methoxy-benzophenone (cr)		118.6 \pm 1.6	
2,2'-dihydroxy-4-methoxy-benzophenone (cr)		100.7 \pm 0.9	
2,2',4,4'-tetrahydroxy-benzophenone (cr)		159.8 \pm 3.1	
2,2'-dihydroxy-4,4'-dimethoxybenzophenone(cr)		139.4 \pm 2.4	

^a Uncertainties in this table are twice standard deviations.

^b Taken from Table 4.3.4 and Table 4.3.5.

In order to compensate for the lack of enthalpic data as well as to validate the available results, the gas-phase formation enthalpies for substituted acetophenones and benzophenones were estimated with help of quantum chemical method G4. The search for stable alkoxy-amines conformers was

carried out with the CREST program package [191] Structures of molecules were optimised with the MM3[192] and the B3LYP/6-31g(d,p) method [193].

We found several deep-lying conformers in all molecules. For example, there were at least 4 possible stable arrangements in 2-hydroxy-benzophenone (see Figure 4.3.1). Energies E_0 and enthalpies H_{298} of each of the stable conformers found were calculated using the G4 method.

The thermal population P_i of the conformers at $T = 298.15$ K is given by a Boltzmann distribution of conformers:

$$P_i = \frac{e^{-\frac{\Delta G_i}{RT}}}{1 + \sum_{i=1}^n e^{-\frac{\Delta G_i}{RT}}}; \quad \Delta G_i = G_i - G_{st} \quad (4.3.10)$$

where free energies of conformers G_i are related to the appropriate most stable conformer G_{st} . Results on P_i were used for calculation of the energies and enthalpies of the equilibrium mixture of conformers at $T = 298.15$ K and finally applied for calculation $\Delta_f H_m^o(g, 298.15 \text{ K})$ -values of compounds of interest:

$$\Delta_f H_m^o(g, 298.15 \text{ K}) = \sum_i p_i \Delta_f H_m^o(g, 298.15 \text{ K}) \quad (4.3.11)$$

To our surprise, the enthalpy of formation of the equilibrium mixture of conformers, $\Delta_f H_m^o(g, 298.15 \text{ K})_{eq}$, calculated for each compound according to Eq. (4.3.11), and the enthalpy of formation of the most stable conformer $\Delta_f H_m^o(g)_{MSC}$ generally do not differ too much (within $1 \text{ kJ}\cdot\text{mol}^{-1}$). The similar trend was also observed for the significantly more flexible molecule 2-amino-ethanol just recently [194]. For 2-amino-ethanol with 13 relatively stable conformations, the conformational enthalpy contributions of other conformers that coexist at 298.15 K are all together only $-2.9 \text{ kJ}\cdot\text{mol}^{-1}$ [194]. And even for glycerol, which is present in the gas phase as an equilibrium mixture at least of 126 conformers [195], the contribution of the conformational enthalpy of $-4.1 \text{ kJ}\cdot\text{mol}^{-1}$ was surprisingly small and fair comparable with the “chemical accuracy” which is ascribed to the high-level composite methods. In this context, do we need the dimensionless computational effort in order to take into account all possible stable conformers? Maybe it is enough to just locate a limited group of 3-4 relatively stable conformers and use them for the time-consuming high-level calculations? In order to testing this suggestion out of 13 stable conformations of 2-aminoethanol, only three conformers that come closest to the most stable were involved in calculation according to Eqs. (4.3.10) and (4.3.11). The comparison of two values $\Delta_f H_m^o(g, 298.15 \text{ K})_{eq} = -203.5 \text{ kJ}\cdot\text{mol}^{-1}$ and $\Delta_f H_m^o(g, 298.15 \text{ K})_{MSC} = -204.1 \text{ kJ}\cdot\text{mol}^{-1}$ shows that neglecting 10 other relatively stable conformations hardly contributes to the overall conformational enthalpy contribution. According to this experience, it is obvious that only a few most stable conformers contribute significantly to the *theoretical* enthalpy of formation, provided that the differences in their energies do not exceed them

1-3 kJ·mol⁻¹. Conformers with the energy difference ≥ 10 kJ·mol⁻¹ are practically not populated in the gas phase. Such a simplification can be used for large molecules with abundant flexibility with sufficient accuracy. With this experience, the energies of the most stable conformers for each molecule were calculated using the composite G4 method, since the conformational analysis of molecules examined does not reveal the presence of energetically close conformers.

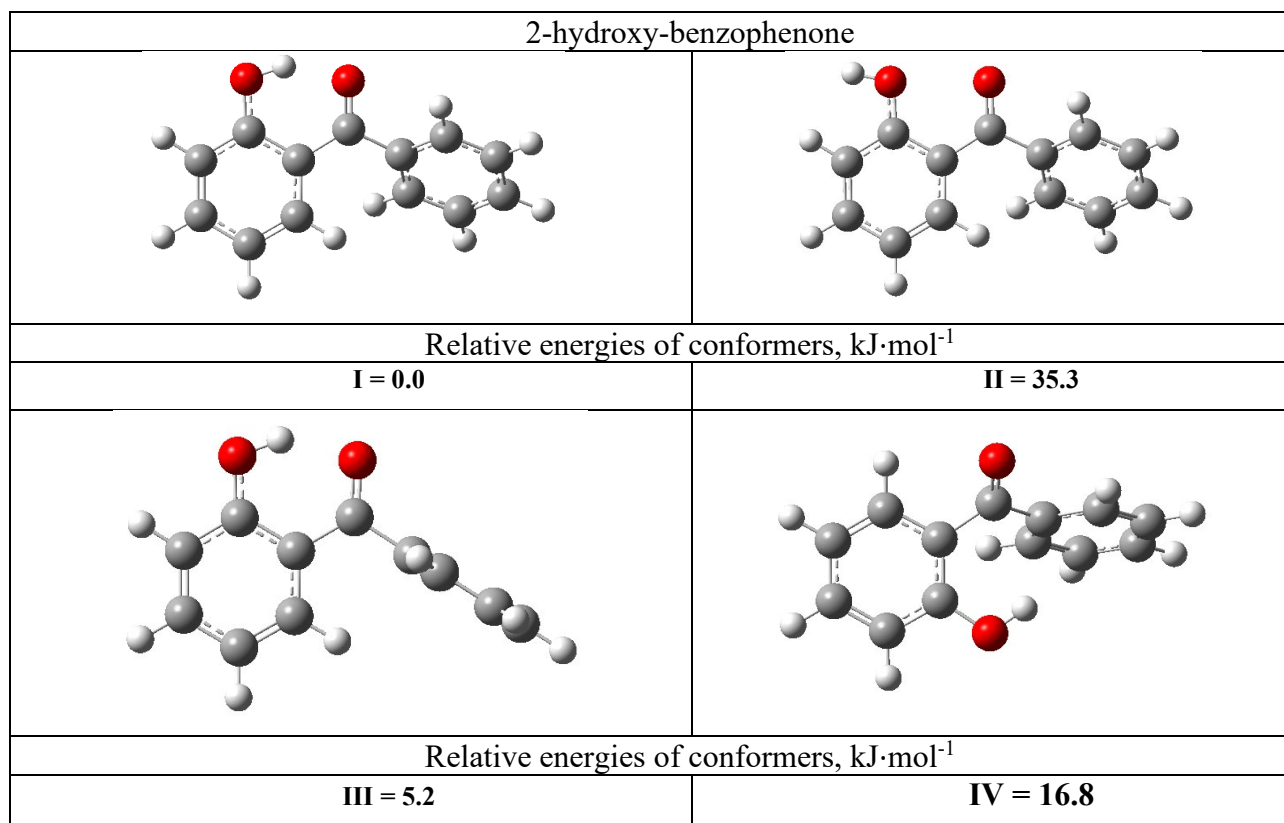
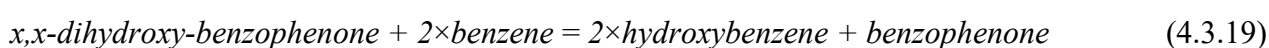
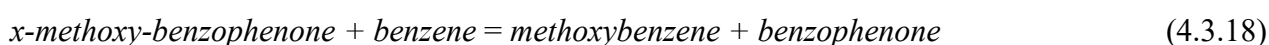
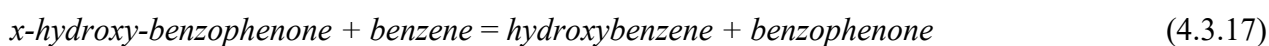
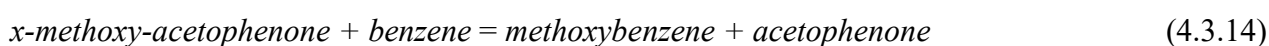


Figure 4.3.1 Stable conformers for 2-hydroxy-benzophenone as calculated with the G4.

The H_{298} enthalpies of the most stable conformers were converted into the *theoretical* enthalpies of formation, $\Delta_f H_m^0(\text{g})_{\text{G4}}$, using the *experimental* gas phase standard molar enthalpies of formation $\Delta_f H_m^0(\text{g}, 298.15 \text{ K})$ of auxiliary compounds (see Table 4.3.13) using the following well-balanced reactions (WBR):



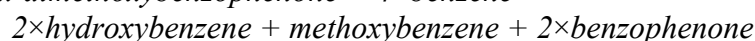
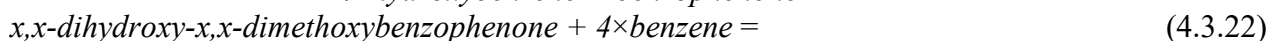
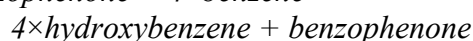
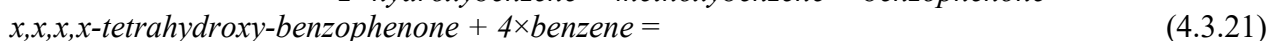
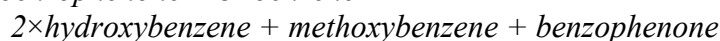
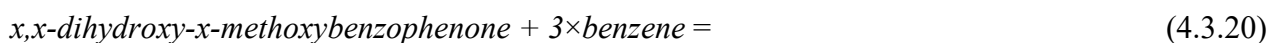


Table 4.3.13 Thermochemical data at $T = 298.15$ K ($p^\circ = 0.1$ MPa) for auxiliary reference compounds (in $\text{kJ}\cdot\text{mol}^{-1}$).

	$\Delta_f H_m^\circ$ (liq)	$\Delta_f^\circ H_m^\circ$	$\Delta_f H_m^\circ(\text{g})_{\text{exp.}}$
benzene	49.0±0.9 [116]	33.9±0.1 [116]	82.9±0.9 [116]
methyl-benzene	12.0±1.1 [116]	38.1±0.1 [116]	50.1±1.1 [116]
phenol	-150.5±1.2 [182]	58.0±0.3 [182]	-92.5±1.2 [182]
methoxy-benzene	-116.9±0.7 [182]	46.6±0.2 [182]	-70.3±0.7 [182]
acetophenone	-142.5±1.0 [156]	55.4±0.3 [159]	-87.1±1.0
1,2-dimethoxy-benzene (liq) [187,196]	-270.5±3.1	64.5±0.3	-206.0±3.1
1,3-dimethoxy-benzene (liq) [187,196]	-283.3±1.9	59.7±0.2	-223.6±1.9
1,4-dimethoxy-benzene (cr) [187,196]	-296.5±0.9	80.3±0.2	-216.2±0.9
1,4-dimethoxy-benzene (liq) [187,196]		61.6±0.2	
2-methoxy-phenol (liq) [187,196]	-308.7±1.8	61.4±0.3	-247.3±1.8
2-hydroxy-phenol (cr)	-354.1±1.1 [197]	88.7±0.7 [198]	-265.4±1.3
2-hydroxy-phenol (liq)	-265.4±1.5	70.7±0.7 [198]	
3-hydroxy-phenol (cr)	-368.0±0.5 [199]	95.6±0.6 [198]	-272.4±0.8
3-hydroxy-phenol (liq)	-350.8±1.5	78.4±1.3 [198]	
4-hydroxy-phenol (cr) [200]	-369.3±0.9 [200]	104.3±0.3	-265.0±0.9
4-hydroxy-phenol (liq)	-349.4±1.1	84.4±0.7	

The *theoretical* enthalpies of formation of substituted acetophenones and benzophenones calculated by G4 methods are given in Table 4.3.11 and Table 4.3.12 in the last column. The *theoretical* gas-phase enthalpies of formation calculated by WBR are in very good agreement with the experiment (within the boundaries of the experimental uncertainties). This observation is essential for using of composite methods for validation of available $\Delta_f H_m^\circ(\text{g})_{\text{exp}}$ data which are frequently in disarray or are existing as a single experimental determination. The consistent sets of thermochemical data for substituted acetophenones and benzophenones evaluated in Table 4.3.2, Table 4.3.3, Table 4.3.4, Table 4.3.5, Table 4.3.10, Table 4.3.11, and Table 4.3.12 have been used for the development of a “centerpiece” group-contribution approach as follows.

4.3.5. Development of the “centerpiece” group-contribution approach

4.3.5.1. Construction of a strain-free theoretical framework

The idea of this approach (see Figure 4.3.2) is that to select a “centerpiece” molecule (*e.g.*, benzene or acetophenone, or benzophenone or *etc.*) with the well-established thermodynamic properties [187]. Various substituents (*e.g.*, methyl, hydroxy, methoxy, *etc.*) can be attached to these “centerpieces” in different positions on the benzene ring. The enthalpic contributions for these

substituents can be easily quantified (see Figure 4.3.3) from the differences between the enthalpy of the substituted benzene and the enthalpy of the benzene itself. Using this scheme, the contributions, *e.g.*, $\Delta H(\text{H} \rightarrow \text{OH})$, $\Delta H(\text{H} \rightarrow \text{C}=\text{O}(\text{CH}_3))$, and $\Delta H(\text{H} \rightarrow \text{CH}_3\text{O})$ can be derived (see Table 4.3.14) using the reliable thermochemical data for acetophenone, methoxybenzene, and benzene compiled in Table 4.3.13.

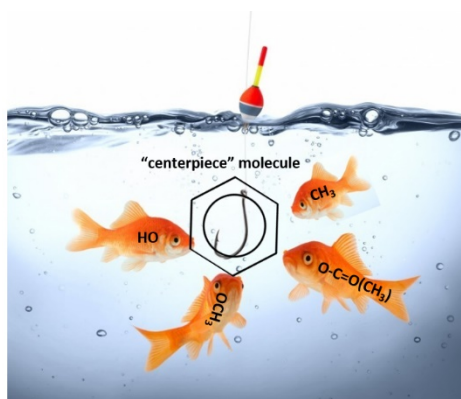


Figure 4.3.2 Graphical presentation of the idea of a “centerpiece” group-contribution approach

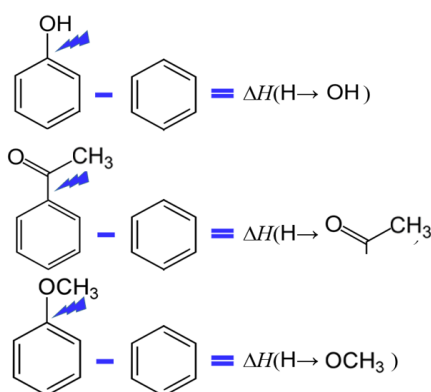


Figure 4.3.3 Quantification of the enthalpic contributions for the hydroxy-, carbonyl-, and methoxy substituents. The scheme is valid for the for the standard molar enthalpies of vaporization, as well as for the gas-phase standard molar enthalpies of formation.

Table 4.3.14 Parameters and pairwise nearest and non-nearest neighbour interactions of substituents on the “centerpieces” for calculation of thermodynamic properties of substituted benzenes and benzophenones at 298.15 K (in $\text{kJ}\cdot\text{mol}^{-1}$).

Centerpiece	$\Delta_f H_m^0(\text{g})$	$\Delta_1^g H_m^0$
<i>benzene</i>	82.9	33.9
<i>acetophenone</i>	55.4	-87.1
<i>benzophenone</i>	57.7	78.0
Contributions		
$\Delta H(\text{H} \rightarrow \text{C}=\text{O}(\text{CH}_3))$	-170.0	21.5
$\Delta H(\text{H} \rightarrow \text{CH}_3)$	-32.8	4.2
$\Delta H(\text{H} \rightarrow \text{CH}_3\text{O})$	-153.2	12.7
$\Delta H(\text{H} \rightarrow \text{OH})$	-175.4	24.1
Interactions		

<i>ortho</i> C=O(CH ₃) - CH ₃	9.2	-0.4
<i>meta</i> C=O(CH ₃) - CH ₃	-0.2	0.3
<i>para</i> C=O(CH ₃) - CH ₃	-0.9	1.9
<i>ortho</i> C=O(CH ₃) - OH	-31.5	-21.0
<i>meta</i> C=O(CH ₃) - OH	-2.0	5.2
<i>para</i> C=O(CH ₃) - OH	-2.1	9.3
<i>ortho</i> C=O(CH ₃) - CH ₃ O	6.4	-3.3
<i>meta</i> C=O(CH ₃) - CH ₃ O	0.7	-2.2
<i>para</i> C=O(CH ₃) - CH ₃ O	-1.0	2.3
<i>ortho</i> OH - OH	2.5	-11.4
<i>meta</i> OH - OH	-4.5	-3.7
<i>para</i> OH - OH	2.9	2.3
<i>ortho</i> OH - CH ₃ O	-1.6	-9.3
<i>meta</i> OH - CH ₃ O	4.5	4.1
<i>para</i> OH - CH ₃ O	11.4	3.0
<i>ortho</i> CH ₃ O - CH ₃ O	17.5	5.2
<i>meta</i> CH ₃ O - CH ₃ O	-0.1	0.4
<i>para</i> CH ₃ O - CH ₃ O	7.3	2.3

These enthalpic contributions $\Delta H(\text{H} \rightarrow \text{OH})$, $\Delta H(\text{H} \rightarrow \text{C}=\text{O}(\text{CH}_3))$, and $\Delta H(\text{H} \rightarrow \text{CH}_3\text{O})$ can be now applied to construct a framework of any desired hydroxy- or methoxy-substituted acetophenone or benzophenone (e.g. see 3-methoxy-acetophenone and 2,4-dihydroxy-benzophenone given in Figure 4.3.4), starting arbitrary from one of the “centerpieces” namely acetophenone, benzophenone, or even from the benzene.

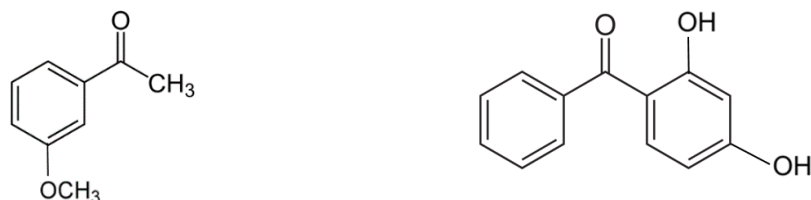


Figure 4.3.4 Construction of a strain-free theoretical framework for 3-methoxy-acetophenone and 2,4-dihydroxy-benzophenone. The scheme is valid for the standard molar enthalpies of vaporization, as well as for the gas-phase standard molar enthalpies of formation

In terms of energy, however, this framework is not perfect due to the lack of energetics of the interactions between the substituents.

4.3.5.2. Pairwise interactions of substituents on the benzene ring

Nearest (e.g. ortho-interactions) and non-nearest neighbour interactions (e.g. meta- or para-interactions) of substituents on the “centerpieces” (benzene, acetophenone, benzophenone, etc.) are generally stipulating the overall amount of the non-additive interactions specific for each particular molecule. For practical reasons, however, it is first necessary to subdivide the entire non-additive interactions into easily definable pairwise interactions. The mutual enthalpic pairwise interactions of substituents in the benzene ring can be accounted for by the three types of contributions that are

specific for the ortho, para, and meta positions of substituents placed in the benzene ring. How the pairwise interactions can be derived is shown in Figure 4.3.5.

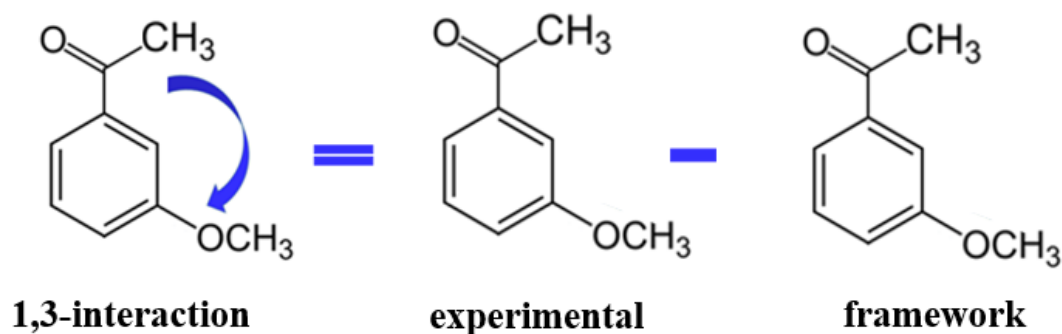


Figure 4.3.5 Example for a quantification of the 1,3-non-nearest neighbour interactions of the carbonyl-group with the CH_3O substituent in the 3-methoxyacetophenone. The scheme is valid for the standard molar enthalpies of vaporization, as well as for the gas-phase standard molar enthalpies of formation.

Indeed, to quantify the enthalpic contribution “*meta* $\text{C}=\text{O}(\text{CH}_3) - \text{CH}_3\text{O}$ ” for the non-bonded interaction of the carbonyl and CH_3O -groups in the *meta*-position on the acetophenone (taken as the “centerpiece”) we must first construct the “theoretical framework” of the 3-methoxyacetophenone (see Figure 4.3.5). To do that, we simply add the contribution $\Delta H(\text{H} \rightarrow \text{CH}_3\text{O})$ from Table 4.3.14 to the experimental enthalpy (enthalpy of vaporization or enthalpy of formation) of the acetophenone from Table 4.3.11. Alternatively, we could add contribution $\Delta H(\text{H} \rightarrow \text{C}=\text{O}(\text{CH}_3))$ and $\Delta H(\text{H} \rightarrow \text{CH}_3\text{O})$ to the benzene as the “centerpiece”. This “theoretical framework” of 3-methoxyacetophenone does not contain the “*meta* $\text{C}=\text{O}(\text{CH}_3) - \text{CH}_3\text{O}$ ” interaction. However, this interaction is present in the real 3-methoxyacetophenone (it is symbolised in Figure 4.3.5 with a blue arrow). The arithmetic difference between the experimental enthalpy (enthalpy of vaporization or enthalpy of formation) of 3-methoxyacetophenone and the enthalpy of the “theoretical framework” therefore provides the quantitative size of the pairwise interaction “*meta* $\text{C}=\text{O}(\text{CH}_3) - \text{CH}_3\text{O}$ ” directly (see Table 4.3.14). Using the same logic, the enthalpic contributions for the “*ortho* $\text{C}=\text{O}(\text{CH}_3) - \text{CH}_3\text{O}$ ” and “*para* $\text{C}=\text{O}(\text{CH}_3) - \text{CH}_3\text{O}$ ” can be derived from experimental data for 2-methoxy- and 4-methoxyacetophenone by using the parameters $\Delta H(\text{H} \rightarrow \text{CH}_3\text{O})$ and $\Delta H(\text{H} \rightarrow \text{C}=\text{O}(\text{CH}_3))$ respectively. In the same way, the required enthalpic contributions for the *ortho*-, *meta*-, and *para*-pairwise interactions of substituents were obtained and summarized in Table 4.3.14.

4.3.5.3. Practical application of the centerpiece approach for prediction of vaporization enthalpies of substituted benzophenones.

The discussion of the magnitudes of the pairwise interactions with respect to $\Delta_1^{\text{g}}H_{\text{m}}^{\text{o}}$ is rather limited since these contributions reflect the tightness of the molecular packing in the liquid. However,

these contributions are not of negligible size (see Table 4.3.14, last column) and they must be considered as empirical constants for the correct prediction of the vaporization energetics.

It makes oneself conspicuous, that the pairwise non-covalent interactions in Table 4.3.14 were derived exclusively with help of substituted benzenes. Are these energetic values of the nearest and non-nearest interactions transferable to the e.g. substituted benzophenones with the benzophenone as the “centerpiece” molecules? To answer this question, we have calculated the enthalpy of vaporization of the 2-methyl-benzophenone using the “centerpiece” approach with the numerical values from Table 4.3.14. The algorithm of calculations is given in Figure 4.3.6

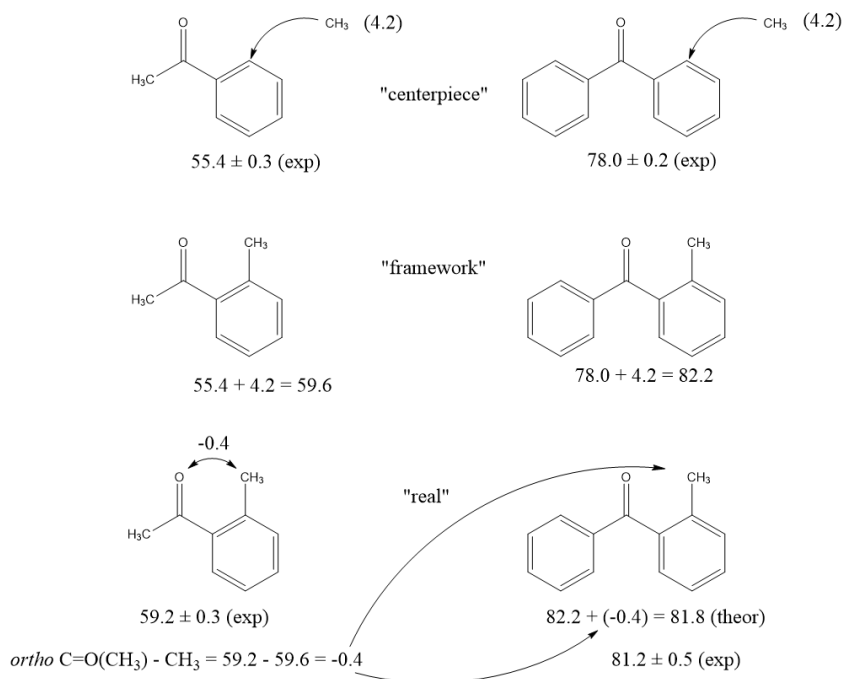


Figure 4.3.6 Example of calculation of the enthalpy of vaporization, $\Delta_1^g H_m^o(298.15 \text{ K})$, of the 2-methylbenzophenone using the “centerpiece” approach with the numerical values from Table 4.3.14. All numbers are given in $\text{kJ}\cdot\text{mol}^{-1}$.

As it obvious from Figure 4.3.6, the *theoretical* enthalpy of vaporization of 2-methylbenzophenone, $\Delta_1^g H_m^o(298.15 \text{ K}) = 81.8 \text{ kJ}\cdot\text{mol}^{-1}$, is in good agreement with the experimental value, $\Delta_1^g H_m^o(298.15 \text{ K}) = 81.2 \pm 0.5 \text{ kJ}\cdot\text{mol}^{-1}$, evaluated in Table 4.3.4.

Another example, we have calculated the enthalpy of vaporization of the 2-hydroxybenzophenone using the “centerpiece” approach with the numerical values from Table 4.3.14. The algorithm of calculations is given in Figure 4.3.7

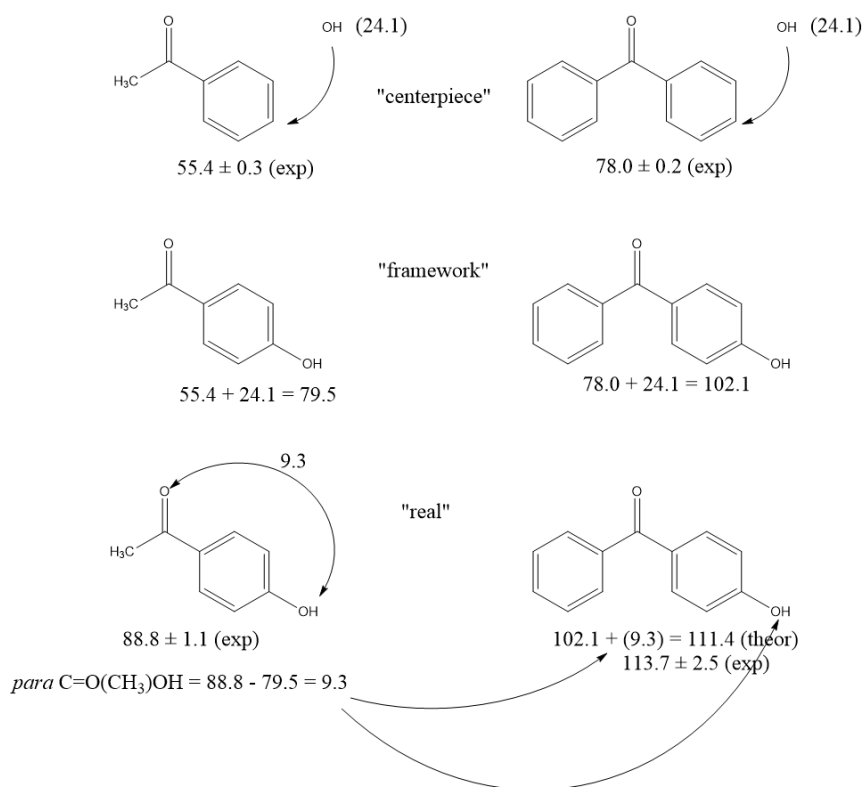


Figure 4.3.7 Example of calculation of the enthalpy of vaporization, $\Delta_1^g H_m^o(298.15 \text{ K})$, of the 2-hydroxy-benzophenone using the “centerpiece” approach with the numerical values from Table 4.3.14. All numbers are given in $\text{kJ}\cdot\text{mol}^{-1}$.

As it can be seen in Figure 4.3.7, the *theoretical* enthalpy of vaporization of 2-hydroxy-benzophenone, $\Delta_1^g H_m^o(298.15 \text{ K}) = 111.4 \text{ kJ}\cdot\text{mol}^{-1}$, is in good agreement with the experimental value, $\Delta_1^g H_m^o(298.15 \text{ K}) = 113.7 \pm 2.5 \text{ kJ}\cdot\text{mol}^{-1}$, evaluated in Table 4.3.5. Hence, we can now conclude, that the numerical values (see Table 4.3.14) of contributions responsible for vaporization energetics are transferrable to other types of aromatic systems, e.g., on the benzophenone derivatives.

In order to ascertain this conclusion, it is reasonable to demonstrate the principle applicability of the “centerpiece” approach for the case that at least two substituents are attached to the benzophenone as the “centerpiece”. In Figure 4.3.8 is shown the algorithm of calculation the vaporization enthalpy of the 2,4-dihydroxy-benzophenone using the “centerpiece” approach with the numerical values from Table 4.3.14.

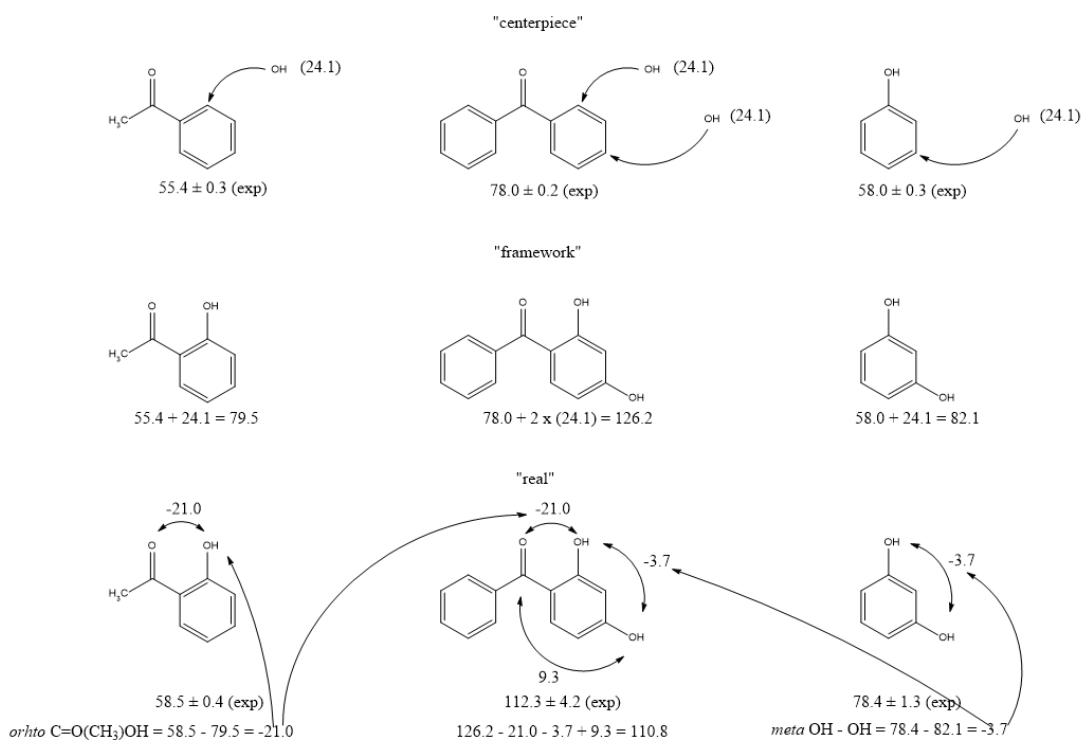


Figure 4.3.8 Example of calculation of the enthalpy of vaporization, $\Delta_1^g H_m^0(298.15 \text{ K})$, of the 2,4-dihydroxy-benzophenone using the “centerpiece” approach with the numerical values from Table 4.3.14. All numbers are given in $\text{kJ}\cdot\text{mol}^{-1}$.

It has turned out that also in this case, the *theoretical* enthalpy of vaporization of 2,4-dihydroxy-benzophenone, $\Delta_1^g H_m^0(298.15 \text{ K}) = 110.8 \text{ kJ}\cdot\text{mol}^{-1}$, is in good agreement with the experimental value, $\Delta_1^g H_m^0(298.15 \text{ K}) = 112.3 \pm 4.2 \text{ kJ}\cdot\text{mol}^{-1}$, evaluated in Table 4.3.5. Hence, the “centerpiece” approach can be successfully applied for prediction of vaporization enthalpies of substituted benzophenones and other aromatic systems with the contributions derived in Table 4.3.14. Now we are going to apply the “centerpiece” approach for prediction the gas-phase enthalpies of formation of substituted benzophenones

4.3.5.4. Practical application of the “centerpiece” approach for prediction of gas-phase enthalpies of formation of substituted benzophenones

The discussion of the magnitudes of the pairwise interactions with respect to $\Delta_f H_m^0(\text{g})$ is more meaningful, because these non-covalent interactions are generally responsible for the distribution of the electron density inside the molecule, or they can be used to derive the strength of the intramolecular hydrogen bonding present in the 2-hydroxy-substituted acetophenones and benzophenones. Quantitatively, the strength of the non-covalent interactions depends strongly on the type of *ortho*-, *meta*- or *para*-pairs. Let us consider the intensity of pairwise interactions in terms of $\Delta_f H_m^0(\text{g})$. From Table 4.3.14 it can be seen that the *ortho*-hydroxy-acetophenone shows a strong stabilization of $-31.5 \text{ kJ}\cdot\text{mol}^{-1}$ due to the intra-molecular hydrogen bonding. In contrast, the *ortho*-

dimethoxy-benzene and ortho-methoxy-acetophenone show a strong destabilization of $17.5 \text{ kJ}\cdot\text{mol}^{-1}$ and of $6.4 \text{ kJ}\cdot\text{mol}^{-1}$ due to the sterical repulsions of bulky methoxy groups. From our experiences, the *meta*- and *para*-interactions of substituents on the benzene ring are less profound compared to *ortho*-interactions [116,187]. Indeed, the *meta*- and *para*-interactions of the Me, OH, CH₃O substituents with the *carbonyl* group can be considered as negligible since they are below $2 \text{ kJ}\cdot\text{mol}^{-1}$ (see Table 4.3.14). In contrast, the significant destabilization at the level from 4.5 to $11.4 \text{ kJ}\cdot\text{mol}^{-1}$ is observed for the *para*-isomers of dimethoxy-benzene and methoxy-phenol. These noticeable destabilizing effects can be explained by the specific electron density distribution within the substituted benzene ring.

Also, the pairwise non-covalent interactions in terms of $\Delta_f H_m^0(g)$ were derived exclusively with help of substituted benzenes (see Table 4.3.14). Therefore, the validity of these contributions for the transfer to benzophenone derivatives has to be checked. We have calculated the enthalpy of formation of the 2-methyl-benzophenone using the “centerpiece” approach with the numerical values from Table 4.3.14. The algorithm of calculations is given in Figure 4.3.7. Therefore, the “centerpiece” approach can also be used successfully to prediction of enthalpies of formation of substituted benzophenones and other aromatic systems with with the contributions derived in Table 4.3.14.

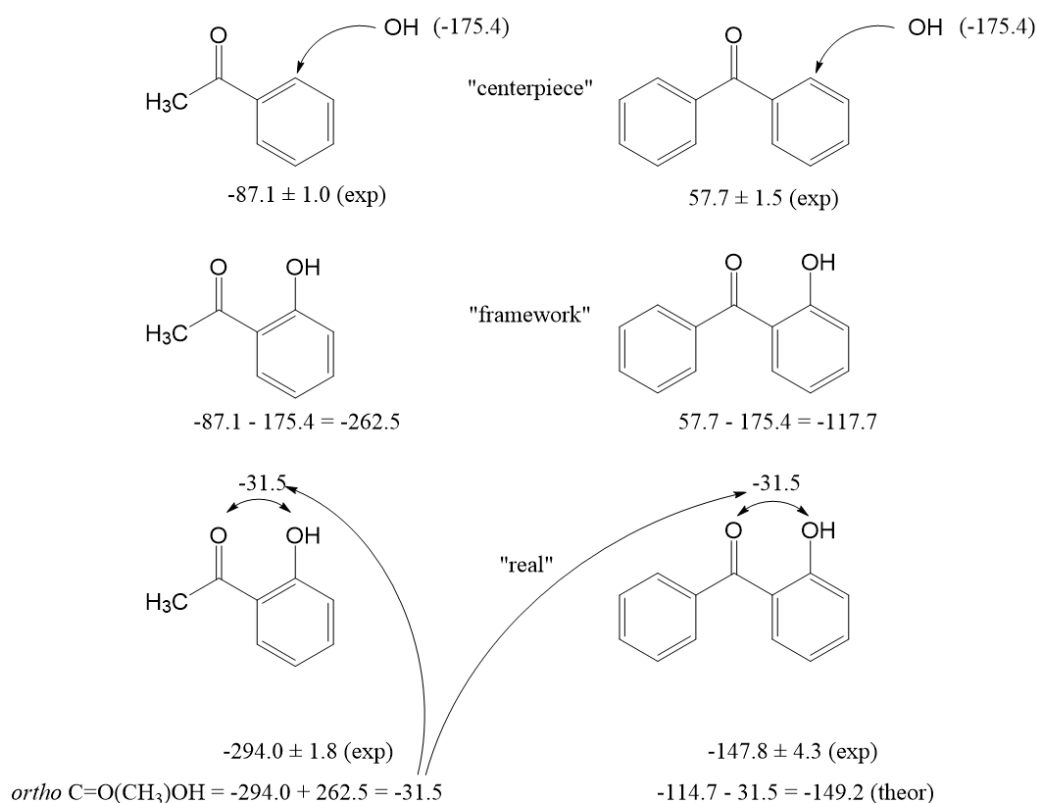


Figure 4.3.9 Example of calculation of the enthalpy of formation, $\Delta_f H_m^0(g, 298.15 \text{ K})$, of the 2-hydroxy-benzophenone using the “centerpiece” approach with the numerical values from Table 4.3.14. All numbers are given in $\text{kJ}\cdot\text{mol}^{-1}$.

As it obvious from Figure 4.3.9, the *theoretical* enthalpy of formation of 2-hydroxy-benzophenone, $\Delta_f H_m^0(\text{g}, 298.15 \text{ K}) = -149.2 \text{ kJ}\cdot\text{mol}^{-1}$, is in very good agreement with the experimental value, $\Delta_f H_m^0(\text{g}, 298.15 \text{ K}) = -147.8 \pm 4.3 \text{ kJ}\cdot\text{mol}^{-1}$, evaluated in Table 4.3.12.

Another example is the calculation of the enthalpy of formation of the 2-hydroxy-4-methoxy-benzophenone using the “centerpiece” approach with the numerical values from Table 4.3.14. The algorithm of calculations is given in Figure 4.3.10. The *theoretical* enthalpy of formation of 2-hydroxy-4-methoxy-benzophenone, $\Delta_f H_m^0(\text{g}, 298.15 \text{ K}) = -298.9 \text{ kJ}\cdot\text{mol}^{-1}$, is in very good agreement with the experimental value, $\Delta_f H_m^0(\text{g}, 298.15 \text{ K}) = -297.4 \pm 4.7 \text{ kJ}\cdot\text{mol}^{-1}$, evaluated in Table 4.3.12.

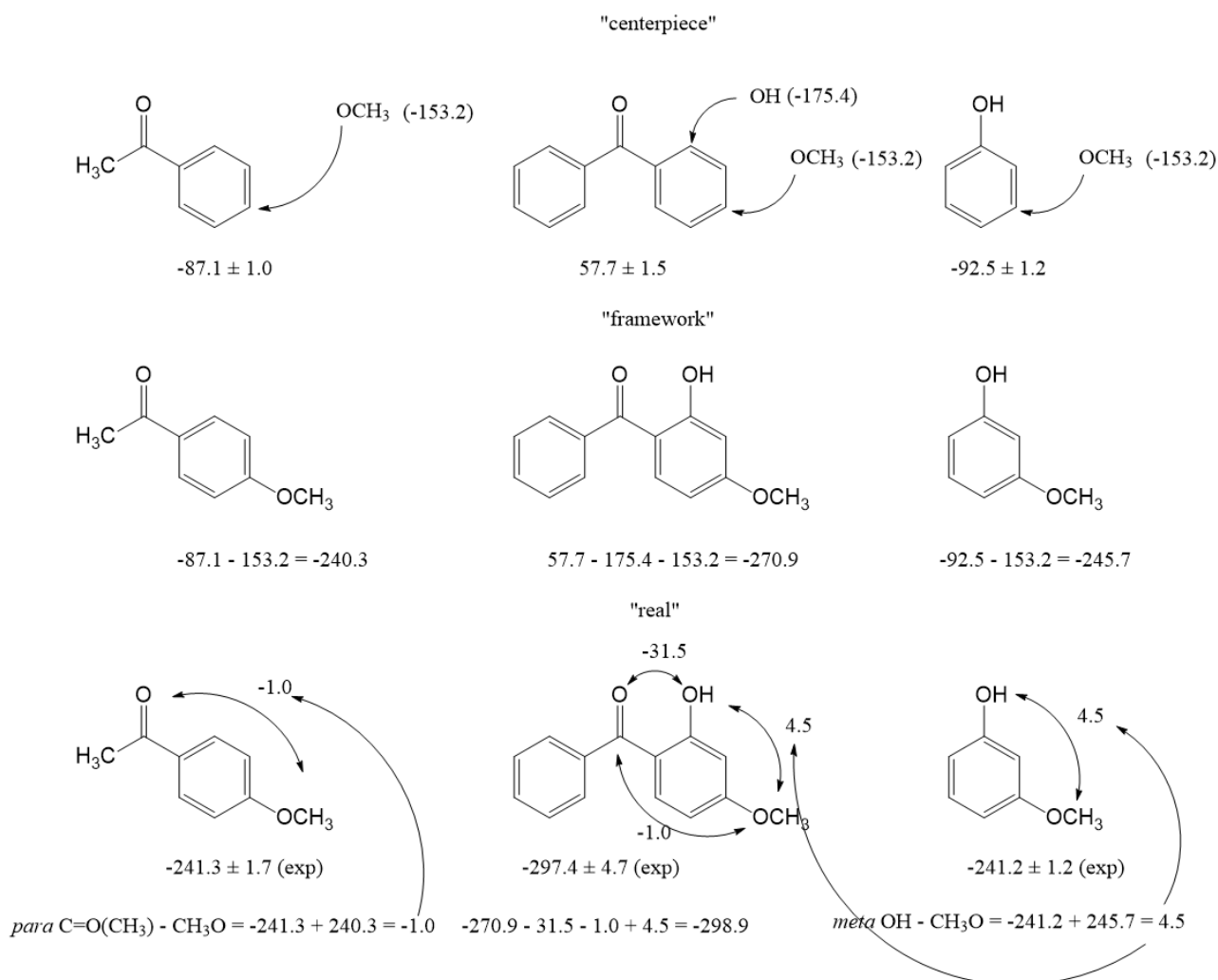


Figure 4.3.10 Example of calculation of the enthalpy of formation, $\Delta_f H_m^0(\text{g}, 298.15 \text{ K})$, of the 2-hydroxy-4-methoxy-benzophenone using the “centerpiece” approach with the numerical values from Table 4.3.14. All numbers are given in $\text{kJ}\cdot\text{mol}^{-1}$.

4.3.5.5. Agglomeration of substituents on the benzene ring: the third bothers you?

It is apparent (see blue arrows in Figure 4.3.11), that the introduction of the third substituent on the benzene ring in dimethoxy-acetophenones (see Figure 4.3.12) is expected to increase the intensity of the mutual interactions of the substituents compared to two substituents.

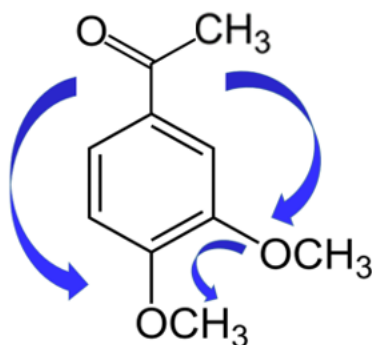


Figure 4.3.11 Agglomeration of the enthalpic contributions for the nearest and non-nearest neighbour interactions in the three substituted benzene derivatives.

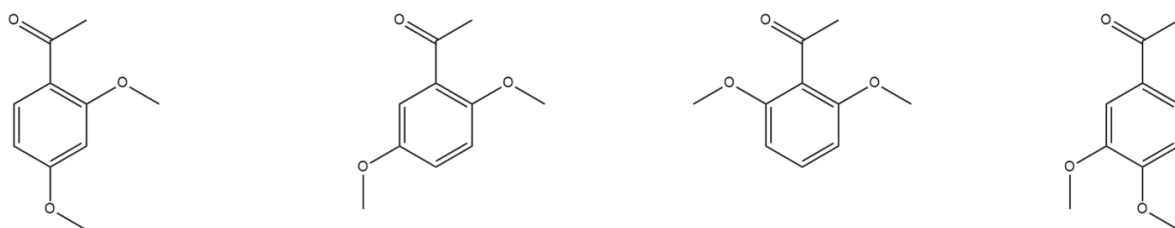


Figure 4.3.12 Isomeric 2,4-dimethoxyacetophenone, 2,5-dimethoxyacetophenone, 2,6-dimethoxyacetophenone, and 3,4-dimethoxyacetophenone: agglomeration of the enthalpic contributions for the nearest and non-nearest neighbour interactions in the three substituted benzene derivatives.

As can be seen in Figure 4.3.11, all three possible types of *ortho*-, *meta*- and *para*-interactions are present simultaneously in 3,4-dimethoxyacetophenone. Is the energetics of these interactions additive with the growing number of substituents? Can we just summarize the individual contributions? Or are there additional effects due to a perturbation in the electron density within the congested benzene ring?

In order to get the answer in terms of $\Delta_f H_m^0(g)$, we calculated the “theoretical framework” ($\Delta H(H \rightarrow C=O(CH_3)) + 2 \times \Delta H(H \rightarrow CH_3O) = -393.5 \text{ kJ}\cdot\text{mol}^{-1}$) for the “dimethoxyacetophenone”. The difference between the $\Delta_f H_m^0(g)$ of the real molecule and the enthalpy of its model, $-393.5 \text{ kJ}\cdot\text{mol}^{-1}$, represented by the “theoretical framework” provides (see Table 4.3.15, column 3) the real total amount of pairwise nearest and non-nearest neighbour interactions of substituents on the “centerpieces” in terms of $\Delta_f H_m^0(g)$.

Table 4.3.15 Analysis of the total amount of pairwise nearest and non-nearest neighbour non-covalent interactions of substituents on the “centerpieces” in terms of $\Delta_f H_m^0(g)$ for di-methoxy-substituted acetophenones at 298.15 K (in $\text{kJ}\cdot\text{mol}^{-1}$).

Compound	$\Delta_f H_m^0(g)_{\text{exp}}^a$	Actual amount of interactions ^b	Theoretical amount of interactions ^c	Δ^c
1	2	3	4	5
2,4-dimethoxyacetophenone	-384.6 ± 2.4	8.9	5.5	3.4
2,5-dimethoxyacetophenone	-378.3 ± 3.1	15.2	14.4	0.8

2,6-dimethoxy-acetophenone	-367.2±2.1	26.3	12.7	13.6
3,4-dimethoxy-acetophenone	-376.6±2.4	16.9	17.2	-0.3

^a Results from Table 4.3.11.

^b Calculated as the difference between the $\Delta_f H_m^0(\text{g})_{\text{exp}}$ given in column 2 and $\Delta_f H_m^0(\text{g})_{\text{framework}} = -393.5 \text{ kJ}\cdot\text{mol}^{-1}$.

^c Calculated as the sum of pairwise interactions of CH₃O and carbonyl group given in Table 4.3.14.

^d Difference between column 3 and 4.

The actual number of interactions in 2,4-, 2,5-, and 3,4-dimethoxy-acetophenones is given in Table 4.3.15, column 3 and it is quite comparable (within uncertainties ascribed to $\Delta_f H_m^0(\text{g})$ -values) to the theoretical sum of nearest and non-nearest neighbour interactions of substituents (Table 4.3.15, column 4). This means that there are no additional interactions between three substituents in the benzene ring. However, with 2,6-dimethoxy-acetophenone, the excessive additional interaction of $13.6 \text{ kJ}\cdot\text{mol}^{-1}$ was observed (see Table 4.3.15, last column). This excess is quite understandable from a structural point of view. Indeed, in this molecule the substituents are in the 1,2,3 sequence in the benzene ring. The methoxy groups are spacious and their close proximity to the carbonyl group increases the steric repulsions of all three groups causes the additional energetic contribution. Hence, the additional strain effects must be considered as special excess contributions for the 1,2,3 sequence of substituents.

To summarize observations regarding the $\Delta_f H_m^0(\text{g})$ -values we can conclude that overall interactions of three substituents placed in the benzene ring (with the exception due to the 1,2,3 sequence) are comparable to the theoretical value (collected from the sum of the pairwise interactions).

4.4. Conclusions

The consistent sets of standard molar thermodynamic properties of formation and phase transitions for substituted acetophenones and benzophenones were evaluated in this work with help of complementary measurements of vapor pressures, sublimation/vaporization, and fusion enthalpies, as well as with help of empirical and high-level quantum-chemical calculations. Thermodynamic properties of substituted acetophenones and benzophenones were recommended as reliable benchmark properties for thermochemical calculations. The evaluated vaporization and formation enthalpies were used to design and develop the “centerpiece” approach for prediction of thermodynamic properties of the aromatic systems.

5. Ionic systems: dispersion forces from the thermodynamic properties

The determination vapor pressure curves and vaporization enthalpies, $\Delta_1^g H_m^0$, for ionic liquids is more challenging than for molecular liquids. Firstly, the vapor pressures are very low and hardly measurable. Moreover, the species that evaporate into the gas phase are unknown. Meanwhile, it is clear that neutral rather than charged species are transferred from the liquid into the gaseous state. Are these simple ion-pairs or even larger neutral clusters? If it is ion-pairs, are those similar to those

in the liquid phase in terms of binding characteristics? All these questions we address in the next chapter.

5.1. Dispersion forces in aprotic ammonium and phosphonium ionic liquids from the vaporization enthalpy.

Ionic liquids (ILs) bearing the tetra-alkyl-ammonium cation and tetra-alkyl-phosphonium cation (see Figure 5.1.1) belong to the most common class of these neoteric solvents. Ionic liquids are described by a delicate balance of Coulomb interaction, hydrogen bonding and dispersion forces. Dissecting the different types of interaction from thermodynamic properties is still a challenge. The vaporization enthalpy has been shown to be a useful tool to derive dispersion forces in molecular systems. What about more complex ionic systems?

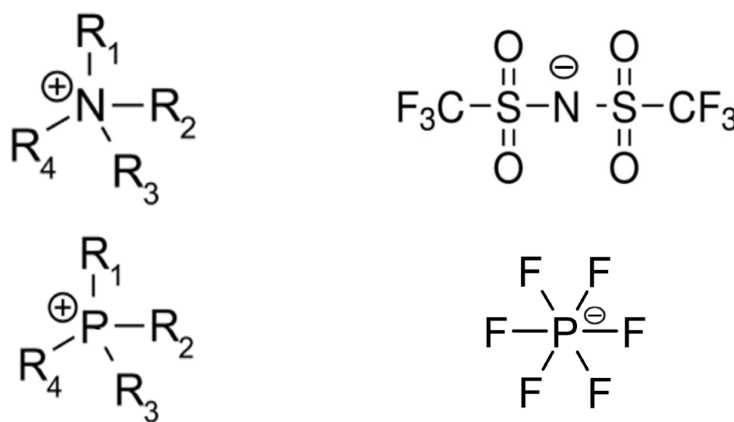


Figure 5.1.1 Structures of cations and anions: tetra-alkyl-ammonium cation based ILs and tetra-alkyl-phosphonium cation; bis[(trifluoromethyl)sulfonyl]imide = [NTf₂]⁻ anion and hexafluorophosphate = [PF₆]⁻ anion.

If the standard molar vaporization enthalpies, $\Delta_1^g H_m^0(298\text{ K})$, of n-alkanes are monotonically grows with the growing chain-length (see Figure 1.3), is this also common for *ionic* compounds? Surprisingly, not so long ago there was a lot of controversy over this question [4]. However, it is already known today that the vaporization enthalpies of aprotic ionic liquids also have the linear chain length dependencies (except for a few special cases caused by a possible nanostructuring of ILs with long alkyl chains bounded to the cation) [4]. An example of such impeccable linear dependence for 1-methyl-3-alkyl-imidazolium based ILs with the [NTf₂]⁻ anion is given on Figure 5.1.2a.

For the ILs based on tetra-alkylammonium and tetra-alkylphosphonium, the straight line was also observed as a function of the chain lengths of the enthalpy of vaporization (see Figure 5.1.2b). From this point of view, we should consider the *molecular* and *ionic* systems to be generally similar. Let us nevertheless try to realize this observation on a molecular basis by comparing similarly shaped *ionic* and *molecular* homologous series. For example, for the *ionic* series of 1-methyl-3-alkyl-imidazolium based ILs, the similarly shaped *molecular* homologous series is the row of n-

alkylimidazoles (see Figure 5.1.2a). What is interesting about comparing the enthalpies of vaporization in these two series?

In Figure 5.1.3 we show the differences between $\Delta_1^g H_m^o(298\text{ K})$ -values for these *ionic* and the corresponding *molecular* compounds. As can be seen in Figure 5.1.3, nothing spectacular can be observed for the pairs 1-methyl-3-alkyl-imidazolium based ILs and alkyl-imidazoles, namely the differences between $\Delta_1^g H_m^o(298\text{ K})$ -values are decreasing insignificantly with the elongation of the alkyl chain. This decrease could be understood from the competition between the corresponding van der Waals and Coulomb interactions [4].

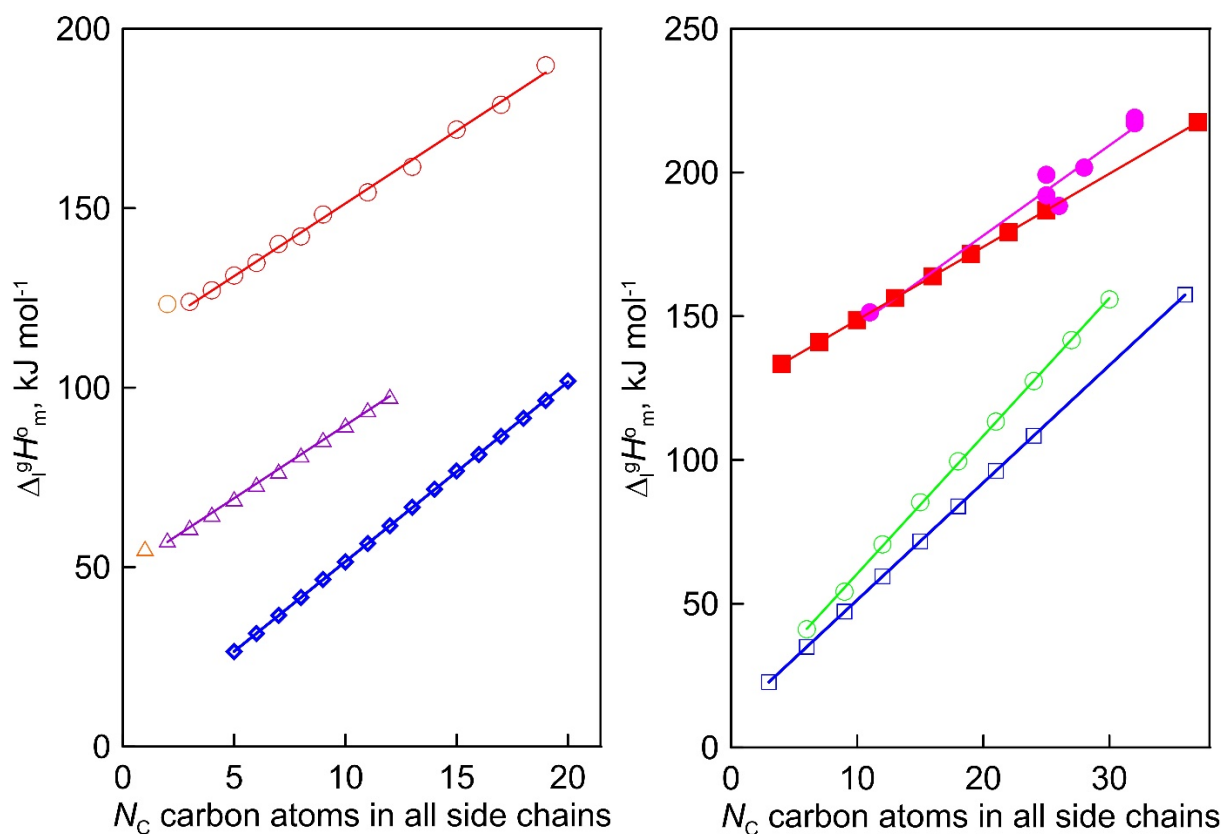


Figure 5.1.2 Vaporization enthalpies $\Delta_1^g H_m^o(298\text{ K})$ chain-length dependences of molecular and ionic compounds: alkanes (opened diamonds, \diamond) [201,202], alkyl-imidazoles (opened triangles, \triangle) [203] and 1-methyl-3-alkyl-imidazolium based ILs (opened circles, \circ) [4], tri-alkylamines [68] (opened squares, \square), tri-alkyl-phosphines (opened circles, \circ) [203], tetra-alkylammonium based ILs (solid squares, \blacksquare) [8], and tetra-alkylphosphonium based ILs (solid circles, \bullet) [204].

the isolated from the liquid phase individual ionic pair does not bear any dispersion interactions flying in the gas phase. How to quantify the portion of dispersion forces in these ILs?

We recently showed that for ILs with “hairy” cations such as tetraalkylammonium, the dispersion interactions of alkyl chains in the gas phase contribute significantly to the energetics of evaporation [207]. It is also known that in long-chain alkanes, the weak dispersion interactions between chain segments are responsible for the stability of very unusual conformers such as hairpins [3]. The tetra-alkylammonium and tetra-alkylphosphonium ILs with the long alkyl chains are qualitatively predestined for intensive dispersion interactions between the chain segments. The “step by step” protocol based on the experimental vaporization enthalpies was developed [8,204] to quantify dispersion interactions in the tetra-alkylammonium and tetra-alkylphosphonium-based ILs with [NTf₂] and [PF₆] anions (see Figure 5.1.1). The results of the calculations carried out using the “step by step” protocol are summarized in Table 5.1.1 and Table 5.1.2 and shown graphically in Figure 5.1.4, Figure 5.1.5, and Figure 5.1.6.

The idea of the first step is simply to cut off the alkyl chains attached to the cation as they are the main cause of the dispersion interactions. The “bald” cation produced in this way can be used as a reference for quantifying the dispersion forces. To execute this idea, linear vaporization enthalpy chain-length dependences of general formula:

$$\Delta_1^g H_m^o(298 \text{ K})/\text{kJ}\cdot\text{mol}^{-1} = Y + Q \times (N_C) \quad (5.1.1)$$

is developed for the IL homologous series for [NR₄][NTf₂], [PR₄][NTf₂], [PR₄][PF₆], as well as for n-alkanes for the sake of comparison CH₃ – (CH₂)_n – CH₃.

Table 5.1.1 Quantification of dispersion forces for tetra-alkylammonium-based ILs with the [NTf₂] anion (in kJ·mol⁻¹) [8].

Compound	N_C^a	$\Delta_1^g H_m^o(298 \text{ K})^d$	Y	$\Delta_1^g H_m^o((\text{CH}_2)_n)$	$-E_{disp}((\text{CH}_2)_n \text{ gas})$
[N1123]	7	140.5±1.9		24.2	10.9
[N1114]	7	143.7±1.9		27.3	7.8
[N1115]	8	145.7±2.2		29.3	10.8
[N1224]	9	147.4±2.2		31.0	14.1
[N2225]	11	150.1±2.6	116.4	33.6	21.5
[N1444]	13	152.1±2.7		35.6	29.6
[N2228]	14	156.8±3.2		40.3	30.0
[N2666]	20	172.7±4.2		56.3	44.0
[N6666]	24	182.4±4.8		66.0	54.4
[N1888]	25	191.8±6.0		75.4	49.9

Table 5.1.2 Quantification of dispersion forces for tetra-alkylphosphonium-based ILs and alkyl phosphines (in kJ·mol⁻¹) [204].

Compound	$\Delta_1^g H_m^o(298 \text{ K})$	Y	$\Delta_1^g H_m^o((\text{CH}_2)_n)$	$-E_{disp}((\text{CH}_2)_n \text{ gas})$
[P ₆₆₆₅][PF ₆]	177.7±3.0		80.8	34.7
[P ₆₆₆₆][PF ₆]	181.3±2.8	96.7	84.6	35.8
[P ₆₆₆₇][PF ₆]	184.7±3.3		88.0	37.3

[P ₆₆₆₈][PF ₆]	188.1±3.5		91.4	38.8
[P ₂₂₂₅][NTf ₂]	151.3±5.0		35.3	19.8
[P ₆₆₆₇][NTf ₂]	199.0±5.7		83.0	42.3
[P ₈₈₈₁][NTf ₂]	192.3±5.0		77.0	48.3
[P ₄₄₄₁₄][NTf ₂]	193.0±5.4	116.0	77.0	53.2
[P ₄₄₄₁₆][NTf ₂]	202±13		85.7	54.7
[P ₆₆₆₁₄][NTf ₂]	217.0±7.2		101.7	59.9
[P ₆₆₆₁₄][NTf ₂]	219.0±5.0		103.0	58.0
P(C ₂ H ₅) ₃	41.1		27.8	1.4
P(C ₃ H ₇) ₃	54.2		41.7	3.3
P(C ₄ H ₉) ₃	70.6		57.3	1.9
P(C ₅ H ₁₁) ₃	85.3		72.0	2.5
P(C ₆ H ₁₃) ₃	99.5	13.2	86.2	2.9
P(C ₇ H ₁₅) ₃	113.3		100.0	4.5
P(C ₈ H ₁₇) ₃	127.4		114.1	5.5
P(C ₉ H ₁₉) ₃	141.7		128.4	4.9
P(C ₁₀ H ₂₁) ₃	155.8		142.5	7.5

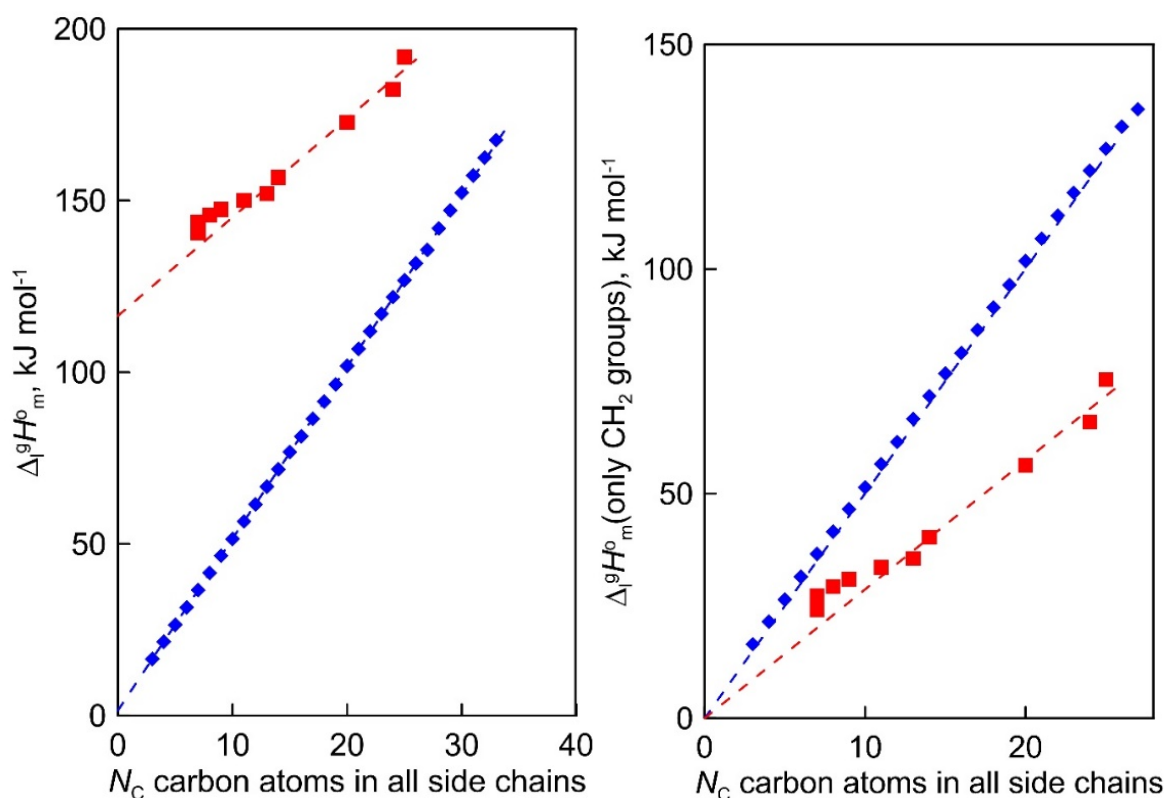


Figure 5.1.4 (a) The chain length dependence of the $\Delta_1^g H_m^0(298\text{ K})$ for n-alkanes, $C_n H_{2n+2}$ (diamonds, \blacklozenge); ammonium-based ILs with $[NTf_2]^-$ anion, (squares, \blacksquare). (b) The dispersion part of the vaporization enthalpy $\Delta_1^g H_m^0(298\text{ K})$ due to the alkyl chains.

The extrapolation these lines to an imaginary case with the $N_C = 0$ (no alkyl chain at all). The graphic interpretation of this step for ILs and for n-alkanes is given in Figure 5.1.4a. In all series taken for comparison, the intercept Y of the linear fit (see Table 5.1.1 and Table 5.1.2) refers to the “residual” vaporization enthalpy, that is imaginatively released from dispersion interactions by alkyl

chains. From a physical point of view, the quantity of the intercept Y is very different for the molecular and for the ionic compounds examined.

In the case of ionic liquids $[\text{NR}_4][\text{NTf}_2]$ ($Y = 116.4 \text{ kJ}\cdot\text{mol}^{-1}$) the intercept represents the vaporization enthalpy of a hypothetical “armless” $[\text{NH}_4][\text{NTf}_2]$ ionic liquid. This value encompasses not only the contribution to vaporization enthalpy from the isolated “ammonium” cation, but also the overall number of Coulomb interactions presented in the liquid phase. It is not to be overlooked, that the corresponding intercept Y for $[\text{NR}_4][\text{NTf}_2]$ series studied in this work is indistinguishable from those ($Y = 116.0 \text{ kJ}\cdot\text{mol}^{-1}$) for tetra-alkylphosphonium-based ILs $[\text{PR}_4][\text{NTf}_2]$ (see Table 5.1.2). This observation shows that the Y intercept can be further used as a measure of Coulomb interactions between ion pairs in the liquid state.

For the n -alkanes $\text{CH}_3 - (\text{CH}_2)_n - \text{CH}_3$, the intercept $Y = 1.5 \text{ kJ}\cdot\text{mol}^{-1}$ was derived from the chain-length dependence of experimental vaporization enthalpies. As a rule, the inaccuracy of the experimental data on n -alkanes is mostly below than $1 \text{ kJ}\cdot\text{mol}^{-1}$ and for this reason it is reasonable to consider the intercept $Y = 1.5 \text{ kJ}\cdot\text{mol}^{-1}$ as an empirical factor that is not negligible for further calculations.

After we have determined the contribution Y to vaporization enthalpies $\Delta_1^g H_m^o(298 \text{ K})$ of ammonium- and phosphonium based ILs by completely cutting off the alkyl chains from the real molecules, we are now ready for the second step of quantifying the dispersion forces due to the multitude of van der Waals interactions of alkyl chain segments. It seems obvious that according to Eq. (5.1.1):

$$\Delta_1^g H_m^o((\text{CH}_2)_n) = \Delta_1^g H_m^o(\text{exp}) - Y \quad (5.1.2)$$

the subtractions of the individual contribution Y (specific but quantified above for each series) from the real experimental vaporization enthalpies, $\Delta_1^g H_m^o(\text{exp})$, bring the desired total measure of the dispersion forces, $\Delta_1^g H_m^o((\text{CH}_2)_n)$, as expressed in terms of enthalpy of vaporization. The latter values (see Figure 5.1.4b) could immediately be ascribed to the intensity of dispersive alkyl chains interactions in the liquid phase if the dispersive forces in the gas phase are completely absent. However, this speculation does not appear to be correct for all the series examined in this work. If the dispersion forces are only present in the liquid phase, the chain length dependency shown in Figure 5.1.4b for the molecular and ionic series should more or less merge with one another, in particular due to sufficiently long tails. Figure 5.1.4b shows, however, that if the $\Delta_1^g H_m^o((\text{CH}_2)_n)$ -values for the series of molecules are only slightly different, the deviations for the ionic series are already noticeable. It seems to be, that the reason is that the n -alkanes have typical linear zig-zag structures in the gas phase, in which an occasional raveling of the chain due to dispersion forces is possible but not favorable [3]. Therefore, in n -alkanes, the amount of dispersion forces drawn into the gas phase

could be viewed as small, and the $\Delta_1^g H_m^o((CH_2)_n)$ -values are only responsible for this series of dispersion interactions in the liquid phase. The line in Figure 5.1.4b developed for the ammonium based ILs is significantly below the line shown for *n*-alkanes. The line in Figure 5.1.5b developed for the phosphonium based ILs is also significantly below the line shown for *n*-alkanes. These observations are clear evidence that the remaining dispersive interactions between alkyl chains dragged from the liquid phase into the gas are of particular importance for the ionic compounds.

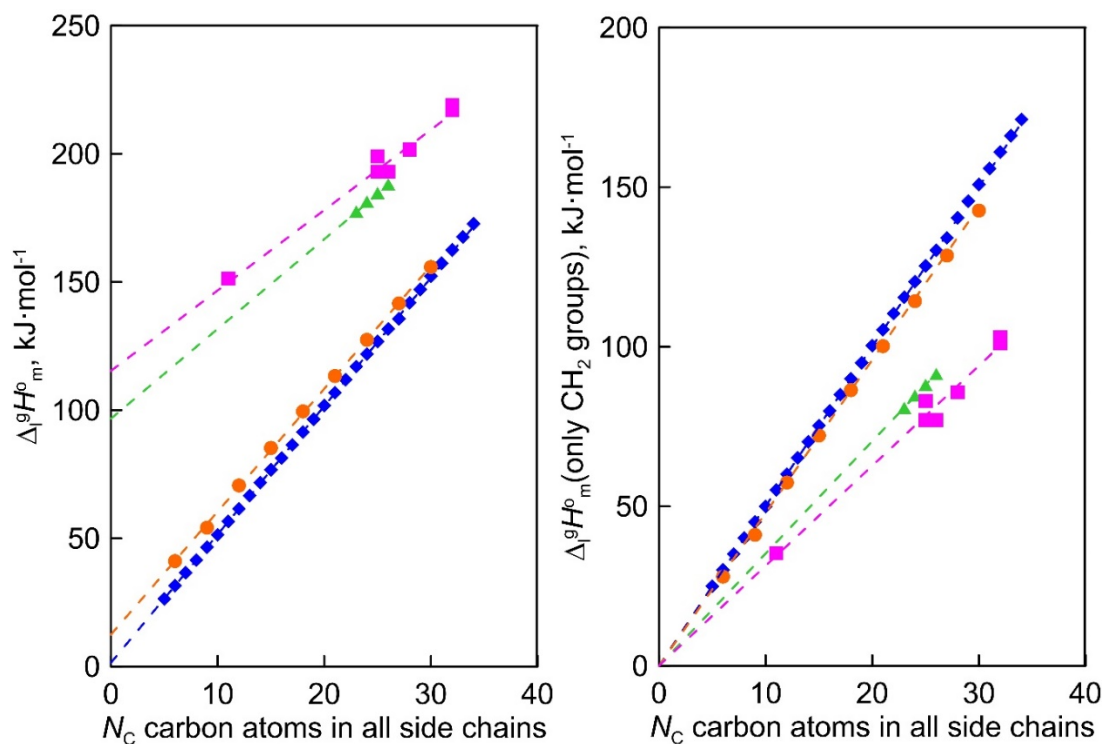


Figure 5.1.5 (a) The chain length dependence of the $\Delta_1^g H_m^o(298\text{ K})$ for *n*-alkanes, $C_n H_{2n+2}$ (diamonds, \blacklozenge); trialkylphosphines, $P(C_n H_{2n+1})_3$ (circles, \bullet); phosphonium-based ILs with $[PF_6]^-$ anion, $[P_{nnnm}][PF_6]$ (triangles, \blacktriangle); phosphonium-based ILs with $[NTf_2]^-$ anion, $[P_{nnnm}][NTf_2]$ (squares, \blacksquare). (b) The dispersion part of the vaporization enthalpy $\Delta_1^g H_m^o(298\text{ K})$ due to the alkyl chains.

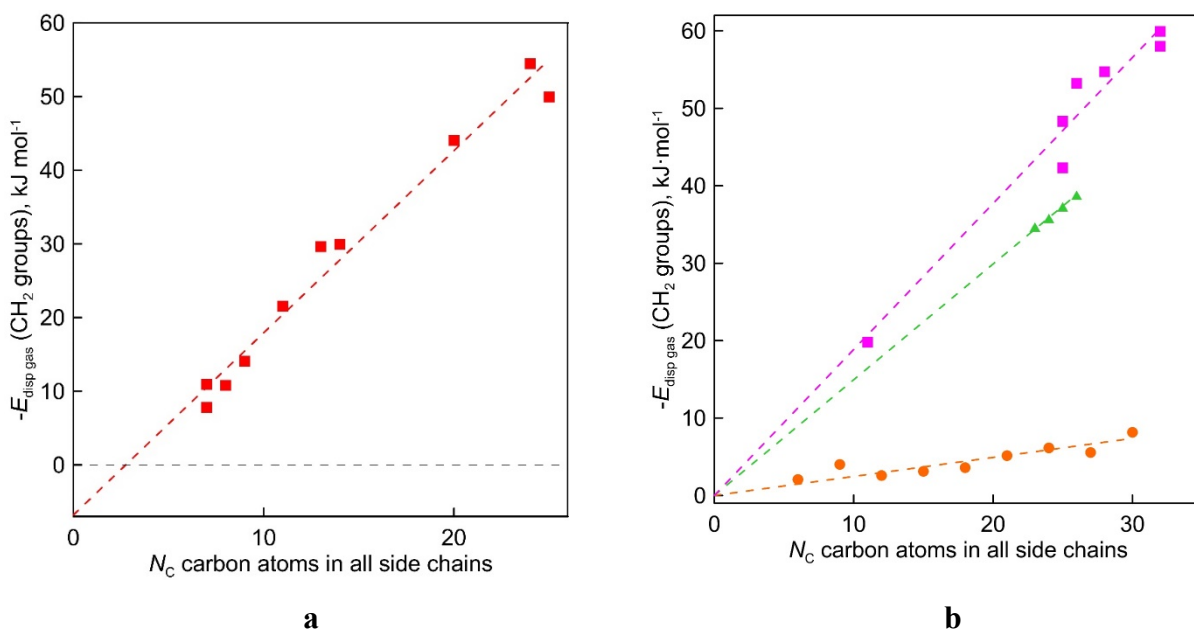


Figure 5.1.6 a) The gas phase dispersive interaction between alkyl chains for ammonium-based ILs with $[\text{NTf}_2]^-$ anion, as derived from experimental vaporization enthalpies $\Delta_1^g H_m^o(298 \text{ K})$. b) The gas phase dispersive interaction between alkyl chains for trialkylphosphines, $\text{P}(\text{C}_n\text{H}_{2n+1})_3$ (circles, ●); phosphonium-based ILs with $[\text{PF}_6]^-$ anion, $[\text{P}_{n n n m}][\text{PF}_6]$ (triangles, ▲); phosphonium-based ILs with $[\text{NTf}_2]^-$ anion, $[\text{P}_{n n n m}][\text{NTf}_2]$ (squares, ■).

To determine this amount of dispersion forces, we finally propose the third step to calculate the interactions between alkyl chains $E_{disp}((\text{CH}_2)_n \text{ gas})$ in the gas phase through space:

$$E_{disp}((\text{CH}_2)_n \text{ gas}) = \Delta_1^g H_m^o((\text{CH}_2)_n \text{ in ILs}) - \Delta_1^g H_m^o((\text{CH}_2)_n \text{ in } \text{C}_n\text{H}_{2n+2}) \quad (5.1.3)$$

The evaluated for ammonium based ILs values are given in Figure 5.1.6a. It is apparent from this figure that the tetra-substituted ammonium ions take the large amount (up to $55 \text{ kJ}\cdot\text{mol}^{-1}$) of dispersive interactions between chains and between chains and anion in the gas phase. First of all, this fact can explain the generally lower vaporization enthalpies of tetra-alkylammonium based ILs $[\text{NR}_4][\text{NTf}_2]$ compared to imidazolium-based ILs with the identical number of C-atoms in the alkyl chains. For example, the value $\Delta_1^g H_m^o(298 \text{ K}) = 152.1 \pm 2.7 \text{ kJ}\cdot\text{mol}^{-1}$ [8] for $[\text{N}_{1444}][\text{NTf}_2]$ (see Table 5.1.1) is significantly lower in comparison to those $\Delta_1^g H_m^o(298 \text{ K}) = 162.2 \pm 3.5 \text{ kJ}\cdot\text{mol}^{-1}$ derived for $[\text{C}_{12}\text{mim}][\text{NTf}_2]$ (averaged result from ref. [208,209]). Secondly, the gas phase dispersive interaction between alkyl chains for ammonium-based ILs with $[\text{NTf}_2]^-$ anion (see Figure 5.1.6a), are the key for the understanding of phenomena questioned in the introduction (see Figure 5.1.3). The dramatically decreasing differences between $\Delta_1^g H_m^o(298 \text{ K})$ -values of tetra-alkylammonium based *ionic* liquids and the corresponding *molecular* tri-alkylamines are obviously the consequence of a systematic accumulation of the gas-phase dispersion interactions at the tetra-alkylammonium cation with increasing chain length. These dispersion interactions are not so pronounced in the tri-alkylamines,

that is why the $\Delta_1^g H_m^\circ(298\text{ K})$ -differences indicate the amount of dispersion forces disrupted in the liquid phase along the vaporisation but taken into storage in the gaseous phase.

The evaluated for phosphonium based ILS values are given in Figure 5.1.5b. It is clear from this figure that tetra-substituted phosphonium ions in $[P_{nnnm}][PF_6]$ and $[P_{nnnm}][NTf_2]$ also take the large amount of dispersive interactions between CH_2 to the gas phase, up to $60\text{ kJ}\cdot\text{mol}^{-1}$ in the case of $[P_{nnnm}][NTf_2]$. These findings are crucial for the general reconsideration of the IL's vaporization thermodynamics, since the vaporizing molecules can no longer be regarded as a "star-shaped" conformation with the non-interacting tails (see *e.g.*, Figure 5.1.7, left). Instead, the tetraalkylsubstituted ammonium and phosphonium based ILS must be considered as entangled hairy balls (see Figure 5.1.7, right) with the significant dispersion interactions between the chain segments, as well as dispersion interactions of the long alkyl chains with the anion.

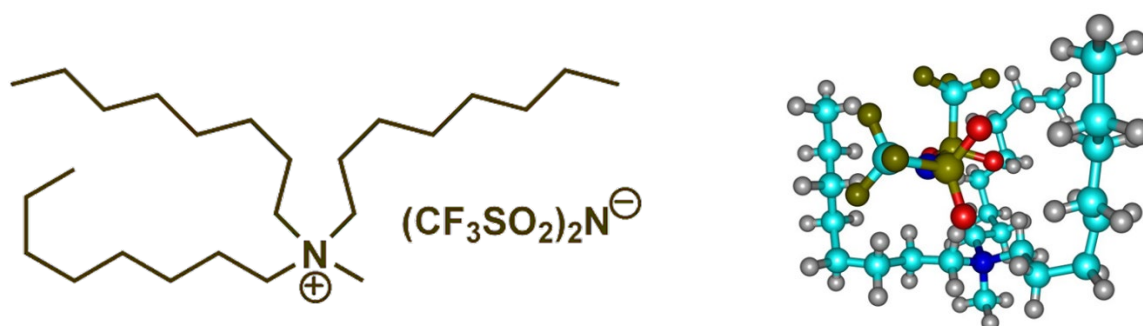


Figure 5.1.7 Illustration of the long-chained tetra-alkylammonium based IL $[N_{1888}][NTf_2]$ with the structurally predestinated dispersion interactions between the chain segments.

5.2. Dispersion forces in aprotic ammonium ionic liquids from DFT

The dispersion energy contributions were evaluated according to a method described in Section 6.4. The results of dispersion energy evaluation given in Table 5.2.1 were evaluated as follows:

$$E_{\text{disp-D3}}(\text{gas})_{\text{QC}} = E_{\text{tot}}(\text{B3LYP/cc - pvtz(D3BJ)}) - E_{\text{tot}}(\text{B3LYP/cc - pvtz}) \quad (5.2.1)$$

$$E_{\text{disp}}((\text{CH}_2)\text{gas})_{\text{QC}} = E_{\text{disp}}([\text{NR}_4][\text{NTf}_2]\text{gas}) - E_{\text{disp}}([\text{NH}_4][\text{NTf}_2]\text{gas}) \quad (5.2.2)$$

where $E_{\text{disp}}(\text{gas})$ corresponds to gas phase dispersion forces in studied ionic liquids, $E_{\text{disp}}((\text{CH}_2)\text{gas})$ corresponds to gas phase dispersion contribution of CH_2 groups in studied ionic liquids.

Table 5.2.1 Quantum chemical quantification of dispersion forces for tetra-alkylammonium-based ILS with the $[NTf_2]$ anion (in $\text{kJ}\cdot\text{mol}^{-1}$) [8].

Compound	$-E_{\text{disp}}(\text{gas})_{\text{QC}}$	$-E_{\text{disp}}((\text{CH}_2)_n \text{ gas})_{\text{QC}}$	$-E_{\text{disp}}((\text{CH}_2)_n \text{ gas})_{\text{exp}}$
[N1123]	232.6	119.5	10.9
[N1114]	230.1	117.1	7.8
[N1115]	246.8	133.7	10.8
[N1224]	266.9	153.8	14.1

[N2225]	302.1	189.1	21.5
[N1444]	327.7	214.6	29.6
[N2228]	360.2	247.1	30.0
[N2666]	463.6	350.5	44.0
[N6666]	517.4	404.4	54.4
[N1888]	532.6	419.6	49.9

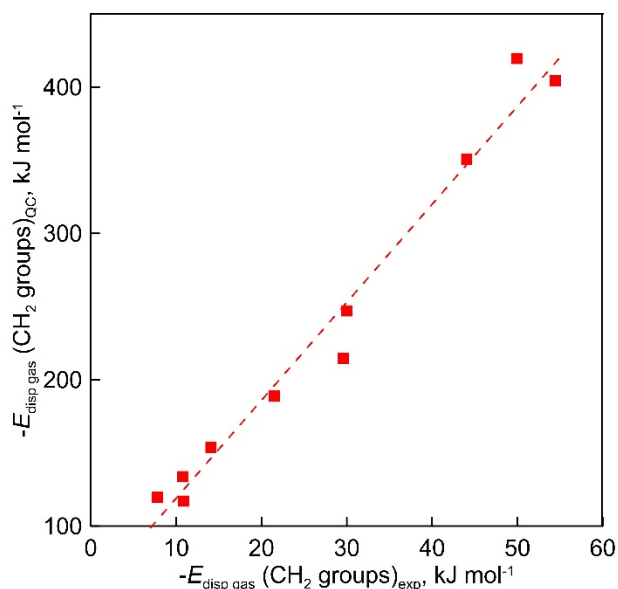


Figure 5.2.1 The correlation gas phase dispersive interaction between alkyl chains for ammonium-based ILs with $[\text{NTf}_2]^-$ anion calculated at D3(BJ) corrected B3LYP level of theory and results of experimental evaluation with “step by step” method.

Apparently, the direct comparison of QC-evaluated and experimental dispersion forces derived from vaporization enthalpies in previous chapter is not relevant. The experimental values were calculated with alkanes as reference compounds and the corresponding along the chain dispersion contribution is absolutely removed from consideration. The corresponding values provide the spatial dispersion forces due to the close position of not-chemically bonded C and H atoms. The results of QC calculations provide the total dispersion interaction of all CH_2 groups in studied ILs. At the same time, the very good correlation between experimental and QC-calculated dispersion forces:

$$E_{disp}((\text{CH}_2)\text{gas})_{\text{QC}} = 6.70 E_{disp}((\text{CH}_2)\text{gas})_{\text{exp}} + 52 \text{ with } (R^2 = 0.975) \quad (5.2.3)$$

obviously shows (see Figure 5.2.1), that both experimental “step by step” and QC methods are consistent and can quantitatively describe general trends of increasing dispersion interactions with the growing chain length.

5.3. Trend shift in hexafluorophosphate cation based ionic liquids

Since 1999, ionic liquids (ILs) have been intensively studied as new promising materials for broad industrial applications [210]. Vapor pressures of ILs at ambient temperatures are extremely low

and make the direct determination of vapor pressures and enthalpies of vaporization of ILs a demanding task, while measurements at the high temperatures can be associated with possible thermal decomposition.

The current study focuses on imidazolium-based ILs that contain hexafluorophosphate (PF_6^-) cation (see Figure 5.3.1).

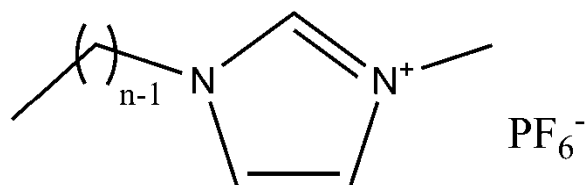


Figure 5.3.1 Structures of imidazolium-based ILs 1-alkyl-3-methylimidazolium hexafluorophosphate $[\text{C}_n\text{mim}][\text{PF}_6]$ family with $n = 2, 4, 6, 8, 10, 12, 14, 16,$ and 18 .

It has been shown that ILs with (PF_6^-) anions have a very moderate thermal stability and easily release HF as one of the decomposition products with a low activation energy of $E_A = 68 \text{ kJ}\cdot\text{mol}^{-1}$ [211]. For this reason, reliable experimental studies on ILs with (PF_6^-) at elevated temperatures are rare [211–213]. The first attempts to measure the vapor pressures for $[\text{PF}_6^-]$ containing IL ($[\text{C}_4\text{mim}][\text{PF}_6]$) was carried out with the classic Knudsen technique [211,212]. However, it was not possible to separate the mass loss rate due to vaporization and decomposition of the sample. The temperature desorption investigation of $[\text{C}_8\text{mim}][\text{PF}_6]$ in combination with the analysis by means of line of sight mass spectrometry (LOSMS) [4] has shown that vaporization and decomposition take place independently of one another, and thus the pure vaporization of the $[\text{C}_8\text{mim}][\text{PF}_6]$ was studied [213]. The evaporation/decomposition behavior of $[\text{C}_4\text{mim}][\text{PF}_6]$ was investigated by Volpe *et al.* [214] in the overall temperature range 425–551 K by means of the molecular effusion-based techniques Knudsen effusion mass loss (KEML) and Knudsen effusion mass spectrometry (KEMS). Additional experiments performed by non-isothermal thermogravimetry-differential thermal analysis (TG-DTA). All three techniques demonstrated the simultaneous evaporation/decomposition, although the conventional decomposition temperature derived from TG curves is much higher than the temperatures covered in effusion experiments.

In order to correctly determine the vaporization enthalpies of ILs with $[\text{PF}_6^-]$, one should avoid the decomposition during the study. This is only possible if the vapor pressure measurements are carried out at the lowest possible temperatures, at which the vapor pressures can still be measured, but the decomposition still does not occur.

The quartz crystal microbalance (QCM) technique was developed for such studies [215] and successfully used for vapor pressure measurements on $[\text{C}_n\text{mim}][\text{PF}_6]$ family with $n = 2-18$ [91,216].

The reliability of the vaporization enthalpies obtained for this set was checked by FTIR analysis and comparison of the thermodynamic parameters obtained with first-principle calculations and solution calorimetry [216]. The compilation of experimental values of the enthalpies of vaporization for $[C_n\text{mim}][\text{PF}_6]$ are listed in Table 5.3.1.

Table 5.3.1 The molar enthalpies of vaporization for $[C_n\text{mim}][\text{PF}_6]$ family derived from QCM results.

IL	T-range K	T_{av} K	$\Delta_1^{\text{g}}H_{\text{m}}^{\text{o}}(T_{\text{av}})$ kJ·mol ⁻¹	$\Delta_1^{\text{g}}G_{\text{m}}^{\text{o}}(T_{\text{av}})^{\text{a}}$ kJ·mol ⁻¹	$\Delta_1^{\text{g}}C_{\text{p,m}}^{\text{o}}{}^{\text{b}}$ J·K ⁻¹ ·mol ⁻¹	$\Delta_1^{\text{g}}H_{\text{m}}^{\text{o}}(298.15\text{ K})^{\text{c}}$ kJ·mol ⁻¹	
1	2	3	4	5	6	7	8
1	$[\text{C}_2\text{mim}][\text{PF}_6]$	414 - 457	435.2	129.9 ± 0.5	78.2 ± 1.5	-74	140.0 ± 2.8
2	$[\text{C}_4\text{mim}][\text{PF}_6]$	403 - 450	425.7	137.1 ± 0.6	78.6 ± 1.4	-74	146.5 ± 2.6
							145.3 ± 2.9 [214]
3	$[\text{C}_6\text{mim}][\text{PF}_6]$	408 - 455	430.7	140.0 ± 0.7	78.7 ± 1.5	-81	150.8 ± 2.7
4	$[\text{C}_8\text{mim}][\text{PF}_6]$	410 - 458	433.7	143.4 ± 0.8	80.2 ± 1.5	-85	154.9 ± 2.8
							165 ± 10 [213]
5	$[\text{C}_{10}\text{mim}][\text{PF}_6]$	413 - 461	436.3	148.5 ± 0.6	81.7 ± 1.5	-93	161.4 ± 2.8
6	$[\text{C}_{12}\text{mim}][\text{PF}_6]$	421 - 468	443.9	154.2 ± 0.5	82.6 ± 1.5	-97	168.3 ± 3.0
7	$[\text{C}_{14}\text{mim}][\text{PF}_6]$	426 - 473	448.9	161.4 ± 0.3	83.9 ± 1.5	-102	176.8 ± 3.0
8	$[\text{C}_{16}\text{mim}][\text{PF}_6]$	438 - 484	460.6	168.8 ± 1.0	83.5 ± 1.5	-108	186.3 ± 3.4
9	$[\text{C}_{18}\text{mim}][\text{PF}_6]$	448 - 496	471.5	175.7 ± 1.0	85.5 ± 1.6	-116	195.8 ± 3.6

^a The standard Gibbs energies of vaporization were evaluated using calibration coefficient $K = 9.5 \cdot 10^{-6}$.

^b Calculated from the experimental and evaluated volumetric properties.

^c Adjusted to 298.15 K using $\Delta_1^{\text{g}}C_{\text{p,m}}^{\text{o}}$ -values from column 7, the uncertainties are corrected for uncertainty in heat capacity difference equal to $20\text{ J}\cdot\text{K}^{-1}\cdot\text{mol}^{-1}$.

In Figure 5.3.2 (left) the vaporization enthalpy, $\Delta_1^{\text{g}}H_{\text{m}}^{\text{o}}(298.15\text{ K})$, alkyl chain length dependence for $[C_n\text{mim}][\text{PF}_6]$ is presented.

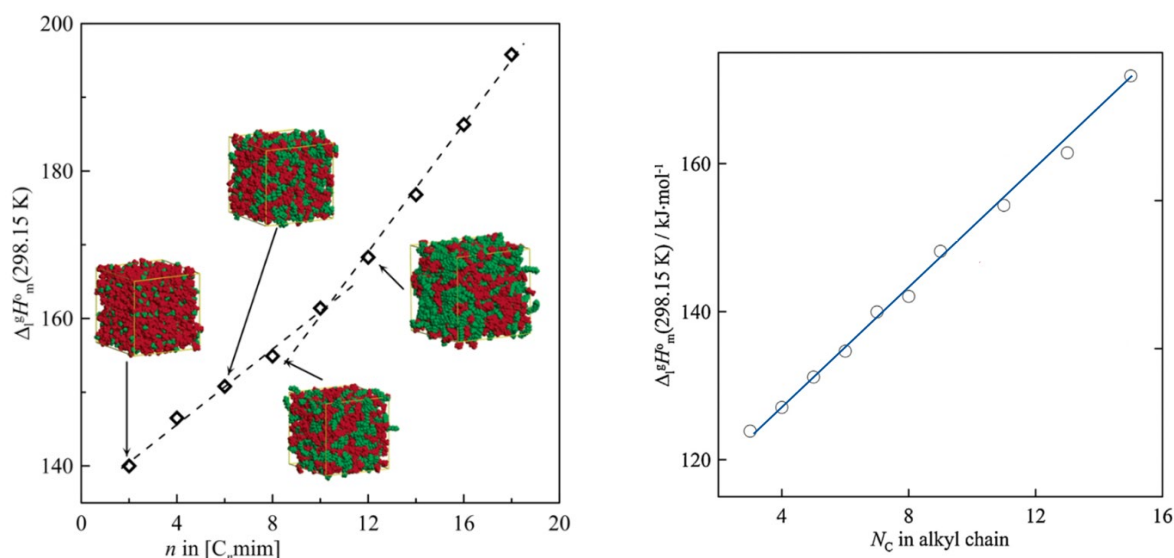


Figure 5.3.2 The alkyl chain length dependence of the enthalpy of vaporization for $[C_n\text{mim}][\text{PF}_6]$ (left) and for $[C_n\text{mim}][\text{NTf}_2]$ from [4] (right)

The trend of the alkyl chain length dependence observed for $[C_n\text{mim}][\text{PF}_6]$ have a change in the value of $\Delta\Delta_1^{\text{g}}H_{\text{m}}^{\text{o}}(\text{CH}_2)$ in the region of $n \sim 10$. In the experimental determination of the enthalpies of vaporization for imidazolium-based ILs with $[\text{NTf}_2]$ -anions [4] such a change of the trend was not observed (see Figure 5.3.2, right).

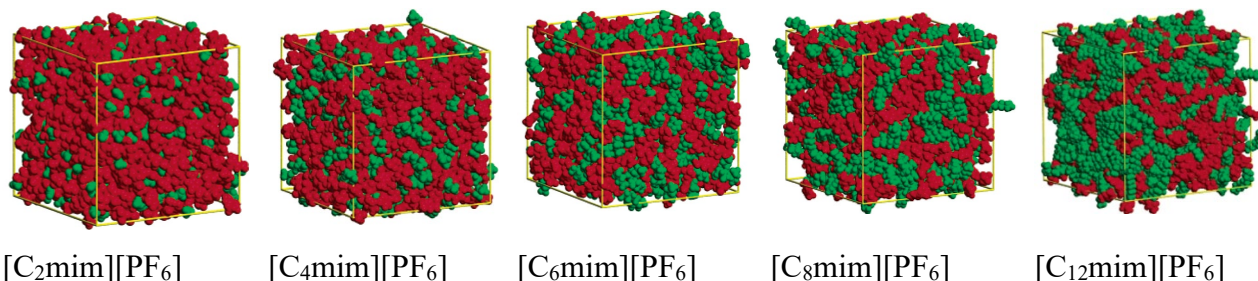


Figure 5.3.3 Visualizations of the nano-structuring in $[C_n\text{mim}][\text{PF}_6]$ series from MD simulations [217].

Nanometer-scale structuring in $[C_n\text{mim}][\text{PF}_6]$ series was demonstrated from MD simulations [217]. For ionic liquids with alkyl side chains longer than or equal to C_{10} , aggregation of the alkyl chains in nonpolar domains was observed. These domains permeate a tridimensional network of ionic channels formed by anions and by the imidazolium rings of the cations. The nanostructures were visualized in those work by color coding the two types of domains (red = polar and green = nonpolar in Figure 5.3.3). As the length of the alkyl chain increases, the nonpolar domains become larger and more connected and cause swelling of the ionic network, in a manner analogous to systems exhibiting microphase separation. The consequences of these nano-structural features on the vaporization enthalpies are apparent in Figure 5.3.2 and they lead to the trend-shift due to competition between the Coulomb and van der Waals forces in the IL. Qualitatively, the increase of the alkyl chain length leads to the linear increase of the van der Waals forces. At the same time Coulomb interaction of the charged parts of the molecules is decreased due to their separation through the alkyl-chain domains. Quantitatively, the chain length dependence for $[C_n\text{mim}][\text{PF}_6]$ vaporization enthalpies must be separated in two equations depending on the number of carbon atoms in the chain:

$$\Delta_1^{\text{g}}H_{\text{m}}^{\text{o}}(298.15 \text{ K})/\text{kJ}\cdot\text{mol}^{-1} = (2.6 \pm 0.3) \times N_{\text{C}} + (135.4 \pm 1.7) \quad N_{\text{C}} \leq 10 \quad (5.3.1)$$

$$\Delta_1^{\text{g}}H_{\text{m}}^{\text{o}}(298.15 \text{ K})/\text{kJ}\cdot\text{mol}^{-1} = (4.3 \pm 0.3) \times N_{\text{C}} + (117.0 \pm 4.5) \quad N_{\text{C}} \geq 10 \quad (5.3.2)$$

where N_{C} , is the number of carbon atoms in the alkyl chain.

It is interesting to compare the CH_2 increment in enthalpy of vaporization for $[C_n\text{mim}][\text{PF}_6]$ with the corresponding increments for other molecular and ionic compounds (see Table 5.3.2).

Table 5.3.2 Contributions for CH₂ group into the enthalpy of vaporization, $\Delta_1^{\text{g}}H_{\text{m}}^{\circ}(298.15 \text{ K})$, for different classes of molecular and ionic compounds.

Compounds	$\Delta\Delta_1^{\text{g}}H_{\text{m}}^{\circ}(\text{CH}_2)$, $\text{kJ}\cdot\text{mol}^{-1}$	Reference
[C _n mim][PF ₆] $n < 10$	2.6 ± 0.3	this work
[C _n mim][PF ₆] $n \geq 10$	4.3 ± 0.3	this work
[C _n mim][NTf ₂]	3.9 ± 0.2	[4]
[C _n Py][NTf ₂]	3.6 ± 0.2	[218]
[C _n C _l Pyrr][NTf ₂]	3.5 ± 0.4	[219]
C _n H _{2n+1} CN	4.44 ± 0.12	[32]
C _n H _{2n+1} OH	4.71 ± 0.08	[55]
C _n H _{2n+1} C ₆ H ₅	4.48 ± 0.04	[132]
C _n H _{2n+2}	4.95	[220]
CH ₂ =CH-C _n H _{2n+1}	4.97	[220]
HS-C _n H _{2n+1}	4.76	[220]
Cl-C _n H _{2n+1}	4.85	[220]
Br-C _n H _{2n+1}	4.80	[220]
C _n H _{2n+1} CO ₂ -CH ₃	5.03	[220]

The $\Delta\Delta_1^{\text{g}}H_{\text{m}}^{\circ}(\text{CH}_2)$ value found for $n \geq 10$ of [C_nmim][PF₆] agrees with the values for ionic liquids with [NTf₂] anion within combined uncertainty. Thus, the CH₂ increment in the enthalpy of vaporization for ionic liquids can be assumed to be at the level of 3.8 – 3.9 $\text{kJ}\cdot\text{mol}^{-1}$ for alkyl chains longer than ≈ 10 carbon atoms. In the case of short chains the CH₂ increment value can deviate significantly from that observed for longer alkyl chains, as it was observed [4] for [C₁mim][NTf₂] and for [C_nmim][PF₆] family in this work. It is obvious, that ILs with the short alkyl chains, the vaporization enthalpies, $\Delta_1^{\text{g}}H_{\text{m}}^{\circ}(298.15 \text{ K})$, can significantly deviate from the additivity, and this fact should be taken in account when evaluating the corresponding correlation or group contribution methods.

In the previous Sections 5.1 and 5.2 we showed that for ionic liquids based on ammonium and phosphonium cations, the dispersion interactions between the alkyl chains contribute significantly to the enthalpy of vaporization. The trend-shift in vaporization enthalpies of [C_nmim][PF₆] shown in Figure 5.3.2 could be also attributed to the dispersion forces growing with the elongation of the chain length. The amount of dispersion interactions, $E_{\text{disp-D}}$, was calculated in the same way as in Sections 5.1 and 5.2 and these values are given in Table 5.3.3.

Table 5.3.3 Chain-length dependence of dispersion forces, $E_{\text{disp-D}}$, in [C_nmim][PF₆] series at 298.15 K in $\text{kJ}\cdot\text{mol}^{-1}$

IL	$E_{\text{disp-D3}}$
[C ₂ mim][PF ₆]	-68.6
[C ₄ mim][PF ₆]	-97.2
[C ₆ mim][PF ₆]	-105.5
[C ₈ mim][PF ₆]	-128.6
[C ₁₀ mim][PF ₆]	-131.8
[C ₁₂ mim][PF ₆]	-182.1

$[C_{14}mim][PF_6]$	-189.3
$[C_{16}mim][PF_6]$	-212.4
$[C_{18}mim][PF_6]$	-242.0

A visualization of these results is given in Figure 5.3.4

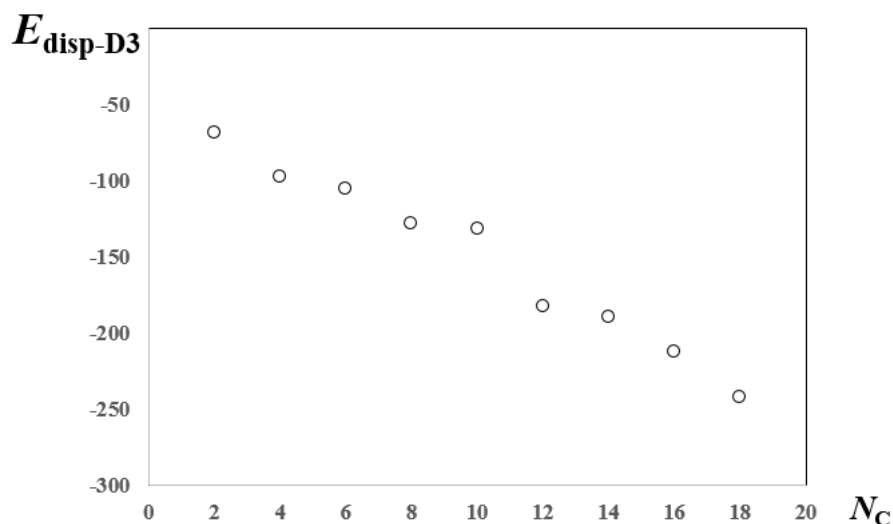


Figure 5.3.4 Chain-length dependence of dispersion forces, $E_{\text{disp-D}}$, in $[C_n\text{mim}][PF_6]$ series at 298.15 K (in $\text{kJ}\cdot\text{mol}^{-1}$).

It is quite obvious from this figure, that for the short-chained ILs the $E_{\text{disp-D}}$ contributions are very individual and the chain-length dependence for $N_C = 2, 4,$ and 6 is not monotone. The significant irregular fluctuations of the $E_{\text{disp-D}}$ -values are observed for the $N_C = 8, 10,$ and 12 . These fluctuations are most probably due to competition between the Coulomb and van der Waals forces and they are in agreement with the observation from MD-simulations as well as with the trend-shift at $N_C = 10$ shown for vaporization enthalpies in Figure 5.3.2. And only from $N_C \geq 14$, the expected monotone increasing of $E_{\text{disp-D}}$ -values can be considered as a manifestation of the victory of the van der Waals forces over the Coulomb forces. Thus, the similarity of trends observed for experimental vaporization enthalpies and theoretical dispersion forces could be considered as the mutual validation of the experimental and theoretical results evaluated for the $[C_n\text{mim}][PF_6]$ series.

6. Experimental part.

6.1. Transpiration or gas saturation method.

Transpiration is a conventional method for indirect vapour pressure measurements. In the gas-saturation method, a saturated vapor phase is generated by passing an inert gas through a column packed either with the pure compound of interest or with an analyte-coated inert carrier. The analyte is collected from a known volume of the saturated vapor using a cryogenic trap and the amount of the analyte is determined by an appropriate method. This method has several advantages, that is, it is not

influenced by small amounts of volatile impurities, it is possible to measure the equilibrium vapor pressure within a short time, and it is also possible to take measurements in any atmosphere by changing the carrier gas. This offers the key advantage that the vapor pressure can be measured over temperature ranges close to the ambient temperature, instead of relying on extrapolation of the results of high temperature measurements, a method that always carries the risk of producing incorrect values. The transpiration method is basically free of serious errors and has proven to be very good in agreement with other established methods for determining the vapor pressures of pure substances and vaporization enthalpies from the temperature dependence of the vapor pressure.

The transpiration method is particularly successful at low vapor pressures of around 100 Pa and below and can be used near ambient temperature, where the data are particularly relevant for assessing the fate and behaviour of environmental pollutants. The restriction for the pressure range is apparent because of the simple treatment of the experimental data obtained by the transpiration method using the ideal gas law [55].

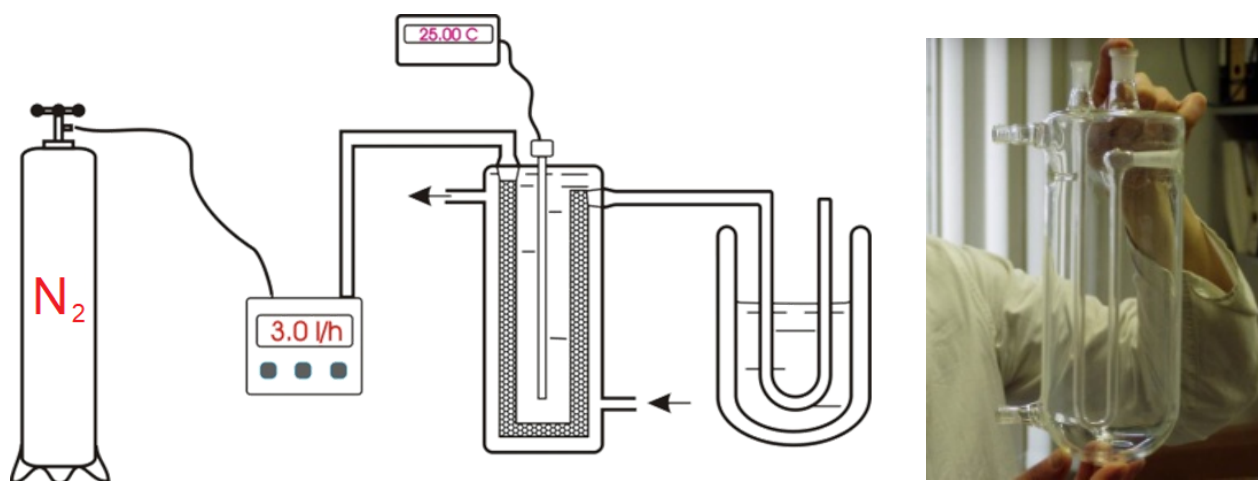


Figure 6.1.1 Transpiration apparatus scheme (left) and a photo of a saturator (right).

To carry out an experiment, we need approx. 0.7-1.0 g of a sample, which we distribute over the portion of glass beads (1.0 mm diameter, # 11079110, BioSpec Products) to provide a large surface area for saturation. The glass beads covered with the sample are placed in a U-shaped tube that is called as saturator (Figure 6.1.1 (right)). The U-shaped tube is kept at desired temperature (± 0.1 K) with a thermostat.

For study of solid samples, they were dissolved in volatile solvents such as methanol or acetonitrile to cover the surfaces of the glass beads after evaporation of the solvent. To remove possible volatile impurities, the sample was preconditioned in the saturator by flushing nitrogen (flow rate approx. 1-2 l/h) through the saturator with the sample in it for about one hour at 20-60° C. The degree of removal of the impurities was followed by gas chromatography.

The flow rate of the nitrogen flow in the saturator should not be too low, to avoid the transport of the material out of the U-tube by diffusion, and not too high, to achieve the saturation of the nitrogen flow with the compound. To determine the plateau in the plot of the apparent pressure against the flow rate of the carrier gas at a suitable temperature (preferably the mean value), several preliminary tests must be carried out. The saturation of the gas must be checked by determining whether the value obtained for the vapor pressure varies with the flow rate. Our setup was tested at different flow rates of the carrier gas to check the lower limit of the flow, below which the contribution of the vapor condensed in the trap by diffusion becomes comparable with that which is transpired. In our apparatus, the contribution due to diffusion was negligible at flow rates of more than $0.45 \text{ dm}^3 \cdot \text{h}^{-1}$. The upper limit for our apparatus where the nitrogen flow rate could already disturb the equilibration was at flow rate of $9.0 \text{ dm}^3 \cdot \text{h}^{-1}$. Thus, we performed the experiments at flow rates in the range $(0.7 \text{ to } 4) \text{ dm}^3 \cdot \text{h}^{-1}$, which ensured that the transporting gas was at the saturated equilibrium with the coexisting liquid phase in the saturation tube. The gas flow was measured using a Hewlett-Packard 0101-0113 soap film flow meter and verified using a Bronkhorst Hi-Tec E-7500-AAA digital gas flow controller. The mass, m_i , of compound, which is transported from the saturator and collected in the cold trap was determined by GC analysis using an external standard (hydrocarbon $n\text{-C}_n\text{H}_{2n+2}$).

The analyte collected in the cold trap was washed out with a suitable solvent and 200 μl of the solution with the known amount of alkane were added. The solution was injected in the GC three times. The gas chromatograph was equipped with a capillary column HP=5 (stationary phase crosslinked 5% PH ME silicone) with a length of 30 m, an inside diameter of 0.32 mm, and having a film thickness of 0.25 μl . The GC calibration was carried out individually for each examined sample.

6.1.1. Data processing

In the transpiration method, the absolute vapour pressure is derived with the equation (6.1.1). In the equation, the absolute vapour pressure p_i at a temperature T_i is proportional to the mass of the condensed substance m_i within a certain period:

$$p_i = \frac{m_i R T_a}{V M_i} \quad (6.1.1)$$

In this equation R is the universal gas constant, T_a – is the temperature of a bubble flow meter that was used to measure the flow rate, M_i – is molar weight of the substance I and V is a sum of volumes of the substance itself and of the nitrogen stream saturated with the substance $V = V_i + V_{N_2}$ according to Dalton's law [55].

The experimental vapour pressures were approximated with the equation (6.1.2) to get the b correlation parameter that is used for sublimation or vaporization enthalpy $\Delta_{l,cr}^g H_m^o(T)$ calculation according to equation (6.1.3) [55].

$$R \cdot \ln(p_i/p_{\text{ref}}) = a + \frac{b}{T} + \Delta_{\text{l,cr}}^{\text{g}} C_{\text{p,m}}^{\text{o}} \cdot \ln\left(\frac{T}{T_0}\right) \quad (6.1.2)$$

$$\Delta_{\text{l,cr}}^{\text{g}} H_{\text{m}}^{\text{o}}(T) = -b + \Delta_{\text{l,cr}}^{\text{g}} C_{\text{p,m}}^{\text{o}} T \quad (6.1.3)$$

where a and b are correlation parameters and $\Delta_{\text{l,cr}}^{\text{g}} C_{\text{p,m}}^{\text{o}}$ is the difference of the molar heat capacities of the gas $C_{\text{p,m}}^{\text{o}}(\text{g})$ and of the crystalline or liquid phase $C_{\text{p,m}}^{\text{o}}(\text{cr, l})$. T_0 is a reference temperature that was arbitrarily chosen as $T_0 = 298.15 \text{ K}$, $p_{\text{ref}} = 1 \text{ Pa}$ and R is the gas constant.

Consequently, vaporization or sublimation entropies at given temperatures T can be also derived from pressure-temperature dependencies with the aid of equation (6.1.4)

$$\Delta_{\text{cr,l}}^{\text{g}} S_{\text{m}}^{\text{o}}(T) = \Delta_{\text{l}}^{\text{g}} H_{\text{m}}^{\text{o}}/T + R \cdot \ln(p_i/p^{\text{o}}) \quad (6.1.4)$$

with $p^{\text{o}} = 0.1 \text{ MPa}$.

The uncertainties both for enthalpies and entropies are expressed as the standard uncertainty (at 0.68 level of confidence, $k = 1$) and are calculated in accordance with the method described in [29]. It includes experimental errors, uncertainties of vapour pressure, equation fitting and temperature adjustment to the 298.15 K.

6.1.2. Heat capacity differences determination

The determination of the difference between the molar heat capacities of the gas and the crystalline or liquid phase $\Delta_{\text{l}}^{\text{g}} C_{\text{p,m}}^{\text{o}}$ is an untrivial and complex task that include several approaches. The choice of a particular approach is mainly based on data availability and the feasibility of experiments.

6.1.2.1. Direct semi-empirical approach.

The values of $C_{\text{p,m}}^{\text{o}}(\text{cr, l})$ can be measured experimentally with the aid of adiabatic calorimetry or differential scanning calorimetry (DSC) [221]. The heat capacity of substance in a gaseous state is difficult to measure experimentally and therefore this parameter is estimated with group additivity method [222] or statistical thermodynamics [223]. For calculation of the $\Delta_{\text{l,cr}}^{\text{g}} C_{\text{p,m}}^{\text{o}}(298.15 \text{ K})$ Chickos and Acree [224,225] suggested an empirical approach

$$\Delta_{\text{l}}^{\text{g}} C_{\text{p,m}}^{\text{o}}(298.15 \text{ K}) = -0.26 \cdot C_{\text{p,m}}^{\text{o}}(\text{l}, 298.15 \text{ K}) + 10.58 \quad (6.1.5)$$

$$\Delta_{\text{cr}}^{\text{g}} C_{\text{p,m}}^{\text{o}}(298.15 \text{ K}) = 0.15 \cdot C_{\text{p,m}}^{\text{o}}(\text{cr}, 298.15 \text{ K}) + 0.75 \quad (6.1.6)$$

where $C_{\text{p,m}}^{\text{o}}(\text{cr}, 298.15 \text{ K})$ is an experimental value or a value calculated with the group additivity procedure [16].

6.1.2.2. Determination of $\Delta_{\text{l}}^{\text{g}} C_{\text{p,m}}^{\text{o}}$ with the aid of Clarke and Glew equation

If a broad pressure-temperature dependency data is provided with a temperature range of about 100-150 K (this is usual case for vapor pressures measured over liquids), we can use the Clarke and Glew equation [17] that is able to provide reliable $\Delta_{\text{l}}^{\text{g}} C_{\text{p,m}}^{\text{o}}$ values.

$$R \ln \left(\frac{p}{p_0} \right) = -\frac{\Delta_1^g G_m^o(\theta)}{\theta} + \Delta_1^g H_m^o(\theta) \cdot \left(\frac{1}{\theta} - \frac{1}{T} \right) + \Delta_1^g C_{p,m}^o(\theta) \cdot \left[\frac{\theta}{T} - 1 + \ln \left(\frac{T}{\theta} \right) \right] \quad (6.1.7)$$

where p is the vapour pressure at the temperature T , p^0 – is an arbitrary reference pressure, *e.g.*, of 1 Pa, θ is an arbitrary reference temperature, *e.g.*, 298.15 K, R – is the molar gas constant, $\Delta_1^g G_m^o(\theta)$ is the difference in the standard molar Gibbs energy between the gaseous and the liquid phases at the selected reference temperature θ , $\Delta_1^g H_m^o(\theta)$ – is the standard molar enthalpy of vaporisation. The use of this equation offers reliable results and is related to the thermodynamic functions of vaporization.

6.1.2.3. Determination of $\Delta_1^g C_{p,m}^o$ with the use of volumetric properties.

There is a sophisticated and indirect approach for $\Delta_1^g C_{p,m}^o$ estimation that is based on the experimental volumetric properties of a liquid phase of a studied substance, namely thermal expansion of the liquid sample α_p , isothermal compressibility κ_T , and molar volume V_m [4,226].

$$\Delta_1^g C_{p,m}^o(298.15 \text{ K}) = -2R - (C_{p,m}^o - C_{v,m}^o)_1 \quad (6.1.8)$$

The difference of heat capacities can be expressed as:

$$(C_{p,m}^o - C_{v,m}^o)_1 = \frac{\alpha_p^2}{\kappa_T} V_m T \quad (6.1.9)$$

The direct measurements of isothermal compressibility from the density pressure dependence are relatively demanding but κ_T can be derived from the speed of sound measurements in liquid phase:

$$\kappa_T = \frac{1}{\rho} \cdot \left(\frac{1}{w_a^2} + \frac{\alpha_p^2 T M}{C_{p,m}^o} \right) \quad (6.1.10)$$

Where ρ is density of the liquid, w_a is the adiabatic speed of sound, and M is the molar mass of the studied compound.

When the speed of sound for a particular substance is not available a following equation can be used:

$$(C_{p,m}^o - C_{v,m}^o)_1 = n \cdot \alpha_p (\Delta_1^g H_m^o - RT) \quad (6.1.11)$$

Where n is an adjustable parameter that is usually $n = 1.10 \pm 0.04$.

6.1.2.4. Determination of $\Delta_1^g C_{p,m}^o$ from the Kirchoff Law

The experimental $\Delta_1^g C_{p,m}^o$ value can also be derived if two test series with significantly different temperature ranges are available in the literature. For example, for the first set the sublimation enthalpy $\Delta_{cr}^g H_m^o(T_{avl})$, measured at elevated temperatures and referenced to T_{avl} . For the second set the sublimation enthalpy $\Delta_{cr}^g H_m^o(T_{avlII})$, measured at significantly low temperatures and

referenced to T_{avII} . Thus, the $\Delta_{cr}^g C_{p,m}^o$ -value can be derived from the Kirchhoff Law according to Eq. (6.3.1):

$$\Delta_{cr}^g C_{p,m}^o = [\Delta_{cr}^g H_m^o(T_{avI}) - \Delta_{cr}^g H_m^o(T_{avII})] / (T_{avII} - T_{avI}) \quad (6.1.12)$$

In this work the temperature adjustment of vaporization/sublimation enthalpies has been performed by using all described method, depending on the available input information.

6.2. Mass loss Knudsen effusion method

The Knudsen effusion method is an experimental approach that makes it possible to measure vapor pressures in the range from 0.01 to 100 Pa and is used in three variations. The first one is the torsion effusion method (or recoil momentum technique) where effusion exerts a force on the cylindrical cell causing a torque on the suspension wire. The torque produces an angular twist opposed by the torsional stiffness of the suspension. This torque is directly proportional to the vapour pressure.

$$p = \frac{2\phi K}{A_1 l_1 f_1 + A_2 l_2 f_2} \quad (6.2.1)$$

where ϕ is the angular twist, K is the torsion constant, A_1 , A_2 , l_1 , l_2 , are the effective areas of the orifices and their distances from the rotation axis, respectively, and f_1 , f_2 are force factors related to Clausing orifice transmission probabilities (geometrical factors derived from radius and thickness of the effusion hole) [171]

The second technique is a differential technique based on the thermogravimetry, in which the mass loss is measured continuously. A light measuring cell is suspended in a thermostatted chamber from the holder of a commercial microbalances. The mass loss is automatically recorded during the experiment. The effusion rate and, consequently, the mass loss depends on the time exposure and temperature of experiment. The mass loss is proportional to vapor pressure [171].

Both techniques have the same disadvantage: the measuring cell is suspended in the vacuum chamber and the temperature cannot be measured directly in the sample. This fact caused the strong fluctuations in the "true" evaporation temperature, which led to systematic errors.

A third modification is free from this disadvantage since the measuring cell is placed in a cavity of a thermostated heating block and a measuring probe is placed directly under the cell. The mass loss during the experiment is determined by weighing the cell before and after the effusion. The cylindrical cell with the sample is tightly closed with a lid with a small orifice at the top. The sample effuses through this opening into a vacuum chamber during the experiment.

The vapour pressure at the temperature of the cell T is usually calculated with Eq. (6.2.2)

$$p^* = \frac{\Delta m}{kAt} \cdot \sqrt{\frac{2\pi RT}{M}} \quad (6.2.2)$$

where t is the vacuum exposure time, M – molar mass of vapour, Δm – mass loss, A – orifice area, R – molar gas constant, and k – transmission probability factor. The factor k is a complex factor that is a function of membrane thickness l , orifice radius r , and Knudsen number Kn and considers effusing gas isotropy failure according to Wahlbeck [227]

In first approximation it is assumed that the vapour reaches full saturation. In fact, that is an unrealistic situation. The phenomenon of undersaturation was studied by Nesmeianov [228]. From his work it can be concluded that the undersaturation cannot be left unconsidered especially for solid substances. The reason for undersaturation is that the effusion rate is higher than the rate of sublimation itself. Zaitsau [229] in his work analysed the issue and transformed the equation (6.3.1) into the following corrected form:

$$p_{\text{sat}} = \frac{\Delta m}{kAt} \cdot \sqrt{\frac{2\pi RT}{M}} \cdot (1 + kA \cdot (\alpha\gamma A_{\text{sub}}))^{-1} = p^* \cdot (1 + kA \cdot (\alpha\gamma A_{\text{sub}}))^{-1} \quad (6.2.3)$$

where α is the condensation coefficient, γ is the roughness coefficient and A_{sub} is ideal geometrical surface of the sample from which the sublimation occurs.

The new Knudsen-Effusion setup was constructed and tested at the University of Rostock. A general scheme and photo are given in Figure 6.2.1 and Figure 6.2.2.

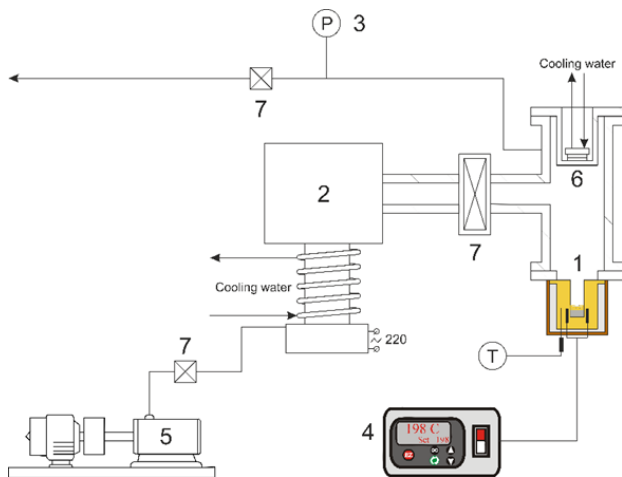


Figure 6.2.1 Knudsen apparatus scheme:
 1 – heating chamber with the Knudsen cell,
 2 – vacuum chamber, 3 – vacuum gauge,
 4 – heating controller, 5 – pump, 6 – cooling trap, 7 – valves

Figure 6.2.2 Photo of Knudsen apparatus

The heating chamber or heating block of our apparatus is a brass cylinder with an indentation for one cell, channels for thermometer and a heating rod connected to a heating controller. The

constant temperature in the measuring cell was maintained within the brass heating block with the stability of 0.02 K in the interval (300 to 470) K provided by a Watlow EZ-ZONE PM EXPRESS PM6C1CA-AAAAAAA controller equipped with a 3-wires Pt 100 Ohm resistance thermometer. The temperature in the heating block was measured using a precise platinum resistance thermometer Pt100 GTF 401 1/10 DIN -50 ... +400 °C, 1/10 DIN Class B ($\pm 0,03$ °C at 0 °C) Greisinger GMH 3710 with 4-wire connection calibrated according to DIN EN 60751 by the German Calibration Service (DKD).

The chamber is wrapped with an insulation based on polyamide band Kapton and SLENTEX mineral insulation. This prevents the chamber from temperature fluctuations related to heat exchange with the environment. The block is attached to the vacuum chamber with the aid of a blank steel flange (ISO100BK-304 with centring ring) with an orifice for the heating chamber. The vacuum chamber is a T-shaped vacuum tube. It is connected to the pumping system via gate valve and joined with a cold trap.

The cold trap has purpose of catching effused substance in one place to avoid vacuum chamber contamination. It is a stainless-steel cylinder with a closed bottom that contains two consequent Peltier elements that create low temperature for the trap that allow to condensate the effused vapour. The Peltier elements in turn are cooled with a plate heat exchanger Watercool HEATKILLER® NSB Rev3.0 Nickel connected to a cold-water source.

The pumping system includes piping and a pump Agilent Technologies DS202 that is providing vacuum creation of 10^{-5} Pa. The depth of vacuum is measured with Full Range Pirani Bayard-Alpert Gauge Agilent Technologies FRG-720.

The effusion cell is a two-part cylinder (see Figure 6.2.3 and Figure 6.2.5) where first part is a bottom that is supposed to contain analysed substance and the second part is a lid with an orifice. The bottom part is an open top cylinder. It is made of stainless steel 316Ti and has diameter of 25 mm and the height of 10 mm. The lid can be equipped with a golden round membrane having an orifice of either 0.5 mm, 1 mm, 1.4 mm, or 2 mm diameter (see Figure 6.2.4). The orifices were made with the aid of drilling machine of corresponding sizes. The precise dimensions of the orifices were obtained with the aid of a microscope Olympus SZX16 and provided in Table 6.2.1 The lid and the bottom have screw-threads for fastening complemented with a PTFE ring for sealing.

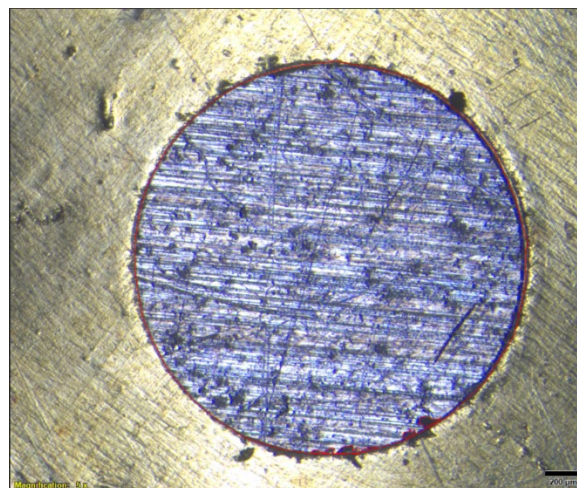
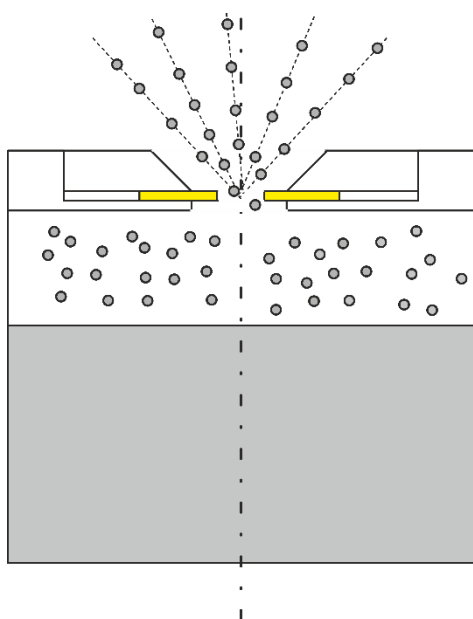


Figure 6.2.3 Scheme of the Knudsen cell with an effusing substance

Figure 6.2.4 5x scaled microscopic image of the 2 mm membrane



Figure 6.2.5 Photos of the Knudsen cell. From left to right: bottom view of the brass lid, top view of the brass lid, steel container.

Table 6.2.1 The precise dimensions of the orifices used in this work

Membrane	$10^4 d, \text{ m}$	$10^7 A, \text{ m}^2$	$l, \text{ m}$
0.5 membrane	4.942	1.918	0.00005
1.0 membrane	10.90	9.365	0.00005
1.4 membrane	14.12	15.66	0.00005
2.0 membrane	20.19	33.18	0.00005

The choice of the cell materials is explained by temperature gradient that is required for the process. The gradient prevents substance from condensation on the lid and lets the particles to pass unhindered. Otherwise, the particles adhere to the membrane and therefore clog the orifice, affect the membrane thickness, thermal conductivity, and flow dynamics. Thereby the choice of brass for the heating chamber and the lid of the cell is a trade-off between thermal conductivity, chemical inertness, and metal hardness.

6.2.1. Experimental procedure

The effusion cell is loaded with analysed substance of about $\frac{3}{4}$ of the cell volume and then the substance is compacted with a hydraulic press with a piston to achieve a maximal thermal contact of the substance with the bottom of the cell and to make the structure of the substance uniformly dense

and without voids. The presence of voids in the substance worsens the thermal contact and sample heating that in turn produces lowered pressure values for a study. After that, the cell with the lid is weighed with high precision balances ($\pm 1 \cdot 10^{-5}$ g) Sartorius Secura 225D-1S and is placed into the indentation of the thermal block. Subsequently, the temperature is set, and the block is left for temperature stabilisation (thermostating) for 30 minutes. Following the thermostating phase the gate valve is opened providing vacuum creation. The time measurement begins after reaching 10^{-3} Pa in the vacuum chamber and ends after predefined time with the gate valve closing. After that the cell is stored at ambient temperature on a cork mat for 30 minutes to reduce cell temperature and to allow adsorption of gases on the cell surface. Subsequently, the cell is being weighed and the mass loss determined. The criteria for a successful experiment would be a mass loss of more than 9-10 mg, preserved full thermal contact of the substance with the cell, and visual absence of thermal decomposition (change of colour, smell etc.)

6.2.1.1. Testing the setup

To qualify the new apparatus a series of experiments was performed. For that purpose, benzoic acid in ranges from 0.14 Pa to 20.67 Pa was measured within a temperature range from 299.75 K to 347.45 K. The compound is recommended as a standard for enthalpy of sublimation measurements. Benzoic acid (CAS 65-85-0) was obtained from Parr inc. with a mass fraction purity of 99.9+% No further additional purification was performed. A series of measurements with benzoic acid was conducted with orifices of about 0.5-, 1.0-, 1.4-, and 2-mm diameter. The precise areas A , mass losses Δm , vacuum exposure time t , Knudsen number Kn , diameters d , and transmission probability factors k , of the effusion orifices used in the measurements are given in Table 6.2.2.

Table 6.2.2 Results of the test experiments with benzoic acid

Membrane diameter, mm	T , K	Δm , g	t , s	k	Kn	p_{sat} , Pa
0.5	331.82	0.00501	1880	1.07	1.02	5.091
0.5	317.13	0.01381	25790	0.96	4.44	3.001
0.5	321.99	0.01501	16623	0.99	2.72	1.836
0.5	326.84	0.00821	5420	1.03	1.69	1.109
0.5	337.73	0.03833	8342	1.13	0.62	8.457
0.5	342.09	0.01509	1960	1.18	0.39	13.676
0.5	347.45	0.02294	1804	1.22	0.25	22.024
1.0	302.02	0.01153	30374	0.97	13.6	0.965
1.0	307.13	0.01065	15872	0.99	7.87	1.718
1.0	317.10	0.01376	6527	1.04	2.68	2.872
1.0	322.03	0.01253	3242	1.09	1.54	0.316
1.0	326.82	0.01221	1830	1.14	0.94	0.179
1.4	299.75	0.03075	62040	0.99	13.63	0.403
1.4	307.85	0.00934	7087	1.01	5.35	1.452
1.4	314.93	0.00851	3064	1.06	2.67	0.153
1.4	320.48	0.01077	2176	1.10	1.58	2.544
1.4	325.49	0.01594	1782	1.16	0.93	0.833
2.0	301.98	0.01395	11848	1.01	8.42	0.317
2.0	305.15	0.01016	6008	1.02	5.96	0.621
2.0	310.95	0.00839	2509	1.05	3.15	1.048

2.0	315.87	0.01516	2650	1.09	1.92	1.816
2.0	321.19	0.01770	1750	1.15	1.15	0.221

The $\ln p - 1/T$ dependency data is graphically presented in Figure 6.2.6

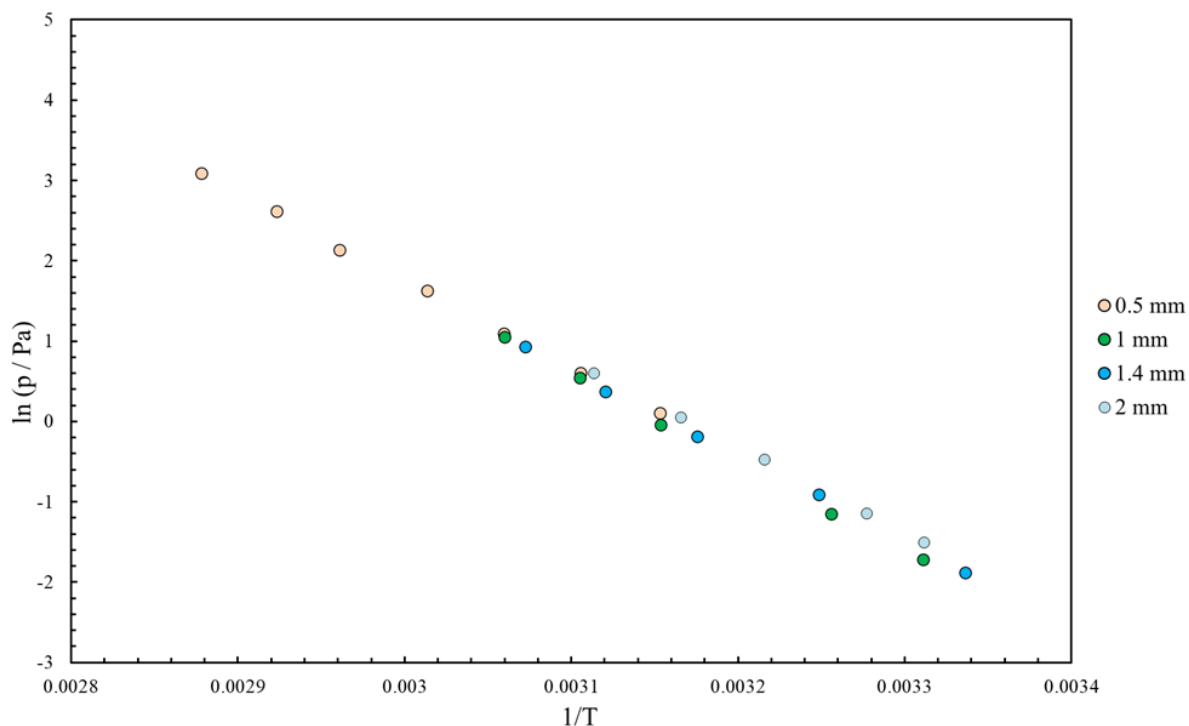


Figure 6.2.6 Results of Knudsen effusion test experiments with benzoic acid

The vapor pressures for benzoic acid measured with our new setup seem to agree well with the values from most of the available literature data. Two sources of observed literature data were excluded from overall comparison since they deviate from the most of data for more than 15-30% [230,231] The deviations are shown in Figure 6.2.7.

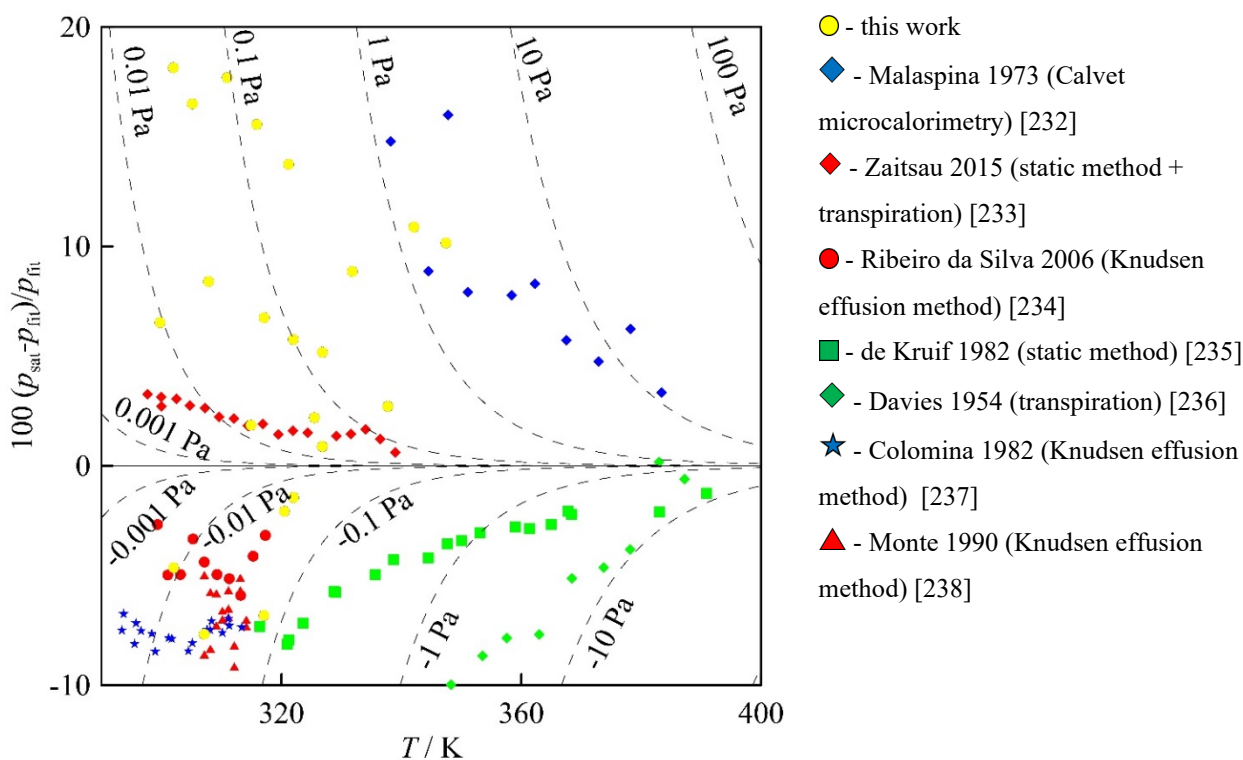


Figure 6.2.7 Deviation plot of experimental values from fitting equation for benzoic acid

The results have the best agreement with Zaitsau [233], Ribeiro da Silva [234], Monte [238], and Colomina [237]. The obtained data has slightly higher pressure values of the most of observed data and are on relatively the same level with Malaspina [232] in terms of deviations from the fitting equation.

6.3. Differential scanning calorimetry

In our research we measure standard molar enthalpies of fusion $\Delta_{\text{cr}}^{\text{l}}H_{\text{m}}^{\text{o}}$ with a conventional method – differential scanning calorimetry (DSC) [239]. The measurement is performed with commercial DSC devices Mettler Toledo 822e and Mettler 823e equipped with Huber TC125 series coolers.

To measure the enthalpy a small sample of approximately 10 mg is placed in the standard aluminium crucible with pin of 40 μl volume. The weighing of 10 mg of the substance is made in high precision microbalances (Sartorius MSE3.6P-000-DM) with the standard uncertainty of $5 \cdot 10^{-6}$ g. For substances with melting point exceeding approximately 200° C we pierce the crucible to avoid the crucible disruption due to high pressures arising inside of it.

For every sample we develop an individual heating and cooling program. This is explained not only by the different melting temperatures but also by the behaviour of the crystals, in particular their formation. Sometimes the difficulty in crystallization is exacerbated with several crystalline phases formation that requires a tedious and a scrupulous tweaking of the heating and cooling program.

The most general case of the temperature program is a cycle of heating of the sample with a heating rate of 10 K/min up to a temperature that is higher for about 30-40 K than the melting temperature of a studied substance. After that the sample is cooled down until crystallization with the cooling rate of 10 K/min. The cycle is repeated at least 5 times to deliver reasonable and reproducible data, and to check whether the substance has not decomposed. The first cycle is not considered since at the first run the substance not melted yet and hence not having a full thermal contact with the crucible.

The DSC devices were calibrated and checked with melting behaviour of indium, gallium, lead, and octane samples that are usually used as references in differential-scanning calorimetry. The double standard deviation of the enthalpy of fusion in the test measurements was $\pm 0.3 \text{ kJ}\cdot\text{mol}^{-1}$ and 0.3 K for the melting temperature. The uncertainties of the enthalpies of fusion include uncertainties from fusion experiment itself and from calibration. The transition temperatures were evaluated as the onset temperature of observed transition adjusted to the zero-heating rate.

Thermochemical calculations are commonly performed at the reference temperature $T = 298.15 \text{ K}$. The adjustment of the fusion enthalpy is made with the aid of the equation below [240]:

$$\Delta_{\text{cr}}^{\text{l}}H_{\text{m}}^{\circ}(298.15 \text{ K}) = \Delta_{\text{cr}}^{\text{l}}H_{\text{m}}^{\circ}(T_{\text{fus}}) - (\Delta_{\text{cr}}^{\text{g}}C_{\text{p,m}}^{\circ} - \Delta_{\text{l}}^{\text{g}}C_{\text{p,m}}^{\circ}) \cdot [(T_{\text{fus}}) - 298.15 \text{ K}] \quad (6.3.1)$$

where $\Delta_{\text{cr}}^{\text{g}}C_{\text{p,m}}^{\circ}$ and $\Delta_{\text{l}}^{\text{g}}C_{\text{p,m}}^{\circ}$ are the difference of the molar heat capacities of a studied substance of the gas and the crystal or liquid phases respectively. Uncertainties in the temperature adjustment are estimated to contribute approximately 30% to the total adjustment [241].

6.4. Computational methods

The contribution of the dispersion interactions in the stability of studied compounds can be evaluated as difference in total energy of the molecules optimized at B3LYP/cc-tzvp level of theory with and without D3 dispersion correction from Grimme [9,10] with Becke and Johnson damping) [242]. The most important challenging task in the theoretical study of molecular or ionic compounds with long side alkyl chains is to correctly establish the conformational ensemble. We applied Conformer Rotamer Ensemble Sampling Tool (CREST) by Grimme [191] utilizing GFN2-xtb method [243,244] for tight optimization of found conformers and evaluation of relative total energy. The complete evaluation of the dispersive energy for whole ensemble of conformers is time and resource consuming. Therefore, to the energies of GFN2-xtb method were used for evaluation of the enthalpy correction of the conformational ensemble at 298 K. The closest by the corrected energy conformer was chosen as representative for evaluation of the dispersive contribution.

7. References

- [1] T. Schwabe, S. Grimme, Double-hybrid density functionals with long-range dispersion corrections: higher accuracy and extended applicability, *Physical Chemistry Chemical Physics*. 9 (2007) 3397–3406. <https://doi.org/10.1039/B704725H>.
- [2] S. Grimme, P.R. Schreiner, Steric crowding can stabilize a labile molecule: Solving the hexaphenylethane riddle, *Angewandte Chemie International Edition*. 50 (2011) 12639–12642. <https://doi.org/https://doi.org/10.1002/anie.201103615>.
- [3] N.O.B. Lüttschwager, W.N. Tobias, R.A. Mata, M.A. Suhm, The last globally stable extended alkane, *Angewandte Chemie International Edition*. 52 (2012) 463–466. <https://doi.org/10.1002/anie.201202894>.
- [4] S.P. Verevkin, D.H. Zaitsau, V. Emel'yanenko, V.A. Yermalayeu, C. Schick, H. Liu, E.J. Maginn, S. Bulut, I. Krossing, R. Kalb, V.N. Emel'yanenko, V.A. Yermalayeu, C. Schick, H. Liu, E.J. Maginn, S. Bulut, I. Krossing, R. Kalb, Making sense of enthalpy of vaporization trends for ionic liquids: new experimental and simulation data show a simple linear relationship and help reconcile previous data., *The Journal of Physical Chemistry B*. 117 (2013) 6473–6486. <https://doi.org/10.1021/jp311429r>.
- [5] J. Chickos, T. Wang, E. Sharma, Hypothetical thermodynamic properties: Vapor pressures and vaporization enthalpies of the even n-alkanes from C40 to C76 at T = 298.15 K by correlation-gas chromatography. Are the vaporization enthalpies a linear function of carbon number?, *Journal of Chemical and Engineering Data*. 53 (2008) 481–491. <https://doi.org/10.1021/je7005852>.
- [6] J.P. Wagner, P.R. Schreiner, London dispersion in molecular chemistry — reconsidering steric effects, *Angewandte Chemie International Edition*. 54 (2015) 12274–12296. <https://doi.org/https://doi.org/10.1002/anie.201503476>.
- [7] R. Ludwig, The effect of dispersion forces on the interaction energies and far infrared spectra of protic ionic liquids, *Physical Chemistry Chemical Physics*. 17 (2015) 13790–13793. <https://doi.org/10.1039/C5CP00885A>.
- [8] D.H. Zaitsau, R. Ludwig, S.P. Verevkin, Determination of the dispersion forces in the gas phase structures of ionic liquids using exclusively thermodynamic methods, *Physical Chemistry Chemical Physics*. 23 (2021) 7398–7406. <https://doi.org/10.1039/D0CP05439A>.

- [9] S. Grimme, A. Hansen, J.G. Brandenburg, C. Bannwarth, Dispersion-corrected mean-field electronic structure methods, *Chemical Reviews*. 116 (2016) 5105–5154. <https://doi.org/10.1021/acs.chemrev.5b00533>.
- [10] F. Weigend, R. Ahlrichs, Balanced basis sets of split valence, triple zeta valence and quadruple zeta valence quality for H to Rn: Design and assessment of accuracy, *Physical Chemistry Chemical Physics*. 7 (2005) 3297–3305. <https://doi.org/10.1039/B508541A>.
- [11] V.N. Emel'yanenko, P. Stange, J. Feder-Kubis, S.P. Verevkin, R. Ludwig, Dissecting intermolecular interactions in the condensed phase of ibuprofen and related compounds: The specific role and quantification of hydrogen bonding and dispersion forces, *Physical Chemistry Chemical Physics*. 22 (2020) 4896–4904. <https://doi.org/10.1039/c9cp06641a>.
- [12] W. V. Steele, R.D. Chirico, S.E. Knipmeyer, A. Nguyen, N.K. Smith, I.R. Tasker, Thermodynamic properties and ideal-gas enthalpies of formation for cyclohexene, phthalan (2,5-dihydrobenzo-3,4-furan), isoxazole, octylamine, dioctylamine, trioctylamine, phenyl isocyanate, and 1,4,5,6-tetrahydropyrimidine, *Journal of Chemical & Engineering Data*. 41 (1996) 1269–1284. <https://doi.org/10.1021/je960093t>.
- [13] N. Nichols, I. Wadsö, Thermochemistry of solutions of biochemical model compounds 3. Some benzene derivatives in aqueous solution, *The Journal of Chemical Thermodynamics*. 7 (1975) 329–336. [https://doi.org/10.1016/0021-9614\(75\)90169-X](https://doi.org/10.1016/0021-9614(75)90169-X).
- [14] G.L. Hall, W.E. Whitehead, C.R. Mourer, T. Shibamoto, A new gas chromatographic retention index for pesticides and related compounds, *Journal of High Resolution Chromatography*. 9 (1986) 266–271. <https://doi.org/10.1002/JHRC.1240090503>.
- [15] NIST Chemistry WebBook, (2021). <https://webbook.nist.gov/>.
- [16] J.S. Chickos, S. Hosseini, D.G. Hesse, J.F. Liebman, Heat capacity corrections to a standard state: a comparison of new and some literature methods for organic liquids and solids, *Structural Chemistry* 1993 4:4. 4 (1993) 271–278. <https://doi.org/10.1007/BF00673701>.
- [17] E.C.W. Clarke, D.N. Glew, Evaluation of thermodynamic functions from equilibrium constants, *Trans. Faraday Soc.* 62 (1966) 539–547. <https://doi.org/10.1039/TF9666200539>.
- [18] W. Acree, J.S. Chickos, Phase Transition Enthalpy Measurements of Organic and Organometallic Compounds. Sublimation, Vaporization and Fusion Enthalpies From 1880 to 2015. Part 1. C1-C10, *Journal of Physical and Chemical Reference Data*. 45 (2016) 33101. <https://doi.org/10.1063/1.4948363>.

- [19] M. Ducros, J.F. Gruson, H. Sannier, Estimation des enthalpies de vaporisation des composés organiques liquides. Partie 1. Applications aux alcanes, cycloalcanes, alcènes, hydrocarbures benzeniques, alcools, alcanes thiols, chloro et bromoalcanes, nitriles, esters, acides et aldéhydes., *Thermochimica Acta*. 36 (1980) 39–65. [https://doi.org/10.1016/0040-6031\(80\)80109-2](https://doi.org/10.1016/0040-6031(80)80109-2).
- [20] M. Ducros, J.F. Gruson, H. Sannier, I. Velasco, Estimation des enthalpies de vaporisation des composés organiques liquides. Partie 2. Applications aux éthersoxydes, thioalcanes, cétones et amines, *Thermochimica Acta*. 44 (1981) 131–140. [https://doi.org/10.1016/0040-6031\(81\)80035-4](https://doi.org/10.1016/0040-6031(81)80035-4).
- [21] S.P. Verevkin, V.N. Emel'yanenko, V. Diky, C.D. Muzny, R.D. Chirico, M. Frenkel, New group-contribution approach to thermochemical properties of organic compounds: hydrocarbons and oxygen-containing compounds, *Journal of Physical and Chemical Reference Data*. 42 (2013) 33102. <https://doi.org/10.1063/1.4815957>.
- [22] A.A. Efimova, V.N. Emel'yanenko, S.P. Verevkin, Y. Chernyak, Vapour pressure and enthalpy of vaporization of aliphatic poly-amines, *The Journal of Chemical Thermodynamics*. 42 (2010) 330–336. <https://doi.org/10.1016/J.JCT.2009.09.003>.
- [23] S.P. Verevkin, Y. Chernyak, Vapor pressure and enthalpy of vaporization of aliphatic propanediamines, *The Journal of Chemical Thermodynamics*. 47 (2012) 328–334. <https://doi.org/https://doi.org/10.1016/j.jct.2011.11.004>.
- [24] W. V. Steele, The standard enthalpies of formation of the triphenyl compounds of the Group V elements 1. Triphenylamine and the Ph-N bond-dissociation energy, *The Journal of Chemical Thermodynamics*. 10 (1978) 441–444. [https://doi.org/10.1016/0021-9614\(78\)90091-5](https://doi.org/10.1016/0021-9614(78)90091-5).
- [25] M. V. Forward, S.T. Bowden, W.J. Jones, S 26. Physical properties of triphenyl compounds of group VB elements, *Journal of the Chemical Society (Resumed)*. (1949) S121–S126.
- [26] D. Lipkind, C. Plienrasri, J.S. Chickos, A Study of the Vaporization Enthalpies of Some 1-Substituted Imidazoles and Pyrazoles by Correlation-Gas Chromatography, *The Journal of Physical Chemistry B*. 114 (2010) 16959–16967. <https://doi.org/10.1021/jp1090334>.
- [27] C. Gobble, J. Vikman, J.S. Chickos, Evaluation of the Vaporization Enthalpies and Liquid Vapor Pressures of (R)-Deprenyl, (S)-Benzphetamine, Alverine, and a Series of Aliphatic Tertiary Amines by Correlation Gas Chromatography at T/K = 298.15, *Journal of Chemical and Engineering Data*. 59 (2014) 2551–2562. <https://doi.org/10.1021/JE500358R>.

- [28] S.P. Verevkin, A.Yu. Sazonova, V.N. Emel'yanenko, D.H. Zaitsau, M.A. Varfolomeev, B.N. Solomonov, K.V. Zherikova, Thermochemistry of Halogen-Substituted Methylbenzenes, *Journal of Chemical and Engineering Data*. 60 (2015) 89–103. <https://doi.org/10.1021/JE500784S>.
- [29] V.N. Emel'yanenko, S.P. Verevkin, Benchmark thermodynamic properties of 1,3-propanediol: Comprehensive experimental and theoretical study, *The Journal of Chemical Thermodynamics*. 85 (2015) 111–119. <https://doi.org/10.1016/j.jct.2015.01.014>.
- [30] W.E. Acree, Thermodynamic properties of organic compounds: Part 4. First update of enthalpy of fusion and melting point temperature compilation, *Thermochimica Acta*. 219 (1993) 97–104. [https://doi.org/10.1016/0040-6031\(93\)80486-T](https://doi.org/10.1016/0040-6031(93)80486-T).
- [31] E.L. Krasnykh, S.P. Verevkin, B. Koutek, J. Doubisky, Vapour pressures and enthalpies of vaporization of a series of the linear n-alkyl acetates, *The Journal of Chemical Thermodynamics*. 38 (2006) 717–723. <https://doi.org/10.1016/J.JCT.2005.08.003>.
- [32] V.N. Emel'yanenko, S.P. Verevkin, B. Koutek, J. Doubisky, Vapour pressures and enthalpies of vapourization of a series of the linear aliphatic nitriles, *The Journal of Chemical Thermodynamics*. 37 (2005) 73–81. <https://doi.org/10.1016/J.JCT.2004.08.004>.
- [33] E. Kováts, Gas-chromatographische Charakterisierung organischer Verbindungen. Teil 1: Retentionsindices aliphatischer Halogenide, Alkohole, Aldehyde und Ketone, *Helvetica Chimica Acta*. 41 (1958) 1915–1932. <https://doi.org/10.1002/HLCA.19580410703>.
- [34] C.T. Peng, S.F. Ding, R.L. Hua, Z.C. Yang, Prediction of retention indexes : I. Structure—retention index relationship on apolar columns, *Journal of Chromatography A*. 436 (1988) 137–172. [https://doi.org/10.1016/S0021-9673\(00\)94575-8](https://doi.org/10.1016/S0021-9673(00)94575-8).
- [35] V.N. Emel'yanenko, A.A. Pimerzin, V. V. Turovtsev, S.P. Verevkin, Benchmark Thermochemistry of N-Methylaniline, *Journal of Physical Chemistry A*. 119 (2015) 2142–2152. <https://doi.org/10.1021/JP5129854>.
- [36] V.N. Emel'yanenko, S.P. Verevkin, Enthalpies of formation and substituent effects of ortho-, meta-, and para-aminotoluenes from thermochemical measurements and from ab initio calculations, *The Journal of Physical Chemistry A*. 109 (2005) 3960–3966. <https://doi.org/10.1021/jp045450i>.
- [37] S.P. Verevkin, Thermochemistry of amines: experimental standard molar enthalpies of formation of some aliphatic and aromatic amines, *The Journal of Chemical Thermodynamics*. 29 (1997) 891–899. <https://doi.org/10.1006/JCHT.1997.0212>.

- [38] R.M. Stephenson, S. Malanowski, *Handbook of the Thermodynamics of Organic Compounds*, Springer Netherlands, 1987. <https://doi.org/10.1007/978-94-009-3173-2>.
- [39] A.O. Surov, G.L. Perlovich, V.N. Emel'yanenko, S.P. Verevkin, Thermochemistry of Drugs. Experimental and First-Principles Study of Fenamates, *Journal of Chemical & Engineering Data*. 56 (2011) 4325–4332. <https://doi.org/10.1021/je200128y>.
- [40] V. Majer, V. Svoboda, *Enthalpies of vaporization of organic compounds: a critical review and data compilation*, United Kingdom, 1986.
- [41] F. Xu, L.X. Sun, Z.C. Tan, J.G. Liang, R.L. Li, Thermodynamic study of ibuprofen by adiabatic calorimetry and thermal analysis, *Thermochimica Acta*. 412 (2004) 33–57. <https://doi.org/10.1016/J.TCA.2003.08.021>.
- [42] F. Espitalier, B. Biscans, P.S. Peyrigain, C. Laguérie, Ternary diagram: alpha-(3-benzoylphenyl)-propionic acid (ketoprofen) in acetone-water mixtures at different temperatures. Experimental data and predicted results, *Fluid Phase Equilibria*. 113 (1995) 151–171. [https://doi.org/10.1016/0378-3812\(95\)02806-8](https://doi.org/10.1016/0378-3812(95)02806-8).
- [43] R. Soto, M. Svärd, V. Verma, L. Padrela, K. Ryan, Å.C. Rasmuson, Solubility and thermodynamic analysis of ketoprofen in organic solvents, *International Journal of Pharmaceutics*. 588 (2020) 119686. <https://doi.org/10.1016/J.IJPHARM.2020.119686>.
- [44] H. Buchholz, V.N. Emel'yanenko, H. Lorenz, S.P. Verevkin, An Examination of the Phase Transition Thermodynamics of (S)- and (RS)-Naproxen as a Basis for the Design of Enantioselective Crystallization Processes, *Journal of Pharmaceutical Sciences*. 105 (2016) 1676–1683. <https://doi.org/10.1016/J.XPHS.2016.02.032>.
- [45] S.P. Verevkin, M.E. Konnova, V.N. Emel'yanenko, A.A. Pimerzin, Weaving a web of reliable thermochemistry around lignin building blocks: Vanillin and its isomers, *The Journal of Chemical Thermodynamics*. 157 (2021) 106362. <https://doi.org/10.1016/J.JCT.2020.106362>.
- [46] S. P. Verevkin, V. V. Turovtsev, I. V. Andreeva, Y. D. Orlov, A. A. Pimerzin, Webbing a network of reliable thermochemistry around lignin building blocks: tri-methoxy-benzenes, *RSC Advances*. 11 (2021) 10727–10737. <https://doi.org/10.1039/D1RA00690H>.
- [47] V.N. Emel'yanenko, D.H. Zaitsau, A.A. Pimerzin, S.P. Verevkin, Benchmark properties of diphenyl oxide as a potential liquid organic hydrogen carrier: Evaluation of thermochemical data with complementary experimental and computational methods, *The Journal of Chemical Thermodynamics*. 125 (2018) 149–158. <https://doi.org/10.1016/J.JCT.2018.05.021>.

- [48] C.G. de Kruif, J.C. van Miltenburg, J.G. Blok, Molar heat capacities and vapour pressures of solid and liquid benzophenone, *The Journal of Chemical Thermodynamics*. 15 (1983) 129–136. [https://doi.org/10.1016/0021-9614\(83\)90151-9](https://doi.org/10.1016/0021-9614(83)90151-9).
- [49] V. Štejska, M. Fulem, K. Růžička, P. Morávek, New static apparatus for vapor pressure measurements: Reconciled thermophysical data for benzophenone, *Journal of Chemical & Engineering Data*. 61 (2016) 3627–3639. <https://doi.org/10.1021/acs.jced.6b00523>.
- [50] W.V. Steele, R.D. Chirico, A. Nguyen, I.A. Hossenlopp, N.K. Smith, Determination of ideal-gas enthalpies of formation for key compounds, *AIChE Symp. Ser.* 86 (1990) 138–154.
- [51] S.P. Verevkin, Thermochemistry of aromatic ketones. Experimental enthalpies of formation and structural effects, *Thermochimica Acta*. 310 (1998) 229–235. [https://doi.org/10.1016/S0040-6031\(97\)00231-1](https://doi.org/10.1016/S0040-6031(97)00231-1).
- [52] D.H. Zaitsau, V.N. Emel'yanenko, P. Stange, S.P. Verevkin, R. Ludwig, Dissecting the vaporization enthalpies of ionic liquids by exclusively experimental methods: Coulomb interaction, hydrogen bonding, and dispersion forces, *Angewandte Chemie International Edition*. 58 (2019) 8589–8592. <https://doi.org/10.1002/anie.201904813>.
- [53] M. Colomina, M. V. Roux, C. Turrión, Thermochemical properties of naphthalene compounds IV. Enthalpies of combustion and formation of 2-methoxynaphthalene, 2-ethoxynaphthalene, and 2,3- and 2,7-dihydroxynaphthalenes, *The Journal of Chemical Thermodynamics*. 8 (1976) 869–872. [https://doi.org/10.1016/0021-9614\(76\)90164-6](https://doi.org/10.1016/0021-9614(76)90164-6).
- [54] R. Maxwell, J. Chickos, An Examination of the Thermodynamics of Fusion, Vaporization, and Sublimation of Ibuprofen and Naproxen by Correlation Gas Chromatography, *Journal of Pharmaceutical Sciences*. 101 (2012) 805–814. <https://doi.org/10.1002/JPS.22803>.
- [55] D. Kulikov, S.P. Verevkin, A. Heintz, Enthalpies of vaporization of a series of aliphatic alcohols: Experimental results and values predicted by the ERAS-model., *Fluid Phase Equilibria*. 192 (2001) 187–207. [https://doi.org/10.1016/S0378-3812\(01\)00633-1](https://doi.org/10.1016/S0378-3812(01)00633-1).
- [56] H.C. Brown, G.K. Barbaras, H.L. Berneis, W. Hallam Bonner, R.B. Johannesen, M. Grayson, K. LeRoi Nelson, Strained homomorphs. 14. General summary, *Journal of the American Chemical Society*. 75 (1953) 1–6. <https://doi.org/10.1021/ja01097a001>.
- [57] R. Ludwig, The effect of hydrogen bonding on the thermodynamic and spectroscopic properties of molecular clusters and liquids, *Physical Chemistry Chemical Physics*. 4 (2002) 5481–5487. <https://doi.org/10.1039/B207000F>.

- [58] R. Ludwig, F. Weinhold, T.C. Farrar, Quantum cluster equilibrium theory of liquids: molecular clusters and thermodynamics of liquid ethanol, *Molecular Physics*. 97 (1999) 465–477. <https://doi.org/10.1080/00268979909482847>.
- [59] R. Ludwig, F. Weinhold, T.C. Farrar, Structure of liquid N-methylacetamide: Temperature dependence of NMR chemical shifts and quadrupole coupling constants, *Journal of Physical Chemistry A*. 101 (1997) 8861–8870. <https://doi.org/10.1021/jp971360k>.
- [60] R. Ludwig, F. Weinhold, T.C. Farrar, Theoretical study of hydrogen bonding in liquid and gaseous N-methylformamide, *The Journal of Chemical Physics*. 107 (1997) 499–507. <https://doi.org/10.1063/1.474411>.
- [61] R. Ludwig, O. Reis, R. Winter, F. Weinhold, T.C. Farrar, Quantum cluster equilibrium theory of liquids: Temperature dependence of hydrogen bonding in liquid N-methylacetamide studied by IR spectra, *Journal of Physical Chemistry B*. 102 (1998) 9312–9318. <https://doi.org/10.1021/jp971575u>.
- [62] R. Ludwig, F. Weinhold, T.C. Farrar, Quantum cluster equilibrium theory of liquids part I: Molecular clusters and thermodynamics of liquid ammonia, *Berichte Der Bunsengesellschaft/Physical Chemistry Chemical Physics*. 102 (1998). <https://doi.org/10.1002/bbpc.19981020210>.
- [63] R. Ludwig, The structure of liquid methanol, *ChemPhysChem*. 6 (2005) 1369–1375. <https://doi.org/10.1002/cphc.200400663>.
- [64] R. Ludwig, F. Weinhold, Quantum cluster equilibrium theory of liquids: Freezing of QCE/3-21G water to tetrakaidecahedral “Bucky-ice,” *The Journal of Chemical Physics*. 110 (1998) 508–515. <https://doi.org/10.1063/1.478136>.
- [65] G.L. Perlovich, S.V. Kurkov, L.K. Hansen, A. Bauer-Brandl, Thermodynamics of sublimation, crystal lattice energies, and crystal structures of racemates and enantiomers: (+)- and (±)-ibuprofen, *Journal of Pharmaceutical Sciences*. 93 (2004) 654–666. <https://doi.org/https://doi.org/10.1002/jps.10586>.
- [66] K. S. Pitzer, E. Catalano, Electronic correlation in molecules. III. The paraffin hydrocarbons, *Journal of the American Chemical Society*. 78 (1956) 4844–4846. <https://doi.org/10.1021/ja01600a006>.
- [67] M.D. Wodrich, C.S. Wannere, Y. Mo, P.D. Jarowski, K.N. Houk, P. von R. Schleyer, The concept of protobranching and its many paradigm shifting implications for energy evaluations,

Chemistry – A European Journal. 13 (2007) 7731–7744.
<https://doi.org/https://doi.org/10.1002/chem.200700602>.

- [68] J.B. Pedley, R.D. Naylor, S.P. Kirby, J.B. Pedley, Thermochemical data of organic compounds., 2nd ed., Chapman & Hall, London, 1986.
- [69] S. Gronert, The folly of protobranching: Turning repulsive interactions into attractive ones and rewriting the strain/stabilization energies of organic chemistry, *Chemistry – A European Journal*. 15 (2009) 5372–5382. <https://doi.org/https://doi.org/10.1002/chem.200800282>.
- [70] S. P. Verevkin, M. Nölke, H.-D. Beckhaus, C. Rüchardt, Enthalpies of formation of hexaethylethane, octamethylhexane, and tri-tert-butylmethane. Extremely strained hydrocarbons, *The Journal of Organic Chemistry*. 62 (1997) 4683–4686. <https://doi.org/10.1021/jo9702002>.
- [71] M.A. Flamm-Ter Meer, H.-D. Beckhaus, C. Rüchardt, Thermolabile kohlenwasserstoffe. XXVI. Bildungsenthalpie von 1,1,2,2-tetra-tert-butylethan [Thermolabile hydrocarbons. XXVI. Formation enthalpies of 1,1,2,2-tetra-tert-butylethan], *Thermochimica Acta*. 80 (1984) 81–89. [https://doi.org/https://doi.org/10.1016/0040-6031\(84\)87185-3](https://doi.org/https://doi.org/10.1016/0040-6031(84)87185-3).
- [72] A. Baeyer, Ueber Polyacetylenverbindungen [About polyacetylene compounds], *Berichte Der Deutschen Chemischen Gesellschaft*. 18 (1885) 2269–2281. <https://doi.org/https://doi.org/10.1002/cber.18850180296>.
- [73] P. von R. Schleyer, J.E. Williams, Blanchard K. R., Evaluation of strain in hydrocarbons. The strain in adamantane and its origin, *Journal of the American Chemical Society*. 92 (1970) 2377–2386. <https://doi.org/10.1021/ja00711a030>.
- [74] A. Greenberg, J.F. Liebman, Strained Organic Molecules, 1st ed., Academic Press Inc. (London) Ltd., London, 1978.
- [75] S.W. Benson, Thermochemical kinetics: methods for the estimation of thermochemical data and rate parameters, Wiley, New York, 1976.
- [76] H.-D. Beckhaus, Anwendung von Kraftfeldrechnungen, IV. Ein Kraftfeld für die Berechnung von Struktur und Bildungsenthalpie von Alkylbenzolen und sein Verlässlichkeitstest an hochgespannten Diphenylethanen, *Chemische Berichte*. 116 (1983) 86–96. <https://doi.org/https://doi.org/10.1002/cber.19831160110>.
- [77] C.F.R.A.C. Lima, C.A.D. Sousa, J.E. Rodriguez-Borges, A. Melo, L.R. Gomes, J.N. Low, L.M.N.B.F. Santos, The role of aromatic interactions in the structure and energetics of benzyl

- ketones, *Physical Chemistry Chemical Physics*. 12 (2010) 11228–11237. <https://doi.org/10.1039/C003941A>.
- [78] S.P. Verevkin, Thermochemistry of alcohols: Experimental standard molar enthalpies of formation and strain of some alkyl and phenyl congested alcohols, *Structural Chemistry*. 9 (1998) 375–382. <https://doi.org/10.1023/A:1022471228499>.
- [79] K. Sasse, J. N'guimbi, J. Jose, J.C. Merlin, Tension de vapeur d'hydrocarbures polyaromatiques dans le domaine 10⁻³–10 Torr, *Thermochimica Acta*. 146 (1989) 53–61. [https://doi.org/10.1016/0040-6031\(89\)87075-3](https://doi.org/10.1016/0040-6031(89)87075-3).
- [80] S.P. Verevkin, Thermochemistry of substituted benzenes. Experimental standard molar enthalpies of formation of o-,m-, and p-terphenyls and 1,3,5-triphenylbenzene, *The Journal of Chemical Thermodynamics*. 29 (1997) 1495–1501. <https://doi.org/10.1006/jcht.1997.0265>.
- [81] B.N. Solomonov, M.A. Varfolomeev, R.N. Nagrimanov, V.B. Novikov, D.H. Zaitsau, S.P. Verevkin, Solution calorimetry as a complementary tool for the determination of enthalpies of vaporization and sublimation of low volatile compounds at 298.15 K, *Thermochimica Acta*. 589 (2014) 164–173. <https://doi.org/10.1016/j.tca.2014.05.033>.
- [82] F.W. Reiter, H. Kind, R. Nehren, ChemInform Abstract: Dampfdruckuntersuchungen an polyphenylen und polyphenylmischungen, *Chemischer Informationsdienst. Organische Chemie*. 1 (1970) 470–475. <https://doi.org/10.1002/chin.197033162>.
- [83] M.A.V. Ribeiro da Silva, L.M.N.B.F. Santos, L.M.S.S. Lima, Standard molar enthalpies of formation and of sublimation of the terphenyl isomers, *Journal of Chemical Thermodynamics*. 40 (2008) 166–173. <https://doi.org/10.1016/j.jct.2007.08.008>.
- [84] M.A.V. Ribeiro da Silva, L.M.N.B.F. Santos, L.M.S.S. Lima, Thermodynamic study of 1,2,3-triphenylbenzene and 1,3,5-triphenylbenzene, *Journal of Chemical Thermodynamics*. 42 (2010) 134–139. <https://doi.org/10.1016/j.jct.2009.07.022>.
- [85] C.F.R.A.C. Lima, M.A.A. Rocha, A. Melo, L.R. Gomes, J.N. Low, L.M.N.B.F. Santos, Structural and thermodynamic characterization of polyphenylbenzenes, *Journal of Physical Chemistry A*. 115 (2011) 11876–11888. <https://doi.org/10.1021/jp207593s>.
- [86] C.F.R.A.C. Lima, A.S.M.C. Rodrigues, L.M.N.B.F. Santos, Effect of confined hindrance in polyphenylbenzenes, *Journal of Physical Chemistry A*. 121 (2017) 2475–2481. <https://doi.org/10.1021/acs.jpca.7b00579>.

- [87] I.B. Johns, E.A. McElhill, J.O. Smith, Thermal Stability of Some Organic Compounds, *Journal of Chemical and Engineering Data*. 7 (1962) 277–281. <https://doi.org/10.1021/je60013a036>.
- [88] K.E. Maly, E. Gagnon, J.D. Wuest, Engineering molecular crystals with abnormally weak cohesion, *Chemical Communications*. 47 (2011) 5163–5165. <https://doi.org/10.1039/c1cc10866b>.
- [89] C.F.R.A.C. Lima, M.A.A. Rocha, B. Schröder, L.R. Gomes, J.N. Low, L.M.N.B.F. Santos, Phenyl naphthalenes: Sublimation equilibrium, conjugation, and aromatic interactions, *Journal of Physical Chemistry B*. 116 (2012) 3557–3570. <https://doi.org/10.1021/jp2111378>.
- [90] A.A. Balepin, V.P. Lebedev, E.A. Miroshnichenko, G.I. Koldobskii, V.A. Ostovskii, B.P. Larionov, B.V. Gidasov, Y.A. Lebedev, Energy effects in polyphenylenes and phenyltetrazoles, *Svoistva Veshchestv Str. Mol.* (1977) 93–98.
- [91] D.H. Zaitsau, Private communication, (2021).
- [92] W. Hanshaw, M. Nutt, J.S. Chickos, Hypothetical thermodynamic properties. subcooled vaporization enthalpies and vapor pressures of polyaromatic hydrocarbons, *Journal of Chemical and Engineering Data*. 53 (2008) 1903–1913. <https://doi.org/10.1021/je800300x>.
- [93] K. Nass, D. Lenoir, A. Kettrup, Calculation of the Thermodynamic Properties of Polycyclic Aromatic Hydrocarbons by an Incremental Procedure, *Angewandte Chemie International Edition in English*. 34 (1995) 1735–1736. <https://doi.org/10.1002/anie.199517351>.
- [94] M.A.A. Rocha, C.F.R.A.C. Lima, L.M.N.B.F. Santos, Phase transition thermodynamics of phenyl and biphenyl naphthalenes, *Journal of Chemical Thermodynamics*. 40 (2008) 1458–1463. <https://doi.org/10.1016/j.jct.2008.04.010>.
- [95] R.D. Chirico, W. V. Steele, A.F. Kazakov, Thermodynamic properties of 1-phenyl naphthalene and 2-phenyl naphthalene, *Journal of Chemical Thermodynamics*. 73 (2014) 241–254. <https://doi.org/10.1016/j.jct.2014.01.006>.
- [96] I. Mokbel, T. Guetachew, J. Jose, Vapor pressures and sublimation pressures of 14 polycyclic aromatic hydrocarbons (C₁₁-C₁₈) at pressures in the range from 0.5 Pa to 30 kPa, *ELDATA: Int. Electron. J. Phys.-Chem. Data*. 2 (1995) 167–180.
- [97] V.P. Klochkov, Davlenie nasyschennyh parov nekotoryh aromaticeskikh soedinenii, *Zh. Fiz. Khim.* 32 (1958) 1177–1181.
- [98] C.-F. Shieh, N.W. Gregory, Vaporization characteristics of 9-phenylanthracene, *Journal of Chemical and Engineering Data*. 19 (1974) 11–14.

- [99] B. Stevens, Vapour pressures and the heats of sublimation of anthracene and of 9:10-diphenylanthracene, *Journal of the Chemical Society (Resumed)*. (1953) 2973–2974. <https://doi.org/10.1039/jr9530002973>.
- [100] H. Hoyer, W. Peperle, Dampfdruckmessungen an organischen Substanzen und ihre Sublimationswärmen, *Zeitschrift Für Elektrochemie, Berichte Der Bunsengesellschaft Für Physikalische Chemie*. 62 (1958) 61–66.
- [101] C.F.R.A.C. Lima, J.C.S. Costa, L.M.S.S. Lima, A. Melo, A.M.S. Silva, L.M.N.B.F. Santos, Energetic and Structural Insights into the Molecular and Supramolecular Properties of Rubrene, *ChemistrySelect*. 2 (2017) 1759–1769. <https://doi.org/10.1002/SLCT.201601636>.
- [102] G.W. Smith, Phase behavior of some linear polyphenyls., *Molecular Crystals and Liquid Crystals*. 49 (Letters) (1979) 207–209. <https://doi.org/10.1080/00268947908070413>.
- [103] J. Wąsicki, M. Radomska, R. Radomski, Heat capacities of diphenyl, p-terphenyl and p-quaterphenyl from 180 K to their melting points, *Journal of Thermal Analysis*. 25 (1982) 509–514. <https://doi.org/10.1007/BF01912976>.
- [104] S.S. Chang, Heat capacity and thermodynamic properties of p-terphenyl: Study of order-disorder transition by automated high-resolution adiabatic calorimetry, *The Journal of Chemical Physics*. 79 (1983) 6229–6236. <https://doi.org/10.1063/1.445727>.
- [105] K. Saito, T. Atake, H. Chihara, Thermodynamic Studies on Order-Disorder Phase Transitions of p-Terphenyl and p-Terphenyl-d₁₄, *Bulletin of the Chemical Society of Japan*. 61 (1988) 2327–2336. <https://doi.org/10.1246/bcsj.61.2327>.
- [106] A.S.M.C. Rodrigues, M.A.A. Rocha, L.M.N.B.F. Santos, Isomerization effect on the heat capacities and phase behavior of oligophenyls isomers series, *Journal of Chemical Thermodynamics*. 63 (2013) 78–83. <https://doi.org/10.1016/j.jct.2013.03.026>.
- [107] M.I. Yagofarov, R.N. Nagrimanov, M.A. Ziganshin, B.N. Solomonov, New aspects of relationship between the enthalpies of fusion of aromatic compounds at the melting temperature and the enthalpies of solution in benzene at 298.15 K. Part II, *Journal of Chemical Thermodynamics*. 120 (2018) 21–26. <https://doi.org/10.1016/j.jct.2017.12.022>.
- [108] H. Kambe, I. Mita, R. Yokata, *Thermal Analysis, Volume 3*, in: *Proceedings Third ICTAC, Davos, 1971*: pp. 387–395.
- [109] L. Malaspina, G. Bardi, R. Gigli, Simultaneous determination by Knudsen-effusion microcalorimetric technique of the vapor pressure and enthalpy of vaporization of pyrene and

- 1,3,5-triphenylbenzene, *The Journal of Chemical Thermodynamics*. 6 (1974) 1053–1064. [https://doi.org/10.1016/0021-9614\(74\)90067-6](https://doi.org/10.1016/0021-9614(74)90067-6).
- [110] M.I. Yagofarov, S.E. Lapuk, T.A. Mukhametzyanov, M.A. Ziganshin, C. Schick, B.N. Solomonov, Application of fast scanning calorimetry to the fusion thermochemistry of low-molecular-weight organic compounds: Fast-crystallizing m-terphenyl heat capacities in a deeply supercooled liquid state, *Thermochimica Acta*. 668 (2018) 96–102. <https://doi.org/10.1016/j.tca.2018.08.015>.
- [111] S.S. Chang, A.B. Bestul, Heat capacity and thermodynamic properties of o-terphenyl crystal, glass, and liquid, *The Journal of Chemical Physics*. 56 (1972) 503–516. <https://doi.org/10.1063/1.1676895>.
- [112] S.S.N. Murthy, A. Paikaray, N. Arya, Molecular relaxation and excess entropy in liquids and their connection to the structure of glass, *The Journal of Chemical Physics*. 102 (1995) 8213–8220. <https://doi.org/10.1063/1.469232>.
- [113] B.V. Lebedev, T.A. Bykova, N.N. Smirnova, T.G. Kulagina, Thermodynamics of phenylacetylene, its cyclotrimerization reaction and resulting 1,3,5-triphenylbenzene in the region 0–480K, *Zhurnal Obshchei Khimii*. 52 (1982) 2630–2636.
- [114] J.S. Chickos, W. Hanshaw, Vapor pressures and vaporization enthalpies of the n-alkanes from C 31 to C 38 at T = 298.15 K by correlation gas chromatography, *Journal of Chemical and Engineering Data*. 49 (2004) 620–630. <https://doi.org/10.1021/jc030236t>.
- [115] M.I. Yagofarov, S.E. Lapuk, T.A. Mukhametzyanov, M.A. Ziganshin, C. Schick, B.N. Solomonov, Thermochemical properties of 1,2,3,4-tetraphenylnaphthalene and 1,3,5-triphenylbenzene in crystalline and liquid states studied by solution and fast scanning calorimetry, *Journal of Molecular Liquids*. 278 (2019) 394–400. <https://doi.org/10.1016/j.molliq.2019.01.046>.
- [116] M.V. Roux, M. Temprado, J.S. Chickos, Y. Nagano, Critically evaluated thermochemical properties of polycyclic aromatic hydrocarbons, *Journal of Physical and Chemical Reference Data*. 37 (2008) 1855–1996. <https://doi.org/10.1063/1.2955570>.
- [117] C.F.R.A.C. Lima, J.E. Rodriguez-Borges, L.M.N.B.F. Santos, Exploring the selectivity of the Suzuki-Miyaura cross-coupling reaction in the synthesis of aryl naphthalenes, *Tetrahedron*. 67 (2011) 689–697. <https://doi.org/10.1016/j.tet.2010.11.081>.
- [118] <https://scifinder-n.cas.org/>, (2021).

- [119] K. Saito, T. Atake, H. Chihara, Molar heat capacity and thermodynamic properties of p-quaterphenyl, *The Journal of Chemical Thermodynamics*. 17 (1985) 539–548. [https://doi.org/10.1016/0021-9614\(85\)90053-9](https://doi.org/10.1016/0021-9614(85)90053-9).
- [120] V.A. Postnikov, M.S. Lyasnikova, A.A. Kulishov, V. V. Grebenev, O. V. Borshchev, Solubility and Crystal Growth of p-Quaterphenyl and Its Derivative with Trimethylsilyl Terminal Substituents, *Russian Journal of Physical Chemistry A*. 93 (2019) 1741–1746. <https://doi.org/10.1134/S0036024419090176>.
- [121] T.J. Dingemans, N.S. Murthy, E.T. Samulski, Javelin-, hockey stick-, and boomerang-shaped liquid crystals. Structural variations on p-quinquphenyl, *Journal of Physical Chemistry B*. 105 (2001) 8845–8860. <https://doi.org/10.1021/jp010869j>.
- [122] X. Lu, C. He, P. Liu, A.C. Griffin, Structures and properties of liquid-crystalline polymers based on laterally attached oligo p-phenylenes, *Journal of Polymer Science, Part A: Polymer Chemistry*. 43 (2005) 3394–3402. <https://doi.org/10.1002/pola.20841>.
- [123] P.G. Farrell, F. Shahidi, F. Casellato, C. Vecchi, A. Girelli, DSC studies of aromatic hydrocarbon picrates, *Thermochimica Acta*. 33 (1979) 275–280. [https://doi.org/10.1016/0040-6031\(79\)87051-3](https://doi.org/10.1016/0040-6031(79)87051-3).
- [124] D.N. Bolmatenkov, M.I. Yagofarov, T.A. Mukhametzyanov, M.A. Ziganshin, B.N. Solomonov, The fusion thermochemistry of rubrene and 9,10-diphenylanthracene between 298 and 650 K: Fast scanning and solution calorimetry, *Thermochimica Acta*. 693 (2020) 178778. <https://doi.org/10.1016/j.tca.2020.178778>.
- [125] L.M.N.B.F. Santos, M.A.A. Rocha, A.S.M.C. Rodrigues, V. Štejfá, M. Fulem, M. Bastos, Reassembling and testing of a high-precision heat capacity drop calorimeter. Heat capacity of some polyphenyls at $T = 298.15$ K, *Journal of Chemical Thermodynamics*. 43 (2011) 1818–1823. <https://doi.org/10.1016/j.jct.2011.06.010>.
- [126] J.W. Richardson, G.S. Parks, Thermal Data on Organic Compounds. XIX. Modern Combustion Data for Some Non-Volatile Compounds Containing Carbon, Hydrogen and Oxygen, *Journal of the American Chemical Society*. 61 (1939) 3543–3546. <https://doi.org/10.1021/ja01267a092>.
- [127] E.G. Kiparisova, B.V. Lebedev, The thermodynamic characteristics of cyclotrimers and polycyclotrimers, *Russian Journal of Physical Chemistry A*. 73 (1999) 515–520.

- [128] M.L. Lee, D.L. Vassilaros, C.M. White, M. Novotny, Retention Indices for Programmed-Temperature Capillary-Column Gas Chromatography of Polycyclic Aromatic Hydrocarbons, *Analytical Chemistry*. 51 (1979) 768–773. <https://doi.org/10.1021/ac50042a043>.
- [129] A.F. Shlyakhov, *Gas chromatography in organic geochemistry*, Nedra, Moscow, 1984.
- [130] C.E. Rostad, W.E. Pereira, Kovats and Lee retention indices determined by gas chromatography/mass spectrometry for organic compounds of environmental interest, *Journal of High Resolution Chromatography*. 9 (1986) 328-334. <https://doi.org/10.1002/jhrc.1240090603>.
- [131] H. Beernaert, Gas Chromatographic analysis of polycyclic aromatic hydrocarbons, *Journal of Chromatography A*. 173 (1979) 109–118. [https://doi.org/10.1016/S0021-9673\(01\)80450-7](https://doi.org/10.1016/S0021-9673(01)80450-7).
- [132] S.P. Verevkin, Vapour pressures and enthalpies of vaporization of a series of the linear n-alkyl-benzenes, *The Journal of Chemical Thermodynamics*. 38 (2006) 1111–1123. <https://doi.org/10.1016/J.JCT.2005.11.009>.
- [133] P.A. Irvine, D. Cheng Wu, P.J. Flory, Liquid-crystalline Transitions in Homologous p-Phenylenes and their Mixtures Part 1. - Experimental Results, *Journal of the Chemical Society, Faraday Transactions 1: Physical Chemistry in Condensed Phases*. 80 (1984) 1795–1806.
- [134] D.H. Zaitsau, V.N. Emel'yanenko, A.A. Pimerzin, S.P. Verevkin, Benchmark properties of biphenyl as a liquid organic hydrogen carrier: Evaluation of thermochemical data with complementary experimental and computational methods, *The Journal of Chemical Thermodynamics*. 122 (2018) 1–12. <https://doi.org/10.1016/J.JCT.2018.02.025>.
- [135] S.E. Wheeler, K.N. Houk, P. von R. Schleyer, W.D. Allen, A hierarchy of homodesmotic reactions for thermochemistry, *Journal of the American Chemical Society*. 131 (2009) 2547–2560. <https://doi.org/10.1021/ja805843n>.
- [136] S. P. Verevkin, V. N. Emel'yanenko, S. A. Kozlova, Organic carbonates: Experiment and ab initio calculations for prediction of thermochemical properties, *The Journal of Physical Chemistry A*. 112 (2008) 10667–10673. <https://doi.org/10.1021/jp8024705>.
- [137] H.D. Springall, T.R. White, Heats of combustion and molecular structure. Part II. The mean bond energy term for the carbonyl system in certain ketones, *Journal of the Chemical Society (Resumed)*. (1954) 2764–2766.

- [138] G.R. Nicholson, M. Szwarc, J.W. Taylor, The heats of formation of diacetyl and of benzyl methyl ketone in the vapour phase, *Journal of the Chemical Society (Resumed)*. (1954) 2767–2769. <https://doi.org/10.1039/JR9540002767>.
- [139] J.S. Chickos, S. Hosseini, D.G. Hesse, Determination of vaporization enthalpies of simple organic molecules by correlations of changes in gas chromatographic net retention times, *Thermochimica Acta*. 249 (1995) 41–62. [https://doi.org/10.1016/0040-6031\(94\)01943-B](https://doi.org/10.1016/0040-6031(94)01943-B).
- [140] D.R. Stull, Vapor pressure of pure substances. Organic and inorganic compounds, *Industrial & Engineering Chemistry*. 39 (1947) 517–540. <https://doi.org/10.1021/ie50448a022>.
- [141] V.N. Emel'yanenko, K. V. Zaitseva, F. Agapito, J.A. Martinho Simões, S.P. Verevkin, Benchmark thermodynamic properties of methylanisoles: Experimental and theoretical study, *The Journal of Chemical Thermodynamics*. 85 (2015) 155–162. <https://doi.org/10.1016/J.JCT.2015.02.001>.
- [142] K. V. Zaitseva, V.N. Emel'yanenko, F. Agapito, A.A. Pimerzin, M.A. Varfolomeev, S.P. Verevkin, Benchmark thermochemistry of methylbenzotriles: Experimental and theoretical study, *The Journal of Chemical Thermodynamics*. 91 (2015) 186–193. <https://doi.org/10.1016/J.JCT.2015.07.025>.
- [143] L.A. Curtiss, P.C. Redfern, K. Raghavachari, Gaussian-4 theory, *The Journal of Chemical Physics*. 126 (2007) 084108. <https://doi.org/10.1063/1.2436888>.
- [144] S.P. Verevkin, V.N. Emel'yanenko, R. Siewert, A.A. Pimerzin, Energetics of LOHC: Structure-Property Relationships from Network of Thermochemical Experiments and in Silico Methods, *Hydrogen*. 2 (2021) 101–121. <https://doi.org/10.3390/hydrogen2010006>.
- [145] N.D. Lebedeva, Heats of combustion and formation of aliphatic tertiary amine homologues, *Russian Journal of Physical Chemistry, USSR*. 40 (1966) 1465.
- [146] S.P. Verevkin, V.N. Emel'yanenko, A.A. Pimerzin, E.E. Vishnevskaya, Thermodynamic Analysis of Strain in the Five-Membered Oxygen and Nitrogen Heterocyclic Compounds, *Journal of Physical Chemistry A*. 115 (2011) 1992–2004. <https://doi.org/10.1021/JP1090526>.
- [147] T.M. Krygowski, B.T. Stępień, Sigma- and Pi-Electron Delocalization: Focus on Substituent Effects, *Chemical Reviews*. 105 (2005) 3482–3512. <https://doi.org/10.1021/CR030081S>.
- [148] R.B. Sunoj, Theoretical Aspects of Organoselenium Chemistry, in *Patai's Chemistry of Functional Groups: Organic Selenium and Tellurium Compounds*, Wiley & Sons, UK, 2011.

- [149] S. Verevkin, Thermochemistry of phenols: quantification of the ortho-, para-, and meta-interactions in tert-alkyl substituted phenols, *The Journal of Chemical Thermodynamics*. 31 (1999) 559–585. <https://doi.org/10.1006/jcht.1998.0459>.
- [150] S.P. Verevkin, V.N. Emel'yanenko, A. Klamt, Thermochemistry of Chlorobenzenes and Chlorophenols: Ambient Temperature Vapor Pressures and Enthalpies of Phase Transitions, *Journal of Chemical & Engineering Data*. 52 (2007) 499–510. <https://doi.org/10.1021/jc060429r>.
- [151] S.P. Verevkin, V.N. Emel'yanenko, M.A. Varfolomeev, B.N. Solomonov, K.V. Zherikova, S.V. Melkhanova, Thermochemistry of dihalogen-substituted benzenes: Data evaluation using experimental and quantum chemical methods, *The Journal of Physical Chemistry B*. 118 (2014) 14479–14492. <https://doi.org/10.1021/jp5097844>.
- [152] S.P. Verevkin, Improved group-additivity values for the estimation of the standard enthalpies of formation of imines and carboxylic acids derivatives, *Journal of Thermal Analysis and Calorimetry*. 60 (2000) 437–451. <https://doi.org/10.1023/A:1010193526125>.
- [153] K.V. Zherikova, A.A. Svetlov, M.A. Varfolomeev, S.P. Verevkin, C. Held, Thermochemistry of halogenobenzoic acids as an access to PC-SAFT solubility modeling, *Fluid Phase Equilibria*. 409 (2016) 399–407. <https://doi.org/10.1016/J.FLUID.2015.10.001>.
- [154] S.P. Verevkin, D.H. Zaitsau, V.N. Emel'yanenko, E.N. Stepurko, K.V. Zherikova, Benzoic acid derivatives: Evaluation of thermochemical properties with complementary experimental and computational methods, *Thermochimica Acta*. 622 (2015) 18–30. <https://doi.org/10.1016/j.tca.2015.03.026>.
- [155] R.G. Schmitt, R.C. Hirt, Investigation of the protective ultraviolet absorbers in a space environment. I. Rate of evaporation and vapor pressure studies, *Journal of Polymer Science*. 45 (1960) 35–47. <https://doi.org/10.1002/POL.1960.1204514504>.
- [156] M. Colomina, C. Latorre, R. Perez-Ossorio, Heats of combustion of five alkyl phenyl ketones, *Pure and Applied Chemistry*. 2 (1961) 133–136. <https://doi.org/10.1351/PAC196102010133>.
- [157] D.N. Gray, G. Burton, Evaporation Rates and Vapor Pressure of Some Fluoro- and Trifluoromethyl-Substituted 2-Hydroxy-4-methoxybenzophenones, *Journal of Chemical and Engineering Data*. 11 (1966) 59–60. <https://doi.org/10.1021/JE60028A016>.
- [158] W. V. Steele, R.D. Chirico, A. Nguyen, I.A. Hossenlopp, N.K. Smith, DIPPR project 871. Determination of ideal-gas enthalpies of formation for key compounds, The 1990 project results. *DIPPR Data Series*. 2 (1994) 188–215. <https://doi.org/10.2172/5093919>.

- [159] W. V. Steele, R.D. Chirico, S.E. Knipmeyer, A. Nguyen, Vapor pressure of acetophenone, (\pm)-1,2-butanediol, (\pm)-1,3-butanediol, diethylene glycol monopropyl ether, 1,3-dimethyladamantane, 2-ethoxyethyl acetate, ethyl octyl sulfide, and pentyl acetate, *Journal of Chemical and Engineering Data*. 41 (1996) 1255–1268. <https://doi.org/10.1021/JE9601117>.
- [160] D.M. Price, M. Hawkins, Vapour pressures of hydroxybenzophenone UV absorbers, *Thermochimica Acta*. 329 (1999) 73–76. [https://doi.org/10.1016/S0040-6031\(99\)00005-2](https://doi.org/10.1016/S0040-6031(99)00005-2).
- [161] R.D. Chirico, S.E. Knipmeyer, W. V. Steele, Heat capacities, enthalpy increments, and derived thermodynamic functions for naphthalene between the temperatures 5 K and 440 K, *The Journal of Chemical Thermodynamics*. 34 (2002) 1873–1884. [https://doi.org/10.1016/S0021-9614\(02\)00262-8](https://doi.org/10.1016/S0021-9614(02)00262-8).
- [162] S. Tomitaka, M. Mizukami, F. Paladi, M. Oguni, Thermal and dielectric studies of 2,2'-dihydroxybenzophenone: Progress of crystal nucleation and growth below the glass transition temperature, *Journal of Thermal Analysis and Calorimetry*. 81 (2005) 637–643. <https://doi.org/10.1007/S10973-005-0836-X>.
- [163] M.A.V. Ribeiro da Silva, L.M.P.F. Amaral, F.C.R. Guedes, J.R.B. Gomes, Standard molar enthalpies of formation of methylbenzophenones, *Journal of Physical Organic Chemistry*. 19 (2006) 689–696. <https://doi.org/10.1002/POC.1117>.
- [164] J.Z. Dávalos, A. Guerrero, R. Herrero, P. Jimenez, A. Chana, J.L.M. Abboud, C.F.R.A.C. Lima, L.M.N.B.F. Santos, A.F. Lago, Neutral, Ion Gas-Phase Energetics and Structural Properties of Hydroxybenzophenones, *Journal of Organic Chemistry*. 75 (2010) 2564–2571. <https://doi.org/10.1021/JO100085B>.
- [165] V. Štejfá, M. Fulem, K. Růžička, P. Morávek, New Static Apparatus for Vapor Pressure Measurements: Reconciled Thermophysical Data for Benzophenone, *Journal of Chemical and Engineering Data*. 61 (2016) 3627–3639. <https://doi.org/10.1021/ACS.JCED.6B00523>.
- [166] R.N. Nagrimanov, A.A. Samatov, A.V. Buzyorov, B.N. Solomonov, Determination of sublimation enthalpies of substituted benzophenones, fluorenes and diphenyl ethers by solution calorimetry approach, *Thermochimica Acta*. 655 (2017) 358–362. <https://doi.org/10.1016/J.TCA.2017.08.003>.
- [167] I.V. Andreeva, M.A. Varfolomeev, S.P. Verevkin, Thermochemistry of di-substituted benzenes: Ortho-, meta-, and para-hydroxyacetophenones, *The Journal of Chemical Thermodynamics*. 140 (2020) 105893. <https://doi.org/10.1016/J.JCT.2019.105893>.

- [168] I.V. Andreeva, Thermochemistry of substituted benzenes: acetophenones with methyl, ethyl, cyano, and acetoxy substituents, *Journal of Thermal Analysis and Calorimetry*. 21 (2021) 01085.
- [169] D. Kulikov, S.P. Verevkin, A. Heintz, Determination of Vapor Pressures and Vaporization Enthalpies of the Aliphatic Branched C5 and C6 Alcohols, *Journal of Chemical and Engineering Data*. 46 (2001) 1593–1600. <https://doi.org/10.1021/JE010187P>.
- [170] S.P. Verevkin, V.N. Emel'yanenko, Transpiration method: Vapor pressures and enthalpies of vaporization of some low-boiling esters, *Fluid Phase Equilibria*. 266 (2008) 64–75. <https://doi.org/10.1016/J.FLUID.2008.02.001>.
- [171] S.P. Verevkin, Phase changes in pure component systems: Liquids and gases. Measurement of the thermodynamic properties of multiple phases, in: R.D. Weir, Th.W. De Loos (Eds.), *Experimental Thermodynamics*, Elsevier, 2005: pp. 5–30. [https://doi.org/10.1016/S1874-5644\(05\)80004-9](https://doi.org/10.1016/S1874-5644(05)80004-9).
- [172] V.N. Emel'yanenko, D.H. Zaitsau, E. Shoifet, F. Meurer, S.P. Verevkin, C. Schick, C. Held, Benchmark Thermochemistry for Biologically Relevant Adenine and Cytosine. A Combined Experimental and Theoretical Study, *Journal of Physical Chemistry A*. 119 (2015) 9680–9691. <https://doi.org/10.1021/ACS.JPCA.5B04753>.
- [173] V.V. Serpinskii, S.A. Voitkevich, N.Yu. Lyuboshits, *Trudy Vsesoyuz. Nauch.-Issledovatel. Inst. Sintet. I. Natural. Dushistykh Veshchestv*. 4 (1958) 125-130.
- [174] A. Aihara, Estimation of the Energy of Hydrogen Bonds Formed in Crystals. I. Sublimation Pressures of Some Organic Molecular Crystals and the Additivity of Lattice Energy, *Bulletin of the Chemical Society of Japan*. 32 (1959) 1242–1248. <https://doi.org/10.1246/BCSJ.32.1242>.
- [175] L.M.P.F. Amaral, V.M.F. Morais, M.A.V. Ribeiro da Silva, Standard molar enthalpy of formation of methoxyacetophenone isomers, *The Journal of Chemical Thermodynamics*. 74 (2014) 22–31. <https://doi.org/10.1016/J.JCT.2014.03.027>.
- [176] A.R.R.P. Almeida, M.J.S. Monte, Vapour pressures and phase transition properties of four substituted acetophenones, *The Journal of Chemical Thermodynamics*. 107 (2017) 42–50. <https://doi.org/10.1016/J.JCT.2016.12.012>.
- [177] L.M.P.F. Amaral, M.A.V. Ribeiro da Silva, Experimental and computational thermochemical study of dimethoxyacetophenones, *The Journal of Chemical Thermodynamics*. 152 (2021) 106257. <https://doi.org/10.1016/J.JCT.2020.106257>.

- [178] <https://www.guidechem.com>, (2021).
- [179] A.F. Lago, P. Jimenez, R. Herrero, J.Z. Dávalos, J.L.M. Abboud, Thermochemistry and gas-phase ion energetics of 2-hydroxy-4-methoxy- benzophenone (oxybenzone), *Journal of Physical Chemistry A*. 112 (2008) 3201–3208. <https://doi.org/10.1021/JP7111999>.
- [180] B.A. Vinogradov, Production, composition, properties and application of essential oils, (2021). <http://viness.narod.ru/> (accessed November 1, 2021).
- [181] K.V. Tretyakov, Retention Data. NIST Mass Spectrometry Data Center., (2008).
- [182] S.P. Verevkin, Weaving a web of reliable thermochemistry around lignin building blocks: phenol, benzaldehyde, and anisole, *Journal of Thermal Analysis and Calorimetry* 2021. (2021) 1–13. <https://doi.org/10.1007/S10973-021-10924-X>.
- [183] R.E. Ardrey, A.C. Moffat, Gas-liquid chromatographic retention indices of 1318 substances of toxicological interest on SE-30 or OV-a stationary phase, *Journal of Chromatography A*. 220 (1981) 195–252. [https://doi.org/10.1016/S0021-9673\(00\)81925-1](https://doi.org/10.1016/S0021-9673(00)81925-1).
- [184] S.W. Benson, New Methods for Estimating the Heats of Formation, Heat Capacities, and Entropies of Liquids and Gases, *Journal of Physical Chemistry A*. 103 (1999) 11481–11485. <https://doi.org/10.1021/JP992971A>.
- [185] P. Walden, Über die Schmelzwärme, spezifische Kohäsion und Molekulargrösse bei der Schmelztemperatur, *Zeitschrift Für Elektrochemie Und Angewandte Physikalische Chemie*. 14 (1908) 713–724.
- [186] A. Abdelaziz, D. H. Zaitsau, N. V. Kuratieva, S. P. Verevkin, C. Schick, Melting of nucleobases. Getting the cutting edge of “Walden’s Rule,” *Physical Chemistry Chemical Physics*. 21 (2019) 12787–12797. <https://doi.org/10.1039/C9CP00716D>.
- [187] S.P. Verevkin, M.E. Konnova, V. V. Turovtsev, A. V. Riabchunova, A.A. Pimerzin, Weaving a Network of Reliable Thermochemistry around Lignin Building Blocks: Methoxy-Phenols and Methoxy-Benzaldehydes, *Industrial and Engineering Chemistry Research*. 59 (2020) 10727–10737. <https://doi.org/10.1021/acs.iecr.0c04281>.
- [188] I. Prigogine, R. Defay, *Chemical Thermodynamics*, Wiley, 1954.
- [189] R.N. Nagrimanov, M.A. Ziganshin, B.N. Solomonov, S.P. Verevkin, Thermochemistry of drugs: experimental and theoretical study of analgesics, *Structural Chemistry*. 30 (2019) 247–261. <https://doi.org/10.1007/s11224-018-1188-z>.

- [190] S.P. Verevkin, V.N. Emel'yanenko, R.N. Nagrimanov, Nearest-Neighbor and Non-Nearest-Neighbor Interactions between Substituents in the Benzene Ring. Experimental and Theoretical Study of Functionally Substituted Benzamides, *Journal of Physical Chemistry A*. 120 (2016) 9867–9877. <https://doi.org/10.1021/ACS.JPCA.6B10332>.
- [191] P. Pracht, F. Bohle, S. Grimme, Automated exploration of the low-energy chemical space with fast quantum chemical methods, *Physical Chemistry Chemical Physics*. 22 (2020) 7169–7192. <https://doi.org/10.1039/C9CP06869D>.
- [192] N.L. Allinger, Y.H. Yuh, J.H. Lii, Molecular mechanics. The MM3 force field for hydrocarbons. 1, *Journal of the American Chemical Society*. 111 (1989) 8551–8566. <https://doi.org/10.1021/JA00205A001>.
- [193] A.D. Becke, Density-functional thermochemistry. III. The role of exact exchange, *The Journal of Chemical Physics*. 98 (1998) 5648. <https://doi.org/10.1063/1.464913>.
- [194] S.P. Verevkin, M.E. Konnova, K.V. Zherikova, A.A. Pimerzin, Sustainable hydrogen storage: Thermochemistry of amino-alcohols as seminal liquid organic hydrogen carriers, *The Journal of Chemical Thermodynamics*. 163 (2021) 106591. <https://doi.org/10.1016/J.JCT.2021.106591>.
- [195] S.P. Verevkin, D.H. Zaitsau, V.N. Emel'yanenko, A.A. Zhabina, Thermodynamic properties of glycerol: Experimental and theoretical study, *Fluid Phase Equilibria*. 397 (2015) 87–94. <https://doi.org/10.1016/J.FLUID.2015.03.038>.
- [196] M.A. Varfolomeev, D.I. Abaidullina, B.N. Solomonov, S.P. Verevkin, V.N. Emel'yanenko, Pairwise Substitution Effects, Inter- and Intramolecular Hydrogen Bonds in Methoxyphenols and Dimethoxybenzenes. Thermochemistry, Calorimetry, and First-Principles Calculations, *Journal of Physical Chemistry B*. 114 (2010) 16503–16516. <https://doi.org/10.1021/JP108459R>.
- [197] M.D.M.C. Ribeiro da Silva, M.A.V. Ribeiro da Silva, G. Pilcher, Enthalpies of combustion of 1,2-dihydroxybenzene and of six alkylsubstituted 1,2-dihydroxybenzenes, *The Journal of Chemical Thermodynamics*. 16 (1984) 1149–1155. [https://doi.org/10.1016/0021-9614\(84\)90187-3](https://doi.org/10.1016/0021-9614(84)90187-3).
- [198] S.P. Verevkin, S.A. Kozlova, Di-hydroxybenzenes: Catechol, resorcinol, and hydroquinone: Enthalpies of phase transitions revisited, *Thermochimica Acta*. 471 (2008) 33–42. <https://doi.org/10.1016/J.TCA.2008.02.016>.

- [199] P.D. Desai, R.C. Wilhoit, B.J. Zwolinski, Heat of Combustion of Resorcinol and Enthalpies of Isomerization of Dihydroxybenzenes, *Journal of Chemical & Engineering Data*. 13 (1968) 334–335. <https://pubs.acs.org/sharingguidelines>.
- [200] S.P. Verevkin, Substituent effects on the benzene ring. Prediction of the thermochemical properties of alkyl substituted hydroquinones, *Physical Chemistry Chemical Physics*. 1 (1999) 127–131.
- [201] K. Růžička, V. Majer, Simultaneous treatment of vapor pressures and related thermal data between the triple and normal boiling temperatures for n-alkanes C5–C20, *Journal of Physical and Chemical Reference Data*. 23 (1994) 1–39. <https://doi.org/10.1063/1.555942>.
- [202] J.S. Chickos, W. Hanshaw, Vapor pressures and vaporization enthalpies of the n-alkanes from C31 to C38 at T = 298.15 K by correlation gas chromatography, *Journal of Chemical & Engineering Data*. 49 (2004) 620–630. <https://doi.org/10.1021/je030236t>.
- [203] V.V. Ovchinnikov, L.R. Khazieva, L.I. Lapteva, A.I. Konovalov, Thermochemistry of heteroatomic compounds, *Russian Chemical Bulletin* 2000 49:1. 49 (2000) 33–38. <https://doi.org/10.1007/BF02499061>.
- [204] D.H. Zaitsau, N. Plechkova, S.P. Verevkin, Vaporization thermodynamics of ionic liquids with tetraalkylphosphonium cations, *The Journal of Chemical Thermodynamics*. 130 (2019) 204–212. <https://doi.org/10.1016/j.jct.2018.10.007>.
- [205] V.N. Emel'yanenko, S.V. Portnova, S.P. Verevkin, A. Skrzypczak, T. Schubert, Building blocks for ionic liquids: Vapor pressures and vaporization enthalpies of 1-(n-alkyl)-imidazoles, *The Journal of Chemical Thermodynamics*. 43 (2011) 1500–1505. <https://doi.org/10.1016/J.JCT.2011.05.004>.
- [206] T. Köddermann, D. Paschek, R. Ludwig, Ionic Liquids: Dissecting the enthalpies of vaporization, *ChemPhysChem*. 9 (2008) 549–555. <https://doi.org/10.1002/cphc.200700814>.
- [207] D.H. Zaitsau, V.N. Emel'yanenko, P. Stange, C. Schick, S.P. Verevkin, R. Ludwig, Dispersion and hydrogen bonding rule: Why the vaporization enthalpies of aprotic ionic liquids are significantly larger than those of protic ionic liquids, *Angewandte Chemie International Edition*. 55 (2016) 11682–11686. <https://doi.org/10.1002/anie.201605633>.
- [208] S.P. Verevkin, D.H. Zaitsau, V.N. Emel'yanenko, V.R. Ralys, V.A. Yermalayeu, C. Schick, Vaporization enthalpies of imidazolium based ionic liquids. A thermogravimetric study of the alkyl chain length dependence, *Journal of Chemical Thermodynamics*. 54 (2012) 433–437. <https://doi.org/10.1016/j.jct.2012.05.029>.

- [209] D.H. Zaitsau, S.P. Verevkin, V.N. Emel'yanenko, A. Heintz, Vaporization enthalpies of imidazolium based ionic liquids: dependence on alkyl chain length, *ChemPhysChem*. 12 (2011) 3609–3613. <https://doi.org/10.1002/cphc.201100618>.
- [210] T. Welton, Room-temperature ionic liquids. Solvents for synthesis and catalysis, *Chemical Reviews*. 99 (1999) 2071–2084. <https://doi.org/10.1021/cr980032t>.
- [211] D.H. Zaitsau, Y.U. Paulechka, G.J. Kabo, The kinetics of thermal decomposition of 1-butyl-3-methylimidazolium hexafluorophosphate, *Journal of Physical Chemistry A*. 110 (2006) 11602–11604. <https://doi.org/10.1021/jp064212f>.
- [212] G.J. Kabo, A.V. Blokhin, Y.U. Paulechka, A.G. Kabo, M.P. Shymanovich, J.W. Magee, Thermodynamic properties of 1-butyl-3-methylimidazolium hexafluorophosphate in the condensed state., *Journal of Chemical and Engineering Data*. 49 (2004) 453–461. <https://doi.org/10.1021/je034102r>.
- [213] J.P. Armstrong, C. Hurst, R.G. Jones, P. Licence, K.R.J. Lovelock, C.J. Satterley, I.J. Villar-Garcia, Vapourisation of ionic liquids, *Physical Chemistry Chemical Physics*. 9 (2007) 982–990. <https://doi.org/10.1039/B615137J>.
- [214] V. Volpe, B. Brunetti, G. Gigli, A. Lapi, S. Vecchio Cipriotti, A. Ciccio, Toward the Elucidation of the Competing Role of Evaporation and Thermal Decomposition in Ionic Liquids: A Multitechnique Study of the Vaporization Behavior of 1-Butyl-3-methylimidazolium Hexafluorophosphate under Effusion Conditions, *Journal of Physical Chemistry B*. 121 (2017). <https://doi.org/10.1021/acs.jpcc.7b08523>.
- [215] S.P. Verevkin, D.H. Zaitsau, V.N. Emel'yanenko, A. Heintz, A new method for the determination of vaporization enthalpies of ionic liquids at low temperatures, *Journal of Physical Chemistry B*. 115 (2011). <https://doi.org/10.1021/jp207397v>.
- [216] D.H. Zaitsau, A. V. Yermalayeu, V.N. Emel'yanenko, S. Butler, T. Schubert, S.P. Verevkin, Thermodynamics of imidazolium-based ionic liquids containing PF₆ anions, *The Journal of Physical Chemistry B*. 120 (2016) 7949–7957. <https://doi.org/10.1021/acs.jpcc.6b06081>.
- [217] J.N.A. Canongia Lopes, A.A.H. Pádua, Nanostructural organization in ionic liquids, *Journal of Physical Chemistry B*. 110 (2006) 3330–3335. <https://doi.org/10.1021/jp056006y>.
- [218] D.H. Zaitsau, A. V. Yermalayeu, V.N. Emel'yanenko, S.P. Verevkin, U. Welz-Biermann, T. Schubert, Structure-property relationships in ILs: A study of the alkyl chain length dependence in vaporisation enthalpies of pyridinium based ionic liquids, *Science China Chemistry*. 55 (2012) 1525–1531. <https://doi.org/10.1007/s11426-012-4662-2>.

- [219] D.H. Zaitsau, A. V. Yermalayeu, V.N. Emel'yanenko, A. Heintz, S.P. Verevkin, C. Schick, S. Berdzinski, V. Strehmel, Structure-property relationships in ILs: Vaporization enthalpies of pyrrolidinium based ionic liquids, *Journal of Molecular Liquids*. 192 (2014) 171–176. <https://doi.org/10.1016/j.molliq.2013.07.018>.
- [220] M. Månsson, P. Sellers, G. Stridh, S. Sunner, Enthalpies of vaporization of some 1-substituted n-alkanes., *Journal of Chemical Thermodynamics*. 9 (1977) 91–97. [https://doi.org/10.1016/0021-9614\(77\)90202-6](https://doi.org/10.1016/0021-9614(77)90202-6).
- [221] G. Pei, J. Xiang, G. Li, S. Wu, F. Pan, X. Lv, A Literature Review of Heat Capacity Measurement Methods, *Minerals, Metals and Materials Series*. (2019) 569–577. https://doi.org/10.1007/978-3-030-05955-2_54.
- [222] E.S. Domalski, E.D. Hearing, Estimation of the Thermodynamic Properties of C-H-N-O-S-Halogen Compounds at 298.15 K, *Journal of Physical and Chemical Reference Data*. 22 (1993) 805–1159. <https://doi.org/10.1063/1.555927>.
- [223] D.H. Zaitsau, A.A. Pimerzin, S.P. Verevkin, Fatty acids methyl esters: Complementary measurements and comprehensive analysis of vaporization thermodynamics, *Journal of Chemical Thermodynamics*. 132 (2019) 322–340. <https://doi.org/10.1016/j.jct.2019.01.007>.
- [224] J.S. Chickos, W.E. Acree, Enthalpies of sublimation of organic and organometallic compounds. 1910-2001, *Journal of Physical and Chemical Reference Data*. 31 (2002) 537–698. <https://doi.org/10.1063/1.1475333>.
- [225] J.S. Chickos, W.E. Acree, Enthalpies of vaporization of organic and organometallic compounds, 1880-2002, *Journal of Physical and Chemical Reference Data*. 32 (2003) 519–878. <https://doi.org/10.1063/1.1529214>.
- [226] Y.U. Paulechka, D.H. Zaitsau, G.J. Kabo, A.A. Strechan, Vapor pressure and thermal stability of ionic liquid 1-butyl-3-methylimidazolium Bis(trifluoromethylsulfonyl)amide, *Thermochimica Acta*. 439 (2005) 158–160. <https://doi.org/10.1016/j.tca.2005.08.035>.
- [227] P.G. Wahlbeck, Effusion. VII. The Failure of Isotropy of a Gas in an Effusion Cell and the Transition Region, *Journal of Chemical Physics*. 55 (1971) 1709–1715. <https://doi.org/10.1063/1.1676300>.
- [228] Nesmeianov An. N, Carasso J. I., *Vapour pressure of the elements*, Academic Press, New York, 1963.

- [229] D. Zaitsau, G.J. Kabo, A.A. Kozyro, V.M. Sevruk, The effect of the failure of isotropy of a gas in an effusion cell on the vapor pressure and enthalpy of sublimation for alkyl derivatives of carbamide, *Thermochimica Acta*. 406 (2003) 17–28. [https://doi.org/10.1016/S0040-6031\(03\)00231-4](https://doi.org/10.1016/S0040-6031(03)00231-4).
- [230] W. Zielenkiewicz, G.L. Perlovich, M. Wszelaka-Rylik, The vapour pressure and the enthalpy of sublimation. Determination by inert gas flow method, *Journal of Thermal Analysis and Calorimetry* 57, (1999) 225-234.
- [231] J. Selvakumar, V.S. Raghunathan, K.S. Nagaraja, Vapor pressure measurements of Sc(tmhd)₃ and synthesis of stabilized zirconia thin films by hybrid CVD technique using Sc(tmhd)₃, Zr(tmhd)₄, and Al(acac)₃ [tmhd, 2,2,6,6-tetramethyl-3,5-heptanedione; acac, 2,4-pentanedione] as precursors, *Journal of Physical Chemistry C*. 113 (2009) 19011–19020. <https://doi.org/10.1021/jp906204c>.
- [232] L. Malaspina, R. Gigli, G. Bardi, Microcalorimetric determination of the enthalpy of sublimation of benzoic acid and anthracene, *The Journal of Chemical Physics*. 59 (1973) 387–394. <https://doi.org/10.1063/1.1679817>.
- [233] D.H. Zaitsau, S.P. Verevkin, A.Yu. Sazonova, Vapor pressures and vaporization enthalpies of 5-nonanone, linalool and 6-methyl-5-hepten-2-one. Data evaluation., *Fluid Phase Equilibria*. 386 (2015) 140–148. <https://doi.org/10.1016/j.fluid.2014.11.026>.
- [234] M.A.V. Ribeiro da Silva, M.J.S. Monte, L.M.N.B.F. Santos, The design, construction, and testing of a new Knudsen effusion apparatus, *The Journal of Chemical Thermodynamics*. 38 (2006) 778–787. <https://doi.org/10.1016/j.jct.2005.08.013>.
- [235] C.G. de Kruif, J.G. Blok, The vapour pressure of benzoic acid, *The Journal of Chemical Thermodynamics*. 14 (1982) 201–206. [https://doi.org/10.1016/0021-9614\(82\)90011-8](https://doi.org/10.1016/0021-9614(82)90011-8).
- [236] M. Davies, J.I. Jones, The sublimation pressures and heats of sublimation of some carboxylic acids, *Transactions of the Faraday Society*. 50 (1954) 1042–1047. <https://doi.org/10.1039/TF9545001042>.
- [237] M. Colomina, P. Jimenez, C. Turrion, Vapour pressures and enthalpies of sublimation of naphthalene and benzoic acid, *The Journal of Chemical Thermodynamics*. 14 (1982) 779–784. [https://doi.org/10.1016/0021-9614\(82\)90174-4](https://doi.org/10.1016/0021-9614(82)90174-4).
- [238] M.A.V. Ribeiro da Silva, M.J.S. Monte, The construction, testing and use of a new Knudsen effusion apparatus, *Thermochimica Acta*. 171 (1990) 169–183. [https://doi.org/10.1016/0040-6031\(90\)87017-7](https://doi.org/10.1016/0040-6031(90)87017-7).

- [239] C. Plato, A.R. Glasgow, Differential scanning calorimetry as a general method for determining the purity and heat of fusion of high-purity organic chemicals. Application to 95 compounds, *Analytical Chemistry*. 41 (2002) 330–336. <https://doi.org/10.1021/AC60271A041>.
- [240] W. Acree, J.S. Chickos, Phase transition enthalpy measurements of organic and organometallic compounds and ionic liquids. sublimation, vaporization, and fusion enthalpies from 1880 to 2015. part 2. C11-C192, *Journal of Physical and Chemical Reference Data*. 46 (2017) 013104. <https://doi.org/10.1063/1.4970519>.
- [241] C. Gobble, J.S. Chickos, S.P. Verevkin, Vapor pressures and vaporization enthalpies of a series of dialkyl phthalates by correlation gas chromatography, *Journal of Chemical and Engineering Data*. 59 (2014) 1353–1365. <https://doi.org/10.1021/je500110d>.
- [242] S. Grimme, S. Ehrlich, L. Goerigk, Effect of the damping function in dispersion corrected density functional theory, *Journal of Computational Chemistry*. 32 (2011) 1456–1465. <https://doi.org/10.1002/jcc.21759>.
- [243] C. Bannwarth, S. Ehlert, S. Grimme, GFN2-xTB—an accurate and broadly parametrized Self-Consistent Tight-Binding quantum chemical method with multipole electrostatics and density-dependent dispersion contributions, *Journal of Chemical Theory and Computation*. 15 (2019) 1652–1671. <https://doi.org/10.1021/acs.jctc.8b01176>.
- [244] P. Pracht, E. Caldeweyher, S. Ehlert, S. Grimme, A robust Non-Self-Consistent Tight-Binding quantum chemistry method for large molecules., *ChemRxiv*. Preprint. (2019). <https://doi.org/10.26434/chemrxiv.8326202.v1>.

APPENDIX

A. Supporting information for chapter 2

Table A.1 Results of transpiration method for substituted acetophenones and benzophenones: absolute vapor pressures p , standard molar vaporization enthalpies and standard molar vaporization entropies

$T/$ K ^a	$m/$ mg ^b	$V(\text{N}_2)^c /$ dm ³	$T_a/$ K ^d	Flow/ dm ³ ·h ⁻¹	$p/$ Pa ^e	$u(p)/$ Pa ^f	$\Delta_1^g H_m^o(T)/$ kJ·mol ⁻¹	$\Delta_1^g S_m^o(T)/$ J·K ⁻¹ ·mol ⁻¹
tri-n-butyl-amine: $\Delta_1^g H_m^o(298.15 \text{ K}) = (58.3 \pm 0.6) \text{ kJ} \cdot \text{mol}^{-1}$								
$\ln(p/p_{ref}) = \frac{300.7}{R} - \frac{81599.6}{RT} - \frac{78}{R} \ln \frac{T}{298.15}; p_{ref} = 1 \text{ Pa}$								
289.2	2.58	2.733	292.2	4.00	12.53	0.34	59.0	129.5
292.2	2.41	2.000	292.2	3.00	15.89	0.42	58.8	128.6
295.2	2.70	1.750	292.2	3.00	20.37	0.53	58.6	127.8
298.2	2.48	1.250	293.2	3.00	26.20	0.68	58.3	127.1
301.2	2.52	1.000	292.2	3.00	33.16	0.85	58.1	126.3
304.2	1.52	0.500	293.2	1.50	40.00	1.02	57.9	125.2
307.2	2.51	0.667	292.2	2.00	49.42	1.26	57.6	124.4
310.2	2.78	0.600	293.2	1.80	61.13	1.55	57.4	123.6
313.2	1.71	0.290	293.2	1.20	77.40	1.96	57.2	123.0
316.2	2.59	0.360	292.2	1.44	94.33	2.38	56.9	122.2
319.2	2.74	0.300	293.2	1.20	119.96	3.02	56.7	121.8
322.2	3.37	0.300	292.2	1.20	147.30	3.71	56.5	121.1
325.2	3.95	0.300	293.2	1.20	173.08	4.35	56.2	120.1
328.2	6.38	0.396	293.2	1.44	211.60	5.31	56.0	119.5
331.2	5.52	0.280	293.2	1.20	258.52	6.49	55.8	118.9
334.2	7.05	0.300	293.2	1.20	308.09	7.73	55.5	118.1
337.2	8.53	0.300	293.2	1.20	372.51	9.34	55.3	117.5

tri-n-pentyl-amine: $\Delta_1^g H_m^o(298.15 \text{ K}) = (71.6 \pm 0.5) \text{ kJ} \cdot \text{mol}^{-1}$

$\ln(p/p_{ref}) = \frac{324.6}{R} - \frac{96355.1}{RT} - \frac{83}{R} \ln \frac{T}{298.15}; p_{ref} = 1 \text{ Pa}$								
310.2	2.53	7.595	293.2	5.06	3.57	0.09	70.6	142.5
313.2	2.61	5.907	294.2	5.06	4.76	0.12	70.4	141.9
314.2	2.86	5.933	293.2	3.56	5.17	0.15	70.3	141.6
316.2	2.61	4.641	293.2	5.06	6.03	0.18	70.1	141.0
319.2	2.82	3.797	293.2	5.06	7.96	0.22	69.9	140.4
322.2	2.89	3.067	293.2	4.00	10.09	0.28	69.6	139.6
325.2	2.81	2.400	293.2	4.00	12.54	0.34	69.4	138.6
328.2	3.13	2.133	293.2	4.00	15.73	0.42	69.1	137.8
331.2	2.96	1.600	292.2	3.00	19.73	0.52	68.9	137.0
334.2	3.41	1.500	293.2	3.00	24.36	0.63	68.6	136.2
337.2	2.96	1.000	292.2	3.00	31.58	0.81	68.4	135.8
340.2	2.84	0.800	292.2	2.40	37.85	0.97	68.1	134.8
343.2	2.98	0.667	293.2	2.00	47.96	1.22	67.9	134.3
343.2	2.97	0.667	292.2	2.00	47.64	1.22	67.9	134.2
346.2	2.63	0.480	292.2	1.44	58.49	1.49	67.6	133.5
349.2	3.20	0.480	292.2	1.44	71.08	1.80	67.4	132.7
352.2	3.24	0.400	293.2	1.20	86.82	2.20	67.1	132.0
355.2	2.99	0.300	292.2	1.20	106.49	2.69	66.9	131.4
358.2	3.54	0.290	292.2	1.20	130.14	3.28	66.6	130.8
361.2	4.32	0.290	292.2	1.20	158.73	3.99	66.4	130.2

tri-n-hexyl-amine: $\Delta_1^g H_m^o(298.15 \text{ K}) = (82.7 \pm 0.8) \text{ kJ} \cdot \text{mol}^{-1}$

$$\ln(p/p_{ref}) = \frac{344.1}{R} - \frac{109241.9}{RT} - \frac{89}{R} \ln \frac{T}{298.15}; p_{ref} = 1 \text{ Pa}$$

328.2	1.08	6.919	293.2	5.06	1.41	0.04	80.0	151.0
334.2	1.02	4.000	293.2	4.00	2.30	0.06	79.5	149.1
337.2	0.90	2.800	293.2	4.00	2.92	0.08	79.2	148.2
340.2	2.85	6.780	293.2	3.60	3.80	0.10	79.0	147.5
343.4	1.26	2.280	293.2	3.60	5.01	0.15	78.7	146.8
346.2	2.61	3.797	293.2	5.06	6.20	0.18	78.4	146.0
348.2	1.31	1.667	293.2	4.00	7.11	0.20	78.3	145.4
352.2	2.87	2.616	293.2	5.06	9.91	0.27	77.9	144.6
355.2	2.54	1.860	293.2	3.60	12.35	0.33	77.6	143.8
357.2	0.96	0.600	293.2	2.00	14.42	0.39	77.5	143.3
358.2	2.13	1.250	293.2	3.00	15.44	0.41	77.4	143.1
360.2	0.97	0.500	293.2	2.00	17.46	0.46	77.2	142.4
361.2	2.62	1.200	293.2	3.60	19.71	0.52	77.1	142.5
364.2	2.64	1.000	293.2	3.00	23.83	0.62	76.8	141.6
366.2	1.21	0.400	293.2	1.20	27.41	0.71	76.7	141.2
367.2	2.13	0.667	293.2	2.00	28.83	0.75	76.6	140.8
370.2	2.57	0.667	293.2	2.00	34.79	0.89	76.3	139.9

tri-n-heptyl-amine: $\Delta_f^{\text{g}}H_m^{\text{o}}(298.15 \text{ K}) = (95.7 \pm 0.8) \text{ kJ} \cdot \text{mol}^{-1}$

$$\ln(p/p_{\text{ref}}) = \frac{372.1}{R} - \frac{125240.8}{RT} - \frac{99}{R} \ln \frac{T}{298.15}; p_{\text{ref}} = 1 \text{ Pa}$$

327.8	1.57	122.233	294.0	9.50	0.100	0.008	92.8	168.3
333.2	2.19	103.193	294.0	9.20	0.167	0.009	92.3	166.3
338.3	1.46	40.403	294.0	9.20	0.283	0.012	91.8	165.0
341.5	1.73	36.033	294.0	9.20	0.377	0.014	91.4	163.9
345.2	1.18	17.733	294.0	9.50	0.522	0.018	91.1	162.7
348.3	1.24	14.250	294.0	9.50	0.682	0.022	90.8	161.7
349.6	1.32	13.391	294.0	9.13	0.774	0.024	90.6	161.4
351.3	1.80	15.333	294.0	9.20	0.920	0.028	90.5	161.1
353.5	2.28	16.434	294.0	9.13	1.089	0.032	90.2	160.3
355.5	1.78	10.733	294.0	9.20	1.301	0.038	90.1	159.8
357.4	1.42	7.152	294.0	9.13	1.555	0.044	89.9	159.4
358.2	1.42	6.808	294.0	9.50	1.634	0.046	89.8	159.0
359.4	1.75	7.667	294.0	9.20	1.790	0.050	89.7	158.6
361.4	1.51	5.420	294.0	8.13	2.183	0.060	89.5	158.4
362.5	1.69	5.420	294.0	8.13	2.445	0.066	89.4	158.2
363.5	1.60	4.743	294.0	8.13	2.645	0.071	89.3	158.0
365.6	1.65	4.201	294.0	8.13	3.076	0.082	89.1	157.2
366.5	2.20	5.285	294.0	8.13	3.269	0.087	89.0	156.9
368.4	1.30	2.710	294.0	8.13	3.773	0.099	88.8	156.3
369.5	2.17	4.065	294.0	8.13	4.191	0.110	88.7	156.2
371.6	1.30	2.033	294.0	8.13	5.007	0.150	88.5	155.7
372.6	2.32	3.388	294.0	8.13	5.379	0.159	88.4	155.4

tri-n-octyl-amine: $\Delta_f^{\text{g}}H_m^{\text{o}}(298.15 \text{ K}) = (106.5 \pm 1.0) \text{ kJ} \cdot \text{mol}^{-1}$

$$\ln(p/p_{\text{ref}}) = \frac{405.8}{R} - \frac{142250.5}{RT} - \frac{120}{R} \ln \frac{T}{298.15}; p_{\text{ref}} = 1 \text{ Pa}$$

348.2	0.21	18.538	298.7	4.47	0.0787	0.0070	100.5	171.7
350.3	0.23	16.753	297.1	4.57	0.0958	0.0074	100.2	170.9
351.2	0.04	2.689	295.3	4.03	0.1037	0.0076	100.1	170.5
353.2	0.30	16.729	303.8	1.25	0.1264	0.0082	99.9	169.9
354.2	0.23	11.854	298.2	4.57	0.1339	0.0083	99.8	169.2
356.2	0.23	9.900	299.3	4.57	0.1664	0.0092	99.5	168.8
357.0	0.09	3.569	296.2	4.04	0.1778	0.0094	99.4	168.4
360.1	0.27	7.722	296.2	4.10	0.2391	0.0110	99.0	167.5
361.0	0.22	5.956	298.2	4.47	0.2587	0.0115	98.9	167.1
363.0	0.09	2.034	297.4	4.07	0.3040	0.0126	98.7	166.3
363.0	0.19	4.263	300.6	4.74	0.3094	0.0127	98.7	166.5

364.9	0.23	4.339	293.2	4.49	0.3677	0.0142	98.5	165.8
365.9	0.11	2.002	299.0	4.00	0.4009	0.0150	98.3	165.5
367.0	0.23	3.764	299.3	4.47	0.4377	0.0159	98.2	165.1
368.9	0.36	4.938	299.0	4.00	0.5189	0.0180	98.0	164.5
368.9	0.22	2.978	298.2	4.47	0.5200	0.0180	98.0	164.5
371.0	0.24	2.582	297.2	4.56	0.6384	0.0210	97.7	164.0
372.7	0.22	2.142	296.2	4.57	0.7253	0.0231	97.5	163.3
372.8	0.23	2.159	300.5	4.05	0.7408	0.0235	97.5	163.4
375.2	0.24	1.899	298.2	4.56	0.9013	0.0275	97.2	162.6
375.7	0.23	1.638	298.3	4.47	0.9648	0.0291	97.2	162.7

^a Saturation temperature measured with the standard uncertainty ($u(T) = 0.1$ K).

^b Mass of transferred sample condensed at $T = 243$ K.

^c Volume of nitrogen ($u(V) = 0.005$ dm³) used to transfer m ($u(m) = 0.0001$ g) of the sample. Uncertainties are given as standard uncertainties.

^d T_a is the temperature of the soap bubble meter used for measurement of the gas flow.

^e Vapour pressure at temperature T , calculated from the m and the residual vapour pressure at the condensation temperature calculated by an iteration procedure.

^f Standard uncertainties were calculated with $u(p_i/\text{Pa}) = 0.005 + 0.025(p_i/\text{Pa})$ for pressures below 5 Pa and with $u(p_i/\text{Pa}) = 0.025 + 0.025(p_i/\text{Pa})$ for pressures from 5 to 3000 Pa. The standard uncertainties for T , V , p , m , are standard uncertainties with 0.683 confidence level. Uncertainty of the vaporization/sublimation enthalpy $U(\Delta_{l,cr}^g H_m^o)$ is the expanded uncertainty (0.95 level of confidence) calculated according to procedure described elsewhere [28,29]. Uncertainties include uncertainties from the experimental conditions and the fitting equation, vapour pressures, and uncertainties from adjustment of vaporization enthalpies to the reference temperature $T = 298.15$ K.

Table A.2 Results of Knudsen effusion method for tri-phenyl-amine: absolute vapor pressures p , standard molar sublimation enthalpies and standard molar sublimation entropies

$T/$ K ^a	$m/$ mg ^b	$t/$ s	$p/$ Pa ^c	$u(p)/$ Pa ^d	$\Delta_{cr}^g H_m^o(T)/$ kJ·mol ⁻¹	$\Delta_{cr}^g S_m^o(T)/$ J·K ⁻¹ ·mol ⁻¹
tri-phenylamine: $\Delta_{cr}^g H_m^o(298.15 \text{ K}) = (121.3 \pm 2.9) \text{ kJ} \cdot \text{mol}^{-1}$						
$\ln(p/p_{ref}) = \frac{387.3}{R} - \frac{136075.7}{RT} - \frac{49.6}{R} \ln \frac{T}{298.15}; p_{ref} = 1 \text{ Pa}$						
374.91	129.06	9955	4.710E+00	-8.256E-02	117.5	230.5
373.24	11.33	4500	3.490E+00	-5.586E-01	117.6	229.6
368.25	14.06	2177	2.460E+00	3.825E-02	117.8	231.7
363.69	10.86	2927	1.460E+00	-3.420E-02	118.0	232.0
358.86	12.73	1919	9.400E-01	5.691E-02	118.3	233.4
353.71	12.15	9521	5.200E-01	2.446E-02	118.5	233.9
348.26	11.42	6018	2.800E-01	1.647E-02	118.8	234.8
343.70	24.72	61080	1.700E-01	1.717E-02	119.0	235.9
338.78	13.08	57660	9.000E-02	6.587E-03	119.3	236.3
328.49	10.19	63060	2.000E-02	-2.077E-03	119.8	236.4
323.26	16.56	235500	1.000E-02	-8.503E-04	120.0	237.3

^a Saturation temperature measured with the standard uncertainty ($u(T) = 0.1$ K).

^b Mass loss of the sample measured by weighing.

^c Vapour pressure at temperature T , calculated from the m .

^d Standard uncertainties were calculated with $u(p_i/\text{Pa}) = 0.005 + 0.025(p_i/\text{Pa})$ for pressures below 5 Pa. Uncertainty of the sublimation enthalpy $U(\Delta_{cr}^g H_m^o)$ is the expanded uncertainty (0.95 level of confidence) calculated according to procedure described elsewhere [28,29]. Uncertainties include uncertainties from the experimental conditions and the fitting equation, vapour pressures, and uncertainties from adjustment of vaporization enthalpies to the reference temperature $T = 298.15$ K.

Table A.3 Results from the Knudsen Method: absolute vapour pressures p_i , standard molar sublimation enthalpies $\Delta_{\text{cr}}^{\text{g}}H_m^{\text{o}}$ and standard molar sublimation entropies $\Delta_{\text{cr}}^{\text{g}}S_m^{\text{o}}$ measured in this work

$T/$ K ^a	$m/$ mg	t/s	$p_i/$ Pa ^b	$u(p_i)/$ Pa ^c	$\Delta_{\text{cr}}^{\text{g}}H_m^{\text{o}}(T)/$ kJ·mol ⁻¹	$\Delta_{\text{cr}}^{\text{g}}S_m^{\text{o}}(T)/$ J·K ⁻¹ ·mol ⁻¹	Exp-calc (%)
flurbiprofen , $\Delta_{\text{cr}}^{\text{g}}H_m^{\text{o}}(298.15 \text{ K}) = (136.1 \pm 0.9) \text{ kJ}\cdot\text{mol}^{-1}$ $\Delta_{\text{cr}}^{\text{g}}S_m^{\text{o}}(298.15 \text{ K}) = (236.0 \pm 1.0) \text{ J}\cdot\text{mol}^{-1}\cdot\text{K}^{-1}$ $\Delta_{\text{cr}}^{\text{g}}G_m^{\text{o}}(298.15 \text{ K}) = (57.68 \pm 0.03) \text{ kJ}\cdot\text{mol}^{-1}$							
$\ln(p_i/p_{\text{ref}}) = \frac{404.2}{R} - \frac{149640.9}{RT} - \frac{45.4}{R} \ln \frac{T}{298.15}; p_{\text{ref}} = 1 \text{ Pa}$							
347.10	10.51	265860	1.69E-02	-1.20E-04	133.9	256.1	-0.71
353.05	12.58	146940	3.69E-02	-3.18E-04	133.6	255.3	-0.86
357.51	9.74	62160	6.77E-02	2.09E-03	133.4	255.0	3.09
363.16	19.06	62168	1.33E-01	8.52E-04	133.2	254.1	0.64
367.66	9.36	18245	2.22E-01	-4.18E-03	132.9	253.4	-1.89
373.38	16.51	58728	4.38E-01	-2.18E-03	132.7	252.8	-0.50
373.59	12.55	12076	4.45E-01	-5.58E-03	132.7	252.7	-1.25
380.27	12.73	20354	9.59E-01	5.98E-03	132.4	252.0	0.62
380.64	13.22	5513	1.00E+00	7.66E-03	132.4	252.0	0.77
(S)-naproxen methyl ester , $\Delta_{\text{cr}}^{\text{g}}H_m^{\text{o}}(298.15 \text{ K}) = (120.9 \pm 0.8) \text{ kJ}\cdot\text{mol}^{-1}$ $\Delta_{\text{cr}}^{\text{g}}S_m^{\text{o}}(298.15 \text{ K}) = (241.6 \pm 1.6) \text{ J}\cdot\text{mol}^{-1}\cdot\text{K}^{-1}$ $\Delta_{\text{cr}}^{\text{g}}G_m^{\text{o}}(298.15 \text{ K}) = (48.90 \pm 0.03) \text{ kJ}\cdot\text{mol}^{-1}$							
$\ln(p_i/p_{\text{ref}}) = \frac{385.8}{R} - \frac{135352.8}{RT} - \frac{48.5}{R} \ln \frac{T}{298.15}; p_{\text{ref}} = 1 \text{ Pa}$							
323.90	13.85	434460	1.301E-02	-5.625E-05	119.6	237.6	-0.43
327.70	11.65	221340	2.158E-02	-2.884E-04	119.5	236.9	-1.34
333.86	19.28	158400	5.021E-02	1.173E-03	119.2	236.3	2.34
338.78	13.64	61379	9.194E-02	5.384E-04	118.9	235.5	0.59
347.91	11.34	61440	2.782E-01	1.850E-03	118.5	234.2	0.66
350.77	12.57	13713	3.758E-01	-1.007E-02	118.3	233.5	-2.68
357.25	13.01	24170	7.994E-01	-5.352E-03	118.0	232.8	-0.67
357.89	22.85	10409	8.767E-01	1.264E-02	118.0	232.9	1.44

^a Experimental temperature ($u(T) = 0.05 \text{ K}$).

^b Vapour pressure at temperature T , calculated from the mass loss m , determined gravimetrically with ($u(m) = 0.00001 \text{ g}$)

^c Uncertainties were calculated with $u(p_i/\text{Pa}) = 0.005 + 0.025(p_i/\text{Pa})$ for pressures below 5 Pa. The uncertainty for the thermodynamic functions of sublimation are standard uncertainties with 0.683 confidence level, calculated according to procedure described elsewhere [28,29]. The standard uncertainty of sublimation enthalpy $u(\Delta_{\text{cr}}^{\text{g}}H_m^{\text{o}})$ includes uncertainties from experimental conditions, uncertainties of vapour pressure, uncertainties from fitting equation, and uncertainties from temperature adjustment to $T = 298.15 \text{ K}$.

B. Supporting information for chapter 3

Table B.1 Results of transpiration method for 1-phenyl-naphthalene: absolute vapor pressures p , standard molar vaporization enthalpies and standard molar vaporization/ entropies

$T/$ K ^a	$m/$ mg ^b	$V(N_2)^c /$ dm ³	$T_a/$ K ^d	Flow/ dm ³ ·h ⁻¹	$p/$ Pa ^e	$u(p)/$ Pa ^f	$\Delta_1^g H_m^o(T)/$ kJ·mol ⁻¹	$\Delta_1^g S_m^o(T)/$ J·K ⁻¹ ·mol ⁻¹
1-phenyl-naphthalene: $\Delta_1^g H_m^o(298.15 \text{ K}) = (83.2 \pm 0.5) \text{ kJ} \cdot \text{mol}^{-1}$								
$\ln(p/p_{ref}) = \frac{341.0}{R} - \frac{110456.0}{RT} - \frac{91.4}{R} \ln \frac{T}{298.15}; p_{ref} = 1 \text{ Pa}$								
313.1	1.20	101.0	293.4	5.31	0.141	0.009	81.8	149.4
318.2	1.83	90.17	294.5	5.27	0.243	0.011	81.4	148.3
323.5	3.29	104.5	303.2	5.31	0.388	0.015	80.9	146.5
329.2	5.98	114.2	297.2	5.31	0.634	0.021	80.4	144.7
331.0	5.42	86.24	297.3	4.84	0.760	0.024	80.2	144.3
333.1	7.06	94.09	296.7	5.31	0.906	0.028	80.0	143.7
335.9	1.51	15.93	296.4	5.31	1.14	0.03	79.8	142.9
339.4	1.88	14.65	296.2	5.31	1.55	0.04	79.4	142.0
342.4	1.67	10.13	294.7	5.31	1.98	0.05	79.2	141.2
345.8	1.99	8.896	293.7	5.31	2.68	0.07	78.9	140.5
350.4	2.70	8.498	294.2	5.31	3.80	0.10	78.4	139.3
354.2	3.81	9.073	296.4	5.31	5.06	0.15	78.1	138.2
357.7	2.86	5.311	294.2	5.31	6.44	0.19	77.8	137.2
362.0	8.28	11.29	297.0	5.31	8.86	0.25	77.4	136.2
362.1	3.20	4.337	298.7	5.31	8.96	0.25	77.4	136.2
362.9	2.34	3.010	294.2	5.31	9.32	0.26	77.3	135.9
365.8	6.23	6.550	301.7	5.31	11.67	0.32	77.0	135.3
366.0	2.91	2.996	296.2	5.31	11.70	0.32	77.0	135.2
369.5	2.81	2.257	294.2	5.31	14.89	0.40	76.7	134.3
369.8	6.88	5.355	296.4	5.31	15.49	0.41	76.7	134.4

^a Saturation temperature measured with the standard uncertainty ($u(T) = 0.1 \text{ K}$).

^b Mass loss of the sample measured by weighing.

^c Vapour pressure at temperature T , calculated from the m .

^d Standard uncertainties were calculated with $u(p_i/\text{Pa}) = 0.005 + 0.025(p_i/\text{Pa})$ for pressures below 5 Pa and with $u(p_i/\text{Pa}) = 0.025 + 0.025(p_i/\text{Pa})$ for pressures from 5 to 3000 Pa. The standard uncertainties for T , V , p , m , are standard uncertainties with 0.683 confidence level. Uncertainty of the vaporization/sublimation enthalpy $U(\Delta_{l,cr}^g H_m^o)$ is the expanded uncertainty (0.95 level of confidence) calculated according to procedure described elsewhere [28,29]. Uncertainties include uncertainties from the experimental conditions and the fitting equation, vapour pressures, and uncertainties from adjustment of vaporization enthalpies to the reference temperature $T = 298.15 \text{ K}$.

Table B.2 Results of Knudsen effusion method for aromatic compounds: absolute vapor pressures p , standard molar vaporization/sublimation enthalpies and standard molar vaporization/sublimation entropies.

$T/$ K ^a	$m/$ mg ^b	$t, \text{ s}$	$p/$ Pa ^c	$u(p)/$ Pa ^d	$\Delta_{l,cr}^g H_m^o(T)/$ kJ·mol ⁻¹	$\Delta_{l,cr}^g S_m^o(T)/$ J·K ⁻¹ ·mol ⁻¹
m-quinquephenyl: $\Delta_1^g H_m^o(298.15 \text{ K}) = (130.5 \pm 1.1) \text{ kJ} \cdot \text{mol}^{-1}$						
$\ln(p/p_{ref}) = \frac{453.4}{R} - \frac{171160.7}{RT} - \frac{136.5}{R} \ln \frac{T}{298.15}; p_{ref} = 1 \text{ Pa}$						
388.68	11.12	80220	6.17E-02	1.52E-04	118.1	185.0
393.59	17.19	79080	9.71E-02	1.69E-04	117.4	183.3
399.16	6.53	18426	1.59E-01	-1.12E-03	116.7	181.3
403.52	12.68	81840	2.33E-01	-3.50E-04	116.1	179.8
409.24	12.03	14137	3.79E-01	1.65E-03	115.3	178.0
p-quinquephenyl: $\Delta_{cr}^g H_m^o(298.15 \text{ K}) = (168.6 \pm 3.4) \text{ kJ} \cdot \text{mol}^{-1}$						
$\ln(p/p_{ref}) = \frac{417.0}{R} - \frac{185108.5}{RT} - \frac{55.3}{R} \ln \frac{T}{298.15}; p_{ref} = 1 \text{ Pa}$						
438.68	20.28	236640	4.24E-02	2.84E-04	160.8	244.7

444.04	11.15	76080	7.29E-02	1.11E-03	160.6	244.1
448.93	14.07	62220	1.13E-01	-2.45E-03	160.3	243.2
456.55	11.7	25775	2.27E-01	-9.09E-03	159.9	242.1
459.50	7.91	12158	3.24E-01	1.52E-02	159.7	242.5
464.21	16.65	17750	4.66E-01	-5.96E-03	159.4	241.4
468.38	12.34	10050	6.71E-01	-1.01E-02	159.2	240.9
472.50	9.75	15721	9.91E-01	1.80E-02	159.0	240.7

1,2,3,4-terphenylnaphthalene: $\Delta_{\text{cr}}^{\text{g}}H_{\text{m}}^{\text{o}}(298.15 \text{ K}) = (156.7 \pm 1.5) \text{ kJ}\cdot\text{mol}^{-1}$

$$\ln(p/p_{\text{ref}}) = \frac{428.0}{R} - \frac{178900.3}{RT} - \frac{74.5}{R} \ln \frac{T}{298.15}; p_{\text{ref}} = 1 \text{ Pa}$$

405.73	9.11	261420	1.32E-02	-1.36E-04	148.7	234.8
423.63	13.88	61620	8.68E-02	1.42E-03	147.3	231.8
428.58	22.17	61320	1.39E-01	1.04E-03	147.0	230.8
443.84	11.03	7341	5.69E-01	1.27E-03	145.8	228.2
448.36	10.54	4795	8.24E-01	-2.23E-02	145.5	227.2
453.05	10.79	3124	1.27E+00	4.31E-03	145.1	226.6
453.21	13.2	13220	1.26E+00	-2.47E-02	145.1	226.4
455.82	14.25	10800	1.64E+00	4.32E-02	144.9	226.4

9,10-diphenyl-anthracene: $\Delta_{\text{cr}}^{\text{g}}H_{\text{m}}^{\text{o}}(298.15 \text{ K}) = (154.6 \pm 2.7) \text{ kJ}\cdot\text{mol}^{-1}$

$$\ln(p/p_{\text{ref}}) = \frac{410.6}{R} - \frac{171866.2}{RT} - \frac{58.0}{R} \ln \frac{T}{298.15}; p_{\text{ref}} = 1 \text{ Pa}$$

415.63	11.92	81660	7.67E-02	7.15E-03	147.8	238.4
434.55	11.73	12529	4.91E-01	4.70E-02	146.7	235.9
428.73	10.71	21600	2.62E-01	5.45E-03	147.0	236.0
404.02	7.52	227400	1.72E-02	-3.10E-03	148.4	237.9
438.88	13.09	10200	6.71E-01	8.10E-03	146.4	234.6
448.91	11.98	3660	1.67E+00	4.74E-02	145.8	233.4
443.63	11.18	6180	9.41E-01	-7.76E-02	146.1	233.2
454.01	11.87	2398	2.49E+00	-2.78E-02	145.5	232.4
433.56	17.24	61260	4.41E-01	3.57E-02	146.7	235.9
428.67	13.54	82500	2.58E-01	3.56E-03	147.0	235.9
463.12	13.62	4030	4.84E+00	-5.23E-01	145.0	230.5

^a Saturation temperature measured with the standard uncertainty ($u(T) = 0.1 \text{ K}$).

^b Mass loss of the sample measured by weighing.

^c Vapour pressure at temperature T , calculated from the m .

^d Standard uncertainties were calculated with $u(p_i/\text{Pa}) = 0.005 + 0.025(p_i/\text{Pa})$ for pressures below 5 Pa. Uncertainty of the vaporization/sublimation enthalpy $U(\Delta_{\text{l,cr}}^{\text{g}}H_{\text{m}}^{\text{o}})$ is the expanded uncertainty (0.95 level of confidence) calculated according to procedure described elsewhere [28,29]. Uncertainties include uncertainties from the experimental conditions and the fitting equation, vapour pressures, and uncertainties from adjustment of vaporization enthalpies to the reference temperature $T = 298.15 \text{ K}$.

Table B.3 Results of transpiration method: absolute vapour pressures p , standard ($p^{\circ} = 0.1 \text{ MPa}$) molar vaporization enthalpies and standard ($p^{\circ} = 0.1 \text{ MPa}$) molar vaporization entropies.

$T/$ K ^a	$m/$ mg ^b	$V(\text{N}_2)^c /$ dm ³	$T_a/$ K ^d	Flow/ dm ³ ·h ⁻¹	$p/$ Pa ^c	$u(p)/$ Pa ^f	$\Delta_{\text{l}}^{\text{g}}H_{\text{m}}^{\text{o}}(T)$ kJ·mol ⁻¹	$\Delta_{\text{l}}^{\text{g}}S_{\text{m}}^{\text{o}}(T)$ J·K ⁻¹ ·mol ⁻¹
------------------------	-------------------------	--	--------------------------	---	-------------------------	----------------------------	--	--

1-phenyl-2-butanone: $\Delta_{\text{l}}^{\text{g}}H_{\text{m}}^{\text{o}}(298.15 \text{ K}) = (63.7 \pm 0.7) \text{ kJ}\cdot\text{mol}^{-1}$

$$\ln(p/p_{\text{ref}}) = \frac{312.7}{R} - \frac{88001.1}{RT} - \frac{81.4}{R} \ln \frac{T}{298.15}; p_{\text{ref}} = 1 \text{ Pa}$$

295.3	1.03	2.737	295.3	5.13	6.28	0.18	64.0	136.2
295.4	1.35	3.377	295.3	1.88	6.66	0.19	64.0	136.6
298.2	1.24	2.566	297.7	5.13	8.13	0.23	63.7	135.5
300.2	0.76	1.301	295.7	2.69	9.67	0.27	63.6	134.9

301.1	1.11	1.796	298.0	5.13	10.34	0.28	63.5	134.6
305.2	0.35	0.405	296.0	0.97	14.56	0.39	63.2	133.5
306.2	1.34	1.348	296.3	3.24	16.57	0.44	63.1	133.7
310.2	1.31	0.971	296.7	3.24	22.45	0.59	62.8	132.5
315.2	1.61	0.809	297.3	3.24	33.22	0.86	62.3	131.2
320.2	1.99	0.711	297.6	2.24	46.82	1.20	61.9	129.7
325.1	0.98	0.249	297.8	1.00	65.77	1.67	61.5	128.4
330.0	1.36	0.249	298.2	1.00	91.05	2.30	61.1	127.1
335.1	1.76	0.232	295.9	0.93	126.25	3.18	60.7	125.8
340.2	2.65	0.239	298.5	0.93	184.94	4.65	60.3	125.0
345.2	3.61	0.239	299.2	0.93	252.71	6.34	59.9	123.8

4-phenyl-2-butanone: $\Delta_f^{\ominus}H_m^{\ominus}(298.15\text{ K}) = (63.2 \pm 0.8)\text{ kJ}\cdot\text{mol}^{-1}$

$$\ln(p/p_{ref}) = \frac{308.8}{R} - \frac{87479.0}{RT} - \frac{81.4}{R} \ln \frac{T}{298.15}; p_{ref} = 1\text{ Pa}$$

293.2	1.03	4.103	294.8	2.39	4.19	0.11	63.6	133.2
296.7	1.30	3.784	294.8	2.39	5.72	0.17	63.3	132.3
302.8	1.38	2.430	294.8	2.39	9.41	0.26	62.8	130.5
305.4	1.27	1.832	294.8	2.39	11.44	0.31	62.6	129.6
308.3	1.27	1.514	294.8	2.39	13.84	0.37	62.4	128.5
311.1	1.32	1.195	294.8	2.39	18.23	0.48	62.2	128.2
313.9	1.35	0.996	294.8	2.39	22.51	0.59	61.9	127.5
316.7	1.35	0.797	294.8	2.39	28.13	0.73	61.7	126.9
317.4	2.48	1.429	294.8	3.50	28.72	0.74	61.6	126.4
319.6	1.33	0.637	294.8	2.39	34.49	0.89	61.5	126.1
322.4	1.33	0.518	294.8	2.39	42.44	1.09	61.2	125.4
325.2	1.48	0.478	294.8	2.39	51.29	1.31	61.0	124.7
328.0	1.85	0.478	294.8	2.39	64.11	1.63	60.8	124.2
330.6	1.97	0.438	294.8	2.39	74.27	1.88	60.6	123.3
330.8	3.27	0.729	294.8	3.50	74.22	1.88	60.6	123.2
333.5	1.92	0.359	294.8	2.39	88.40	2.23	60.3	122.5

1,3-diphenyl-1-propanone: $\Delta_f^{\ominus}H_m^{\ominus}(298.15\text{ K}) = (85.2 \pm 1.0)\text{ kJ}\cdot\text{mol}^{-1}$

$$\ln(p/p_{ref}) = \frac{355.6}{R} - \frac{116387.5}{RT} - \frac{104.6}{R} \ln \frac{T}{298.15}; p_{ref} = 1\text{ Pa}$$

368.8	1.77	2.448	293.7	2.94	8.41	0.24	77.8	133.0
371.8	1.69	1.955	295.9	1.09	10.13	0.28	77.5	131.9
373.0	1.71	1.758	293.7	1.41	11.33	0.31	77.4	131.9
375.0	3.59	3.260	293.7	2.20	12.80	0.34	77.2	131.2
377.9	1.70	1.261	293.7	1.01	15.65	0.42	76.9	130.5
378.0	1.14	0.821	294.7	1.33	16.12	0.43	76.8	130.7
383.2	0.81	0.444	294.7	1.33	21.23	0.56	76.3	128.8
388.4	1.55	0.609	293.7	1.41	29.55	0.76	75.8	127.5
393.2	1.64	0.480	294.2	1.37	39.67	1.02	75.3	126.3
396.3	1.70	0.416	295.9	1.09	47.80	1.22	74.9	125.5
398.3	1.74	0.378	293.7	1.01	53.29	1.36	74.7	125.0
400.5	2.10	0.407	295.9	1.09	60.21	1.53	74.5	124.4
403.4	2.13	0.351	294.7	1.05	70.72	1.79	74.2	123.6

1,3-diphenyl-2-propanone: $\Delta_f^{\ominus}H_m^{\ominus}(298.15\text{ K}) = (89.4 \pm 0.8)\text{ kJ}\cdot\text{mol}^{-1}$

$$\ln(p/p_{ref}) = \frac{368.8}{R} - \frac{120595.6}{RT} - \frac{104.6}{R} \ln \frac{T}{298.15}; p_{ref} = 1\text{ Pa}$$

315.7	0.33	38.034	295.9	2.11	0.1012	0.0075	87.6	162.6
-------	------	--------	-------	------	--------	--------	------	-------

320.6	0.33	23.553	295.9	5.23	0.1620	0.0090	87.1	160.8
325.6	0.41	18.436	295.9	5.40	0.2633	0.0116	86.5	159.0
326.2	0.28	11.786	295.9	5.57	0.2796	0.0120	86.5	158.8
326.7	0.81	31.410	295.9	5.35	0.3006	0.0125	86.4	158.8
330.6	0.37	9.412	295.9	5.38	0.4574	0.0164	86.0	158.0
331.2	0.35	8.813	295.9	5.40	0.4618	0.0165	86.0	157.4
335.3	0.42	6.974	296.4	2.99	0.6973	0.0224	85.5	156.3
335.7	0.55	8.967	295.9	5.38	0.7202	0.0230	85.5	156.2
335.7	0.38	6.277	295.9	5.38	0.7017	0.0225	85.5	156.0
337.7	0.41	5.647	295.7	5.38	0.8506	0.0263	85.3	155.5
338.1	0.38	5.049	295.9	5.32	0.8897	0.0272	85.2	155.4
340.6	0.43	4.661	295.9	5.48	1.0706	0.0318	85.0	154.3
340.7	0.74	8.160	295.9	5.38	1.0656	0.0316	85.0	154.2
344.0	0.40	3.100	295.9	5.32	1.5218	0.0430	84.6	153.7
345.6	0.88	6.187	295.9	5.38	1.6647	0.0466	84.4	152.8
345.7	0.50	3.407	295.9	5.38	1.7229	0.0481	84.4	153.1
350.3	0.57	2.590	296.6	2.99	2.5739	0.0693	84.0	151.8
350.7	0.38	1.736	295.9	5.48	2.5613	0.0690	83.9	151.4
354.0	0.41	1.428	295.9	5.35	3.3205	0.0880	83.6	150.4
355.3	0.50	1.544	296.7	2.99	3.8342	0.1009	83.4	150.3
359.9	0.43	0.934	295.9	2.00	5.4155	0.1604	83.0	148.8
360.3	0.71	1.495	297.0	2.99	5.5403	0.1635	82.9	148.6
363.9	0.52	0.850	295.9	2.00	7.0888	0.2022	82.5	147.4

^a Saturation temperature measured with the standard uncertainty ($u(T) = 0.1$ K).

^b Mass of transferred sample condensed at $T = 243$ K.

^c Volume of nitrogen ($u(V) = 0.005$ dm³) used to transfer m ($u(m) = 0.0001$ g) of the sample. Uncertainties are given as standard uncertainties.

^d T_a is the temperature of the soap bubble meter used for measurement of the gas flow.

^e Vapour pressure at temperature T , calculated from the m and the residual vapour pressure at the condensation temperature calculated by an iteration procedure.

^f Standard uncertainties were calculated with $u(p/\text{Pa}) = 0.005 + 0.025(p/\text{Pa})$ for pressures below 5 Pa and with $u(p/\text{Pa}) = 0.025 + 0.025(p/\text{Pa})$ for pressures from 5 to 3000 Pa. The standard uncertainties for T , V , p , m , are standard uncertainties with 0.683 confidence level. Uncertainties of the vaporization enthalpies are expressed as the expanded uncertainty (0.95 level of confidence, $k = 2$). They were calculated according to a procedure described elsewhere [28,29]. Uncertainties include uncertainties from the experimental conditions and the fitting equation, vapour pressures, and uncertainties from adjustment of vaporization/sublimation enthalpies to the reference temperature $T = 298.15$ K.

C. Supporting information for chapter 4

Table C.1 Results of transpiration method for substituted acetophenones and benzophenones: absolute vapor pressures p , standard molar vaporization/sublimation enthalpies and standard molar vaporization/sublimation entropies

$T/$ K ^a	$m/$ mg ^b	$V(\text{N}_2)^c /$ dm ³	$T_a/$ K ^d	Flow/ dm ³ ·h ⁻¹	$p/$ Pa ^e	$u(p)/$ Pa ^f	$\Delta_{\text{l,cr}}^g H_{\text{m}}^o(T)/$ kJ·mol ⁻¹	$\Delta_{\text{l,cr}}^g S_{\text{m}}^o(T)/$ J·K ⁻¹ ·mol ⁻¹
2'-methoxy-acetophenone: $\Delta_{\text{l}}^g H_{\text{m}}^o(298.15 \text{ K}) = (64.6 \pm 0.4) \text{ kJ} \cdot \text{mol}^{-1}$								
$\ln(p/p_{\text{ref}}) = \frac{306.1}{R} - \frac{88277.0}{RT} - \frac{79.5}{R} \ln \frac{T}{298.15}; p_{\text{ref}} = 1 \text{ Pa}$								
293.1	1.26	11.686	297.3	6.37	2.10	0.06	65.0	132.1
298.1	1.30	7.470	299.0	6.37	3.20	0.09	64.6	130.6
295.6	1.50	10.623	298.1	6.40	2.65	0.07	64.8	131.6
298.1	1.39	7.661	298.3	5.11	3.32	0.09	64.6	130.9
300.7	1.45	6.358	298.8	6.36	4.10	0.11	64.4	130.1
303.1	1.37	4.812	299.7	6.42	5.06	0.15	64.2	129.6
305.6	1.49	4.269	298.2	5.12	6.09	0.18	64.0	128.7

308.2	1.46	3.227	300.7	6.45	7.83	0.22	63.8	128.4
310.6	1.59	3.000	299.4	5.14	9.12	0.25	63.6	127.4
313.2	1.31	1.925	297.3	2.89	11.57	0.31	63.4	127.0
314.1	1.44	1.943	299.2	2.92	12.57	0.34	63.3	126.9
315.6	1.42	1.693	297.7	2.90	14.18	0.38	63.2	126.5
318.2	1.48	1.440	296.3	2.88	17.17	0.45	63.0	125.9
320.7	1.48	1.201	298.5	2.88	20.72	0.54	62.8	125.2
323.2	1.44	0.958	296.0	2.87	24.90	0.65	62.6	124.7
325.7	1.38	0.792	297.9	1.06	29.12	0.75	62.4	123.9
328.1	1.48	0.713	295.6	1.07	34.19	0.88	62.2	123.2
330.7	1.50	0.605	294.0	1.04	40.57	1.04	62.0	122.5
333.1	1.41	0.481	295.0	1.07	48.07	1.23	61.8	122.0
335.7	1.50	0.430	294.0	1.03	57.18	1.45	61.6	121.4
338.2	1.72	0.413	294.4	1.08	68.16	1.73	61.4	120.9
340.6	1.65	0.343	294.6	1.03	78.58	1.99	61.2	120.2
342.2	1.81	0.345	295.2	1.04	85.95	2.17	61.1	119.8
343.2	1.91	0.341	294.6	1.08	91.33	2.31	61.0	119.6
344.2	2.08	0.345	295.4	1.03	98.77	2.49	60.9	119.5
348.1	2.71	0.361	294.1	1.08	122.28	3.08	60.6	118.4

3'-methoxy-acetophenone: $\Delta_1^{\text{g}}H_{\text{m}}^{\text{o}}(298.15 \text{ K}) = (65.8 \pm 0.4) \text{ kJ} \cdot \text{mol}^{-1}$

$$\ln(p/p_{\text{ref}}) = \frac{308.6}{R} - \frac{89512.3}{RT} - \frac{79.5}{R} \ln \frac{T}{298.15}; p_{\text{ref}} = 1 \text{ Pa}$$

293.1	1.23	11.921	297.5	3.41	1.71	0.05	66.2	134.7
300.1	1.54	7.693	294.0	4.44	3.27	0.09	65.7	132.9
296.6	1.43	9.999	298.8	3.08	2.37	0.06	65.9	133.8
303.7	1.65	6.094	298.8	3.48	4.50	0.12	65.4	132.1
307.1	1.39	4.064	298.1	3.05	5.93	0.17	65.1	131.1
307.2	1.41	3.980	298.4	2.99	5.88	0.17	65.1	130.9
310.6	1.42	3.027	299.4	4.54	7.80	0.22	64.8	130.0
314.1	1.41	2.288	297.9	3.05	10.42	0.29	64.5	129.3
317.7	1.56	1.940	297.9	2.91	13.27	0.36	64.3	128.1
321.2	1.63	1.530	297.0	3.06	17.73	0.47	64.0	127.4
324.6	1.79	1.299	297.9	2.89	22.75	0.59	63.7	126.6
328.2	1.50	0.824	296.7	1.10	30.16	0.78	63.4	125.9
335.1	1.58	0.547	296.8	1.09	47.62	1.22	62.9	124.1
342.2	1.71	0.370	296.9	1.11	75.92	1.92	62.3	122.4
349.1	2.65	0.372	297.0	1.12	117.29	2.96	61.8	120.8
356.2	4.40	0.414	296.9	1.13	174.79	4.39	61.2	119.0
363.2	6.35	0.381	296.6	1.14	272.98	6.85	60.6	117.9

4'-methoxy-acetophenone: $\Delta_1^{\text{g}}H_{\text{m}}^{\text{o}}(298.15 \text{ K}) = (70.1 \pm 0.6) \text{ kJ} \cdot \text{mol}^{-1}$

$$\ln(p/p_{\text{ref}}) = \frac{316.1}{R} - \frac{93788.4}{RT} - \frac{79.5}{R} \ln \frac{T}{298.15}; p_{\text{ref}} = 1 \text{ Pa}$$

315.2	1.15	3.535	295.7	4.00	5.33	0.16	68.7	136.3
317.2	1.78	4.534	292.8	4.00	6.38	0.18	68.6	135.9
317.1	0.95	2.402	293.4	3.86	6.43	0.19	68.6	136.0
320.1	1.22	2.432	296.6	3.94	8.24	0.23	68.3	135.3
323.2	1.22	1.959	294.2	2.80	10.19	0.28	68.1	134.3
326.2	1.23	1.516	297.4	3.79	13.33	0.36	67.9	133.8
329.2	1.22	1.212	293.9	2.80	16.34	0.43	67.6	132.9
332.2	1.20	0.943	297.8	3.77	20.96	0.55	67.4	132.4

335.1	1.10	0.704	294.3	2.82	25.44	0.66	67.1	131.6
338.2	1.14	0.597	298.5	1.99	31.41	0.81	66.9	130.8
341.1	0.65	0.268	295.8	1.15	39.47	1.01	66.7	130.3
345.2	1.15	0.374	299.0	1.50	50.76	1.29	66.3	129.1
349.1	0.99	0.248	300.0	0.99	66.20	1.68	66.0	128.3
352.1	1.22	0.244	293.5	0.98	81.21	2.06	65.8	127.7
354.1	1.36	0.245	292.8	0.98	89.79	2.27	65.6	127.0

3'-methyl-benzophenone: $\Delta_1^{\text{g}}H_{\text{m}}^{\text{o}}(298.15 \text{ K}) = (80.4 \pm 0.6) \text{ kJ} \cdot \text{mol}^{-1}$

$$\ln(p/p_{\text{ref}}) = \frac{340.1}{R} - \frac{108842.0}{RT} - \frac{95.4}{R} \ln \frac{T}{298.15}; p_{\text{ref}} = 1 \text{ Pa}$$

303.2	0.13	18.906	297.5	4.93	0.085	0.007	79.92	147.4
308.2	0.13	11.508	295.3	4.93	0.142	0.009	79.44	145.8
308.3	0.02	2.140	295.8	3.05	0.142	0.009	79.43	145.7
313.2	0.14	7.371	296.6	3.05	0.236	0.011	78.97	144.5
318.2	0.12	3.863	296.9	3.05	0.376	0.014	78.49	142.8
320.2	0.14	3.863	297.0	4.93	0.458	0.016	78.30	142.3
323.2	0.15	3.152	296.1	3.05	0.577	0.019	78.01	141.1
323.2	0.14	3.152	297.4	3.05	0.574	0.019	78.01	141.1
328.2	0.16	2.237	296.8	3.05	0.892	0.027	77.54	139.6
333.2	0.23	2.135	299.5	3.05	1.346	0.039	77.06	138.1
338.2	0.21	1.271	297.5	3.05	2.072	0.057	76.58	136.8
341.2	0.24	1.162	295.6	3.03	2.618	0.070	76.29	135.9
344.2	0.24	0.909	296.2	3.03	3.288	0.087	76.01	135.0
347.2	0.25	0.720	296.8	1.96	4.324	0.113	75.72	134.6
350.2	0.25	0.589	297.4	1.96	5.270	0.157	75.44	133.5
353.2	0.25	0.467	297.9	1.00	6.852	0.196	75.15	133.1
356.2	0.25	0.383	298.4	1.00	8.316	0.233	74.87	132.1
359.2	0.24	0.292	298.7	1.00	10.281	0.282	74.58	131.3
362.2	0.25	0.250	298.9	1.00	12.417	0.335	74.29	130.4

2,2'-dihydroxy-benzophenone: $\Delta_1^{\text{g}}H_{\text{m}}^{\text{o}}(298.15 \text{ K}) = (84.9 \pm 0.9) \text{ kJ} \cdot \text{mol}^{-1}$

$$\ln(p/p_{\text{ref}}) = \frac{375.0}{R} - \frac{121793.3}{RT} - \frac{123.6}{R} \ln \frac{T}{298.15}; p_{\text{ref}} = 1 \text{ Pa}$$

363.1	0.69	1.274	295.7	2.94	6.18	0.18	76.9	131.3
368.2	1.55	2.065	295.9	1.18	8.62	0.24	76.3	129.4
363.2	1.31	2.439	295.2	1.18	6.14	0.18	76.9	131.1
368.6	1.29	1.666	295.9	1.02	8.89	0.25	76.2	129.3
373.5	1.62	1.475	295.9	1.18	12.59	0.34	75.6	127.8
373.6	0.53	0.479	295.7	1.07	12.72	0.34	75.6	127.8
375.8	1.31	1.014	295.9	1.01	14.85	0.40	75.3	127.2
378.7	1.71	1.088	295.9	2.04	18.05	0.48	75.0	126.3
378.8	1.52	0.998	295.9	1.02	17.51	0.46	75.0	126.0
383.8	1.53	0.715	295.9	1.02	24.56	0.64	74.4	124.7
383.8	1.55	0.710	295.2	1.01	24.99	0.65	74.4	124.8
383.8	1.29	0.610	295.2	1.18	24.30	0.63	74.4	124.5
387.9	1.25	0.457	295.2	1.14	31.23	0.81	73.8	123.3
388.1	1.09	0.408	295.9	0.98	30.58	0.79	73.8	123.0
388.7	1.80	0.633	295.2	1.00	32.53	0.84	73.8	123.0
393.0	1.02	0.286	295.2	1.14	40.81	1.05	73.2	121.4
393.1	1.33	0.372	295.2	1.01	41.09	1.05	73.2	121.4
398.1	1.36	0.291	295.7	1.03	53.59	1.36	72.6	119.7

398.3	1.15	0.237	295.9	1.02	55.80	1.42	72.6	119.9
403.2	1.72	0.274	295.7	1.03	71.82	1.82	72.0	118.3
408.4	2.11	0.257	295.2	1.03	93.81	2.37	71.3	116.7

2-hydroxy-4-methoxybenzophenone: $\Delta_1^{\text{g}}H_{\text{m}}^{\circ}(298.15 \text{ K}) = (98.4 \pm 1.0) \text{ kJ}\cdot\text{mol}^{-1}$

$$\ln(p/p_{\text{ref}}) = \frac{396.8}{R} - \frac{134317.1}{RT} - \frac{120.5}{R} \ln \frac{T}{298.15}; p_{\text{ref}} = 1 \text{ Pa}$$

341.2	0.16	8.480	299.3	5.09	0.207	0.010	93.2	164.4
343.2	0.15	6.716	296.3	5.04	0.243	0.011	93.0	163.4
346.2	0.15	5.014	300.4	5.01	0.335	0.013	92.6	162.7
348.2	0.05	1.329	298.6	2.05	0.397	0.015	92.4	161.9
348.2	0.15	4.070	299.4	5.09	0.404	0.015	92.4	162.0
350.2	0.18	4.057	298.6	3.01	0.476	0.017	92.1	161.2
350.2	0.15	3.562	299.4	5.09	0.474	0.017	92.1	161.2
353.2	0.15	2.667	295.4	3.02	0.608	0.020	91.8	160.0
353.2	0.15	2.714	299.3	5.09	0.620	0.020	91.8	160.1
357.2	0.16	2.015	298.8	5.04	0.867	0.027	91.3	158.7
358.2	0.10	1.107	295.4	3.02	0.958	0.029	91.2	158.5
359.2	0.14	1.503	298.6	3.01	1.025	0.031	91.0	158.0
359.2	0.15	1.611	301.3	5.09	1.027	0.031	91.0	158.0
360.2	0.15	1.511	299.4	5.04	1.108	0.033	90.9	157.6
362.1	0.15	1.208	299.8	3.02	1.337	0.038	90.7	157.2
363.2	0.16	1.180	301.8	3.08	1.450	0.041	90.6	156.7
365.1	0.15	0.906	300.3	3.02	1.760	0.049	90.3	156.4
366.2	0.16	0.923	301.8	3.08	1.887	0.052	90.2	155.9
367.2	0.18	0.981	300.4	3.02	2.042	0.056	90.1	155.5
368.2	0.14	0.719	299.4	2.98	2.190	0.060	90.0	155.1

2,2'-dihydroxy-4-methoxybenzophenone: $\Delta_1^{\text{g}}H_{\text{m}}^{\circ}(298.15 \text{ K}) = (100.7 \pm 0.9) \text{ kJ}\cdot\text{mol}^{-1}$

$$\ln(p/p_{\text{ref}}) = \frac{412.8}{R} - \frac{141902.1}{RT} - \frac{138.3}{R} \ln \frac{T}{298.15}; p_{\text{ref}} = 1 \text{ Pa}$$

365.1	0.36	5.608	294.7	3.06	0.64	0.02	91.4	151.0
370.2	0.35	3.824	294.2	3.06	0.93	0.03	90.7	148.7
375.0	0.38	2.679	293.7	2.92	1.44	0.04	90.0	147.4
375.3	2.15	14.890	294.2	1.02	1.45	0.04	90.0	147.2
380.3	0.37	1.861	295.2	3.06	1.98	0.05	89.3	144.9
385.3	1.51	5.243	293.2	3.15	2.87	0.08	88.6	143.1
390.3	0.42	1.011	295.9	1.17	4.18	0.11	87.9	141.5
390.4	1.40	3.220	293.7	3.12	4.36	0.11	87.9	141.7
390.7	0.48	1.122	295.2	1.87	4.31	0.11	87.9	141.4
395.4	1.13	1.940	294.7	3.15	5.85	0.17	87.2	139.6
400.2	1.30	1.558	293.7	3.12	8.35	0.23	86.6	138.2
400.4	0.38	0.466	295.9	1.17	8.10	0.23	86.5	137.8
400.7	0.43	0.504	294.7	0.98	8.57	0.24	86.5	138.0
405.4	1.30	1.170	294.7	3.05	11.17	0.30	85.8	136.0
405.4	1.30	1.170	294.7	3.05	11.17	0.30	85.8	136.0
410.6	1.61	0.987	293.7	3.12	16.32	0.43	85.1	134.8
410.9	1.31	0.818	293.7	2.34	16.07	0.43	85.1	134.4
415.5	1.49	0.691	294.2	1.93	21.61	0.57	84.4	133.1
415.9	1.45	0.651	294.7	1.95	22.39	0.58	84.4	133.1
415.9	1.43	0.647	293.7	1.02	22.17	0.58	84.4	133.0
420.9	1.38	0.476	294.2	1.02	28.95	0.75	83.7	131.1

420.9	1.38	0.488	295.2	1.95	28.48	0.74	83.7	130.9
425.9	1.20	0.315	294.2	0.99	38.20	0.98	83.0	129.5
430.9	1.15	0.232	295.2	0.99	49.83	1.27	82.3	127.8

2,2'-dihydroxy-4,4'-dimethoxybenzophenone: $\Delta_{\text{cr}}^{\text{g}}H_{\text{m}}^{\text{o}}(298.15 \text{ K}) = (117.2 \pm 2.9) \text{ kJ}\cdot\text{mol}^{-1}$

$$\ln(p/p_{\text{ref}}) = \frac{452.8}{R} - \frac{162824.5}{RT} - \frac{153.0}{R} \ln \frac{T}{298.15}; p_{\text{ref}} = 1 \text{ Pa}$$

412.6	0.58	1.914	296.2	3.06	2.74	0.07	99.7	154.3
415.0	1.11	3.062	294.2	3.06	3.24	0.09	99.3	153.4
420.0	1.98	3.776	295.2	3.06	4.69	0.12	98.6	151.8
424.0	1.74	2.552	295.2	3.06	6.10	0.18	97.9	150.3
435.1	1.68	1.250	293.7	3.06	11.96	0.32	96.3	146.2

2,2'-dihydroxy-4,4'-dimethoxybenzophenone: $\Delta_{\text{cr}}^{\text{g}}H_{\text{m}}^{\text{o}}(298.15 \text{ K}) = (139.4 \pm 2.4) \text{ kJ}\cdot\text{mol}^{-1}$

$$\ln(p/p_{\text{ref}}) = \frac{401.7}{R} - \frac{155110.8}{RT} - \frac{52.8}{R} \ln \frac{T}{298.15}; p_{\text{ref}} = 1 \text{ Pa}$$

368.5	0.28	96.124	294.2	6.07	0.0258	0.0056	135.7	242.0
372.9	0.54	108.500	295.9	6.00	0.0443	0.0061	135.4	241.5
375.0	0.56	87.944	295.9	6.00	0.0575	0.0064	135.3	241.3
376.0	0.30	42.315	295.9	2.82	0.0628	0.0066	135.3	241.1
376.7	0.31	43.123	295.9	3.06	0.0650	0.0066	135.2	240.5
378.9	0.24	25.296	294.2	6.07	0.0849	0.0071	135.1	240.4
382.9	0.27	18.000	295.9	6.00	0.1361	0.0084	134.9	240.0
383.0	0.27	18.000	292.7	6.00	0.1312	0.0083	134.9	239.6
386.4	0.31	14.419	293.7	6.07	0.1916	0.0098	134.7	239.2
389.0	0.22	7.504	293.7	6.00	0.2663	0.0117	134.6	239.3
392.1	0.34	8.704	295.9	6.00	0.3509	0.0138	134.4	238.4
395.1	0.35	6.100	295.9	6.00	0.5143	0.0179	134.3	238.6
399.3	0.28	3.137	293.7	6.07	0.7853	0.0246	134.0	237.9

^a Saturation temperature measured with the standard uncertainty ($u(T) = 0.1 \text{ K}$).

^b Mass of transferred sample condensed at $T = 243 \text{ K}$.

^c Volume of nitrogen ($u(V) = 0.005 \text{ dm}^3$) used to transfer m ($u(m) = 0.0001 \text{ g}$) of the sample. Uncertainties are given as standard uncertainties.

^d T_{a} is the temperature of the soap bubble meter used for measurement of the gas flow.

^e Vapour pressure at temperature T , calculated from the m and the residual vapour pressure at the condensation temperature calculated by an iteration procedure.

^f Standard uncertainties were calculated with $u(p/\text{Pa}) = 0.005 + 0.025(p/\text{Pa})$ for pressures below 5 Pa and with $u(p/\text{Pa}) = 0.025 + 0.025(p/\text{Pa})$ for pressures from 5 to 3000 Pa. The standard uncertainties for T , V , p , m , are standard uncertainties with 0.683 confidence level. Uncertainty of the vaporization/sublimation enthalpy $U(\Delta_{\text{l,cr}}^{\text{g}}H_{\text{m}}^{\text{o}})$ is the expanded uncertainty (0.95 level of confidence) calculated according to procedure described elsewhere [28,29]. Uncertainties include uncertainties from the experimental conditions and the fitting equation, vapour pressures, and uncertainties from adjustment of vaporization enthalpies to the reference temperature $T = 298.15 \text{ K}$.

Table C.2 Results of Knudsen effusion method for benzophenone derivatives: absolute vapor pressures p , standard molar sublimation enthalpies and standard molar sublimation entropies

T/K^{a}	m/mg^{b}	T/s	p/Pa^{c}	$u(p)/\text{Pa}^{\text{d}}$	$\Delta_{\text{cr}}^{\text{g}}H_{\text{m}}^{\text{o}}(T)/\text{kJ}\cdot\text{mol}^{-1}$	$\Delta_{\text{cr}}^{\text{g}}S_{\text{m}}^{\text{o}}(T)/\text{J}\cdot\text{K}^{-1}\cdot\text{mol}^{-1}$
2,4-di-hydroxy-benzophenone: $\Delta_{\text{cr}}^{\text{g}}H_{\text{m}}^{\text{o}}(298.15 \text{ K}) = (133.0 \pm 2.9) \text{ kJ}\cdot\text{mol}^{-1}$						
$\ln(p/p_{\text{ref}}) = \frac{382.1}{R} - \frac{144576.8}{RT} - \frac{39.0}{R} \ln \frac{T}{298.15}; p_{\text{ref}} = 1 \text{ Pa}$						
403.4	35.5	4417	4.159	-0.031	128.8	235.5
386.5	12.9	8951	0.794	0.017	129.5	237.4
396.6	11.4	2756	2.208	0.040	129.1	236.4
406.8	8.2	14260	5.602	-0.174	128.7	235.0

366.7	11.3	75182	0.084	-0.004	130.3	238.9
376.5	10.2	20355	0.279	0.013	129.9	238.7
2,2',4,4'-tetrahydroxy-benzophenone: $\Delta_{\text{cr}}^{\text{g}} H_{\text{m}}^{\text{o}}(298.15 \text{ K}) = (159.8 \pm 3.1) \text{ kJ} \cdot \text{mol}^{-1}$						
$\ln(p/p_{\text{ref}}) = \frac{404.6}{R} - \frac{172711.7}{RT} - \frac{43.2}{R} \ln \frac{T}{298.15}; p_{\text{ref}} = 1 \text{ Pa}$						
431.8	8.31	17366	0.251	-0.003	154.1	249.6
436.6	11.87	14993	0.414	0.007	153.9	249.4
441.9	20.99	16139	0.676	-0.002	153.6	248.7
448.2	13.67	18965	1.236	0.022	153.4	248.2
448.9	14.96	5987	1.277	-0.020	153.3	247.9
453.8	15.78	13385	1.990	-0.036	153.1	247.4
455.7	15.9	3250	2.433	0.031	153.0	247.5

^a Saturation temperature measured with the standard uncertainty ($u(T) = 0.1 \text{ K}$).

^b Mass loss of the sample measured by weighing.

^c Vapour pressure at temperature T , calculated from the m .

^d Standard uncertainties were calculated with $u(p_i/\text{Pa}) = 0.005 + 0.025(p_i/\text{Pa})$ for pressures below 5 Pa and with $u(p_i/\text{Pa}) = 0.025 + 0.025(p_i/\text{Pa})$ for pressures from 5 to 3000 Pa. The standard uncertainties for T , V , p , m , are standard uncertainties with 0.683 confidence level. Uncertainty of the vaporization/sublimation enthalpy $U(\Delta_{\text{l,cr}}^{\text{g}} H_{\text{m}}^{\text{o}})$ is the expanded uncertainty (0.95 level of confidence) calculated according to procedure described elsewhere [28,29]. Uncertainties include uncertainties from the experimental conditions and the fitting equation, vapour pressures, and uncertainties from adjustment of vaporization enthalpies to the reference temperature $T = 298.15 \text{ K}$.